# Development of a Robotic Trans-oesophageal Ultrasound System and Its Application in Automatic Acquisition

Wang, Shuangyi

*Awarding institution:*
King's College London

# DEVELOPMENT OF A ROBOTIC TRANS-OESOPHAGEAL ULTRASOUND SYSTEM AND ITS APPLICATION IN AUTOMATIC ACQUISITION


**Shuangyi Wang**

**Department of Biomedical Engineering**

**Division of Imaging Science & Biomedical Engineering**

**School of Medicine**

**King's College London**

**This dissertation is submitted for the degree of Doctor of Philosophy**

**September 2017**

*I dedicate this thesis to my parents, Dr. Shijun Wang and Prof. Jinzhi Wang, who offered unconditional love and have always been there for me. I hope this achievement will complete the dream that you had for me all those many years ago when you chose to sacrifice yourself for many things and give me the best education you could.*

# DECLARATION

This dissertation is the result of my own work and includes nothing, which is the outcome of work done in collaboration except where specifically indicated in the text. It has not been previously submitted, in part or whole, to any university of institution for any degree, diploma, or other qualification.

Signed: 王双翌

Date: 22/02/2017

Shuangyi Wang

King's College London

# ABSTRACT

Trans-oesophageal echocardiography (TOE) has been widely utilized for cardiac disease diagnosis and interventional procedure guidance. However, the TOE operator is required to manually manipulate the probe, often for long periods of time and sometimes in an X-ray environment where there is exposure to ionising radiation. Considering these challenges, a robotic TOE system with intelligent functions that can be operated remotely would be a revolutionary design. Though many research works have been done for ultrasound robotics, no work for robotizing the TOE probe and exploring its application has been reported in the literature.

In this thesis, a new design of a robotic TOE system is reported after the review of related knowledge on echocardiography and previous works on ultrasound robotics. The system has four degrees of freedom to remotely operate a commercial TOE probe. The preliminary tests of the robot demonstrate good repeatability performance of the system. Additionally, the kinematic modelling of the system relating the motor parameters to the ultrasound images is developed, verified, and reported. The model has been included into a view-planning platform designed for planning TOE views and robot paths before a surgical procedure using pre-scanned MR images.

With the proposed robot and the view-planning method, an automatic acquisition workflow is reported. This includes an auto-patient adaption method and a tracking method for locating the probe position when applying feedback. Phantom experiments were performed and the results were analysed. Motivated by a reliability problem identified in the workflow, an improved tracking method of the probe is reported. The new experiments indicate reliable performance of the workflow and the mean error in the near field of ultrasound, where most structures of clinical interest are located, is at the same magnitude as heart motions (1 cm). The study is encouraging for the eventual clinical application of robotic-based TOE acquisition.

# ACKNOWLEDGEMENTS

Undertaking this PhD has been a truly life-changing experience for me and it would not have been possible to do without the support and guidance that I received from many people. First and foremost I wish to express my sincere gratitude to my supervisor, Prof. Kawal Rhode, for continuously supporting my PhD study and guiding me into the academic world, for his patience with my study progress, encouragements when I am depressed, and most importantly showing me the wonderful world of robotics and medical imaging. His strong scientific spirit, passion in education, and will for making impacts to people's life greatly influence my attitude towards research and will have life-long impacts to my career. It's my great honour to study with him and I could not have imagined having a better supervisor and mentor for my PhD study.

My deep appreciation goes out to my daily supervisor Dr. Richard Housden, without whom I wouldn't be able to finish this PhD. I greatly appreciate the selfless help and immense time devotion from Dr. Housden for guiding me each single method I utilized for the project and each single sentence I wrote for my papers and thesis. In all my life, I will never forget these significant helps to train me into a professional researcher. Many thanks go to my collaborator and mentor Mr. Davi Singh from Xtronics. Ltd. who kept teaching me different skills in engineering and put significant efforts working with me all the way though my PhD. I am also grateful to his families – for their friendship and the warmth they extended to me during my time in the house at Gravesend.

My thanks also go out to the support I received from Prof. Kaspar Althoefer and Dr. Hongbin Liu for the project and my research. I am indebted to all my colleagues who helped me in different aspects during my study. Special thanks to Dr. Yohan Noh, Mr. Junghwan Back, Dr. Kiran Reddy, Mr. Devapriyan Johnson, and Mr. David Lau. I also gratefully acknowledge the scholarship received for my PhD study from the KCL-CSC scheme and the funding for the project from the National Institute for Health Research (NIHR) Biomedical Research Centre at Guy's and St. Thomas' NHS Foundation Trust and King's College London.

I would also like to say a heartfelt thank you to my parents for always believing in me, sharing happiness and sorrow with me, encouraging me to follow my dreams, and without whom, I would not have had the courage to embark on this journey in the first place. Finally, I want to give a big hug to my wife Mrs. Wang, who has been by my side throughout this PhD, living every single minute of it, and making me a better man.

# CONTENTS

# LIST OF TABLES

# LIST OF FIGURES

# LIST OF ABBREVIATIONS AND ACRONYMS

| | |
|---|---|
| **PRF** | Pulse repetition frequency |
| **CFI** | Colour-flow Doppler image |
| **CWD** | Continuous-wave Doppler |
| **PWD** | Pulsed-wave Doppler |
| **TTE** | Trans-thoracic echocardiography |
| **TOE / TEE** | Trans-oesophageal echocardiography |
| **ICE** | Intra-cardiac echocardiography |
| **LA** | Left atrium |
| **LV** | Left ventricle |
| **RV** | Right ventricle |
| **RA** | Right atrium |
| **ASE** | American Society of Echocardiography |
| **SCA** | Society of Cardiovascular Anaesthesiologists |
| **UG** | Upper oesophageal |
| **MG** | Middle oesophageal |
| **TG** | Trans-oesophageal |
| **DTG** | Deep trans-gastric |
| **ECG** | Electrocardiogram |
| **LAA** | Left atrial appendage |
| **CABG** | Coronary artery bypasses graft |
| **TOEFP** | TOE-assisted fluoroscopically guided procedure |
| **CE** | Conformité Européenne |
| **FDA** | United States' Food and Drug Administration |
| **DOF(s)** | Degree-of-freedom(s) |
| **ESA** | European Space Agency |

| | |
|---|---|
| **TRUS** | Trans-rectal ultrasound |
| **HIFU** | High intensity focused ultrasound |
| **ENT** | Ear-nose-throat |
| **NOTES** | Natural orifice transluminal endoscopic surgery |
| **ROI** | Region of interest |
| **CAD** | Computer-aided engineering |
| **PVA** | Polyvinyl alcohol |
| **ABS** | Acrylonitrile butadiene styrene |
| **MCU** | Microcontroller |
| **FOV** | Field of view |

# 1 INTRODUCTION

## 1.1 Overview of Ultrasound Imaging

### 1.1.1 Basics of ultrasound imaging in medicine

Medical ultrasonography (sonography) is a diagnostic imaging technology widely used in medicine to visualize internal organs, their size, structure and any pathological lesion using high frequency sound waves. The interaction mechanism between ultrasound waves and living systems has been studied since the 1920s after the discovery of the piezoelectric effect by the Curie brothers and its utilization in the construction of high frequency mechanical vibrating sources [1]. This technique was initially developed for RADAR and SONAR technologies used for submarine detection and non-destructive testing of metals [2]. It began to be understood and used in medicine for imaging purposes in the 1940s [3-5] to detect tumours, exudates, abscesses, or gallstones since then, ultrasound has been applied for various medical purposes; by the mid-1950s more than 6,000 publications had been made [6, 7]. The first greyscale images were produced in 1950 and the first real time images were produced by a Siemens device in 1965 [2]. The acceptance of ultrasound as a powerful diagnostic tool was in the 1970s with improvements in real-time 2D images, formed by both mechanical and electronic array scanning [8]. The modern era of medical ultrasonography has witnessed widespread use in daily clinical routines, as well as developments of various new technologies. Substantial improvements in ultrasound scanners with improved image quality, higher frame rate, Doppler imaging mode, and 3D imaging capability have been introduced and widely employed in clinical use.

Average human ears can detect sound waves with frequencies between 20 Hz and 20 kHz. Sound waves with frequencies higher than 20 kHz are classified as ultrasound. In medical ultrasound, frequencies higher than 2.5 MHz and up to 20MHz are generally used. Ultrasound is a longitudinal wave that can be produced using electroacoustic transducers formed by multiple piezoelectric crystals. These crystals can change their static dimension when an external electric field is applied to the material; this is known as the inverse piezoelectric effect. The ceramic lead zirconate titanate is normally used as the piezoelectric material due to its high electro-mechanical conversion efficiency. When in transmitting mode, the piezoelectric crystals are stimulated by electrical signals, vibrating and emitting ultrasound waves. In receiving mode, the crystals are hit by the ultrasound waves reflected from the tissues, forming electric signals vice versa (Fig. 1.1). During emission, each piezoelectric crystal produces an ultrasound wave and the summation of all waves generated by the piezoelectric crystals forms the ultrasound beam. With a sequence of beams (1D scan lines) to cover the sector or volume, 2D or 3D ultrasound images can be formed. Ultrasound waves are generated in pulses that are spaced with enough time in between to permit the sound to reach the target of interest and return to the transducer. Pulse repetition frequency (PRF) is the rate of pulses emitted by the transducer and used to describe the pulse generation frequency. The PRF for medical imaging ranges from 1-10 kHz. The speed of ultrasound varies for different biological media but the average value is assumed to be at a constant value 1,540 m/sec for most human soft tissues.

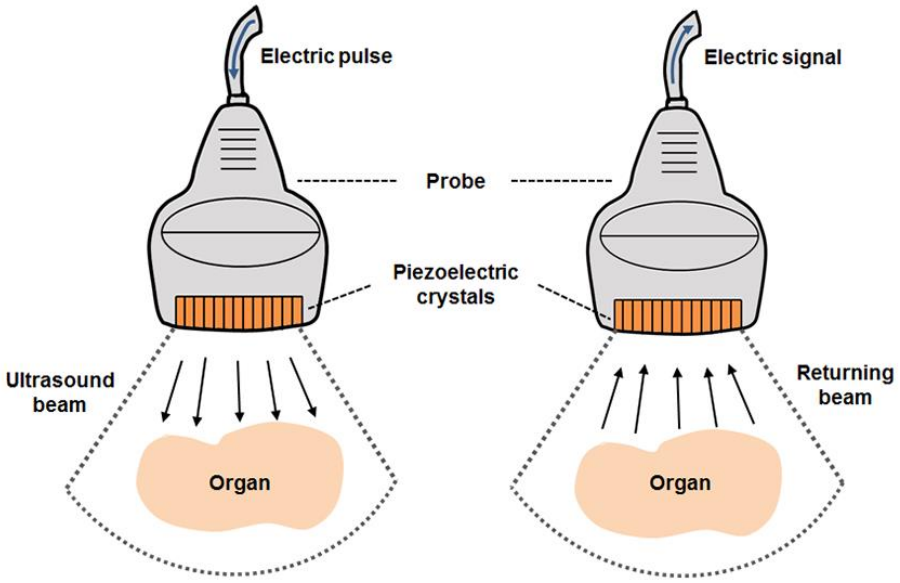


**Fig. 1.1. Schematic diagram of ultrasound generation and receiving with direct and indirect piezoelectric effect, where electrical energy is converted into mechanical and then ultrasound energy and vice versa.**

The frequency of ultrasound has a strong impact on the spatial resolution of the ultrasound image. Axial resolution refers to the ability to distinguish two structures that lie along the axis (as shown in Fig. 1.2) of the ultrasound beam as separate and distinct. Axial resolution is determined by the pulse length where a high frequency wave with a short pulse length will yield better axial resolution, since reflections from structures along the penetration direction are more likely to be distinguished as separate. Lateral resolution refers to the resolution of objects lying side by side (as shown in Fig. 1.2). Lateral resolution is directly related to the ultrasound beam width, which in turn is inversely related to the ultrasound frequency. A high frequency transducer normally emits a wave with a small beam width in its far field, yielding higher lateral resolution as two structures are more likely to be scanned with different beams. In addition, the spatial resolution of an ultrasound image also relies on the number of scan lines (emitting beams) to cover the sector or the volume. Temporal resolution of ultrasound is the ability to detect that an object has moved over time (as shown in Fig. 1.2). For the purposes of medical ultrasound, temporal resolution is synonymous with frame rate. The temporal resolution is related to the PRF which can be influenced by the scanning depth. The sector or volume to scan and the number of scan lines also decide the time to scan for a single frame, thus contributing to the temporal resolution. Moreover, the focusing of the ultrasound beam, which will be discussed in subsequent sections, has an impact on both spatial and temporal resolution.

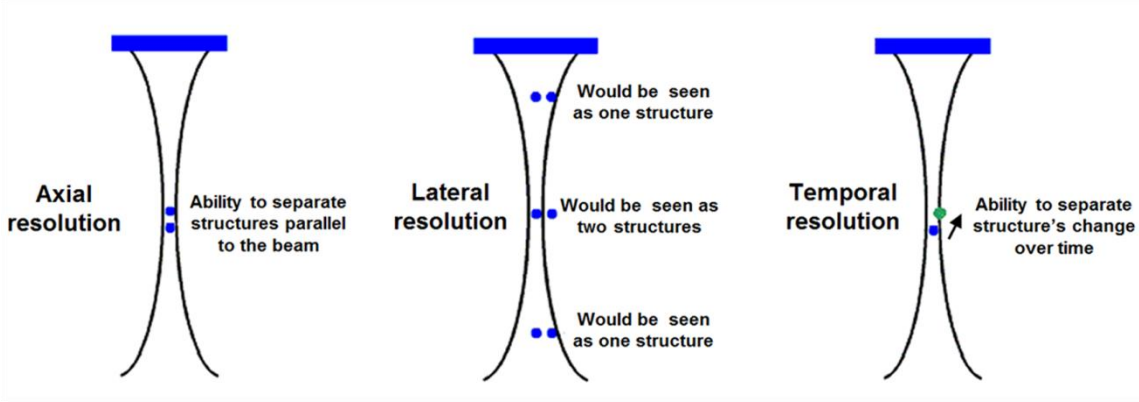


**Fig. 1.2. Schematic representation and explanation of the definitions of axial (left), lateral (middle), and temporal (right) resolution of ultrasound imaging. Figure adapted from [9].**

The interaction of ultrasound with tissue can be summarized in three basic manners: reflection, refraction, and attenuation. Reflection occurs when the ultrasound wave is deflected backwards towards the transducer from the tissue. The extent of reflection is determined by the difference in acoustic impedance of the two tissues at an interface, the angle of incidence of the ultrasound beam, and the width of the tissue boundary.

Specular reflection occurs at flat, smooth interfaces where the transmitted wave is reflected in a single direction (e.g. fascial sheaths, the diaphragm and walls of major vessels). For specular reflection to occur, the wavelength of the ultrasound wave must be smaller than the reflective structure. Reflection in biological tissues when the incident wave encounters an interface that is not perfectly smooth (e.g. surface of visceral organs) is called scattering (diffuse reflection). Echoes from diffuse reflectors are generally weaker than those returning from specular reflectors. Scattering also occurs when the wavelength of the ultrasound wave is larger than the dimensions of the reflective structure (e.g. red blood cells). The incident beam can be also refracted with a change in the direction of the transmitted beam. Refraction occurs only when the speeds of ultrasound are different on each side of the tissue interface. With medical imaging, fat causes considerable refraction and image distortion. Refraction encountered with bone is even more significant leading to a major change in the direction of the incident beam and image distortion. The degree of beam bending is dependent on the change in the speed of ultrasound between interfacing mediums.

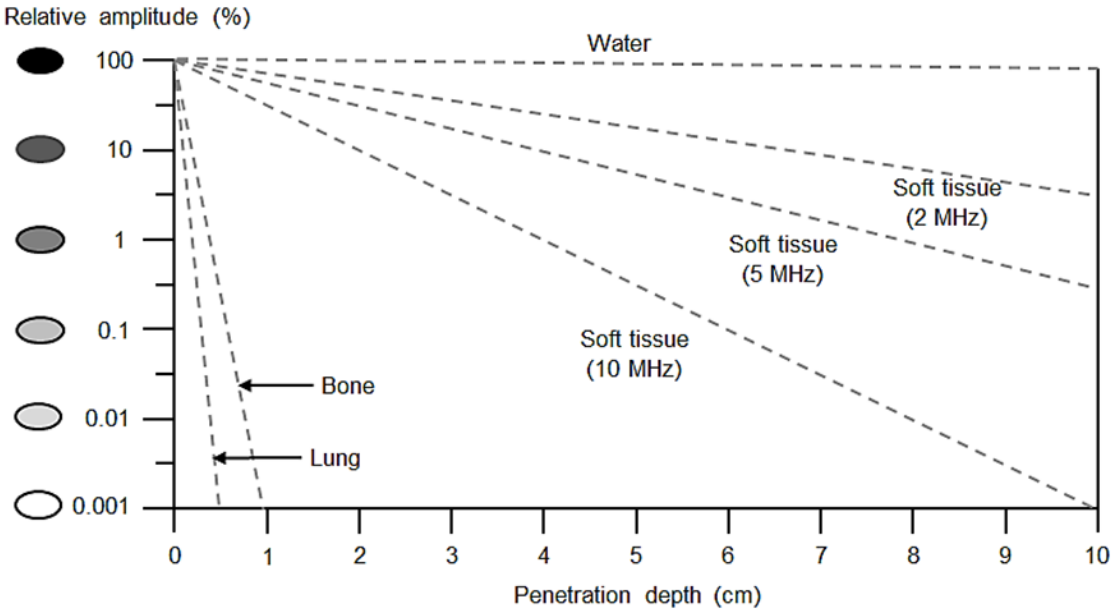


**Fig. 1.3. Effect of attenuation on ultrasound pulse amplitude in relation to penetration depths and ultrasound frequencies for different mediums in the human body. Figure adapted from [9].**

In addition to reflection and refraction, the amplitude of the original ultrasound signal becomes attenuated as the depth of penetration through tissue increases. While both reflection and refraction contribute to attenuation, 80% of attenuation of ultrasound waves in soft tissue is caused by absorption resulting in heat production [10]. Attenuation is represented by the attenuation coefficient of the specific tissue type. For example, bone has a very high attenuation coefficient, which severely limits beam

transmission. The degree of attenuation also varies directly with the frequency of the ultrasound wave. A high frequency wave is associated with high attenuation thus limiting tissue penetration, whereas a low frequency wave is associated with low tissue attenuation and deep tissue penetration. The illustration (Fig. 1.3) shows the decrease in pulse amplitude as ultrasound passes through various materials for different mediums found in the human body [11].

The interactions of ultrasound with tissue directly relate to the advantages and disadvantages of using ultrasound as an imaging approach. Ultrasound images muscle and soft tissue very well and is particularly useful for delineating the interfaces between solid and fluid-filled spaces. It renders real-time live images, enabling rapid diagnoses. In addition, it has no known long-term side effects and rarely causes any discomfort to the patient [12], allowing the technique to be considered as one of the safest imaging approaches. Compared with many other medical imaging modalities, an ultrasound scanner is portable, and the machine can be brought to bedsides or transported to remote locations easily. The technique is substantially lower in cost and is affordable for use worldwide. Today, ultrasound is the second most utilized diagnostic imaging technology in medicine, after X-Rays [13].

As for the disadvantages, ultrasound doesn't penetrate bone or air very well. Therefore, imaging structures behind bones or air is difficult, e.g. imaging the heart through the chest is challenging because the acoustic window between the ribs is small, and the bones and air in the lungs degrade the image. To overcome the difficulties, various intra-operative ultrasound devices based on endoscopic techniques have been introduced, such as trans-oesophageal ultrasound for cardiac diagnosis. Additionally, ultrasound images tend to be more difficult to interpret than many other medical images. Generally, ultrasonography is performed for diagnosis or therapeutic procedure guidance (as summarized in Table 1.1). For extra-corporal scanning, a hand-held probe is placed directly on and moved over patients to acquire images. Alternatively, different endocavital and laparoscopic ultrasound methods with transducers mounted on the tip of endoscopes or special devices are used to access patients' natural orifices or artificial incisions and acquire images from inside the body.

**Table 1.1. The clinical use of ultrasound imaging categorized by different devices**

| Device | Examples of clinical applications |
|---|---|
| Hand-held | Abdominal (liver, kidney, gallbladder, etc.), cardiac, maternity, breast, vascular, urological, ophthalmological, and gynaecological scan. |
| Endoscopic | Trans-oesophageal and trans-nasal: cardiac diagnosis and procedure guidance. |
| | Endobronchial ultrasound: diagnosis of lung cancer, lung infections, etc. |
| | Trans-gastric and trans-duodenal: procedures guidance. |
| Trans-vaginal | Vagina, uterus, and ovarium scan. |
| Trans-rectal | Rectum, prostate, and perirectal space scan. |
| Laparoscopic | Procedure guidance for scanning abdominal, pelvic, and mediastinal region. |
| Intra-operative | Intra-cardiac, intra-ductal (such as: bile duct and Wirsung duct) scan. |

### 1.1.2 Imaging modes and transducer techniques

The early evolution of ultrasound imaging technique started with a hand-held transducer that points a single beam, generating a 1D signal with amplitudes at different penetration depths proportional to the strength of the reflected signal from structures at those depths. This is known as A-mode ultrasound imaging, which is no longer commonly used clinically except in ophthalmology for precise intraocular length measurements [14]. Based on the A-mode data from a single ultrasound beam represented as a function of time, an M-mode ultrasound image displays time on the horizontal axis and depth on the vertical axis. The A-mode signals are converted into dots with different brightness representing amplitudes. M-mode ultrasound is mainly used for motion analysis, such as evaluating valve functions or measuring chamber dimensions in cardiac applications [15].

Since the first introduction of real-time 2D ultrasound imaging in the 1970s, this technique was rapidly adopted clinically and has become the most widely used imaging mode of ultrasound [2]. This kind of real-time 2D imaging is also known as dynamic B-mode imaging. The cross-sectional imaging is achieved by sweeping or steering the ultrasound transmit beam sideway across a plane so that many scan lines will be interrogated sequentially. Each of these beams forms a brightness modulated scan line in which the echo amplitude is represented by a grey level. With this basic principle, different probes for 2D imaging were designed, such as the linear, convex, and phased-array probe. The linear and convex probes are generally classified as array probes, containing arrays of transducer elements. The number of rectangular elements is typically 128 or 256. Array probes select the region of investigating by firing a set of

transducer elements (typically 32 to 64) sequentially [16] as shown in Fig. 1.4a. The beam is stepped along the array to the next set after the current set is finished.

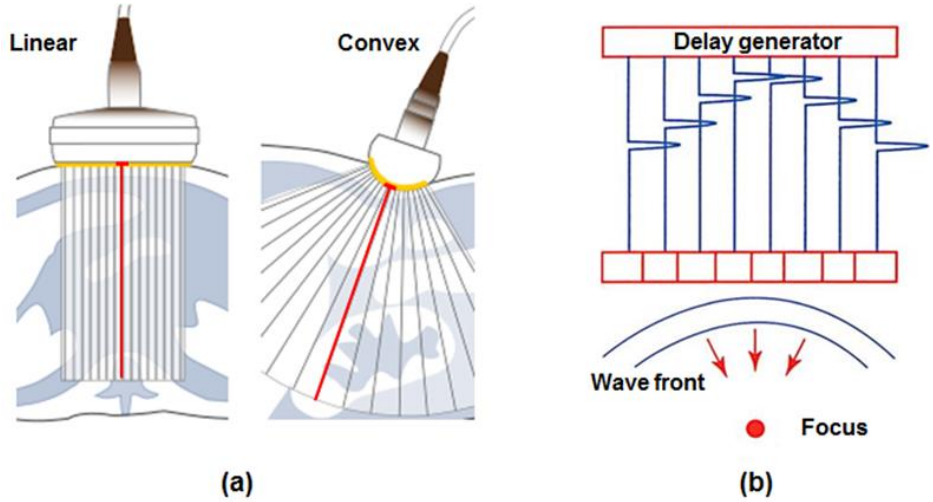


**Fig. 1.4. (a) Examples of array probes (linear and convex). A set of elements (red) within the element array (yellow) is activated at one time to generate a scan line. (b) Principle of electronic beam focusing. Electrical pulsing of the inner elements is delayed with respect to the outer elements. Figure adapted from [17] and [18].**

In the subgroup of these elements, pulsing of the inner elements is delayed with respect to the outer elements, which is known as electronic focusing (Fig. 1.4b). A focused beam, resulting from the interference of the small divergent wavelets from each element, improves lateral resolution as well as sensitivity by increasing the amount of energy in the focal zone. For reception, the electronic signals are delayed individually from the more central element to those of the outer most elements in a similar way to compensate for the differences of acoustic path. When ultrasound scan lines penetrate the human body, several echo sources generate returning waves from different tissue interfaces with their depths known. The dynamic-focusing technique of the received signal allows changes of the focal length automatically in discrete steps with different elements activated for the receiving aperture [19]. However, this technique is unachievable for the transmit beam as the focal length is fixed once it is launched. To obtain optimum focus over the entire depth of field, the multi-zone transmit technique [20] was developed, in which several transmit pulses are sent for each line, focused at a different depth. Then the final image is formed out of the portions of those partial images that are most in focus. Although this technique improves the spatial resolution at more depths, it has the drawback of reducing the frame rate. Moreover, parallel beamforming (also known as multiple line acquisition) [21] with the focusing

mechanism is used to increase the frame rate by transmitting one wide beam and receiving multiple narrow beams in parallel.

However, the linear and convex probes described above are too large for some applications, such as placing between ribs to obtain an ideal acoustic window for a heart scan. The technique also suffers from off-axis beam artifacts resulting from grating lobes [22]. As a way to overcome both problems, the method of phased-arrays (Fig. 1.5a) was introduced to scan a sector field of view with a smaller size of probe. In such systems, all the transducer elements are used to steer the scan line to a particular angle with respect to the transducer face (Fig. 1.5b). This can be combined with the focusing described earlier, providing a steering and focusing mechanism. Electronic beam steering of phased-array probes also enabled the development of simultaneous modes [23], which is especially important for cardiology. Since the beam path is electronically controlled, the direction (vector) of each A-line can be selected at random, which makes it possible to provide a B-mode image in real time with a simultaneous M-mode display. With the simultaneous mode, sonographers can see a very detailed view of the motion of a cardiac valve as well as the location from which it is acquired.

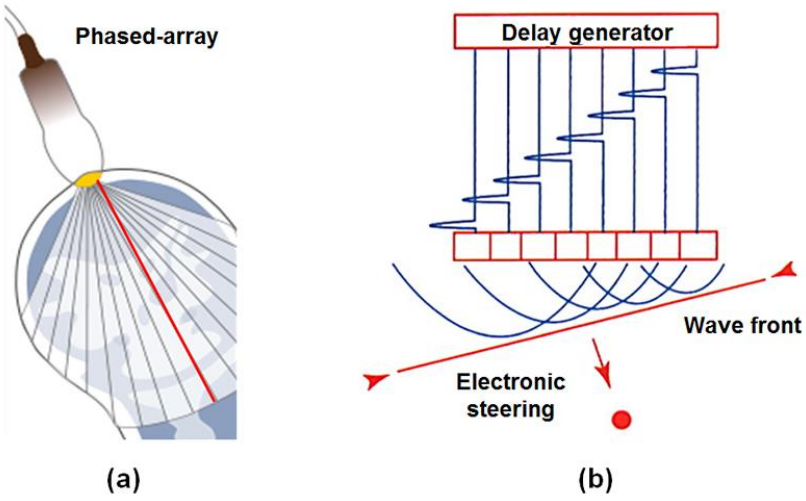


**Fig. 1.5. (a) Examples of phased array probe. All elements within the element array (yellow) are activated at once to generate a scan line. (b) Principle of electronic beam steering. Electrical pulsing of all the elements is delayed according to the steered direction. Figure adapted from [17] and [18].**

Attempts for 3D images started from off-line reconstruction from 2D images by registering different planes. This technique can be achieved either by linear step-by-step motion or rotation/ tilting of the array or phased-array probe [16, 24]. As the mechanical movements of the probe are not fast enough to get adequate images during a single cardiac cycle, the gated sequential acquisition technique [25] using respiratory and ECG gating is used to reduce the misalignment of slices caused by respiration and heart rate

variabilities. In addition, for static targets 3D images can be obtained using self-rotational transducers without the need for external mechanical movements. In this approach, an internal motorized mechanism rotates the transducer array through an angle depending on the application and probe shape, while the 2D images for 3D reconstruction are acquired [26]. Real-time 3D ultrasound imaging without the need for physically moving the probe or transducer is achieved by newly developed 3D transducer technology [2]. To steer the ultrasound beam electronically in 3D space, a 2D piezoelectric array typically consisting of 2,000-3,000 elements in a matrix arrangement format is used [27]. With the beam generated by selected elements, steering in both the azimuthal and elevational plane is achieved and results in a pyramid-shaped 3D volume. Differently to 2D phased-array transducers where beamforming is done within the ultrasound system, a micro-beamforming technique splits the process into pre-beamforming by a custom integrated circuit in the probe handle and the traditional digital beamforming in the ultrasound system [28]. For the 3D display of the acquired images, different rendering techniques [29] have been developed and employed in the ultrasound systems to visualize both surface and inner structures.

Doppler imaging mode, also known as D-mode imaging, is also widely used clinically as a way of imaging and measuring flow based on the changes in frequency (Doppler shift) caused by the reciprocal movement of the sound between generator and the observer. Diagnostic ultrasound uses the change in frequency of ultrasound signals backscattered from red blood cells [30]. The frequency of the reflected ultrasound wave changes according to the direction of blood flow in relation to the transducer. There are generally two approaches for Doppler ultrasonic imaging categorized into colour-flow and spectral modes [30]. In colour-flow Doppler image (CFI) mode, the velocity and direction of blood flows are depicted in a colour map superimposed on the 2D image. The classic colour-flow mode uses two distinct colours, usually variations of red and blue colours, to represent the vascular blood perfusion of a structure. As a variant of the classic colour-flow mode, a power Doppler image displays the power of the Doppler signal, which is related to the number of blood cells in the sample volume. This is often used to increase sensitivity to low flows and velocities. However, power Doppler does not display flow direction or different velocities.

In the spectral mode, blood flow velocity variations are represented as a graphic wave form referred to as a spectrum. The spectral mode can be further divided into two specific approaches: continuous-wave Doppler (CWD) and pulsed-wave Doppler

(PWD). The CWD image mode requires two piezoelectric crystals working continuously. One transmits and the other receives the Doppler signals along the scan-line. CWD is very useful in high velocity signals recording though it cannot locate the Doppler signal source. The PWD image mode uses the same piezoelectric crystal transmitting and receiving the ultrasound signal. PWD mode allows measurement from a small, specific blood volume (e.g. arteries and veins) by providing both blood flow direction and precise determination of Doppler signal source. However, as a result of using the same crystal for both transmission and reception, it cannot accurately give the velocity based on Doppler shift if the measured blood moves too fast. For many cases in practice, combinations of PW and CW are used to determine both velocity and location of a particular blood flow of interest.

### 1.1.3 Ultrasound in cardiology

Since medical ultrasound was introduced in the 1950s, the technique has retained its advantage over other imaging modalities in imaging the beating heart in real time because of fast data acquisition. The application of ultrasound in cardiology, usually referred to as echocardiography, has now become routine in diagnosis, management, and follow-up of patients with any suspected or known heart diseases. Medical ultrasound is now one of the most widely used tests performed as well as one of the most cost-effective diagnostic tools in cardiology.

Trans-thoracic echocardiography (TTE) is a commonly used imaging modality in assessing the structure and function of the heart. A TTE scan is performed by placing either a 2D or a 3D transducer between the ribs. Different angles and positions result in different views and section planes of the heart. These views during a standard TTE scan have their purpose in imaging different structures of the heart or obtaining useful heart performance parameters. TTE allows a variety of assessments of the heart such as those summarized in [31]. These include assessment of the heart motion, ascertaining if the valves are opening and closing properly, checking the ability of the heart to pump the blood, detecting blood clots and tumours, and evaluating cardiomyopathy disease. The most obvious disadvantage of TTE is the difficulty in placing the transducer between the ribs of the patient. The imaging quality of the heart is also influenced by the pathway of the ultrasound beam through bones, muscles, and lung. However, compared with other echocardiography technologies, TTE is cheap, convenient, and less

uncomfortable to patients. Thus, the initial assessment of the heart is usually performed by using TTE.

As alternative ways to perform an echocardiogram, trans-oesophageal echocardiography (TOE / TEE) and trans-nasal echocardiography (both shown in Fig. 1.6a) with flexible endoscopic configurations are used as semi-invasive diagnostic tools. Since the TOE probe is inserted into the oesophagus, upon which the heart rests directly, the ultrasound beam travels only millimetres to access the heart structure. This reduces the attenuation of the ultrasound signal, ultimately resulting in enhanced image and Doppler quality with stronger return signals. Thus, TOE has a natural advantage in image quality when compared with TTE. Specifications and clinical applications of TOE are discussed in detail in the following subsections. A feasibility study of introducing a small trans-nasal ultrasound probe via the nose has shown several advantages over the standard thick TOE probe in terms of patient comfort and prolonged echocardiography monitoring [32]. The standard TOE technique may also have a limitation in monitoring cardiac activities during anesthesia because it may impair tracheal intubation and mask ventilation [33]. In such situations, a trans-nasal ultrasound probe may be considered.

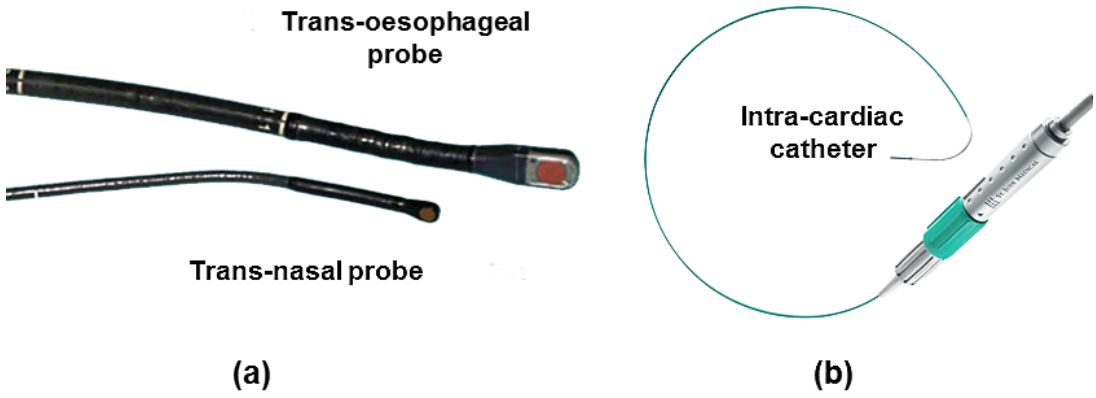


**Fig. 1.6. (a) Comparison of trans-oesophageal probe and trans-nasal probe used for echocardiography. (b) Example of an intra-cardiac catheter used for echocardiography.**

Intra-cardiac echocardiography (ICE) (as shown in Fig. 1.6b) based on a catheter configuration was developed to provide accurate imaging of the intra-cardiac structure. Various improvements in ICE technique in recent years have allowed this imaging tool to be used in more interventional cardiac and electrophysiological procedures as summarized in [34, 35]. There are normally two means of inserting the catheter into the heart: the femoral or the internal jugular approach. Both are under continuous fluoroscopic guidance to advance the catheter to the heart.

## 1.2 Specifications of TOE

### 1.2.1 Equipment and manipulation of TOE

Trans-oesophageal ultrasound scanning is performed with ultrasound scanners and specially elongated probes, known as TOE probes. A TOE probe usually comprises an electronic interface, a control handle, a gastroscope tube, and a miniaturized ultrasound transducer. The electronic interface, which connects the probe to the ultrasound scanner, allows signal transmissions between the ultrasound machine and the ultrasound transducer. The control handle usually includes two independently rotatable knobs which are used to adjust the bi-directional bending of the probe tip via several internal mechanisms. These two knobs, normally with different shapes, are arranged and mounted concentrically one on top of the other. On the side of the control handle, buttons or additional small wheels may also be placed in order to provide the electronic steering function of the ultrasound beam. The gastroscope tube is the structure guided down the oesophagus and in contact with the patients. The tube usually includes a flexible portion extending from the control handle and a rigid head at the distal end on which a miniaturized ultrasound transducer is mounted. Examples of TOE probes from different manufactures are shown in Fig. 1.7. Though general configurations of these TOE probes are similar, variations exist including shapes of probes, approaches to control electronic steering, and properties of transducers.

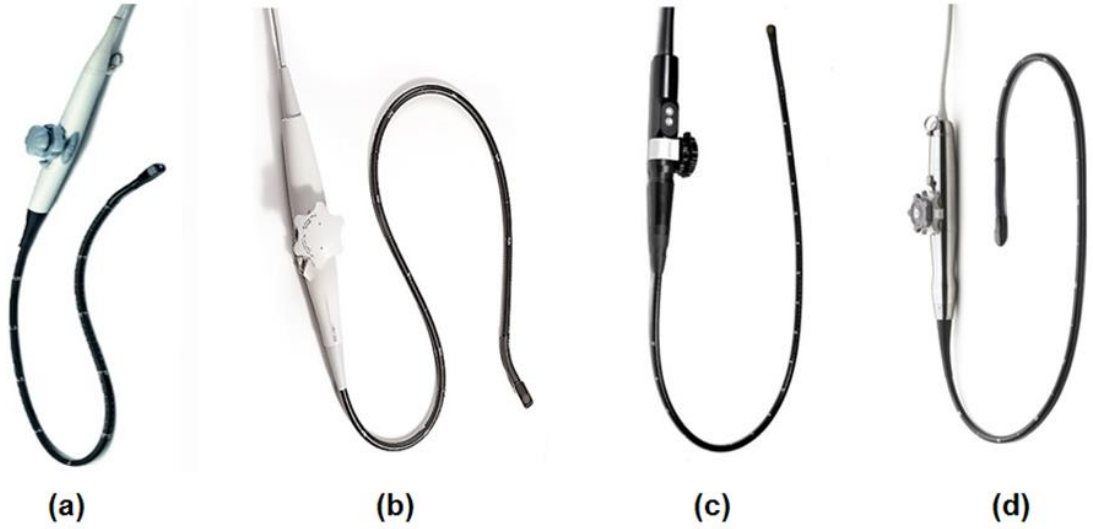


**Fig. 1.7. Examples of TOE probes from different manufactures with similar structures and configurations: (a) Vivid E9 (GE, United States), (b) V5Ms (Siemens, Germany), (c) Motormulti (Oldeft Ultrasound, The Netherlands) and (d) X7-2t (Philips, The Netherlands).**

The studies in this thesis utilize a commercial TOE probe (x7-2t, Philips, The Netherlands) along with a compatible ultrasound machine (iE33, Philips, The Netherlands). Movements of the TOE probe inside of the patient are summarized in Fig. 1.8a. This assumes that the patient is supine in the standard anatomic position, and the TOE transducer is pointing towards the heart from the oesophagus so the imaging plane is anteriorly through the heart. With reference to the heart, superior represents towards the head, inferior towards the feet, posterior towards the spine, and anterior towards the sternum. The terms left and right mean the patient's left and right sides. With this definition of movements of the probe inside of the patient, manipulation of the probe during TOE scanning is also defined. The structural layout and the definition of manipulation axes of the TOE probe are shown in Fig. 1.8b with explanations of each component of the probe. The manipulation of the TOE probe involves inserting the probe down the oesophagus and positioning the transducer to appropriate locations controlled manually by the sonographer, summarized as follows:

- *Translation axis*: the probe can be advanced or withdrawn in the oesophagus by gripping the probe shaft and moving along its long axis. This allows the probe to be pushed distally down to the oesophagus and stomach or pulled back in the opposite direction.

- *Rotation axis*: the orientation of the probe can be controlled by manually rotating the probe handle along its long axis. Looking in the patient's head to feet direction, rotating the probe clockwise within the oesophagus toward the patient's right is called turning to the right, and rotating counter-clockwise is called turning to the left.

- *Left–right bending axis*: the orientation of the probe tip can be adjusted to the left or right by rotating the top knob located on the handle of the probe. Bending of the tip of the probe towards the patient's left and right is called left or right flexing.

- *Anteflex–retroflex bending axis*: the orientation of the probe tip can be adjusted upwards and downwards by rotating the bottom knob on the handle of the probe. Flexing the tip of the probe anteriorly is called anteflexing, and flexing it posteriorly is called retroflexing.

- *Electronic steering axis*: the orientation of the ultrasound beam can be electronically steered (0 degree to 180 degree) by a button pair located on the handle of the probe, and sometimes by operating a button on the ultrasound

machine. Rotating towards 180 degrees is called rotating forward, and rotating in the opposite direction toward 0 degree is called rotating backward. At a transducer angle of 0 degrees (the horizontal or transverse plane), with the imaging plane directed anteriorly from the oesophagus through the heart, the patient's right side appears in the left of the image display (Fig. 1.9a). Rotating the transducer angle forward to 90 degrees (vertical or longitudinal plane) moves the left side of the display inferiorly toward the spine (Fig. 1.9b). The angle of rotation thus occurs in a 'counter-clockwise' manner, as depicted in an icon typically shown on the screen. Rotating the transducer angle to 180 degrees places the patient's left side to the left of the display, the mirror image of 0 degrees (Fig. 1.9c).

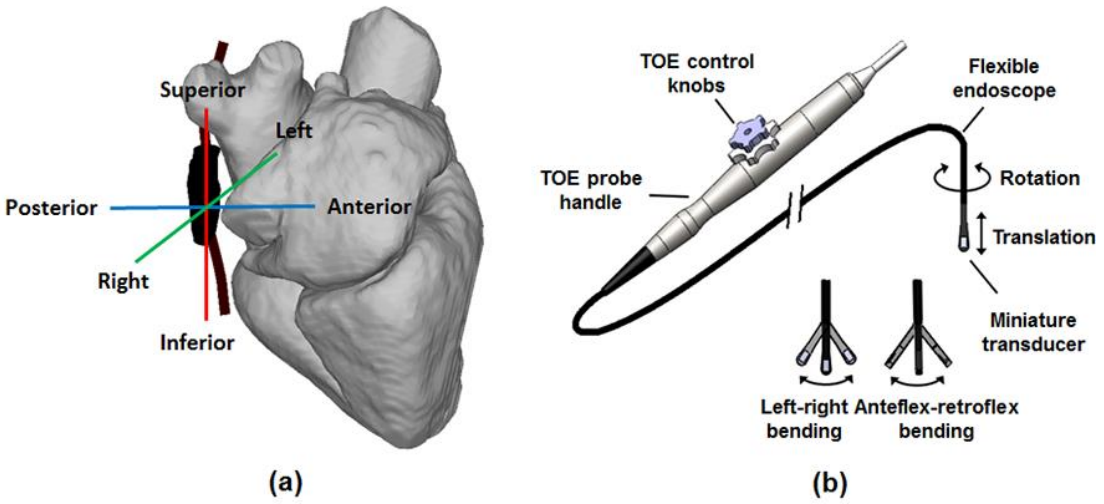


**Fig. 1.8. (a) Terminology and definition of the movements of the TOE probe inside the patient. (b) Components and the manipulation axes of the TOE probe.**

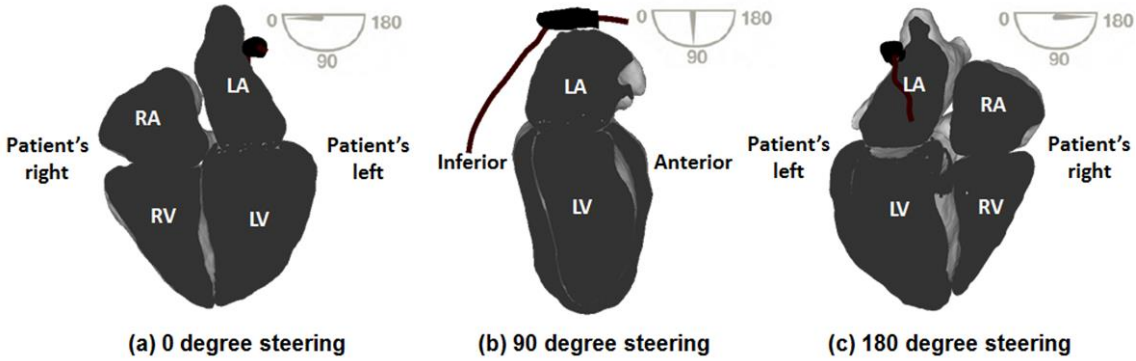


**Fig. 1.9. Illustration of the electronic steering axis. The ultrasound beam rotates about the penetration direction of the ultrasound beam. (a) Image orientation at transducer angle 0 degrees. (b) Image orientation at angle 90 degrees. (c) Image orientation at angle 180 degrees. LA, Left atrium; LV, left ventricle; RV, right ventricle; RA, right atrium.**

The TOE probe in this study uses a cable-actuated steerable system to control the bi-directional steering of the rigid distal end. In this design configuration, several endoscopic flexible links (vertebra) with articulation capability are arranged and connected to cables or wires attached to non-cross-coupling shafts. The shafts are mechanically coupled to the two knobs on the probe control handle as introduced previously. As such, the endoscopic flexible links, and thus the distal end of the probe, can be moved by manual adjustment of the knobs. The non-cross-coupling shafts also include two different rack and pinion gear sets. These convert angular input motion into linear output motion or vice versa. A hollow metal cylindrical shell of varying diameter is used to house the rack and pinion gear sets. The mechanism consists of a prismatic joint, pinion, and a handle. A schematic diagram of the probe bending mechanism is shown in Fig. 1.10.

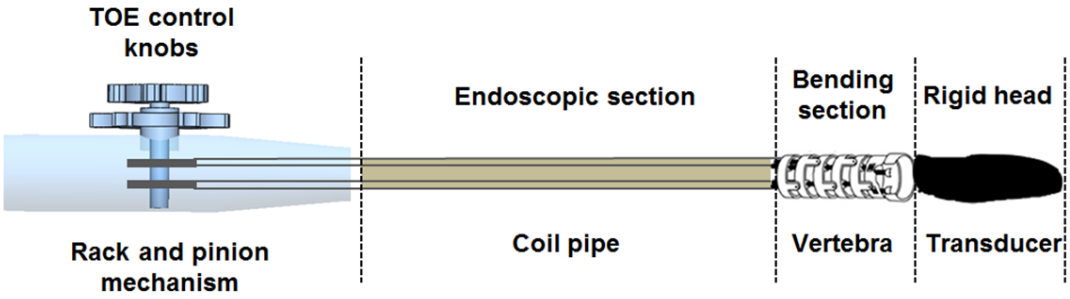


**Fig. 1.10. Schematic representation of the probe bending system with rack and pinion mechanism linked to the user-controllable knobs and cable actuating mechanism to control the bi-directional bending of the probe tip via flexible vertebra structure in the bending section.**

### 1.2.2 Procedure and utilisation of TOE

TOE is a semi-invasive procedure which requires sedation or anesthesia. The current practices for sedation and anesthesia during the performance of TOE have been reviewed in [36]. Generally for the non-surgical use of TOE, numbing medication is first sprayed into the patient's throat. The operator then positions the patient onto the operating bed in the left lateral decubitus position (Fig. 1.11). The echocardiographer stands facing the patient during the scan. The nurse then inserts a mouthpiece, working as a bite block keeping the patient's mouth open and preventing the patient from biting the TOE probe as well as the operator's fingers. Conscious sedation is then applied to the patient. A small percentage of patients might not tolerate probe insertion under moderate sedation or if there is a history of difficulties in achieving sedation. In such cases, deep sedation or anesthesia with more intensive monitoring and additional support is required.

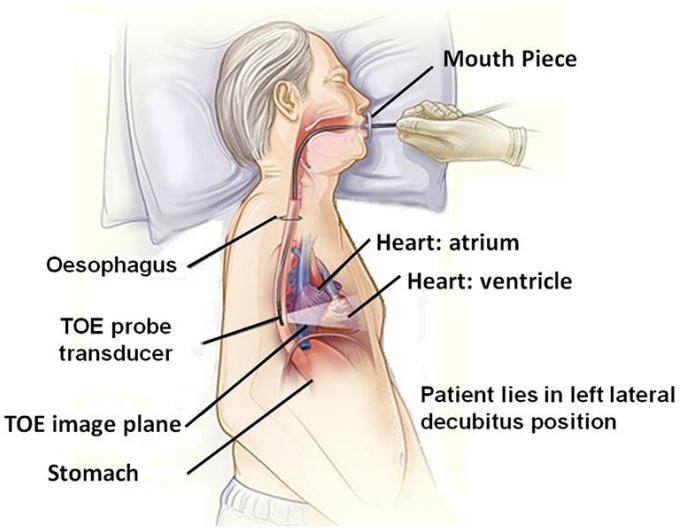


**Fig. 1.11. Illustration of the TOE procedure with the patient in left lateral decubitus position and a TOE probe inserted into the oral cavity by an operator. A mouth piece is used for guiding the probe into the oral cavity. Figure adapted from [37].**

During the insertion of the probe, a protection sheath is used to cover the probe endoscopic portion and tip with adequate ultrasound gel placed inside. The patient is asked to place the chin downwards and breathe slowly while the probe is inserted to the back of the pharynx. With a bite block in place, it is also useful for the operator to insert one or two fingers into the mouth and guide the probe toward the midline, depressing the tongue if it is blocking passage. Once the probe is in the pathway of the oesophagus, the patient is asked to swallow the probe as an assistance of reducing gag. During the whole operation of probe insertion, the probe has to be manipulated in its neutral position without any bending of the probe tip to avoid any possible injury to the patient. Once the probe is successfully inserted, the TOE scan begins with different manipulations of the probe according to standard or custom protocols and depending on the specific clinical needs of the patient. This is usually achieved by a specially trained echocardiographer. The TOE images are shown on the screen of the ultrasound machine and interpreted visually. After the scan is finished, the echocardiographer slowly pulls the TOE probe out from the patient's mouth with the probe returned to its neutral position. If TOE is used as an adjunct monitoring device during cardiac procedures, patients are typically fully anesthetized and intubated. General considerations for probe insertion are the same as for the normal scan, although several differences exist [36]. These may include a different position of the patient, additional agents to facilitate passage of the probe, and respiratory therapists or other professionals capable of managing and monitoring the ventilator.

### 1.2.3 Imaging modes and scanning protocols of TOE

Related techniques for trans-oesophageal ultrasound were first reported in 1971 by Side and Gosling with a device to measure flow in the aortic arch [38]. In their study, a dual-element transducer mounted on a gastroscope was used to obtain CW Doppler of cardiac flow. This was followed by its use with 1D M-mode imaging in 1976 for chronic obstructive pulmonary disease reported by Frazin *et al.* [39]. The first 2-D B-mode ultrasound imaging obtained through the oesophagus was reported by Hisanaga *et al*. in 1977 and 1978 using a rotating single-element transducer and a linear mechanical scanning transducer [40, 41]. The modern era of TOE began in the 1980s, with the important introduction of flexible probes using phased-array transducers and adjustable tips for imaging the heart. From this time forward, 2D TOE scanning with phased-array transducers evolved rapidly with improvements of the miniature transducers, initially as a single, horizontally oriented transducer (monoplane), next as two orthogonally oriented transducers (biplane), and then as adjustable transducers capable of rotating 180 degrees within the tip of the probe (multiplane) [42]. The transducer usually contains 64 to 128 piezoelectric crystals placed side by side, forming a linear pattern. All the elements are pulsed together to form the wavefront for a single scan line. Sequential activation of crystals with the steering and focusing techniques above generates an ultrasound beam that scans back and forth over 90 degrees to sweep through a flat scanning plane or sector. The transducer is mechanically rotated 180 degrees with a motorized mechanism around the long axis of the ultrasound beam to scan a conical-shaped volume.

The 2D multiplane TOE has been widely used clinically since then and a set of 20 trans-oesophageal echocardiographic views, intended to facilitate and provide consistency in training, reporting, archiving, and quality assurance, was published by the American Society of Echocardiography (ASE) and the Society of Cardiovascular Anaesthesiologists (SCA) for performing a comprehensive multiplane TOE examination [43]. This guideline describes the techniques of manipulating the probe to the desired locations (translation, rotation, bending, and electronic steering) for acquiring these 20 views, known as the 2D TOE standard views or 2D TOE protocol. In the description of the 2D TOE standard views, four primary positions within the gastrointestinal tract at different depths (echo window) are used (Fig. 1.12): upper oesophageal (UG), mid oesophageal (MG), trans-gastric (TG), and deep trans-gastric (DTG). Following the primary standard 20 views, some recommendations have added

an additional eight views to the 2D TOE standard views as the result of expansion of indications for TOE [36].

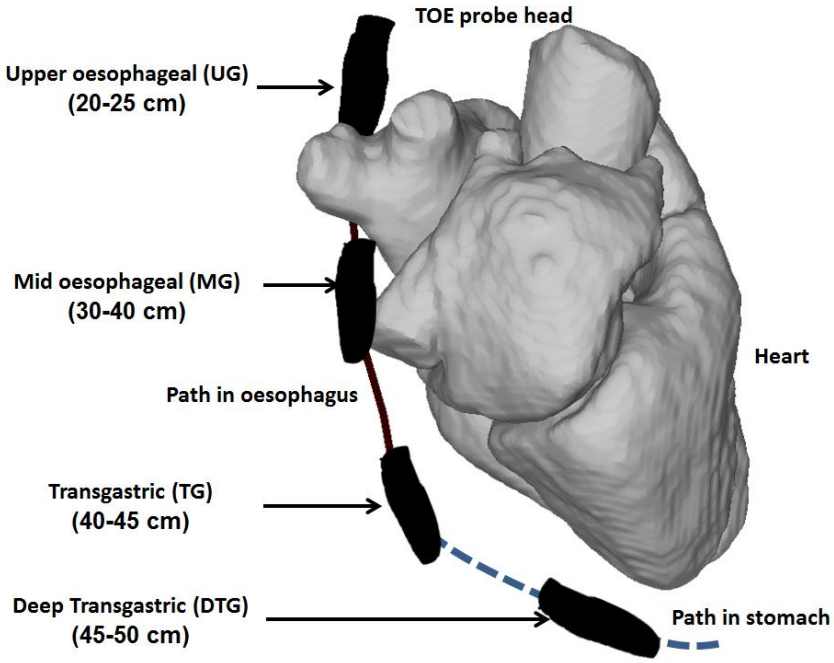


**Fig. 1.12. Four standard transducer positions (UG, MR, TG, and DTG) within the oesophagus and stomach used in the description of the TOE standard views.**

Derived from a 2D stationary TOE probe, 3D TOE was achieved using a 2D transducer by mechanically moving the transducer linearly or rotationally [29]. In the sequential linear method, the TOE probe (monoplane or multiplane) is moved in equal longitudinal steps to provide a series of parallel equidistant 2D images which are constructed to a 3D volume afterwards (Fig. 1.13a). The rotational scanning method is performed with an off-line reconstruction method using the multiplane 2D probe; the TOE probe is held immobile while the ultrasound scanning plane rotates mechanically or electronically to scan a conical-shaped volume at fixed angle increments (Fig. 1.13b). For both techniques described above, the acquisition of each image (slice) is timed to the same portion (R-wave) of the electrocardiogram (ECG). In addition, when the time to obtain multiple 2D images is longer than a tolerable breath hold, respiratory gating is used to acquire images during the same portion of the respiratory cycle [29]. This improves image quality because the distance between the TOE probe and the heart varies with respiration.

More recently, trans-oesophageal echocardiographic probes and systems have been developed that can produce real-time 3D images with a matrix-array transducer (Fig. 1.13c) [29]. With this technique, data acquisition occurs in a very short time and may involve ECG gating for larger volumes but not respiratory gating. Modern matrix array

transducers contain a grid of 50 rows and 50 columns for a total of 2500 independent piezoelectric crystals. The whole transducer is encased in the size of a standard multiplane TOE probe tip. As introduced previously, different piezoelectric crystals within the matrix-array transducer are activated sequentially, generating ultrasound beams which can be steered in both the azimuthal and elevational plane to scan a pyramid shape.

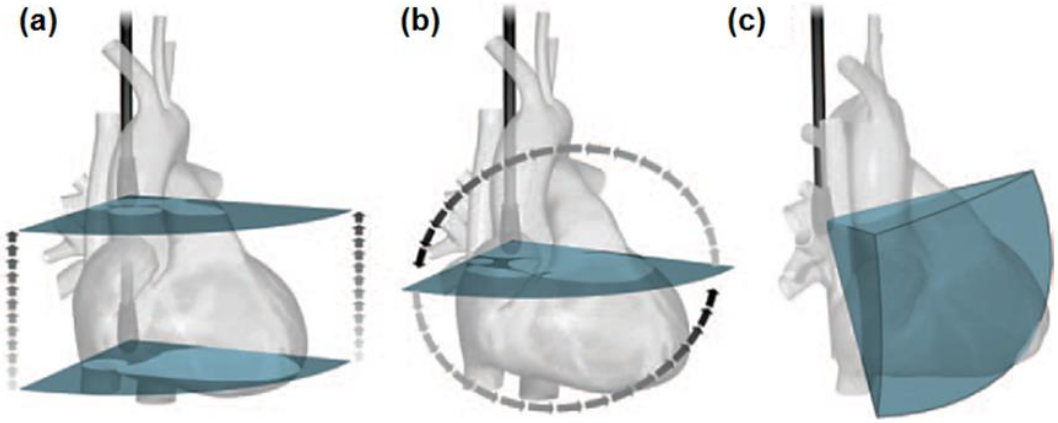


**Fig. 1.13. Techniques used in TOE to acquire raw 3D data include (a) sequential (linear) 2D scanning, (b) rotational 2D scanning, and (c) volume scanning. Figure reproduced from [29].**

In the latest TOE systems, different modes of 3D volume acquisition are available. Currently, the most common modes are live 3D, live 3D zoom, and full volume, as well as full volume colour Doppler acquisitions [27]. Temporal and spatial resolution and volume size of 3D TOE are related to each other. As there is only one transmit beam at a time travelling through the scan volume with a constant speed, the temporal resolution is dependent on the number of scan lines. The number of scan lines is dependent on the size of the scan volume and line density. A comparison of three different 3D TOE modes is summarized in Table 1.2. The volume sizes of these three different 3D TOE modes are illustrated in Fig. 1.14. The matrix-array probe also functions as a standard 2D multiplane TOE probe with its ability of beam steering in both azimuthal and elevational planes. This includes 2D, spectral, and colour Doppler modes. Similar to the 2D protocol, 3D standard views for general scans have also been proposed [36, 44]. A comprehensive 3D TOE examination usually starts with live 3D mode using single-beat acquisition from the mid-oesophageal views to determine the overall function of the left and right ventricles and to identify structural valve abnormalities. A subsequent multiple-beat mode with ECG gating provides a wide-angle acquisition. This improves image quality and permits a wider volume of acquisition. Since a matrix array including

both the area and depth is used for 3D TOE, less probe manipulation for data acquisition is required compared with a standard 2D TOE examination.

**Table 1.2. Summary and comparison of different 3D TOE modes**

| | Full volume | Live 3D | Live 3D Zoom |
|---|---|---|---|
| Dimensions | 90° * 90° by the depth of the 2D image | 60° * 30° by the depth of the 2D image | 20° * 20° to 90° * 90° by a variable height |
| Real time | No (ECG gated) | Yes | Yes |
| Frame rate | 20-40 Hz (4 heart beats)<br>40-50 Hz (7 heart beats) | 20-30 Hz | 5-10 Hz |
| Temporal resolution | Low | Good | Low |
| Spatial resolution | Lowest | Mid | Highest |

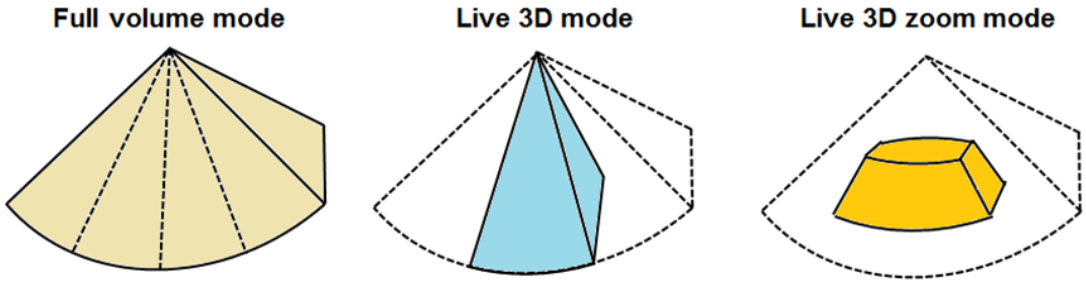


**Fig. 1.14. Schematic representation of different 3D volume acquisition modes. From left to right: full volume composed of four or seven subvolumes; live 3D mode; live 3D zoom mode.**

## 1.3 Clinical Applications of TOE

### 1.3.1 General indications and advantages of TOE

TOE is used not only as a diagnostic tool but also as a monitoring adjunct for operative and percutaneous cardiac procedures. Because of the short distance between the transducer and the heart, increased frequency transducers with shorter wavelength of ultrasound and narrower beam width can be used, yielding better spatial (both axial and lateral) resolution. Additionally, for a given line density, visualization of a structure (e.g., valve) at a smaller depth results in an effectively higher lateral resolution, as the lines have a smaller distance to diverge compared to visualization of a structure at a larger depth. As a result, several structures in the adult heart can be evaluated and better imaged using TOE, including the aorta, left atrial appendage, valves of the heart,

pulmonary artery, both atria, atrial septum, and coronary arteries. A comparison of TOE and TTE in terms of scanning depth and orientation is shown in Fig. 1.15.

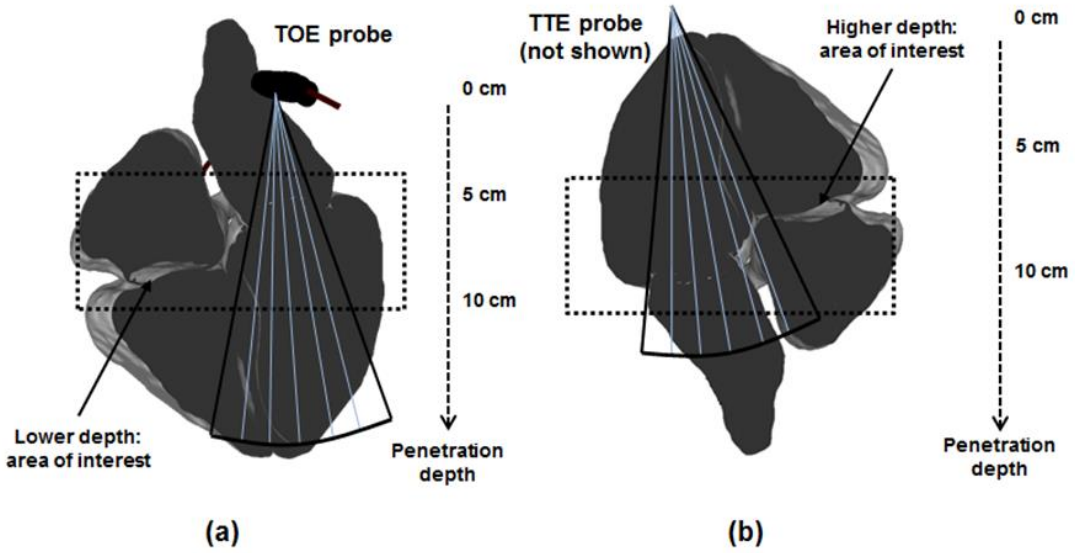


**Fig. 1.15. Schematic illustration of the relation between scanning depth, orientation, and spatial resolution (lateral resolution) from (a) a TOE scan and (b) a TTE scan.**

### 1.3.2 Diagnostic use of TOE

In terms of the diagnostic use of TOE, a complete list of explicit indications is difficult given the diversity of diseases and clinical scenarios in which echocardiography is used or potentially could be used. Because of its moderately invasive nature compared with TTE, TOE is reserved for selected indications in which the potential benefits of making a diagnosis outweigh the risks associated with the procedure. As recommended by several organizations, this mainly includes the situation when TTE is non-diagnostic or TTE is deferred because there is a high probability that it will be non-diagnostic [36, 45, 46]. The non-diagnostic situations where TOE is required can be categorized into a few classes, summarized as follows:

- Detailed evaluation of abnormalities in structures that are typically in the far field of TTE. These structures, such as the aorta and the left atrial appendage, are less well visualized on TTE compared with TOE as they are more distant from the TTE transducer.
- Evaluation of prosthetic heart valves [47]. This is used when the achievable imaging resolution with TTE does not permit a detailed assessment of prosthetic valve function, and the increased imaging resolution provided by TOE is a major advantage in evaluating the prosthetic valve.

- Intensive care unit (ICU) patients with hemodynamic instability [48]. In such cases, multiple chest tubes or mechanical ventilation might be applied which obstruct the acoustic window of TTE while the acoustic windows of TOE from the oesophagus to the heart and great vessels are unobstructed. Clinical reports indicate TOE provides diagnoses that are missed by TTE in up to 40% of cases when mechanical ventilation is applied in patients [49, 50].
- Physical unavailability of TTE. This includes situations in which patients have chest wall injuries or when patients with body habitus (morbidly obese) prevent adequate TTE imaging.

The use of TOE for particular indications varies from institution to institution, but a general summary is presented in Table 1.3. The clinical report indicates TOE is most commonly performed to evaluate potential cardiac sources of emboli, to assess valves for endocarditis, or to exclude left atrial appendage (LAA) thrombi in patients with atrial fibrillation [51]. In another large series from the 1990s, the most common clinical indications for TOE were to evaluate cardiac sources of embolism, endocarditis, prosthetic heart valve dysfunction, native valvular disease, and aortic dissection or aneurysm [52].

**Table 1.3. Summary of the diagnostic use of TOE**

| **Evaluation of cardiac pathology when TTE is non-diagnostic.** |
|---|
| Evaluation of suspected acute aortic pathology (i.e. dissection, trans-section, intramural hematoma). |
| Evaluation of suspected prosthetic valve dysfunction (thrombus, vegetation, or regurgitation). |
| Evaluation of suspected complications of endocarditis (e.g. fistula, abscess). |
| Evaluation of left atrial/LAA thrombus in a patient with atrial fibrillation/atrial flutter to facilitate clinical decision making regarding anticoagulation, cardioversion, or ablation. |
| Evaluation of source of embolism for which a TOE would be performed if the TTE was normal. |
| As follow-up to prior TOE when intervals change would result in a change in therapy. |

### 1.3.3 Procedural adjunct use of TOE

Procedural indications of TOE refer to the perioperative use of TOE assessing cardiac structure and function during cardiac surgery and the guidance of catheter-based intra-cardiac procedures (Table 1.4). The use of perioperative TOE aims to improve surgical outcomes, including selected cardiac operations (i.e. valvular procedures) and thoracic aortic surgical procedures. It is also used in some coronary artery bypass graft (CABG)

surgeries. One of the strongest indications for perioperative use of TOE for valvular procedures is the evaluation of mitral valve during repair. When a systematic approach is used to assess mitral valve morphology, there is an excellent agreement between TOE and surgical findings, with a 92% agreement on mechanism and precise location of pathology [53]. As for the use of TOE during CABG, TOE is used to monitor left ventricular function, which can alter medical therapy or surgical management [54]. For catheter-based intra-cardiac procedures (**e**.g. placement of closure devices, valvuloplasty, atrial appendage obliteration, and percutaneous valves), TOE is widely used as a guidance modality to provide soft tissue information along with X-ray fluoroscopy, which provides high contrast imaging of the intra-operative devices [55].

**Table 1.4. Summary of the procedural adjacent use of TOE**

| Category I<br>Supported by the strongest evidence | Category II<br>Supported by weaker evidence |
|---|---|
| Heart valve repair | Heart valve replacement |
| Most congenital heart surgery requiring cardiopulmonary bypass | Removal of cardiac tumors |
| Endocarditis, particularly with extensive disease or inadequate preoperative evaluation of disease extent | Procedures with increased risk of myocardial ischemia or hemodynamic disturbances |
| Ascending aortic dissection repair when aortic valve involvement is unknown | Intra-cardiac thrombectomy or pulmonary embolectomy |
| Evaluation of life-threatening hemodynamic disturbances when ventricular function is unknown | Suspected cardiac trauma or for detection of foreign bodies |
| Pericardial window procedures | Cardiac aneurysm repair |
| Hypertrophic obstructive cardiomyopathy repair | Thoracic aortic dissection repair without suspected aortic valve involvement |
| | Evaluation of anastomotic sites during heart and/or lung transplantation |
| | Monitoring placement and function of devices |

With the development of real-time 3D TOE in recent years, guidance of catheter-based procedures can be performed using a 3D TOE probe and this approach has been gradually investigated by more organizations ever since the first experience described by Perk *et al*. [56]. Though 2D TOE still gains wider acceptance among cardiologists, as it has been performed for many years and has been carefully standardized for each step of different procedures [57], 3D TOE has a unique advantage in visualizing

catheter and 3D heart structures due to its 3D visualization nature [58, 59]. Studies have indicated that the entire scenario including the catheter, devices, and heart structures (e.g. septum, valve, and appendage) in most catheter-based procedures can be imaged in a single live 3D view [56, 60, 61]. Because of this, 3D TOE has great potential to be used more widely in the future for guiding catheter-based procedures and researchers have already started pursuing a standardized 3D protocol for specific procedures [62].

## 1.4 Safety and Complications of TOE

### 1.4.1 General safety and clinically reported complications

Although considered as a semi-invasive procedure and generally performed with conscious sedation, TOE scanning has been well proved clinically over many years as a highly safe procedure when performed by a trained clinician with an extremely low rate of serious complications. This has been estimated at less than 0.18 to 2.8% [63] for diagnostic TOE and 0.2% [52] for intraoperative TOE. Death during TOE has been rarely reported with the mortality rate less than 0.01% for diagnostic TOE and 0.2% to 1.2% for intraoperative TOE [63, 64]. These reported rates vary from different studies involving use of different TOE probes. In the largest study of intraoperative TOE-related complications to date, a single-centre case series of 7,200 patients [65], Kallmeyer *et al*. reported TOE-associated morbidity and mortality of 0.2% and 0%, respectively.

Prior to beginning the TOE scanning, all patients should have a history and physical examination performed, focusing on factors that increase the risk of an adverse outcome. A list of absolute and relative contraindications to TOE has been summarized in the TOE guideline suggested by the American Society of Echocardiography and the Society of Cardiovascular Anesthesiologists [66]. As an example of the contraindications, patients with recent or active oesophageal perforation or tear should likely not undergo TOE. Complications of TOE vary in reports by different researchers as a function of the setting and the size of the probe used. A partial list of the incidence of such complications as reported in the literature is presented in Table 1.5.

**Table 1.5. Summary of complications of TOE**

| Complications | | Diagnostic TOE | Intraoperative TOE |
|---|---|---|---|
| Minor oropharyngeal and oesophageal injury | Dental injury | ASA/SCA 0.1% [67] | |
| | Lip injuries | ASA/SCA 13% [67] | |
| | Hoarseness | ASA/SCA 12% [67] | |
| | Severe odynophagia | | Kallmeyer *et al.* 0.1% [65] |
| | Minor pharyngeal bleeding | Khandheria *et al.* 0.14% [52]; Daniel *et al.* >0.01% [63]; Seward *et al.* 0.2% [68] | Kallmeyer *et al.* 0.01% [65] |
| | Dysphagia | ASA/SCA 1.8% [67] | |
| Orogastic tract perforation | Hypopharynx (20%) | Daniel *et al.* <0.01% [63] | Kallmeyer *et al.* 0.01% [65]; Chan *et al.* 0:1,500 [69]; Lennon *et al.* 0.3% [70] |
| | Oesophagus (40%) | | |
| | Stomach (5%) | | |
| | Duodenum (35%) | | |
| Cardiovascular Complications | Heart failure | Lennon *et al.* 0.02 % [70] | |
| | Arrhythmia | Kallmeyer *et al.* 0.06% [65]; Lennon *et al.* 0.02 % [70]; Chan *et al.* 0.3% [69] | |
| Respiratory Complications | Bronchospasm | Daniel *et al.* 0.07% [63]; Chan *et al.* 0.06% [69] | |
| | Laryngospasm | Seward *et al.* 0.14% [68] | |
| | Endotracheal tube malposition | | Kallmeyer *et al.* 0.03% [65] |
| | Tracheal intubation | Chan *et al.* 0.02% [69] | |

### 1.4.2 Complications due to manipulation of the TOE probe

Complications clearly related to mechanical effects of TOE (due to probe manipulation) have been rarely reported, as in most cases TOE procedures are usually well controlled by a trained clinician for a limited scanning time. Distinguishing the complications purely due to probe manipulation from the overall TOE complications (such as complications summarized in Table 1.5) is also difficult as many other effects may contribute to the resulting complications. However, in a few situations, several inappropriate manipulations of the TOE probe are highly likely to cause injuries to patients [66]. If the tip of the probe is bent in the pharynx and placed laterally into the pyriform fossa (Fig. 1.16a), advancement of the probe may cause the tip to be furtherly oriented in an extreme anteflexion or retroflexion position. Manipulation of the probe in

the translation axis while oriented in this manner could cause serious oesophageal laceration. Similarly, manipulation of the probe while locked in extreme anteflexion could significantly distort the oesophagus leading to serious mucosal tears or perforation. As for the trans-gastric TOE scan, considerable tension on the tissues of the stomach and gastroesophageal junction exists in trans-gastric probe manipulations if the probe is forcefully retrograded in the flexion state (Fig. 1.16b).

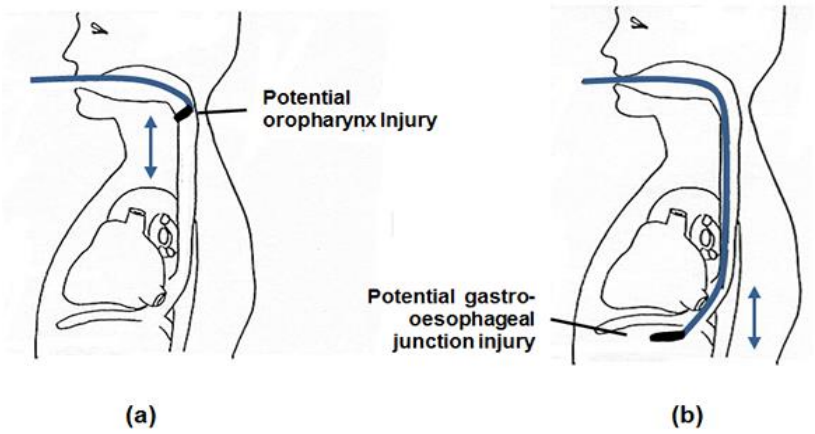


**Fig. 1.16. Illustration of potential injuries to (a) oropharynx and (b) oesophageal junction due to translational movements of the TOE probe when it is in a flexion state.**

In addition to the complications resulting from manipulating (advancing/retracting) the probe in its flexion states, compression due to bending of the probe itself has the potential to cause injury. Though only case reports have been found in the literature, injuries to tissue outside the alimentary tract, injuries on the branches of the posterior division of the recurrent laryngeal nerve, and splenic laceration have been reported [66]. As a complement to the safety studies of TOE in routine daily use with limited scanning time, an animal study has been reported in terms of the effects of prolonged TOE and excessive probe manipulation. The probe was deliberately angulated to its extreme extent for a long period of time in the study and no evidence of mucosal injury was found after the investigation using microscopic and macroscopic devices [71].

## 1.5 Motivations for a Robotic TOE System

### 1.5.1 Radiation safety

Many cardiac procedures where TOE is utilized are usually accompanied by X-ray fluoroscopy imaging, and in a typical setup, the TOE operator is required to stand close

to the path of the X-rays. This is known as a trans-oesophageal echocardiography-assisted fluoroscopically guided procedure (TOEFP) [72] and is increasingly used for catheter-based procedures, in electrophysiology laboratories, and in hybrid cardiac surgeries (combining a conventional surgical part with an interventional part). Though radiation protective clothing is required for the echocardiographer during these procedures, up to 10% of the radiation from X-ray is still able to pass through the shielding, as suggested in the literature [73]. This is not ideal for the duration of the longer procedures, since chronic exposure to ionizing radiation is known to cause cataracts, skin burns, leukemia, several other types of cancer, and damage to the fetus [74-76]. According to studies of low doses of ionizing radiation, the best current evidence suggests that there is no safe level of exposure to radiation and that even low doses can cause several diseases, although the risks are generally proportional to dose [73, 77, 78].

There are generally two sources of radiation for echocardiographers [79]. First, sonographers usually stand very close to patients and frequently drape their arms and bodies over patients who have recently received radioactive agents for diagnostic nuclear studies, thereby rendering the patients transiently radioactive. Second, echocardiographers working in TOEFPs, such as trans-catheter aortic valve replacement, percutaneous mitral valve repair, left atrial occluder device implantation, and atrial septal defect or patent foramen ovale device closure, directly receive radiation from the X-ray system while it is imaging.

According to the suggestions from the Nuclear Regulatory Commission (Fig. 1.17) [80], three protection principles are essential to minimize radiation exposure: limiting the time of exposure to the radioactive source, maximizing distance from the source and using shielding. For TOE procedures, the time of exposure is dependent on the clinical time requirement of the scanning, which is difficult to reduce. The use of shielding includes both wearing protection aprons and equipment-mounted transparent leaded plastic shields, both of which may influence movement of the echocardiographer and is unable to shield 100% of radiation. Particularly, the protection aprons are heavy and can potentially cause orthopaedic injuries to echocardiographers. This will be discussed further in the following subsection. Increasing the distance from the radiation source markedly reduces radiation exposure. Doubling the distance from a radiation source reduces the radiation exposure to one-fourth of the original dose. More obviously, if TOE is operated remotely, in which case the echocardiographer operates in another

room nearby with a protection wall or works from a long-distance remote location, insignificant radiation will reach the echocardiographer. This completely solves the concern of radiation safety for TOE. The remote control of such system could be achieved using a robotic TOE system with a number of communications approaches, such as Bluetooth, Ethernet, and radiofrequency, keeping the echocardiographer away from both radiation sources listed above.

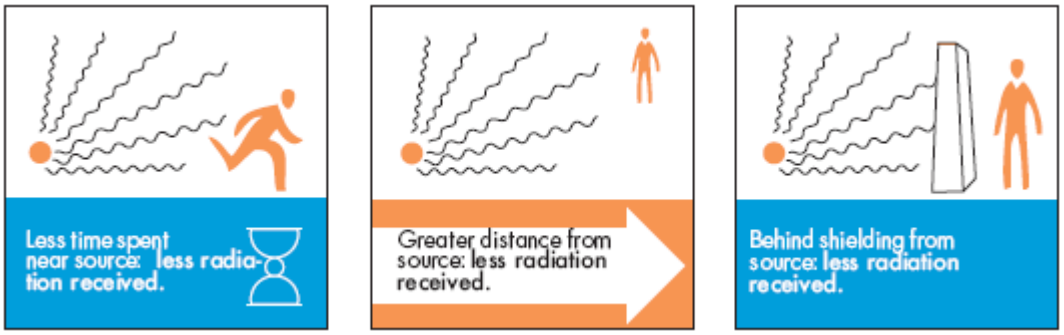


**Fig. 1.17. Protection principles to minimize radiation exposure. Effects of time, distance, and shielding on radiation exposure and dose absorption. Figure reproduced from [80].**

To further illustrate the impacts of using the TOE robot in terms of radiation safety, estimated quantitate radiation exposure doses for operators and patients under different control modes of TOE, along with the equivalent number of single chest radiographs and the time to accumulate comparable natural doses, are summarized in Table 1.6 based on the existing literature [81, 82]. In the traditional manual control mode for using TOE, the operator (either a cardiologist or an anaesthetist) has to work inside the surgical room close to the X-ray source and cannot be too far away from the patient. With the use of a robotic TOE system for master-slave control, the TOE operator could control the TOE probe remotely from a workstation located in a separate room, e.g. the monitor room. This would greatly reduce the effective dose for the operator to 0 mSV as they are no longer working inside the catheter room. However, the master-slave control mode does not provide potential reduction in the dose of the patient as the procedure time and the use of X-ray radiation are not expected to be reduced. For the robotic automatic control mode, the TOE robot is expected to have built-in intelligence to do automatic acquisition based on the simple request of particular views from the operator remotely. Consequently, zero radiation to the operator is expected. Additionally, this mode is expected to reduce the procedure time and the use of X-ray radiation as the result of automation and optimization. This could also result in a reduction of the dose level of the patient based on the estimation from the author.

In addition to the linear no-threshold theory, data from literature has suggested increased cancer risk in the 10 mSv to 100 mSv range. A widely used figure is a 5% excess risk of death from cancer with a 1 Sv (1000 mSv) dose [83]. There is also a published report of radiation induced cataracts of one interventional radiologist and two nurses. Results from recent studies reveal the prevalence of radiation associated posterior lens opacities ranged from 38–52% for interventional cardiologists, and 21–45% for nurses [84]. In addition, interviews from interventional cardiologists in an institute have indicated an average 20% reduction of the white blood cell (self-reported) after a few months' continuous work in the surgical room [85].

**Table 1.6. Estimated quantitative radiation exposure doses for operators and patients**

| Operation modes | Estimated effective doses/ per operation (mSV) | | Equivalent number of single chest radiograph | | Time to accumulate comparable natural background doses | |
|---|---|---|---|---|---|---|
| | Operator | Patient | Operator | Patient | Operator | Patient |
| Manual control | 0.3 - 3 | 3 - 30 | 15 -150 | 150 -1500 | 1 mo – 1 y | 1 – 10 y |
| Master-slave | 0 | 3 - 30 | 0 | 150 -1500 | 0 | 1 – 10 y |
| Robotic automatic | 0 | < 30 | 0 | < 1500 | 0 | < 10 y |

### 1.5.2 Orthopaedic injuries

The X-ray protective clothing for the TOE operator, including an apron and thyroid shield, can cause orthopaedic injuries due to the accumulated effects of bearing the weight over many years with the demanding physical labour and working hours inherent in this career choice. This includes various problems with the spine, hip, knee, and ankle [86]. Though related studies focusing only on TOE are limited in the literature, a study regarding orthopaedic injuries for interventional cardiologists [87], who have the same working environment and wear similar X-ray protection clothing, indicates a high rate of spine problems (42%) among responders from a survey. Of these, 70% were self-described as lumbosacral and 40% as cervical. Problems related to the hips, knees, or ankles were also reported by one-fourth (27%) of all operators. Spine problems were experienced more by respondents who also reported a history of hip, knee, or ankle problems. Importantly, over one-third of those with spine complaints reported that spine problems had caused them to miss work. Apart from the weight consideration, TOE examinations often require that ultrasound technicians hold the probe in one hand while adjusting scanning parameters with the other hand for

prolonged periods of time, and sometimes exerting large forces for prolonged periods of time. A number of studies indicate that the technicians suffer from an unusually high incidence of musculoskeletal disorders, including eye strain, musculoskeletal pain or injury, carpal tunnel syndrome, repetitive strain injuries, stress, burnout, and other hazards [86, 88, 89].

The use of a remote control TOE robotic system would allow echocardiographers to operate the TOE probe without wearing radiation protection clothing, thereby reducing the risk of occupational hazards due to bearing weight. As different control approaches can be provided, such as computer-based software, joystick or haptic devices, and custom master controllers, the echocardiographer can potentially work with a comfortable gesture of their choice, addressing the ergonomic concerns.

### 1.5.3 Training and experience

One of the barriers to the greater utilization of TOE is the need for advanced training. There are several guidelines summarized in [36] addressing training for physicians performing TOE as summarized in Table 1.6. In some of these guidelines, the recommended cases for training may include both TTE and TOE and the recommendation for TOE is not suggested individually. In both developed and developing countries, because of the requirement for highly specialized skills during TOE acquisition, small clinics in remote locations are unlikely to have TOE experts available most of the time. Studies regarding the use of general ultrasound suggest that the lack of training is one of the biggest barriers to reliable image acquisition in low and middle income countries [90, 91]. The problem of skills and training for general ultrasound is made worse for TOE by the views of the heart being relatively complicated to understand. Associated problems due to the expertize requirement of TOE also exist. As cardiac procedures requiring TOE need both a specialized surgeon and an echocardiographer to be available for the entire procedure, the procedures have to be scheduled around both of their timetables. While this may be possible and easier to achieve at large hospitals, smaller hospitals may have difficulties having enough TOE echocardiographers available. Additionally, the highly qualified echocardiographers required for these procedures contribute to the high cost of some of the procedures.

With a robotic TOE system and its built-in intelligence, acquisitions could be made easier with automatic or semi-automatic control and related techniques. This has great potential to deskill the whole TOE procedure so less training is required, and the scan

could be performed by less-qualified physicians. With the remote control ability, robotic TOE procedures could also be performed by an experienced echocardiographer in a remote location so that long-distance diagnosis would be possible. This would make a huge difference to small hospitals or even large hospitals in developing countries, as echocardiographers would not be required on-site all the time.

**Table 1.7. Published recommendations for training in TOE**

| Guideline | ASE and the SCA guidelines for training in perioperative echocardiography (2002, 2006) | | |
|---|---|---|---|
| Skill level | Basic | Advanced | Director |
| Training | 50 cases | 150 cases | 300 cases |
| Guideline | The American College of Cardiology/American Heart Association guidelines for training in TTE and TEE (2003) and COCATS 3 (2008) | | |
| Skill level | Basic | Advanced | Director |
| Training | 150 cases interpreted; 75 cases performed (Both TTE and TOE) | 300 cases interpreted; 150 cases performed (Both TTE and TOE) | 750 cases interpreted 300 cases performed (Both TTE and TOE) |
| Guideline | Canadian Anesthesiologists' Society and the Canadian Society of Echocardiography (2006) | | |
| Skill level | Basic | Advanced | Director |
| Training | 100 cases | 200 cases | 300 cases |
| Guideline | European Society of Echocardiography (2010) | | |
| Skill level | Basic | Advanced | Director |
| Training | 125 cases | NS | NS |

### 1.5.4 Procedure optimization

Other problems may also occur due to the echocardiographer being in the surgical room for the entirety of some cardiac procedures. These include the abundance of people in the operating room during the procedure. While the echocardiographer performs the important function of deploying the TOE down the patient's throat and adjusting its position according to the verbal requests of the interventional cardiologist, he or she has minimal participation for much of the procedure. Also, the interventional cardiologist may have difficulty at times explaining to the echocardiographer exactly how he or she wants the probe end adjusted. With a robotic TOE system, the echocardiographer could work in remote locations as already stated. Moreover, the robotic TOE system can be directly controlled by the interventional cardiologist via a foot pedal on the ground or a control panel attached to the bed. This can potentially solve the problem of communication between echocardiographers and interventional cardiologists.

## 1.6 Objectives and Hypotheses

### 1.6.1 Overall aim

The overall aim of this research is to develop a robotic TOE probe that can be used during cardiac procedures as a remotely operated device. Considering the wide use of commercial TOE probes in clinical routines, the goal is to build an add-on robotic system that can work as an individual piece with such a commercial probe available on the market. In this research, a TOE probe (x7-2t, Philips) as already introduced was used as the design target. However, the concept of the robot should allow easy adaption to other probes available on the market. The aim of the project includes the design and construction of the robot; the testing of the robot in phantoms and potentially in human cadavers; and the final application of the robot for automated TOE acquisitions and device tracking based on view planning and probe tracking methods. The ultimate goal of building a product that can be used in patients is left for future work. Details of the objectives are proposed in the following subsections.

### 1.6.2 Design goal for the TOE robot

The robot should have mechanisms that allow the X7-2t TOE probe to be plugged in and out by the operator. This allows switching between robotic and manual control modes. Furthermore, an eject mechanism would be useful as it enables the user to release the probe from the mechanism immediately if manual control is urgently required during robotic control.

The robot should have two main degrees of freedom (rotation about and translation along the length of the TOE probe) and additional manipulators with two degrees of freedom to steer the probe head via the probe's built-in control knobs. As stated before, these mechanisms for probe actuation are primary designed for the X7-2t TOE probe but should be easily adapted for others. The electronic steering, controlled by two buttons in the X7-2t TOE probe for 2D mode, is not a primary goal for mechanical actuation as this is not required for 3D mode. Potentially it could be an electronic signal directly available from the ultrasound machine for the final product used in patients. This will not be included in the prototype built for this work.

The robot should have a support frame that can be easily mounted and accommodated in the operating room. It should also have a small footprint, allowing it to be positioned

appropriately near to a patient. Ideally, the electronics of the robot should be integrated and built into the mechanical system so that no additional electronics boxes are required. The robot should have the ability of remote control via various communication methods. Control interfaces for both manual remote control and computer control are required. The remote manual control will be via a custom controller, such as a joystick or a dummy probe.

### 1.6.3 Safety requirements for the TOE robot

Several safety requirements for the TOE robot should be taken into consideration. As a general mechatronic device, incorrect robot movements may result from incorrect motor behaviour (such as motor failure), uncontrolled motor current (such as power amplifier failure), or micro-processor failure. Therefore, methods for monitoring the correct movements of the robot are necessary. For the TOE robot which manipulates the TOE probe to access the patient, incorrect robot movements may result in damage to the probe itself and/or cause injury to the patient. The TOE probe is already clinically approved with several built-in safety features and has been used for many years with a low incident rate, as discussed in Section 1.4. A safety feature in which the maximum power of the motors along with the mechanisms will not be able to damage the probe would also be essential.

As also suggested in Section 1.4, the manipulation of the probe manually by a trained echocardiographer may also cause injury to patients. Specifically, manipulating (advancing/retracting) the probe in its flexion states in several situations as summarized in Section 1.4.2 is the main manipulation which is clearly known to cause injuries to patients. To address this concern, primary safety sensors for monitoring the neutralization of the probe tip should be included into the robotic system. As also summarized in Section 1.4.2, limited case reports have suggested that the compression due to bending of the probe itself has the potential to cause injuries to patients. To address this concern, secondary safety sensors may be useful and could be included in the robotic system for monitoring or limiting the forces of the probe bending.

### 1.6.4 Targets for the application of robotic TOE

View planning methods are required so that the echocardiographer can decide which ultrasound views need to be scanned when using the proposed TOE robot for a particular patient. A user interface platform is necessary to allow the echocardiographer

to define the TOE views for the patient based on a virtual environment (e.g. control the robot virtually, obtain simulated ultrasound images, and define views based on these images). Furthermore, an automatic definition of standard views within the platform would be useful if any standard TOE view is required. This allows those standard views to be quickly located in the patient-specific data so that the echocardiographer doesn't need to manually define all the standard views in the protocol for each patient.

Probe tracking methods for the robot are required in order to locate the probe's position within the patient. The accuracy of the tracking method should be adequate enough for the control of the TOE robot. As a primary goal, an accuracy of a few millimetres, similar to that of most commercially available sensors, is expected for the proposed probe tracking method. An automatic acquisition workflow should be designed so the robot can perform a whole automatic TOE acquisition sequence based on the defined views for a patient. The accuracy of the automatic acquisition method should be tested in phantoms and/ or cadavers. The clinical requirement for the accuracy of probe positioning is unclear as TOE acquisition is a feature-based approach. For reference, the amount of movement and deformation of the beating heart is around 1 cm and this is tolerated by the echocardiographer. Therefore this accuracy is set as the target for the automatic acquisition method, so that the automatic probe positioning would place the image plane within 1 cm of the required structures.

### 1.6.5 Hypotheses

The main hypothesis of this thesis is that a newly developed robotic system will be able to remotely control a commercially available TOE probe in a way that allows all degrees of freedom normally used during manual operation to be manipulated safely and with a positional accuracy that is sufficient for performing standard clinical procedures to enable further development and clinical evaluation studies. To determine if this hypothesis is met, the system should meet the following criteria:

- The proposed robotic system will employ built-in features to avoid potential TOE complications, such as probe neutralization sensing and bending force limiting.
- The user will be able to easily define a particular trans-oesophageal ultrasound view of a patient consisting of certain cardiac structures as required by the procedure using software which forms part of the proposed system.
- The proposed robotic system will be reliable in its mechanical design with good repeatability performance of mechanisms for handling each degree of freedom.

Under the same condition with the same motor inputs, the probe tip will be driven to the same position with a mean positioning error less than 1 mm in free space.

- The probe tip's location will be predictable mathematically based on a kinematic model with a mean predication error less than 5 mm in free space.
- The probe tip's location will be directly monitored by an independent positioning tracking method to provide feedback with a mean tracking error less than 2 mm.
- The defined trans-oesophageal ultrasound view will be automatically acquired using the proposed robot with an acquisition accuracy around 1 cm magnitude.

## 1.7 Thesis Structure and Scientific Contributions

In this chapter, an overview of ultrasound imaging and details of TOE have been presented. These provide useful background information on this research and introduce the concepts used in this work. In the following sections, the motivations of a robotic TOE system and the aim of this work were then presented.

In Chapter 2 of this thesis, a comprehensive review of related works on robotic ultrasound systems and ultrasound-guided robotic operations will be studied. These are to understand the novelty of this new proposed robotic system and its application compared with previous works and to extract useful techniques from previous works which can be utilized in this study.

In Chapter 3, the design, implementation, and testing of the new robotic TOE system will be introduced. This system was developed to achieve the aim of having an add-on robot that can work as an individual piece with a commercial probe available on the market. The robot was designed and built by the author in collaboration with Xtronics Ltd. The experiment on testing the robot was designed and performed by the author.

In Chapter 4, a kinematic model of the robotic TOE system and a view-planning platform for TOE views using this model will be introduced. This work aims to accurately model the movement of the TOE probe and provide a visualization platform for the operator to define and plan a TOE acquisition of different views using the robot before the procedure. The work on kinematic modelling and experimental validations was achieved by the author. For the view-planning platform, the author developed the platform by including the verified kinematic model and other functions required for the subsequent experiments into an existing custom-made software described in [92].

In Chapter 5, a complete automatic TOE acquisition workflow proposed by the author will be presented. This work aims to use the developed TOE robot to automatically acquire views defined in the view-planning platform. The work in this chapter intends to fulfil the application goal of the TOE robot. This workflow includes an automatic adaption method for patient-specific data based on the work described in [92], a probe tracking method developed by the author based on a previous registration work [93], and a feedback workflow developed by the author based on the tracking method and an inverse kinematic model. The experiments on validating the whole automatic acquisition workflow were developed and performed by the author.

In Chapter 6, an improved tracking method of the probe and the experiment on validating this new tracking method developed by the author will be presented. This is to address a problem with the tracking method identified in the experiment described in Chapter 5 and demonstrates the complete solution to achieve the application goal of the TOE robot reliably. The second part of this chapter aims to present and discuss different variations of the proposed robot-based automatic acquisition workflow and demonstrate the potential uses of its components in different applications. In addition to the summaries and discussions of each individual topic presented at the end of technical chapters from Chapter 3 to Chapter 6, Chapter 7 will give the overall discussion and conclusion of the whole work at the end of this thesis.

In addition to the contributions by the author as stated, several major contributions from different colleagues and the industry collaborator, whom the author has been mainly working with during his PhD, are also covered in the contents of this thesis. Prof. Kawal Rhode, the lead supervisor of the author, initially proposed the idea of the TOE robotic system and has led the design of the robot and all the scientific experiments included in this thesis from Chapter 3 to Chapter 6. Mr. Davi Singh, the manager of Xtronics Ltd., has made significant contributions to the final mechanical design and manufacture of the TOE robot described in Chapter 3. Dr. James Housden, the day-to-day supervisor of the author, has made significant contributions to the design of the automatic TOE acquisition workflow. This includes the development of the software basis of the view-planning platform introduced in Chapter 4, the inputs to the methodology developments and assistance with all the experiments presented in Chapter 5 and Chapter 6.

During the design and performance evaluation processes of the TOE robot, several clinicians have been involved in different ways to provide clinical guidance and feedback. Dr. Ronak Rajani has been involved in understanding the motivation and the

future clinical use of the TOE robot. Dr. Kiran Reddy has led the initial trial of cadaver experiments using the TOE robot with KCL's facilities for the safety use of the robot. He also made great contributions to the design of the TOE phantoms and performed the first manual experiment on the robotic TOE acquisition. Dr. Henry Chubb has been involved in analysing the performance of the TOE robot and provided clinical evidence for the positioning accuracy requirements. Additionally, Mr. Devapriyan Johnson and Mr. David Lau, both medical students in KCL, have made contributions to the development and validation of the TOE automatic acquisition workflow.

# 2 Related Medical Robotic Systems and Techniques

## 2.1 Introduction

Since the first clinical use of medical robots in the 1980s, numerous works from both research institutions and commercial organizations have been proposed with robotic systems used in many fields such as orthopaedics, minimally invasive surgery, and image-guided interventions. The rapid growth in medical robotic fields has been driven by a combination of technological improvements (such as mechatronics, materials, and control methods), developments in both medical imaging devices (such as MRI and 3D ultrasound) and image processing methods (such as registration and reconstruction), and an increase in surgeon/patient acceptance of robotic assisted procedures. The advantages of using medical robots to replace or assist human operations have been argued by academics, clinicians, and the public. Though the principle advantages of medical robots have been acknowledged by most researchers, such as the improved accuracy, enhanced dexterity, and precise synchronization with preoperative planes, several concerns have been raised regarding the high cost, large space needs, and extensive user training requirements.

The clinical applications of medical robots, as well as the functional requirements of associated systems, vary greatly between different procedures. This has resulted in large numbers of medical robot designs with different configurations and functionalities for

different applications. Though most of these systems were developed for research purposes which may have involved clinical testing, several systems have been successfully commercialized, Conformité Européenne (CE) marked, and cleared by the United States' Food and Drug Administration (FDA), indicating great potential for using medical robots clinically. As one of the most successful medical robots used for general laparoscopy, Intuitive Surgical's da Vinci system, cleared by the FDA for multiple categories of operations, has been discussed in over 8,500 peer-reviewed publications. Over a thousand systems have been installed worldwide, and it was used in 80% of radical prostatectomies performed in the U.S. estimated in 2013 [94, 95]. Behind medical robotic systems, there are various specific scientific topics discussed by numerous works either for theoretical advances or creative practical solutions in order to provide medical robots with intelligence, such as kinematics, control algorithms, ergonomics, telesurgery, intuitive operation, image guidance, etc. Several reviews of medical robots have been presented since the 1990s, providing broad discussions of different systems and techniques. Many such reviews are domain-specific [96-99], for example, focusing on surgical robots, urological robots, spine robots, etc., while some others cover medical robots across various domains with different emphases [100-102], such as basic science, technical advances, marketing issues, social impacts, etc.

In this section, which aims at providing information on previous research work related to the design of a trans-oesophageal ultrasound robot, the review primarily focuses on robotic ultrasound systems in which ultrasound probes are held and manipulated by robots for various applications. This includes extracorporeal and intraoperative ultrasound robotic systems, as well as the ultrasound-integrated surgical systems reviewed in Section 2.2. Summaries of these works aim at introducing the motivations, configurations, functionalities, and employed techniques for existing robotic ultrasound systems. Section 2.3 focuses on the review of ultrasound-based guidance of medical robotic systems, in which either hand-held or robotized ultrasound systems, are used to guide the same or another medical robotic system for different clinical procedures. This section, with an emphasis on the link between ultrasound images and robotic movements, introduces approaches of ultrasound-guidance of robotic motion. Both Sections 2.2 and 2.3 directly relate to the work of this project in terms of robotizing an ultrasound system and automatically performing acquisitions.

In addition to ultrasound robots, non-ultrasound endoscopic robots are reviewed in Section 2.4, as the trans-oesophageal ultrasound probe itself is an endoscope in addition

to its functionality as an ultrasound probe. This section provides more information in terms of robotizing an endoscope and automatic control of such a robotic system. Furthermore, many of these endoscopes have cameras mounted, thus guidance of these robots with images is also covered in Section 2.4. In Section 2.5, a summary is given of the configurations and utilizations of the robots reviewed. Several techniques for robotic vision and motion are discussed. Eventually, inspirations from existing works for other medical robotic systems are discussed for design of a new trans-oesophageal ultrasound system.

## 2.2 Robotic Ultrasound Systems

### 2.2.1 Extracorporeal ultrasound robotic systems

An extracorporeal ultrasound robotic system refers to the configuration in which the robotic system is constructed to hold and manipulate hand-held ultrasound probes for extracorporeal examinations. The research interests in motorizing ultrasound systems started in the late 1990s within the European Union, North America, and Japan [103]. This was motivated by the deficiencies of the on-site manual manipulation of hand-held probes, such as difficulties of maintaining accurate probe positioning for long periods of time using human hands, requirements for experienced sonographers, and the need for mental reconstruction of 3D anatomy from 2D images. Many of these robotic systems were designed in the typical master-slave configuration, whereby the master-side sonographer can be in a remote location to perform the examination and a slave-side robot driving the ultrasound probe mimics the movements of the remote sonographer. These systems were mainly designed for diagnostic purposes but a few of them were also aimed at guidance of interventional procedures or open surgeries. A wide variety of the architectures and target anatomies are summarized in Table 2.1.

Jointed robotic arms, similar to those used in manufacturing, were the most widely utilized architecture by most groups to perform extracorporeal ultrasound examinations. An early diagnostic robot with several related works proposed by Salcudean *et al*. [104, 105], Abolmaesumi *et al*. [106, 107], and Zhu *et al*. [108] was based on the arm-link architecture. It was designed for remote carotid artery examinations using a 4-bar linkage mechanism with counterbalancing and backdrivable joints for safety. Though the robot has 6-Degrees-of-freedom (DOFs) allowing most of the required movements

during the examination, the control of the robot was designed to be semi-automatic with the translation along the vessel controlled by the physician manually while other axes were automatically adjusted by the robot in order to keep the vessel centred in the 2D image plane. This was achieved with a visual servoing technique [109] by tracking the vessel's location from the image [110], and computing the target mechanical movements accordingly. The whole idea was tested in a phantom and then *in vivo* with successful indications of keeping vessels at the centre. With this technique, real-time 3D reconstruction of the carotid artery was also made possible by registering multiple 2D ultrasound images acquired accurately using the robot. Subsequently in the next few years, various versions of arm-based robotic systems were developed providing several improvements and more powerful functions for the examination of the carotid artery. This includes the works from Nakadate *et al*. [111] with completely automatic scanning methods [112, 113] aiming for out-of-plane motion compensation [114] and the more recent work from Seabra *et al*. such as described in [115, 116] with a specific focus on despeckling and reconstruction algorithms so that echogenicity and texture information of vessels could be characterized.

Utilization of robotic systems for abdominal examinations is one of the biggest research directions in the area of ultrasound robotics as it could include scanning of many possible anatomies. Many of these systems were also tested for other applications such as in cardiology and urology after their original design. These works are therefore classified into the category of abdominal and general examinations in this review. Introduced by Gourdon *et al*. [117] and Arbeille *et al*. [118-120] in 1999 and the next few years, a cage-like probe holder containing a robotic wrist was designed for abdominal examination. The configuration of the robot is unique as it doesn't include any translational axes, and was instead held in position manually at the region of scanning. The wrist incorporated three rotational axes, allowing a remote ultrasound expert to orient the probe. In subsequent works, a force feedback mechanism and a master-slave replica probe, which allowed more intuitive control, were introduced and tested clinically, along with the robotic system. The clinical trial demonstrated the feasibility of the robot, regarding the ultrasound imaging tasks, for replacing manual operation, though more examination time was reported in some of the cases.

Encourage by these works, ultrasound robots with more DOFs were designed by several institutions aimed for broader anatomies. The OTELO project [121] for general ultrasound examination, developed by nine partners within the European Union,

emphasized light weight and portability [122]. The research with the 6-DOFs robot included a wide range of topics [123, 124], such as the teleoperation, kinematics, automatic control laws, and ergonomic control [125]. Work presented by Masuda *et al*. introduced platforms with jointed legs on a pair of rails [126, 127]. The leg joints along with the raising/lowering of the platform allowed 6-DOF positioning of an ultrasound probe to perform an abdominal scan [128]. In addition, force sensors and symmetry sensors were included in the system, allowing the contact force and the angle of the probe to the patient to be measured. Another system proposed by Vilchis *et al*. [129-132] described a unique robot with six DOFs aiming for abdominal examinations. In the design, motor-driven cables were supported on the examination table. These cables translated a circular platform, upon which a mounted robotic wrist generated angular orientation. The unique feature of this system was its ability to adapt to the patient's body structure, and in clinical trials it was successfully used to detect aortic and iliac aneurisms. Introduced by Koizumi *et al*., a master-slave robotic system focused on continuous-path control for smooth motion of the ultrasound probe in order to address the problem of synchronization of the master controller and slave robotic effector [133].

In recent years, remote ultrasonography projects at highly commercial level supported by the European Space Agency (ESA) have drawn much attention [134, 135]. Originally developed for ultrasound scanning of astronauts in space, the techniques have now been brought to daily clinical use in secondary hospitals where experts are not available on-site. The initial project ARTIS (Advanced Robotised Tele-echography Integrated Service) produced a compact and light-weight (2.5 kg) semi-automated robotic probe holder (Fig. 2.1a) which allows yaw, pitch and roll as well as instructs the holder to modify the ultrasound probe's position. The system includes an integrated video conferencing option with a remote-controllable webcam. A large-scale experiment organized between the Spanish Ministry of Defence and Afghanistan was conducted for the scientific validation, beginning in 2010. In more recent years, the TESSA (Tele-Echography for ESA) project developed by AdEchoTech [136] has made a huge breakthrough in developing a robotic system named MELODY (Fig. 2.1b). Similar to the architecture of the ARTIS robot, an assistant simply holds the device against the patient and the ultrasound expert can move the probe as if present in the examination room. Full-scale international experiments were conducted with the system in more than 15 hospitals and health institutes in France, Peru, the United States, and

Cyprus. In 2013, the MELODY remote operated ultrasound system was brought to commercialization and to the market after years of research and scientific validation.

(a) (b)

**Fig. 2.1. Example uses of the tele-operated robotic systems on patients from the projects founded by ESA: (a) the robot from the ARTIS project which focused on light weight. (b) TESSA project, which resulted in the commercial robot MELODY. Figure reproduced from [136].**

In addition to the use of ultrasound robots in carotid artery, abdominal, and non-specified general examinations, several systems have been proposed for more specific tasks, such as the examination of lower limb vessels. The system developed by Janvier *et al*. allows the scan of lower limbs with highly accurate 3D reconstruction of vessels using a 2D ultrasound probe scanning evenly in space [137]. A master-slave robotic system called TERMI (Tele-Ecografía Robotizada de los Miembros Inferiores, in Spanish) was proposed by Vilchis *et al*. for diagnosing venous thrombosis in lower limbs [138]. Considering cardiac applications in particular, some of the systems introduced previously investigated the capability of doing cardiac scanning with their initial designs aimed at general examinations. However, the work proposed by Ma *et al.* [139, 140] from a group in King's College London was uniquely aimed at robotizing the trans-thoracic ultrasound system during simultaneous X-ray fluoroscopy for cardiac interventional guidance. The robot, with 6-DOFs controlled by a master haptic device, holds and manipulates the probe. By calibrating and tracking the ultrasound and X-ray systems, 3D ultrasound images were registered with the 2D X-ray images for the use of hybrid guidance. The clinical feasibility of the method was demonstrated during two clinical cases for patients undergoing cardiac pacing studies.

**Table 2.1. Summary of the extracorporeal ultrasound robotic systems in this review**

| Project/First Author(s) | Architecture | Anatomies | Technical notes |
|---|---|---|---|
| Salcudean *et al.*; Abolmaesumi *et al.*; Zhu *et al.* (1999 - 2002) | Parallel linkage | Carotid artery | Semi-automatic scan for keeping structures in the centre of plane with visual servoing. |
| Nakadate *et al.* (2009 - 2011) | Jointed arm | Carotid artery | Automatic tracking and compensation for out-of-plane movements with visual servoing. |
| Seabra *et al.* (2009 - 2012) | Jointed arm | Carotid artery | Despeckling and reconstruction algorithms for echogenicity and texture information. |
| Gourdon *et al.*; Arbeille *et al.* (1999 - 2007) | Platform Wrist | General | No translational axes, held in position manually. |
| OTELO project (2004 - 2009) | Jointed arm | General | Emphasis on light weight and portability. |
| Masuda *et al.* (2000 - 2005) | Legs on rails | General | Unique architecture with force & balance sensing. |
| Vilchis *et al.* (2001 - 2003) | Cable-actuated | General | Ability to adapt to the patient's body structure. |
| Koizumi *et al.* (2009) | Jointed arm | General | Continuous-path control for smooth motion of the probe addressing master-slave synchronization. |
| ARTIS; TESSA (2010 - 2014) | Jointed arm | General | Highly commercial with numerous clinical trials. |
| Janvier *et al.* (2010) | Jointed arm | Lower limb | Highly accurate 3D reconstructions of vessels. |
| Vilchis *et al.* (2007) | Jointed arm | Lower limb | Focused on diagnosing venous thrombosis |
| Ma et al. (2009) | Jointed arm | Cardiac | 3D ultrasound registered with 2D X-ray images |

### 2.2.2 Intraoperative ultrasound robotic systems

In addition to extracorporeal ultrasound systems, efforts have also been made in robotizing intraoperative ultrasound systems in order to provide more stabilized replacements for traditionally manual intraoperative ultrasound examinations. These are summarized in Table 2.2. These systems mainly focus on robotizing currently available intraoperative ultrasound probes by providing separate individual add-on robotic systems.

**Table 2.2. Summary of the intraoperative ultrasound robotic systems in this review**

| Original probe | First Author(s) | Architecture | Technical notes |
|---|---|---|---|
| TRUS probe for prostate evaluations | Han and Kim *et al.* (2011 - 2012) | Motorized TRUS | Works in conjunction with the da Vinci system. Tracking of the probe allows 3D reconstruction. |
| | Adebar *et al.* (2011 - 2012) | Motorized TRUS | Improved capability of elastography. |
| | Schneider *et al.* (2004) | Partially motorized TRUS | Easy registration of needle end-effector with ultrasound images with the coupled design. |
| | Yu et al. (2007) | Motorized TRUS and Needle | Complete robotic prostate brachytherapy systems with motorized TRUS included. |
| ICE catheter for heart evaluations | Loschak *et al.* and Brattain *et al.* (2013 - 2014) | Motorized ICE | The ability of 3D reconstruction with auto-sweeping and the ability of device tracking with automatic orientation methods. |

As one of the most widely-known examples of intraoperative ultrasound, trans-rectal ultrasound has been commonly employed in the guidance of radical prostatectomies. The probe used for these examinations, known as the trans-rectal ultrasound (TRUS) probe, has been robotized with several configurations mainly by the urology group in Johns Hopkins University. The robotized TRUS system for the guidance of radical prostatectomies is usually employed in conjunction with the da Vinci robotic surgical platform in which case the ultrasound imaging robot guides the surgeon to perform minimally invasive prostate operations via the da Vinci robot. Han and Kim *et al.* developed a 4-DOF robotic system to hold a TRUS probe (Fig. 2.2a) for scanning a prostate volume with rotary sweeps using a 2D TRUS probe [141]. The robot allows pivoting of the probe about a fixed point with two rotations for changing the angulation. The drive module allows translation of the probe along and rotation about its axis. Ultrasound scans are controlled directly by the surgeon via a joystick. The system was tested in conjunction with the da Vinci in clinical trials. Both the da Vinci tools and the

blood vessels associated with neurovascular bundles were clearly visualized using TRUS images, and nerve-sparing radical prostatectomy was successfully performed. The novelty of this approach was the mobility of the scan and the automatic tracking capability. The robotic system can measure positions intrinsically without the need for separate tracking systems. Tracking of the probe frame with respect to the reference frame by the robot makes the 3D reconstruction of the prostate possible.

Continuous work [142, 143] on this robotic trans-rectal probe was presented subsequently with an improved probe manipulator, named Euler-2 (Fig 2.2b). In addition to a more mature design and manufacture with a stabilizer adjustment stage, the work also investigated the measurement of forces on the probe inside the rectum, intending to give the user several safety features when moving the probe. Five piezo-resistive force sensors were built into the driver module. The sensors measured the interaction between the TRUS drive units and the probe so that the interaction between the probe and the patient could be estimated. Recently, Adebar *et al*. from the same group improved the capability of the robot to include elastography, a modality for measuring tissue strain characteristics [144]. Methods of automatically tracking existing da Vinci surgical instruments were also discussed in [145].

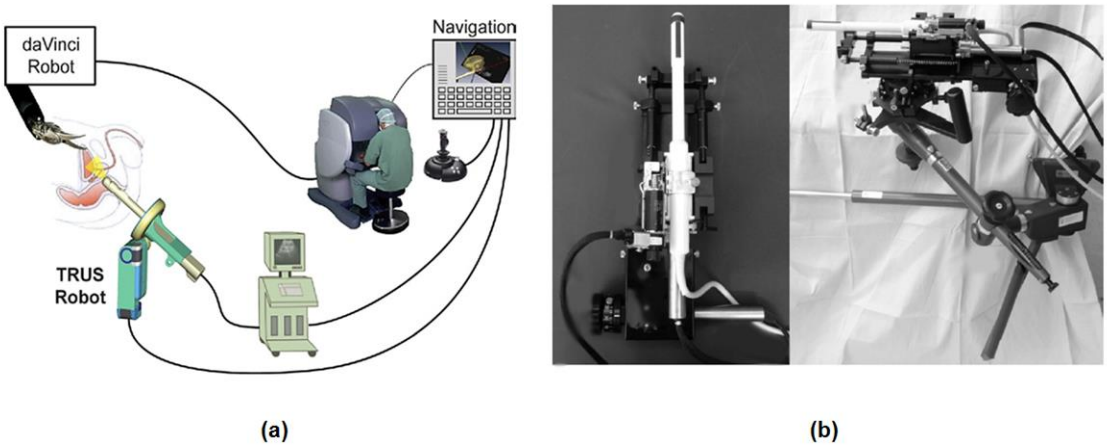


**Fig. 2.2. TRUS robotic systems developed by the group from the Johns Hopkins University: (a) Schematic representation of the original design of the TRUS robot and the working principle with the da Vinci surgical robot; (b) Final implementation of the system with a stabilizer adjustment stage. Figure reproduced from [141] and [142].**

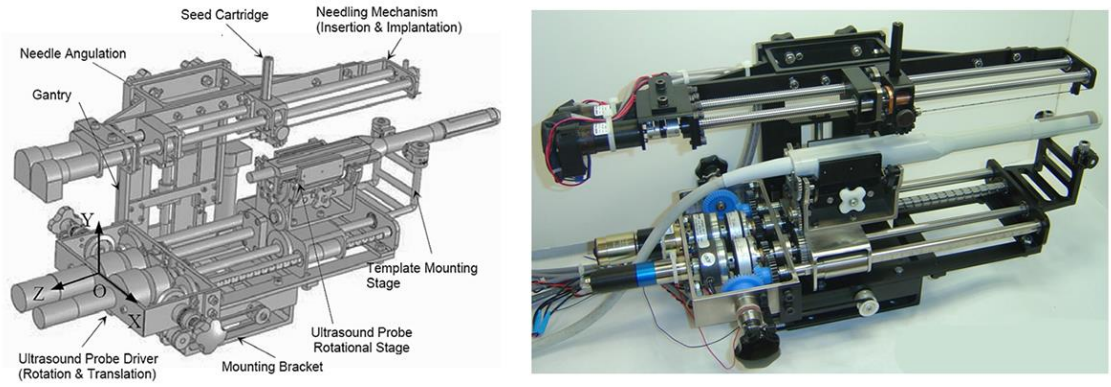


**Fig. 2.3. Complete prostate brachytherapy system, including both the TRUS movement and needle insertion: (left) schematic drawing and (right) fabricated prototype. Figure reproduced from [146].**

In addition to the use of robotic TRUS systems in radical prostatectomies, work presented by Schneider *et al*. described a partially motorized TRUS system with a biopsy needle mounted for use during prostate biopsy procedures [147]. The integration of ultrasound imaging and the biopsy needle allows the registration of the needle end-effector with the ultrasound image easily and precisely, resulting in accurate needle placements. Similar to the prostate biopsy procedure, prostate brachytherapy requires placement of radio-activated sources at a target under the guidance of ultrasound images. While many configurations have the ultrasound probes separately to the needle insertion systems, work from several groups such as that reported by Yu *et al*. [146] (Fig. 2.3) has shown complete robotic prostate brachytherapy systems, including both the TRUS movement and needle insertion, and thus these can also be treated as intraoperative ultrasound robots.

Another important series of work by Loschak *et al*. and Brattain *et al*. from a group in Harvard University described an add-on robotic system which can remotely manipulate a commercial intra-cardiac echocardiography catheter [148-150]. Different to the trans-rectal ultrasound probe, which only allows translation and rotation, the much thicker ICE catheter is a steerable device capable of bi-directional bending of the tip controlled via rotational knobs. The catheter acquires ultrasound images of adjacent tissues from the distal tip, and can be guided through the vasculature to the inside of the heart. The robotizing (Fig. 2.4a) of the ICE catheter is much more complicated in terms of the mechanism as the remote control handle of the device consists of uniquely structured bending knobs. The remote control ability of the proposed 4-DOF system has been demonstrated [151] , but more focus was on several intelligent functions, such as the auto-sweeping of the image plane for 3D reconstruction and automatic pointing at and tracking of targets. The auto-sweeping of the image plane allows the catheter to rotate

about its own coordinate (Fig. 2.4b) and acquire a series of 2D ultrasound images used for 3D reconstruction. The biggest challenge of the auto-sweeping is when the catheter is in a bending state. Rotation about its own axis, rather than the base coordinate, requires all three rotational axes (roll, pitch, and yaw) to work simultaneously with different amounts of movement. This requires a complete modelling of the forward and inverse kinematics, which was presented in their work. However, an EM tracking system was still required for providing the position information of the ultrasound image in order to register the 2D image series.

Another application of this ICE robotic system based on the kinematics and EM tracking system was to automatically track targeted structures or devices with the catheter pointing towards the target (Fig. 2.4c) accordingly. This was mainly to address the need for frequent adjustment of ICE catheters to track other non-imaging catheters and their interactions with surrounding tissue. The automatic tracking was achieved by computing the angle between the target and the ICE imaging plane and commanding a specific movement. The whole work on the ICE robot is encouraging for its use in clinical scanning, as it provides several functions which could not be achieved manually, in addition to providing a replacement for manual control. However, more efforts are required in order to bring the principle from free-space phantom experiments towards constrained-environment *in-vivo* experiments.

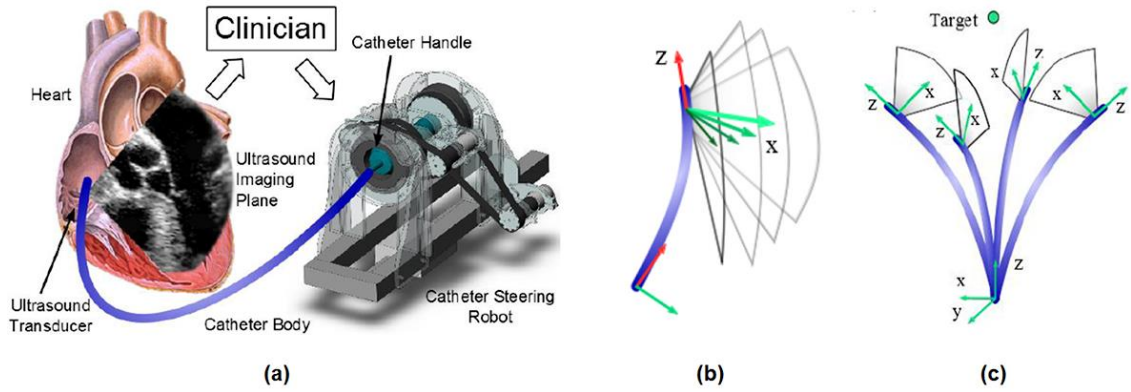


**Fig. 2.4. ICE robotic systems developed by the group from Harvard University: (a) Schematic representation of the original design of the ICE robot and the working principle; (b) Illustration of the auto-sweeping function; (c) Illustration of the automatic pointing function. Figure reproduced from [148] and [150].**

### 2.2.3 Ultrasound-integrated robotic surgical systems

There is great potential in ultrasound-integrated robotic surgical systems, wherein a surgical robot also has the capability of performing ultrasound scanning during surgical procedures. There are several advantages to this approach, such as the direct control of ultrasound imaging by surgeons, which has the potential to streamline workflow within the operating room. The ultrasound-integrated surgical robots are mainly for laparoscopic surgery in which the ultrasound probe is placed directly on solid organs via a laparoscopic device, and the laparoscopic device is manipulated robotically. An early system for laparoscopic ultrasound imaging, called MIDSTEP, was developed in 1998 by de Cunha *et al*. [152] for ultrasound-guided telesurgery. With the system, a remote ultrasound expert could control the movements of a robotically mounted ultrasound probe to help on-site surgeons. Stolka *et al*. [153] developed a robotic ultrasound-guided system for planning and milling implant beds in the lateral skull base as a specific example for orthopaedic surgery. Their system consisted of a milling machine and a 3D ultrasound probe, both of which were mounted on the same 6-DOF robotic arm. This arm performed 3D ultrasound scans along paths traced by an optically tracked pointer, enabling volume reconstruction and planning of implants.

More recently, several groups have developed tools specifically to work with the da Vinci surgical system. Budde *et al*. [154] described a robotic laparoscopic ultrasound imaging system in which the mini-transducer was manipulated by the da Vinci system over the unstabilised and stabilised epicardium to identify the target artery, obtaining a scout scan and both transverse and longitudinal images. In their design, a custom made metal probe holder enabled manipulation of the transducer by the end-effectors of the da Vinci instruments. Similar ideas of directly integrating an ultrasound transducer with a da Vinci system have also been explored by the group from Johns Hopkins with Leven *et al*.'s initial efforts [155] on a rigid laparoscopic probe, Schneider *et al*.'s works [156, 157] on an articulated laparoscopic probe, and Billings *et al*.'s incorporation of elastography [158]. With an Optotrak system used and rigid tracking body incorporated, methods for ultrasound calibration, registration, autonomous robot motion, and the display of registered 2D and 3D ultrasound images were explored.

## 2.3 Ultrasound-based Guidance of Medical Robotic Systems

### 2.3.1 Ultrasound-guided robotic surgical procedures

With the interpretation either by surgeons or computer-based algorithms, ultrasound images are widely used to guide robotic surgical systems to perform targeted movements during various procedures. This includes both the use of manual-control ultrasound systems and robotic-based ultrasound system as the method of manipulation, as well as the mental interpretation of the ultrasound images by surgeons or automatic interpretation by computer algorithms as the method of processing. As for the applications, surgical robots guided by ultrasound are used in many scenarios where soft tissue or blood flow information is required, such as cardiac surgery, keyhole neurosurgery, prostatectomy, laparoscopic procedures, etc. Many of these works were mainly designed with ultrasound integrated to work with the da Vinci surgical system as reviewed in Section 2.2.3. With this configuration, registrations between ultrasound images and robotic frames are usually easy to perform, thus providing direct links between the guiding ultrasound images and robotic surgical tools. With the registration, automatic robot control or image overlay with other modalities would be possible, allowing more powerful functions for procedure guidance. Apart from integrating ultrasound systems into the surgical robots, several works used separate robotic ultrasound imaging systems working adjacent to the surgical robots. One of the applications is to robotize the trans-rectal ultrasound system for guidance of prostatectomy. This has also been reviewed in Section 2.2.2 as an intraoperative ultrasound robotic system. The use of these robots allows accurate positioning of the probe at predicted positions. Consequently, 3D reconstruction based on a series of 2D ultrasound images becomes possible.

As for the use of hand-held ultrasound in the guidance of surgical robots, one of the early examples developed by Davies *et al*. [159] presented a method of using hand-held 3D ultrasound to guide a neurosurgery robot Neurobot. As a complementary imaging modality to the pre-operative MRI used for planning, the real-time ultrasound imaging through a burr-hole in the skull addressed the problem of brain shift caused by leakage of cerebrospinal fluids. With the ultrasound probe tracked by a localizer, ultrasound images were registered to the pre-operative MRI data. The combined information was used for navigation of the Neurobot. More recently, Ahmadi *et al*. employed ultrasound imaging with the neurosurgical robotic system ROBOCAST [160]. 3D ultrasound and

power Doppler images were used to generate a blood vessel map to plan robot trajectories.

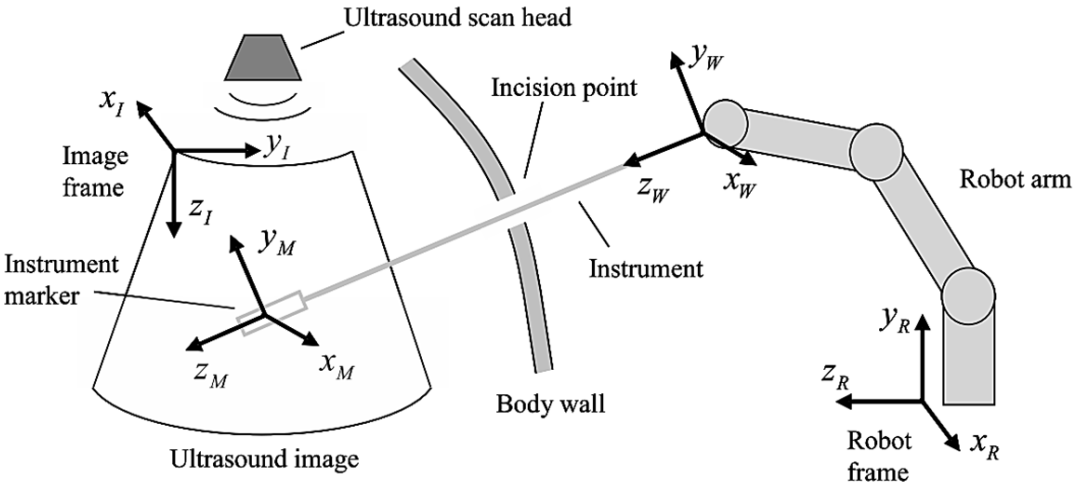


**Fig. 2.5. Diagram of overall system for the visual servoing in the studies, including the ultrasound image, surgical instrument, driving robot, and coordinate reference frames. Figure reproduced from [161].**

Ultrasound guidance used in robotic cardiac procedures has been attempted by several groups. Based on visual servoing techniques which detect the surgical robotic end-effector from 2D ultrasound images and compute the targeted robotic movements, a minimally invasive robot for cardiac surgery was successfully guided towards the goal defined in the US image for both phantom and *in vivo* animal experiments, presented by Vitrani *et al*. [162] and Ortmaier *et al*. [163]. The system was remarkable in the context of a medical application, as it allows for not using any additional external localizer for registration. Instead, a series of computer vision algorithms were used for real-time tracking of the robotic end-effector in the ultrasound plane. After localization, a differential kinematic calculation is performed to describe the relationship between the position error and the desired robotic movements. Another work presented by Novotny *et al*. [161] and Stoll *et al*. [164] described the method of tracking their robotic tool's passive instrument marker by analysing 3D ultrasound images with line detection algorithms and actuating the robot based on visual servoing (Fig. 2.5). Experiments indicated the system was able to track the instrument and converged to the target point with an error less than 1 mm. Work from the same group presented by Yuen *et al*. intended to address the problem of cardiac motion [165]. A 1-DOF system was employed to synchronize instruments with tissue motions that are approximated to one-dimensional. More recently, Thienphrapa *et al*. investigated a minimally invasive means of fragment retrieval from the heart [166]. In their system, a fixed mounted TOE

ultrasound system was used to track fragment movement and generated a probability map of its location. This then suggested a retrieval strategy moving the robot end-effector to the position with the highest spatial probability.

### 2.3.2 Ultrasound-guided robotic needle procedures

Numerous medical procedures require accurate placement of needles, ranging from biopsy procedures to more complex interventions such as brachytherapy. These could be achieved by employing robotic needle systems with the ability to reach sub-millimetres accuracy. A few examples with needles coupled to the probe, working as ultrasound-needle robotic systems, have been reviewed in Section 2.2.3. This section extends the content to free-hand ultrasound systems in guiding needle procedures with more example systems for biopsies and brachytherapy reviewed.

As for biopsy, nearly all robotic systems follow the same general procedure that the ultrasound scan is performed at the very beginning, then the biopsy target and insertion point is specified, and eventually the needle is inserted under the real-time ultrasound guidance. One of the most important tasks before needle insertion is to co-register the robotic and ultrasound coordinate systems so the robot can orient the needle along the required trajectory. The registration is usually accomplished through optical tracking, electromagnetic tracking, or rigid coupling if the needle is mounted onto the probe. Examples include a robotic needle system presented by Megali *et al*. using a registration method based on optical tracking of infrared LEDs on the ultrasound probe [167] and a robotic arm presented by Kettenbach *et al*. using external fiducials for registration [168]. Some other systems also indicated additional functions apart from accurate positioning, such as the system presented by Mallapragada *et al*. which has the ability of simultaneous needle insertion and manipulation of a tumour in real time by applying controlled external force such that the tumour does not deviate from the path of the needle during breast biopsies [169]. Robotic brachytherapy systems have mainly been designed for treating prostate cancer, in which case the use of the robot improves accuracy of the radioactive source placement and allows more complex insertion trajectories to avoid anatomic structures. Among these works, Fichtinger *et al*. [170] were the first group to report clinical trials of a robotic brachytherapy system (Fig. 2.6) on patients. Large placement errors were observed to occur much less frequently than in conventional manual procedures. More recently, several other systems have been

introduced with more functions, such as the ability of seed mapping, rotational DOFs for oblique insertion, real-time 3D tracking and prostate motion compensation [103].

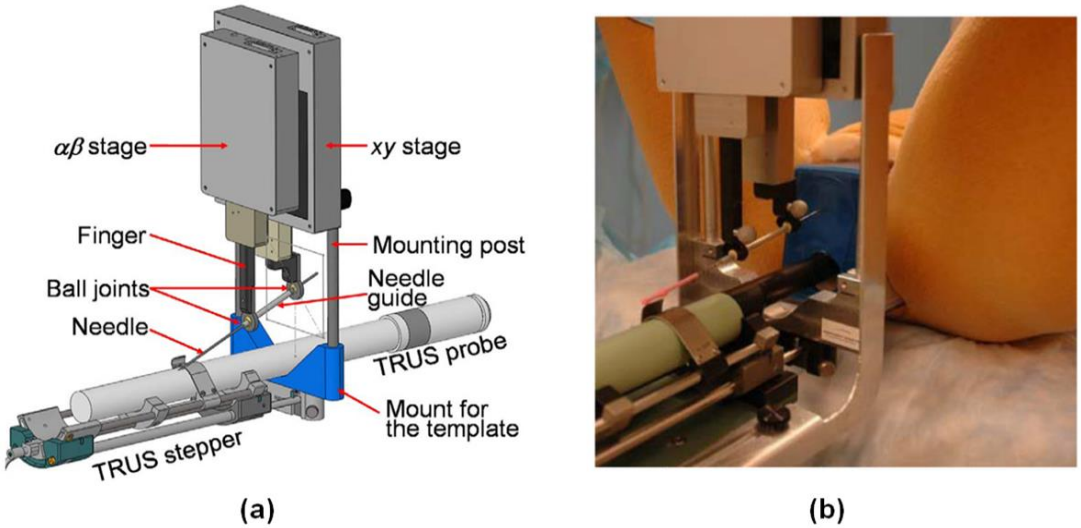


**Fig. 2.6. Example of a robotic brachytherapy system under the guidance of ultrasound presented in [170]. (a) CAD model of the brachytherapy robot mounted over the TRUS probe. (b) Example of clinical setup of the robotic system in phantom experiments. Figure reproduced from [170].**

### 2.3.3 Ultrasound-guided external energy therapy

Ultrasound-guided external therapy robotic systems have been developed for use with High intensity focused ultrasound (HIFU) ablation [171-174]. HIFU refers to the process of introducing high-intensity focus ultrasound waves on a small region of tissue, which is rapidly heated and destroyed without the use of ionizing radiation. This procedure is usually performed with robotic HIFU device as they can cycle though a matrix focus points when ablating a volume. Though MR is often used for the guidance as well as monitoring temperature, ultrasound imaging is a valid alternative with lower cost and higher frame rate. In such cases, ultrasound is used for preoperative scanning as a way of defining the target HIFU volume, as well as tracking the ablation process in real time during the therapy. The problems that need to be addressed during a robotic HIFU procedure are similar to needle placement, such as registration of the ultrasound image transducer coordinates to the HIFU transducer coordinates and compensation for target motion.

## 2.4 Non-ultrasound Endoscopic Robotic Systems

### 2.4.1 Ear-nose-and-throat (ENT) diagnostic robot

A special flexible endoscope used in ear-nose-throat (ENT) diagnoses is employed clinically in order to diagnose tumours or polyps within the nasal cavity. The endoscope includes a flexible distal tip with a mounted camera controlled by a bending lever on the handle and a flexible shaft containing multiple glass fibres used to transmit the images to the physician. With its bendable feature, the flexible shaft of the endoscope can be driven through a non-straight path in the nasal cavity, thus facilitating the examination of anatomic structures. The clinical use of this device has indicated problems with manipulating the orientation of the tip based only on the images, as described by a group from Technische Universitaet Muenchen. Their efforts were to develop a hand-held robotic ENT diagnostic endoscope (Fig. 2.7) aimed at improving the control of the orientation [175, 176]. This was achieved by an add-on 2-DOFs robotic device which manipulated the rotation of the whole endoscope and one-directional bending of the endoscope tip.

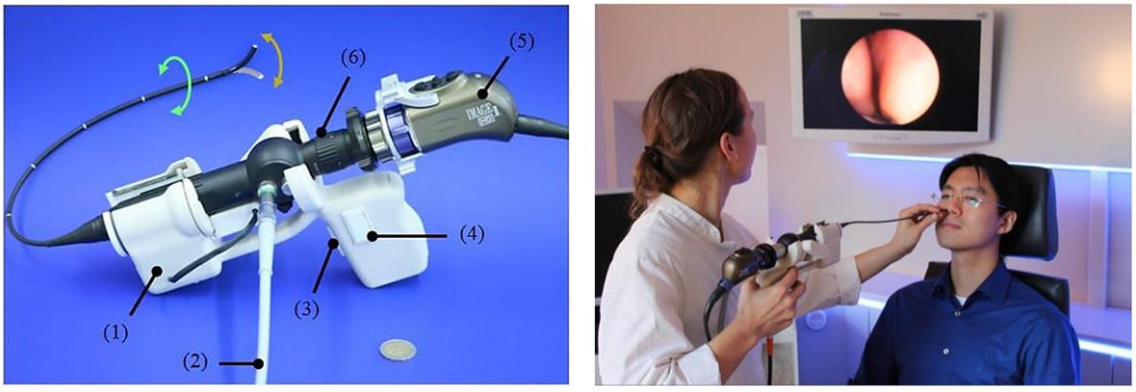


**Fig. 2.7. (a) Implementation of the manipulator system: (1) manipulator, (2) light cable, (3) pushbutton for bending tip, (4) pushbutton for rotation of the endoscope, (5) endoscopic camera, (6) flexible rhino endoscope. (b) Diagnosis of the nasal cavity with the designed robotic manipulator system. Figure reproduced from [176].**

The add-on design configuration has the advantage that the use of the new system is still based on commercial endoscopes already being used clinically. The robotic system allows both manual and automatic controls. The manual control was achieved via two pushbuttons arranged on the add-on robotic manipulator which could be held by the operator directly. The automatic control employed a vision technique to extract the dark region from the image, which represents the distant inner space of the nasal cavity and

indicates the heading direction of the endoscope. Robotic kinematics was proposed based on the modelling of the endoscope in order to automatically orient the endoscope according to the indicated heading direction. Phantom experimental results showed that the image-guided steering is significantly faster than traditional manual steering and that the measured accuracy of the system meets current clinical requirements.

### 2.4.2 Robotic endo-laryngeal scope

Conventional manual control of the endo-laryngeal scope includes 3-DOF manipulation: bending of the scope's tip using the scope handle, rotation of the scope about its axis, and translation of the scope along the axis of the airway. With manual control, problems have been identified in which the scope needs to be manipulated with two hands controlled by one surgeon for holding and actuating purposes while another surgeon is required to be around the patient operating the treatment tools, such as forceps and lasers. This leads to a crowded working environment around the patient, as well as coordination problems between the two surgeons.

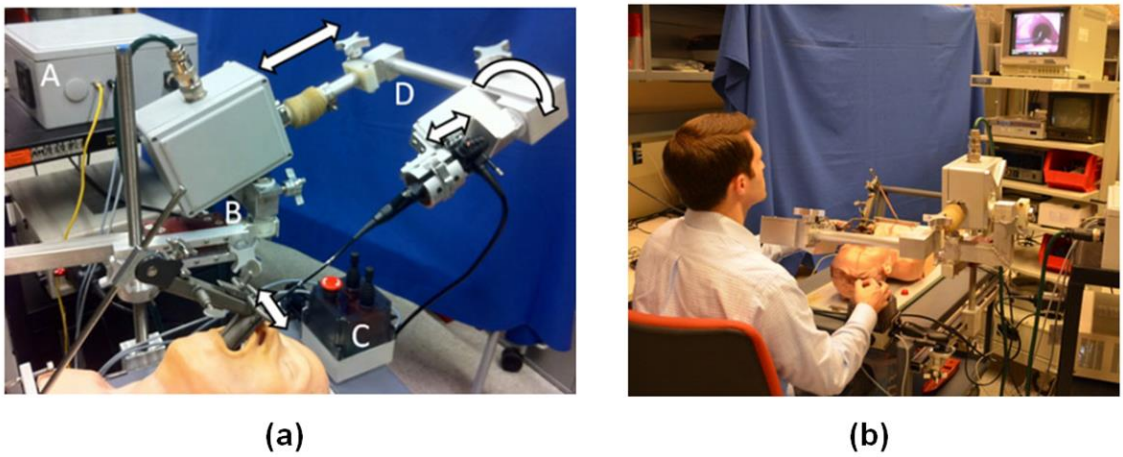


**Fig. 2.8. (a) Implementation of the manipulator system: A. Electronics enclosure, B. 5-DOF positioning arm, C. joystick enclosure, D. robot system. (b) Evaluation of the system with joystick control by a single operator using a rubber head and neck phantom. Figure reproduced from [177].**

Motivated by these problems, a group from Johns Hopkins University has designed an add-on robotic system (Fig. 2.8) making use of an unmodified clinical endo-laryngeal scope [177, 178]. The 3-DOF end-effector of the robot holds and actuates the conventional scope. A 5-DOF passive positioning arm at the back of the robot allows the adjustment of the endoscope insertion. In addition, 2-DOF passive lockable mechanisms allow the robotic system to be locked in case of emergency. The whole system is controlled by a custom joystick interface so the surgeon can operate all movements of the endoscope with one hand while use the other hand to operate the

treatment tools. Both phantom and cadaver studies were performed and the results indicated that the robot-aided approach was superior to hand manipulation of conventional endoscopes.

### 2.4.3 Robotic endoscopes for colonoscopy and gastroscopy

Flexible endoscopes are also widely used for performing colonoscopies and gastroscopies. Control of these endoscopic devices, similar to the situations with other endoscopes introduced before, usually requires two hands. This drawback has been identified by several groups, motivating several robotic systems designed to replace the conventional endoscopes for colonoscopy and gastroscopy. Among those works, many focused on robotizing the endoscope for natural orifice transluminal endoscopic surgery (NOTES), which involves a powerful device including both cameras and surgical tools.

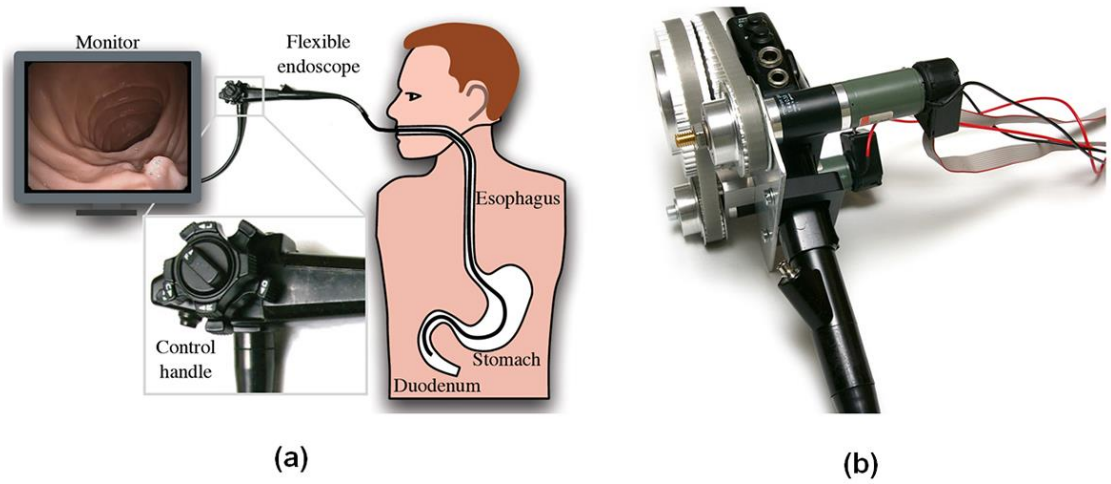


**Fig. 2.9. (a) Conventional gastroscopy: The physician uses the endoscope control handle to steer the endoscope through the patient's gastrointestinal tract while observing the endoscopic images on the monitor. (b) The robotically steered gastroscope with motors and several mechanisms. Figure reproduced from [179].**

Work presented by Reilink *et al*. introduced image-based steering methods for a robotized gastroscope, including a method based on optical flow and a method based on image intensity [180]. In phantom experiments, the robotically steered endoscope performed 68% better in terms of keeping the lumen centred in the image compared to manual control. Further work from Reilink *et al*. focused on the investigation of intuitive steering control [181]. An experiment was performed using a 6-DOF haptic device, along with the motorized endoscope, as a comparison with the conventional manual control. Experimental results indicated that experts appeared faster when using

the conventional steering method compared to motorized steering methods, while students who had done flexible endoscopy training showed no significant differences.


**Fig. 2.10. (a) Exploded view of the coupling mechanism: (1) Drive unit, (2) Remote control, (3) Holder remote control, (4) Plug, (5) Sterile interface, (6) Docking station, (7) Sterile bag, (8) Endoscope. (b) Phantom experimental setup showing the control of the robotic NOTES endoscope. Figure reproduced from [182].**

Another motorized flexible endoscope (Fig. 2.9) developed by Ott *et al*. [179] focused on tracking a region of interest (ROI) despite breathing motion during NOTES so that the physician would be able to focus on the manipulation of the surgical tools. In their partially robotized system, the navigation wheels controlling the bending of the endoscope tip have been replaced by two hollow shaft rotary motors that drive the two coaxial shafts coming out from the handle. A study of visual-servoing technique provided the link between the robot and the anatomic target. The control method allows stabilization of the endoscopic view and *in vivo* experiments were performed validating the proposed solution for improving the manipulation of flexible endoscopes. Different to the above works, a hybrid setup presented by Ruiter *et al*. demonstrated mobile as well as stationary use of a robotic NOTES endoscope with an emphasis on light-weight and intuitive control [182] (Fig. 2.10). Antagonistic cable pairs between the stationary motor unit and the mobile drive unit actuate the navigation wheels of the endoscope. This allows the heavy motor components to be positioned away from the endoscopic system in a separate control box. As for the remote control, a thumb joystick and a touchpad were integrated to function as input, allowing intuitive control of the tip steering with a single hand. A passive docking station for positioning the endoscope was employed. The whole system was evaluated for its usability. Results indicated using touchpad or joystick control increases efficiency and satisfaction, while the effectiveness was not significantly affected by robotic steering.

## 2.5 Summary and Discussion

### 2.5.1 Previous works on robotic ultrasound

Abundant research studies have demonstrated that both extracorporeal and intraoperative ultrasound acquisitions, as highly specialized tasks requiring on-site operations, can be remotely operated by employing robotic techniques. These systems, with different DOFs of movements and various mechanisms for holding and manipulating conventional hand-held probes, were primary designed and utilized to replace or assist with manual control. With robotically-operated ultrasound, higher accuracy and more stable manipulation over long periods of time becomes possible as a benefit of the mechanical nature of robots. One of the most important features that most of these systems provide is the ability of remote control. This enables a distant experienced sonographer to be precisely mimicked by robots for patient diagnosis, which can potentially resolve problems such as the lack of experienced sonographers in rural areas. Additionally, several intraoperative ultrasound systems are utilized for guidance of surgery, where surgeons need to work and communicate with sonographers. The potential advantage of robotic intraoperative ultrasound is that it may allow direct control of the ultrasound image acquisition by the surgeon while manipulating surgical tools with reference to hidden structures, such as needle insertion procedures for biopsy.

In addition to simple reproduction of operator motions, robotic ultrasound has the potential to be more powerful than human operation with computer intelligence built in. Various systems have been shown capable of surpassing human operation, such as the automatic regulation of transducer contact, evenly spaced imaging for 3D reconstructions from 2D images, and even automatic or semi-automatic scanning. These functions have strong relationships with automatic interpretation of ultrasound images and actuate the robotic systems with control algorithms. More general uses of ultrasound in guiding other medical robots are also reviewed in this chapter to provide more information relating to the links between ultrasound images and robotic motions. For the control of an ultrasound robot or a separate surgical robot using ultrasound images, several techniques are of great value, such as device tracking, ultrasound to robot registration, visual servoing, robotic kinematics, and feedback control algorithms. These works set up strong links between ultrasound robots and image processing techniques, working mutually as a whole system in many cases.

Despite numerous robotic ultrasound systems developed in laboratories, there are only limited technologies that have been commercialized and disseminated, and very few ultrasound robots that have received FDA approval. One of the greatest obstacles is justifying the expense of remote-operated robotic ultrasound, because its implementation requires significant training and investment. The use of these systems usually requires change of the conventional clinical setups and routines, which is also challenging to be accepted by clinicians. Furthermore, most of the intraoperative ultrasound robotic technologies reviewed have been limited to phantom and *ex vivo* testing, while extracorporeal systems are more widely employed in human testing. The difference between experimental environments and clinical practice usually results in the problem that the accuracy obtained experimentally cannot be translated into clinical use.

The recent success of the MELODY ultrasound robot in commercialization and clinical translation indicates large amounts of clinical experiments with gradual improvements of the system over long periods of time are needed for an ultrasound robot to be clinically accepted and translated. The review of ultrasound robots also indicates additional functions included in the design, which cannot be achieved with manual control, are important for the device in order to be more valuable as replacements or assistants of manual control.

### 2.5.2 New innovation of the proposed TOE robot

- New requirements for innovative design

For trans-oesophageal ultrasound, no other publication was found in the literature proposing any detailed robotized system apart from this work. Though various extracorporeal and intraoperative ultrasound systems have been introduced, the idea of robotizing a trans-oesophageal ultrasound probe is different. The most similar works on intraoperative ultrasound systems, as reviewed in Section 2.2.2, include the motorization of the TRUS probe and ICE catheter. However, both devices are very different from the TOE probe. The TRUS probe only moved in 2-DOFs with an unbendable scanning head while the 4-DOF ICE catheter has a totally different architecture of the probe as well as the bending control method. The concept of a remote-operated trans-oesophageal ultrasound system has been proposed By Philips [183] in their patent as a potential replacement of the hand-held probe. Though many approaches and possibilities were discussed, there is not any detailed design and

solution given. Therefore, the current robotic systems reviewed in the literature for intraoperative ultrasound devices are not suitable for the control of a TOE probe.

As the trans-oesophageal ultrasound probe has an endoscopic configuration similar to many other devices, reviews of other non-ultrasound endoscopic robots have been provided as well. This includes the work described in Section 2.4 for the ENT endoscope, endo-laryngeal scope, colonoscopy device and gastroscope device. Similar to the intraoperative ultrasound devices, the size, structure, DOFs, and bending control structures for these endoscopes vary greatly from the TOE probe. Therefore, the robotic systems aiming at robotizing these endoscopes or probes are very different from the robot required here in many aspects and cannot be applied to the TOE probe.

- New innovation on functionalities

As for the functionalities and applications, there is only very limited work on specific use of ultrasound robots for cardiology including the robotizing of a TTE probe described in Section 2.2.1 and an ICE catheter described in Section 2.2.2. Both devices are different to the way TOE is operated. Besides, these works focused on specific functionality rather than an automatic ultrasound scanning solution for different views. The work on the TTE probe focused on multi-modality image fusion, while the work on the ICE catheter focused on 2D to 3D reconstruction and automatic orientation of the probe for tracking other devices. Many extracorporeal ultrasound robots reviewed in Section 2.2.1 designed for general use have the potential to be utilized in cardiology. However, the automatic acquisition of different TTE views using these general robots is challenging and there is no specific work reporting such a topic. To conclude, a whole automatic acquisition solution for different ultrasound views of the heart has not been proposed so far because of the complexity of the heart and limited ultrasound robots specifically designed for cardiac imaging purposes.

In terms of automatic acquisition for non-cardiac ultrasound, there are a few existing works on robotic assisted acquisitions for carotid artery as reviewed in Section 2.2.1. These works explore visual servoing techniques for tracking particular features, e.g. tracking the carotid artery using an extracorporeal ultrasound robot. Further works have been extended by other researchers to automatic scanning of the carotid artery using motion compensation based on this tracking. The idea of automatic acquisition is also employed in other types of medical robots, such as an eye-in-hand endoscopic robotic

system used for physiology motion rejection in natural orifice transluminal endoscopic surgery as reported in Section 2.4.3. These works are regarding non-cardiac ultrasound or camera images, mainly focused on motion compensation in local areas for automatic acquisition of targets where the initial positioning for different scanning views still requires manual operation. In addition, using visual servoing techniques based on feature extraction for cardiac ultrasound acquisitions is challenging due to the complexity of the heart structure. This makes these methods not suitable for the aim of the TOE robot described in Chapter 1.

The target for the application of the TOE robot proposed in this study is to allow the echocardiographer to define the TOE views for the patient before the procedure when TOE is used during surgeries and then automatically acquire these views using the robot. According to the findings of this literature review, no such system has been proposed. To achieve the aim described in Chapter 1, a complete novel automatic acquisition workflow, which is not available in any literature, needs to be developed including pre-planning, tracking, and automatic positioning for use with the new TOE robot.

### 2.5.3 Inspirations from previous works on detailed methods

Although there is no other work found in the literature which is specifically for the TOE robotic system or the automatic cardiac ultrasound acquisition workflow, several engineering and mathematical techniques widely employed in the works reviewed in this chapter are useful for developing the TOE robotic system and achieving its application goal proposed in Chapter 1. This includes the kinematic technique for modelling the probe's movement, the pre-planning methods for deciding the robotic paths, and the feedback solutions during the robotic procedures.

Since the bi-directional bending movements of the TOE probe are similar to several other types of probe or endoscope reviewed in this chapter, the kinematic modelling techniques for those systems would be useful for the TOE robot-probe system. In the work of the robotic ICE catheter reviewed in Section 2.2.2, the work of the robotic ENT endoscope reviewed in Section 2.4.1, and the work of the robotized gastroscope reviewed in Section 2.4.3, similar techniques using a geometry relationship based on a 'constant curvature' assumption were used to model the movements of the probe bending. This method has an advantage for these add-on robotic systems as it does not require joint information of the articulation mechanisms. Therefore it is easily employed

by these works for understanding the probe's behaviour and thus automatically controlling them with the robot.

These works on kinematics have similar solutions for the forward approach which aims to predict the pose of the probe head when certain bending movements controlled by the knobs are given. However, different methods were employed for the inverse approach which aims to find out the required bending movements of the bending control knobs when a target pose of the probe head is given. In the work presented for the ICE catheter robot, a theoretical geometrical derivation of the inverse kinematics based on an 'unfolding strategy' of the forward kinematics was proposed. Different to this approach, the work described for the robotized gastroscope utilized differential kinematics where a numerical iteration strategy was employed to address the inverse kinematics.

For the TOE robot-probe system discussed in this work, one of the most important differences towards these works is the constrained environment of the oesophagus where the probe is located. Though similar models as used in these works could be employed for the TOE system, the constrained environment should be taken into consideration when addressing both the forward and inverse kinematics. Another difference is that the aim of this work focuses on obtaining standard ultrasound views. Therefore, both the kinematics for the forward and inverse approach should be extended to the image coordinates. In addition, the mechanical assumptions used in the kinematic model for other types of probe should be tested with the TOE probe to verify the feasibility of the method. To conclude, the basic concept and mathematical details of the bending modelling for other probes reviewed here would be useful for the TOE robot. However, detailed methods to address several differences compared to the previous works should be proposed to meet the different application goal of this work. Detailed methods to work with the TOE robot will be discussed in more detail in Chapter 4.

Using a pre-planning method based on pre-operative images for medical robotic procedures is a useful approach to decide the target position and paths for the robotic end-effector. Though limited work has been found in the literature for robotic systems which hold and manipulate ultrasound probes, the method is widely used for surgical robots. An example of an ultrasound-guided surgical robot is reviewed in Section 2.3.1. This used pre-operative MRI images for planning the positioning of a neurosurgical robot. A similar idea of pre-planning used for ultrasound-guided biopsy robots is reviewed in 2.3.2 where the biopsy target and insertion point are specified after an initial ultrasound scan. Since global information of the heart from MR or CT images

always exist in many cardiac surgical procedures when TOE is used as the real-time guidance, a view-planning platform with associated methods could be designed so the trans-oesophageal ultrasound views could be planned in advance from these pre-operative images. This would be an ideal way to decide the positioning of the probe and detailed methods will be investigated in Chapter 4.

Since the TOE robot has the eye-in-hand configuration where the ultrasound image itself can provide information on the position of the probe, use of the TOE image to guide the robot would be a natural operation to provide feedback to the robot. This topic was first covered in Section 2.2.1 under the category of the extracorporeal robotic ultrasound systems where several examples use visual servoing analysing ultrasound images of the carotid artery to provide information for repositioning of the probe. A similar topic is also reviewed in Section 2.3 where ultrasound images are used to guide another surgical robot. For automatic control, typical methods also use a visual servoing technique by analysing ultrasound images to detect the end-effector of the surgical robot and guiding the repositioning. As mentioned in the above subsection, these methods of using ultrasound images as feedback would be difficult to adapt for the TOE robot because of the difficulty of analysing the complicated cardiac ultrasound images for visual servoing. Therefore, alternative ways of using ultrasound images for feedback should be investigated for the TOE robot such as registering the images to the pre-operative MR/CT images. This will be discussed in more detail in Chapter 5.

In addition to the use of ultrasound images for feedback, electromagnetic tracking systems are also widely employed in ultrasound robotic systems to track the position of the probe and provide useful information to guide the positioning, such as the work reviewed for the ICE catheter in Section 2.2.2. An obvious advantage of using EM tracking is the real-time reliable performance though an additional sensor attached to the original probe. In addition, registration of the EM tracking coordinates to the patient coordinates or the robotic coordinates for different applications require different detailed solutions. These topics will be investigated in more detail in Chapter 6.

# 3 DESIGN AND IMPLEMENTATION OF THE TOE ROBOTIC SYSTEM

## 3.1 Introduction and Overview of the TOE Robot

This chapter aims to describe the design and implementation of the TOE robotic system, the remote control approaches of this device, and the initial experiment to test the repeatability performance of the proposed system. The work is to achieve the aim of having an add-on robotic system for a TOE probe and allowing the remote control of the system as described in Chapter 1. In addition, this work is the foundation of the whole thesis as all the works and applications introduced in the subsequent chapters are based on the robotic system introduced in this chapter. It should be noted that the works introduced in this chapter regarding the design and manufacture of the robotic system were completed in collaboration with Xtronics Ltd where the manager Mr. Singh has made significant contribution to the final mechanical design and helped with the manufacture.

In this introduction section 3.1, a brief overview of the robotic system will first be presented for its static system, implementation and control. The work on the details of the robotic system and the experiments will be described in the following sections. The description starts from the mechanical design described in Section 3.2, followed by the electronics and control described in Section 3.3, and eventually focuses on the safety features of the system in Section 3.4. In Section 3.5, the basic experiments aimed at

verifying the correct working of the mechanism and controls using optical tracking are presented. In Section 3.6, the whole design and implementation of the robot is summarized and the results from the experiments are discussed. The main works introduced in this chapter have been summarized and included in the published papers [184, 185].

### 3.1.1 Static system description

The proposed TOE add-on robot holds the probe handle and manipulates four of the five DOFs that are available in manual handling of the probe. Manipulation of the electronic steering buttons is not yet implemented: this can still be achieved by directly operating the button on the ultrasound machine. The robot comprises three structures, as shown in Fig. 3.1: the handle control structure providing two DOFs to rotate the knobs; a one-DOF probe rotation mechanism to rotate the whole probe together with the handle control structure; and a final one-DOF structure providing linear translation of the probe and all other structures. The handle control structure consists of two rotational wheels precisely formed to mate with and drive the two knobs on the TOE probe handle via belt mechanisms. Magnetic sensing devices are embedded into the wheels to track the initial home or neutral position, serving as a primary safety feature for the probe manipulation. The probe rotation structure consists of a gear train mechanism driven by a balanced two-motor design. The final translation structure uses a linear belt and rail system.

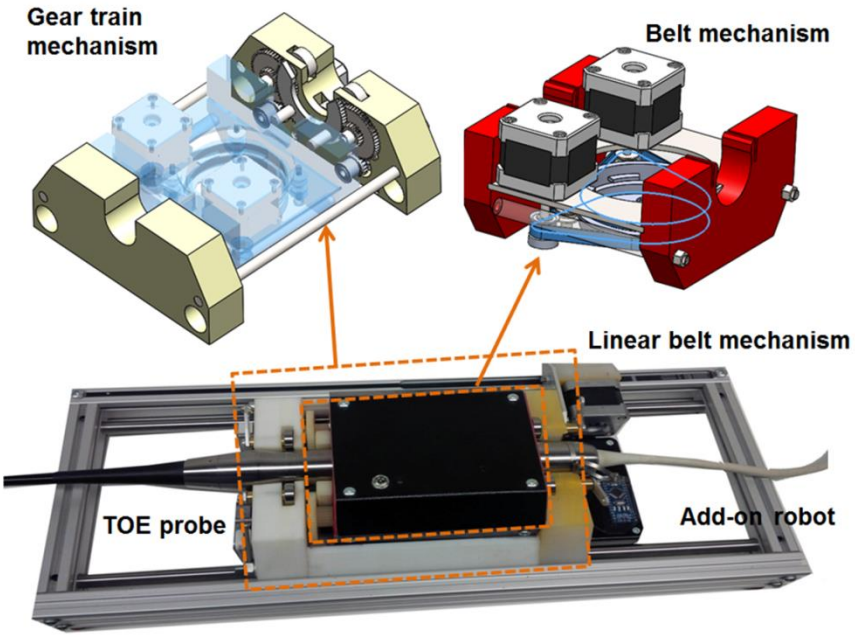


**Fig. 3.1. Overview of the proposed robotic system for TOE with a photo of the final implementation (bottom row) and schematic drawings of the internal mechanisms (top row).**

### 3.1.2 Implementation and control of the system

The whole robot was designed in a computer-aided engineering (CAD) software (Solidworks 2013) and produced through rapid prototyping (3D printing) and machining. The overall rotation diameter of the handle control structure is 110 mm. The dimensions of the whole robot are 500×210×40 mm. The robot utilizes five stepper motors (NEMA 17, 5V, 1.2A, Adafruit Industries). Two of the stepper motors for the steering mechanism are controlled by a single-board microcontroller with an operating frequency of 16 MHz (Arduino Nano, Adafruit Industries). The controller is embedded into the handle control structure with a Bluetooth module (HC-06, 10 metres range, Adafruit Industries), magnetic sensors and a voltage regulator attached. The whole handle control piece is a wireless individual device powered by a rechargeable battery pack. The other three motors for rotation and translation mechanisms are separately controlled by another microcontroller (Arduino Nano). A PC works as the master device and two Arduino-Nano microcontrollers, integrated into the handle control structure and the rail structure, are used as the slave processors. The PC runs a custom made software written in C#, which communicates with the Arduino Nano via a custom protocol. The software itself provides the ability to control the robot in different modes. The software can also be interfaced with other control devices connected to the PC, such as a gamepad, a joystick, or a custom-made dummy probe.

## 3.2 Design and Implementation of the TOE Robot

### 3.2.1 3D modelling of TOE probe's handle

The design of the robotic TOE system started with 3D modelling of the TOE probe's handle. Important dimensions of the handle of the TOE probe were obtained and a 3D model was established as shown in Fig. 3.2. The process of obtaining precise dimensional measurements involved physical measurements, photography, and supporting patent documents [186]. The simplified 3D model provides accurate information on the probe's handle diameter and the contours of the two knobs while the button and the small lever on the probe handle are ignored as they are not required to be motorized.

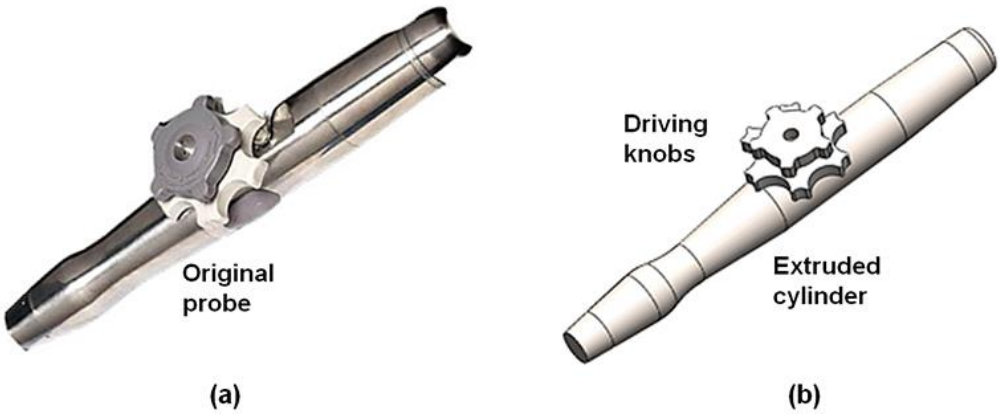


**Fig. 3.2. 3D model of the TOE probe handle. (a) Real probe's handle, including two rotating knobs and an extruded cylinder shaped handle. (b) The 3D simplified model with some features ignored.**

### 3.2.2 Design of the handle control mechanism

The two-axis motorized driving mechanism is designed to mate with the two knobs and drive them separately in order to control the movements of the two knobs. Two discs, derived from plastic timing pulleys, are shown in Fig. 3.3. The internal contours of the two discs were carefully designed to mate with the external contours of the two knobs. Each of the two pulleys has 110 teeth (2.032mm pitch) which can fit into a matching toothed timing belt linked and geared to a stepper motor. The two driving discs are concentric to each other and placed in two parallel planes to mate with two knobs. For construction, the MXL025 Plastic Timing Pulley (PP110MXL025MI, BeltingOnline) with 110 teeth and brass inside was utilised as the original piece, and the inside contour was then machined.

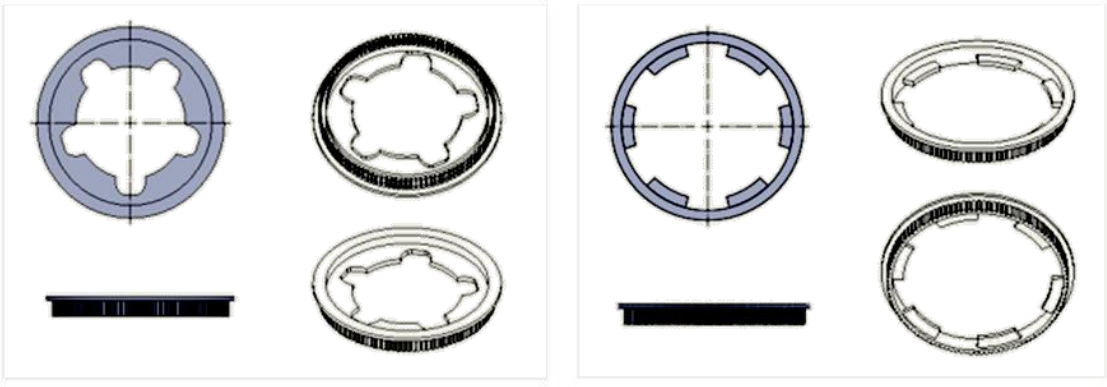

**Fig. 3.3. Schematic drawing of the driving disc used to mate with the TOE probe handle knobs. This is then manufactured from an MXL025 Plastic Timing Pulley (110 teeth).**

Two stepper motors (NEMA17 40mm) are used to drive the two discs separately. The two motors are mounted on the top of a steel plate. Another two timing pulleys are attached to the motor shafts to mate with the timing belts and two driving discs. These

two pulleys are placed in different planes according to the different depths of the two discs (Fig. 3.4a). These timing belts are used for power transmission between the motor shafts and the discs that are not axially aligned as well as to ensure that the driven discs are always rotating at a fixed speed ratio to the driving pulley.

In additional to the belt driving mechanism relating the motors and discs, supporting mechanisms were designed to retain the discs in position and hold the TOE probe's handle. Four pairs of small pulleys fixed to the steel plate with pins and screws from the bottom are used to mate with the flange of the discs as a way to hold them in place. Each of the pulley's notches is in the same plane as the flange of the discs in order to hold and support the disc (Fig. 3.4b). The four pairs of the assembly pieces are placed 45 degrees towards each other (Fig. 3.4c). Another two blocks are utilized to hold the TOE probe's handle with two supporting beams added to keep structures in position (Fig. 3.4d). For the manufacture, the steel plate, supporting beams, and two blocks were constructed by machining.

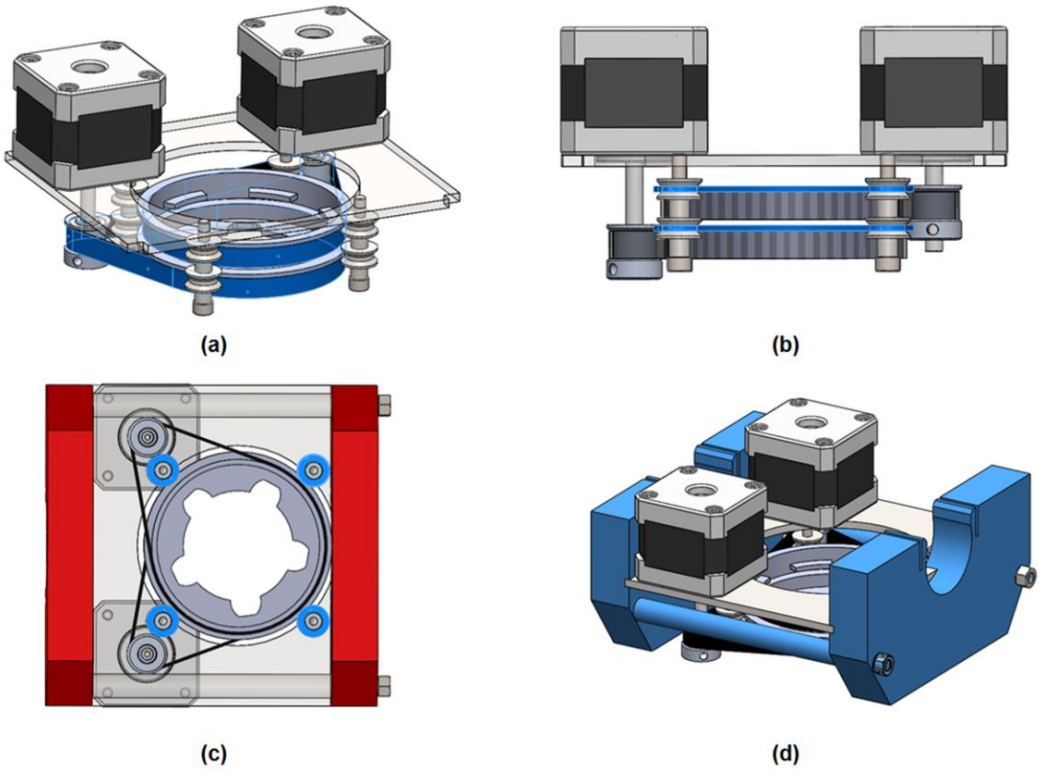


**Fig. 3.4. Schematic drawing of the handle control structure. (a) Belt mechanism with two timing pulleys driving the two discs. (b) The flanges of the discs are used to retain the position of the discs. (c) Four pairs of small pulleys are used to mate with the two flanges. (d) Blocks and beams working as supports for the handle control structure.**

### 3.2.3 Design of the rotation control mechanism

The rotation control mechanism of the robot can rotate the whole probe along its long axis together with the handle control mechanism described in the previous section. The whole structure is shown in Fig. 3.5. In the design, the handle control structure rotates driven by the off-centered cam. The cam mates with two spur gear trains, which attach to the front block. The whole structure is driven by the gear mechanism with a balanced motor design. The rotation diameter of the design is less than 110 mm. The design of the rotation structure takes the usability of the robot into consideration. The size of the robot needs to be compact to reduce interference with the patient and other medical devices in the cardiac catheter room. The concern about the size motivates the use of two small motors and a gear mechanism to transmit motions between different axes. The two motors can be linked to provide more power to drive the rotation structure. During the manufacture of the rotation control structure, 3D printing techniques were utilized to achieve highly accurate dimensions. The two blocks with complicated internal structures and the three types of spur gear are all directly printed.

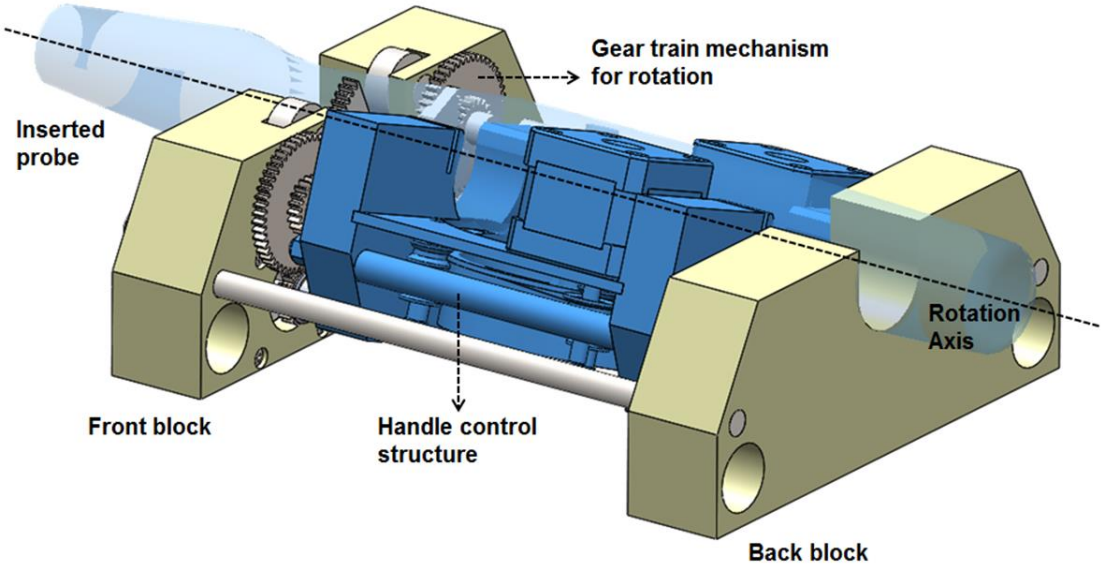


**Fig. 3.5. Rotation control mechanism for the rotation DOF assembled with the probe's handle control structure (dark blue) and the inserted probe (transparent light blue).**

The front block is the fundamental part of the rotation-control structure. The block is one of the main structures where the TOE probe's extruded steel cylinder is placed. An extruded circular cut is designed to mate with the probe's handle cylinder. Fig. 3.6a shows the design of the front block, which was printed by a 3D printer. The front block also serves as the base for mounting the motors with two cavities. Another three cavities are designed to contain three bearings. These bearing are intended to provide free

rotational movement of the probe around its fixed axis. This constrains the relative movement between the probe and the block, and reduces the friction between these two structures. Two NEMA 17 motors are mounted inside the motor cavities. Three ball bearings are inserted into the bearing cavities with their shafts across the bearings. These bearings rotate freely on their individual shafts when the probe rotates along its fixed long axis on the block.

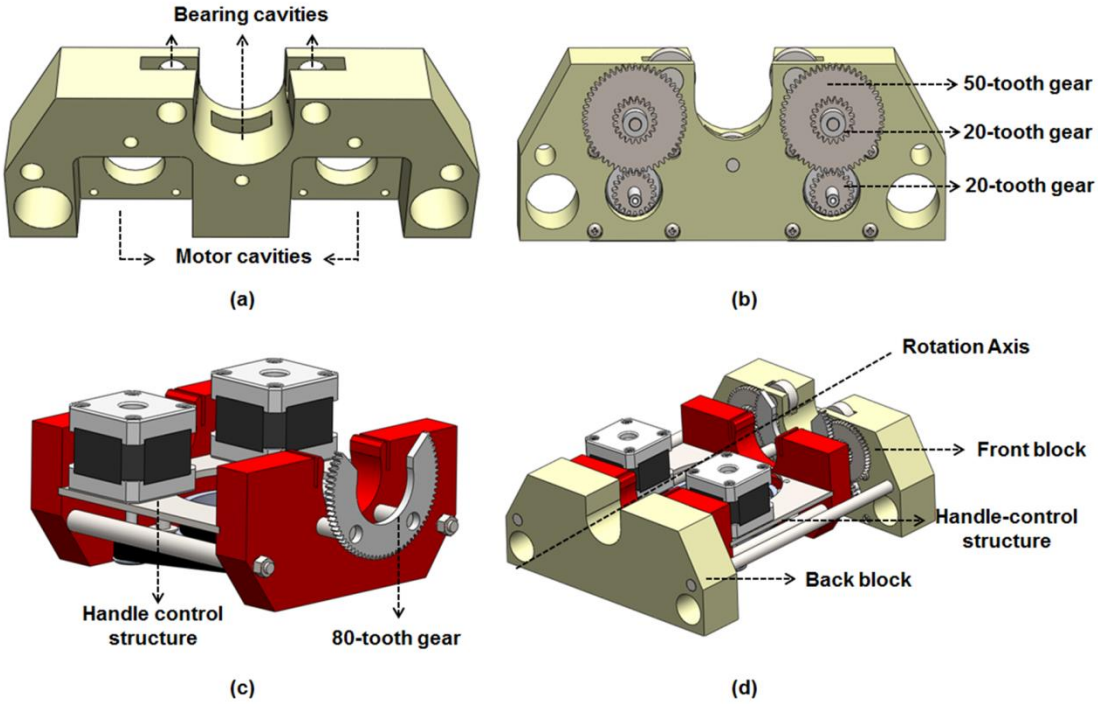


**Fig. 3.6. (a) Design of the front block with motor and bearing cavities. (b) Six spur gears with three on each side are assembled and attached to the front block. (c) A large 80-tooth spur gear is attached to the handle control structure. (d) The assembly of the rotation structure and the handle control structure.**

Gears and gear trains are used as the rotation mechanism to drive the probe rotation by transmitting motion from the motor shaft axes to the main rotation axis. The gear trains in this design consist of 7 gears. On the block side, six spur gears (three on each side) are assembled and attached to the front block as shown in Fig. 3.6b. Two 20-tooth spur gears are attached to the motor shafts. They mate exactly with another two 50-tooth gears attached to the front block sitting on the top of the two small gears. The gears serving as the drive effectors are another two small 20-tooth spur gears which attach to the same shaft as the large 50-tooth gears. Therefore, the rotation of the small gears on the motor shaft will result in the rotation of the two small gears on top. These finally drive a large 80-tooth spur gear to rotate the whole handle control structure introduced in the previous section. The two motors in the design can be further linked together to provide double power to the rotation system. The large 80-tooth spur gear is attached to

the handle control structure as shown in Fig. 3.6c. The inside contour of the large spur gear is cut to mate with the probe's outer profile. The whole handle control structure then mates with the block assembly via the gear train of the 20-tooth small gear and the 80-tooth large gear. The two motors in the design work together cooperatively to drive the whole rotation DOF. Fig. 3.6d shows the final 3D assembly of the rotation structure and the handle control structure.

### 3.2.4 Design of the translation control mechanism

A linear belt drive mechanism and two rails attached to the base frame were designed to provide the fourth DOF: translational movement of the probe (Fig. 3.7). The length of the frame and rails is 70cm, which provides enough movement for the probe translating inside of the oesophagus.

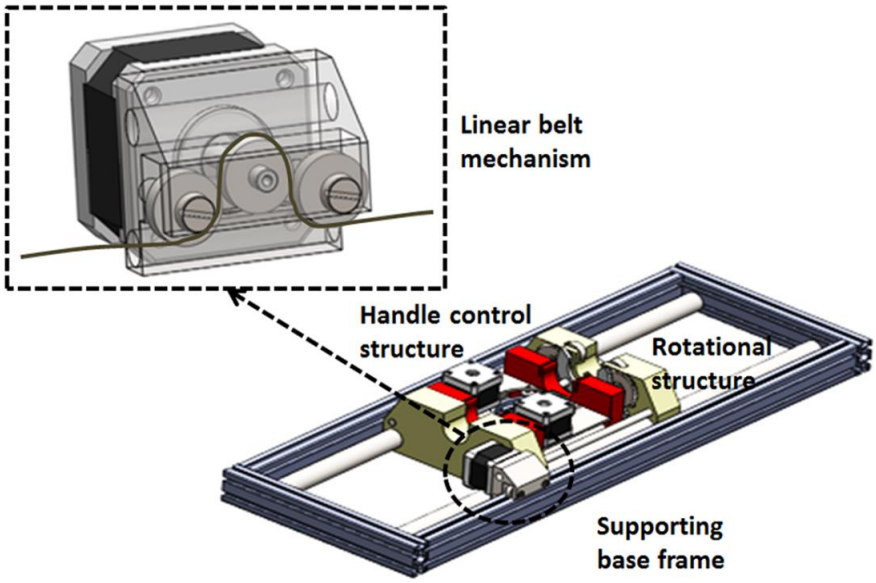


**Fig. 3.7. 3-D assembly drawing of the whole robot. One NEMA 17 motor is mounted to the back block driving the linear belt mechanism. Two bearings are placed on two sides of the motor shaft pulley, providing a belt path through which the linear belt extends.**

One NEMA 17 motor is mounted to the back block of the rotation structure. A small linear motor seat was designed with two bearings inside the seat. The two bearings are placed on either side of the motor shaft. A small motor shaft pulley is attached to the right position on the motor shaft. It works together with the two bearings, providing a belt path which actuates the block translating along the rail. The linear belt extends through the belt path constrained by the two bearings and the motor shaft pulley. Both ends of the linear belt are attached and fixed to the end point of the frame. Therefore, the mechanism will drive the relative movement of the back block when the motor shaft

rotates. The back block is linked with the front block and holds the handle control structure in its position. The movement of the back block will therefore drive all the structures on the rail translating along the long axis.

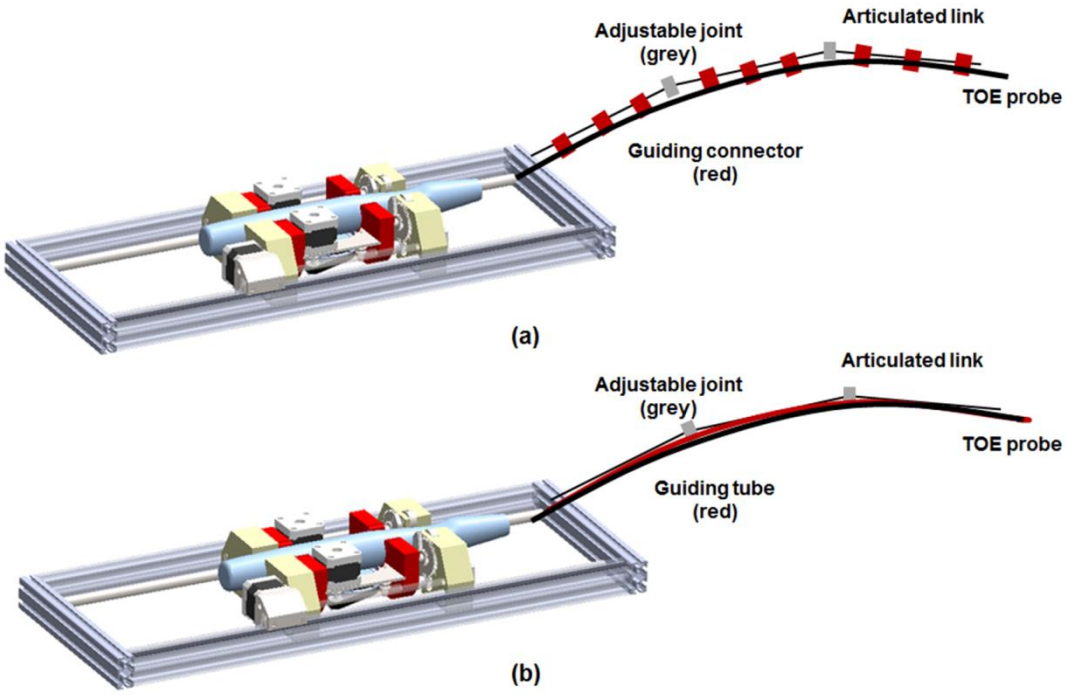


**Fig. 3.8. Illustration of the guiding mechanism for transferring the translational motion of the robotic stage to the probe tip in patients with (a) the use of guiding connectors or (b) the use of a guiding tube and an articulated link.**

In practice, when the robot is used for scanning a patient, a guiding mechanism for the probe's endoscopic portion is required to lead the probe from the robotic system to the patient's oral cavity. This structure is important as it guarantees the translational movements of the robotic stage in driving the probe can be correctly transferred to the movement of the probe tip inside the patient's oral cavity and oesophagus. Several ideas using articulation links with guiding connectors or a tube are shown in Fig. 3.8. The guiding mechanism includes articulation links and a few adjustable joints. The articulation joints can be easily adjusted with screws, forming an ideal path for the endoscopic portion of the probe. For the design with guiding connectors (Fig. 3.8a), each of the connectors can be partly opened, allowing the insertion of the endoscopic portion of the probe and the attachment to the bars. With a few guiding connectors attached to the bars, the probe can be driven so that it follows the path smoothly without any undesired movement in other axes. For the solution using a guiding tube (Fig. 3.8b) a semi-flexible tube with the ability to be curved is mounted onto the articulation links to provide the path for the probe. It should be noted that the design for the guiding

mechanism was intended for the phantom and cadaver experiments. A similar concept could be adapted and further improved with better features in terms of patient acceptance for clinical trials in the future.

## 3.3 Electronics and Control of the TOE Robot

### 3.3.1 Electronic architecture

The electronic design and architecture of the robot can be divided into two parts: the control circuit for the two-axis motorized handle drive and the control circuit for the translational and rotational axes. Since the two-axis handle control structure needs to rotate about the long axis of the robot, electronic wires coming out from this structure have a chance to be cut while the piece rotates and thus cause failures to the handle control structure. To solve this potential problem, a fully wireless design is employed for the handle control piece, in which all electronics, including the powering system, are integrated into the mechanical structures. By separating the electronics of the handle control piece with the other two axes, the handle control piece can also be used as an individual piece.

The interfacing circuit for the handle control piece includes the power system, in which a voltage regulator is used to provide two voltage levels for motors, motor drivers (A4988, Adafruit Industries), magnetic position sensor modules, and an Arduino Nano microcontroller. The Bluetooth module (HC-09, Adafruit Industries) is attached to the Arduino Nano serial lines for remote communication and the motor drivers in the system are connected to the Arduino's digital pins. The magnetic position sensor modules are specifically utilized for safety purposes which will be explained in a subsequent subsection. The electronic architecture of the handle control piece is shown in Fig. 3.9c and Fig. 3.9d. All electronics are wired inside of the handle control piece and protected with a bottom protection piece on the handle control structure as shown in Fig. 3.9e and Fig. 3.9f.

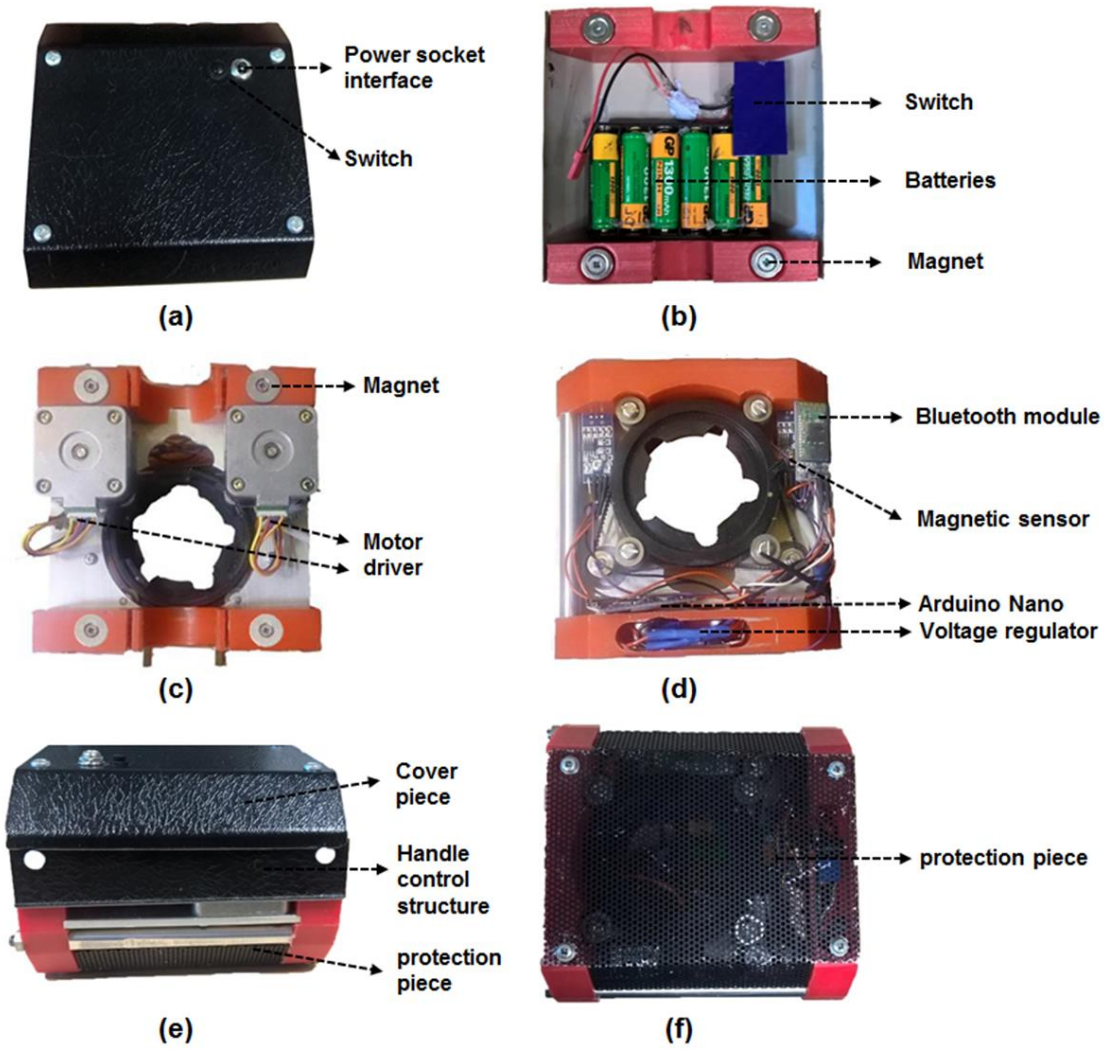


**Fig. 3.9. Electronic architecture of the handle control piece. (a) Top view of the cover piece. (b) Bottom view of the cover piece. (c) Top view of the handle control structure. (d) Bottom view of the handle control structure. (e) Side view of the complete piece. (f) Bottom view of the complete piece.**

The whole piece is powered by six rechargeable batteries (9V) packed into a covering piece (Fig. 3.9a and Fig. 3.9b). This covering piece has two magnets embedded at the bottom, allowing it to be tightly placed onto the handle control piece, which accordingly also has the other two magnets for mating. In order to easily charge the batteries while running the robotic system, the covering piece includes a female power socket interface built on the top, allowing those embedded batteries to be charged via an external power supply using a 9V DC male power adapter. The piece also has a power switch on the top as shown in Fig. 3.9a, allowing the power to be immediately enabled or disabled by connecting or disconnecting the battery output and the electronics. A power indication red LED is included into the plastic piece (front block) of the handle control structure, serving as an alert.

The interface circuits for the drives of the other translational and rotational axes, including another Arduino Nano, motor drivers, and the voltage regulator, are all embedded into a small black box mounted onto the end block of the robot (Fig. 3.10a). This electronics box, as part of the robot system, moves along with the whole structure on the rail. The electronic wires from the motors to the electronics box are protected and fixed into a sheath, mounted beneath the whole robot (Fig. 3.10b). These interface circuits and the motors for the translation and rotation are powered by a separate external power supply, which can be directly plugged into the electronics box via a power socket interface on the top of the black box. The Arduino Nano used for controlling the motors for the translation and rotation is temporarily connected via USB cable for the convenience of programming the microcontroller in the development stage. However, the same Bluetooth module used for the handle control structure can be easily implemented.

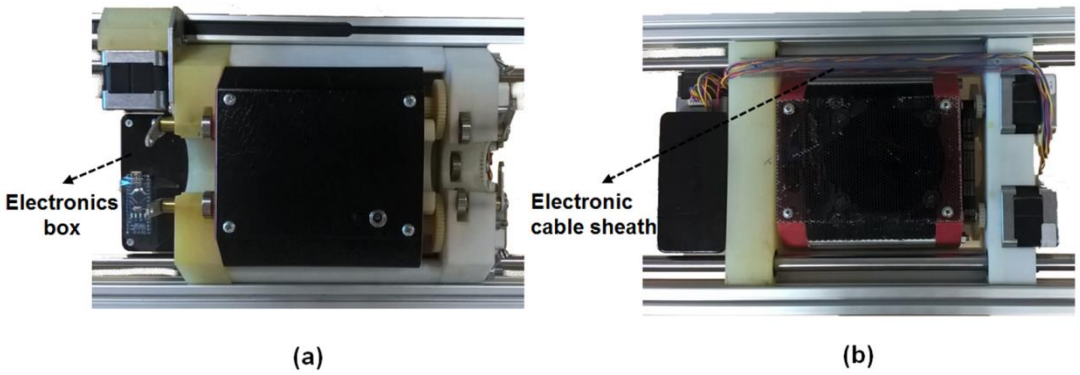


**Fig. 3.10. Electronic architectures of the translational and rotational axes. (a) Front view with the electronics box shown. (b) Back view with the electronic cable sheath shown.**

### 3.3.2 Software control of the TOE robot

The control of the robot is based on a master-slave configuration. A PC works as the master device where Visual C# is utilized as the programming language. An Arduino Nano microcontroller is used as the slave processor. This microcontroller has its own programming language, Arduino C, which is used to pre-program the microcontroller to operate sensors, motors, and interfacing circuits. The Arduino can communicate with the PC via standard serial communication. It listens to the serial commands received from the PC and executes certain operations according to the pre-programmed code loaded into the controller. For this system, a custom TOE robot protocol was developed, which involves motor control, sensor processing, manipulation of I/O pins, and data exchange. This protocol serves as an interface where one side of it guides the hardware operation of the robot and the other side can be interfaced with various control options.

There are four different control options available for the TOE robot, including software control, gamepad control, dummy probe control, and haptic control. The whole working principle of the TOE robot control is shown in Fig. 3.11.

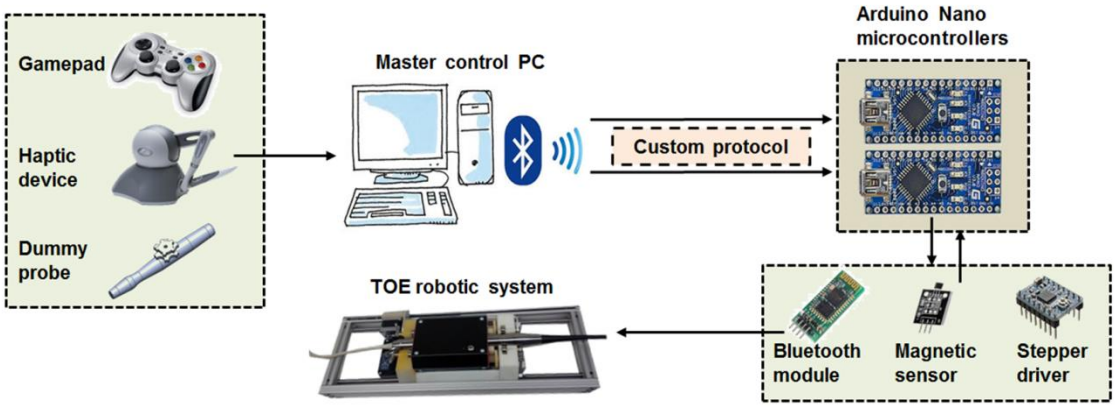


**Fig. 3.11. Flow diagram of the control method for the TOE robot. Different control options including software, gamepad, haptic device, and dummy probe, can be interfaced with the control master PC. The slave Arduino Nano microcontrollers, using the custom protocol, drive the electronics of the TOE robot.**

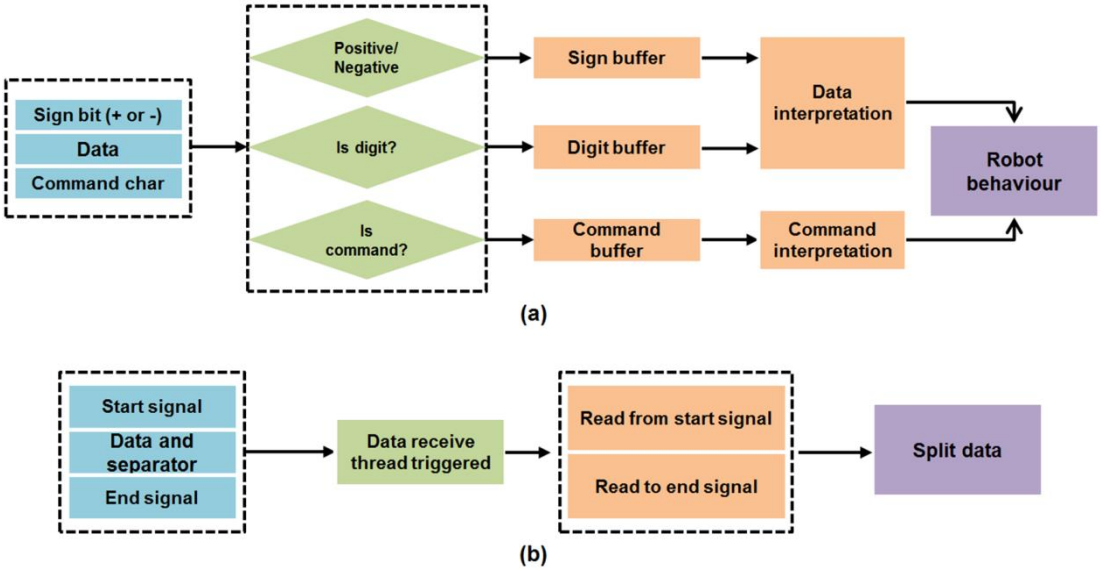


**Fig. 3.12. Data sending and receiving workflow. (a) Data transmission protocol for sending data from the PC to the microcontrollers of the robot. (b) Data transmission protocol for receiving data to the PC.**

The custom TOE robot protocol mainly includes the function of automatic robot detection, sending instructions to the robot, sending data to the robot, and receiving data from the robot. For automatic Arduino detection, the user needs to establish the Bluetooth communication first and pair the robot with the computer. By sending a PING message and listening to the response from the Arduino, the robot can be automatically detected and connected with the PC. To send instructions via the protocol,

a verification mechanism was established between the PC and the Arduino. In order to simplify this protocol and increase the speed of the Arduino, transmitted instructions consist only of characters. By using this custom protocol, a single character sent by the PC corresponds to a particular action carried out by the Arduino. The protocol of sending data from the PC to the Arduino includes basic motor control information and other data for I/O manipulations. This is done by designing a data transmission and receiving protocol (Fig. 3.12a) which is pre-programmed into the Arduino and triggered by the PC main program [187].

For the software control of the robot, different control modes can be selected, including a direct motor move, motor jogging or continuous move, and sequence move. A direct motor move allows individual driving of the five motors in the system, controlling the 4-DOF movement. In each axis, the controls can drive the motor with different speed and acceleration, set the current position to be the zero position, and go to a desired absolute position referenced to the current zero position. The motor jogging or continuous move mode allows two different motor control modes for each axis. In motor jogging mode, each motor runs in micro steps. By clicking the buttons, the motor will run a certain number of steps. In continuous mode, the motor will keep running when the button is pressed and held, and it will stop running when the button is released. The sequence control mode allows a number of motors to run simultaneously and with different pre-designed sequences.

### 3.3.3 Control of the TOE robot using hand-held devices

In this section, three different control options of the TOE robot using hand-held devices are introduced, including using a gamepad, a dummy probe, and a haptic device. This is mainly to investigate the possibility of hand-held devices for controlling the TOE robot. It is expected using these devices may have better intuitive controls of the robot compared to the mouse-based software control since the operator can hold the control device while at the same time focus on looking at the screen of the ultrasound machine. In addition, the dummy probe introduced in this section has a similar structure to the original TOE probe which may make it easier to be used by the operator when working with the TOE robot. This section focuses on introducing the basic method for incorporating these control options with the robot and the control software. It should be noted that only the preliminary correct working of the individual control options of the robot has been tested. A comparative study with other control options and a user

experience study are not included in this work because of the unavailability of a realistic TOE environment for robotic test and because the focus has been on the automatic control aspects of the study. This will be discussed in more detail in the last section of this chapter.

- Control of the TOE robot using a gamepad

Apart from the software control, a gamepad is another choice for control of the TOE robot. The gamepad is interfaced with C# via DirectX provided by Microsoft [188]. DirectX is a set of low-level application programming interfaces (APIs) for creating applications. The C# application takes all the input from the gamepad, processes those input data, and then sends appropriate commands to the Arduino via the protocol. The gamepad control of the robot is similar to the continuous move mode in the software control option. By holding physical buttons on the gamepad, the appropriate axes are actuated (Fig. 3.13).

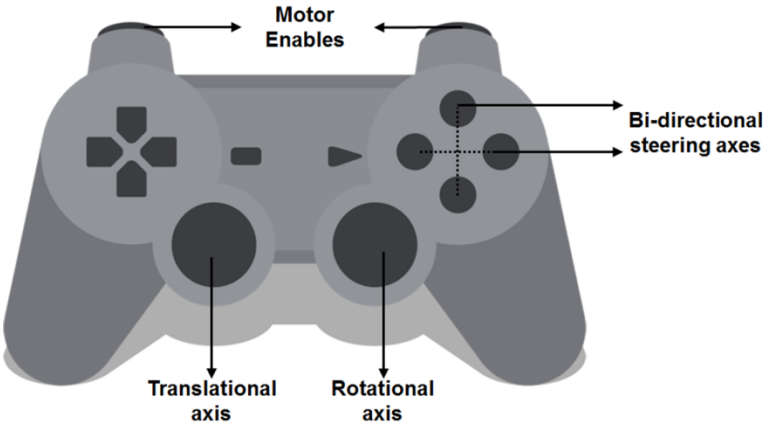


**Fig. 3.13. Diagram of the gamepad input assignments for the TOE robot control.**

- Control of the TOE robot using a dummy probe

For control of the robot using a dummy probe, a dummy probe handle has been developed, serving as the master control device, for intuitive remote operation of the robot (Fig. 3.14). This dummy probe has a similar shape to the original TOE probe handle and has built-in sensors to interpret users' inputs. A pair of buttons on the dummy probe translate the probe by driving the linear motion of the robot. A rotating handle, which can rotate about the long axis of the dummy probe, is used for actuating the rotation axis of the robot. The rotating handle, with notches inside of the structure,

mates with the main dummy probe's back extension and can rotate freely about its long axis with the utilization of low-friction plastic. A potentiometer embedded inside of the rotating handle, with four grab screws pushing against its shaft for fixing, is used to sense the amount of rotational movement. Several gaps are designed for the purpose of assembling the rotating handle to the main dummy probe as it allows the rotating handle to deform slightly with the plastic torsion. This gives enough tolerance for the assembly while also keeps the rotating handle tightly mated with the dummy probe.

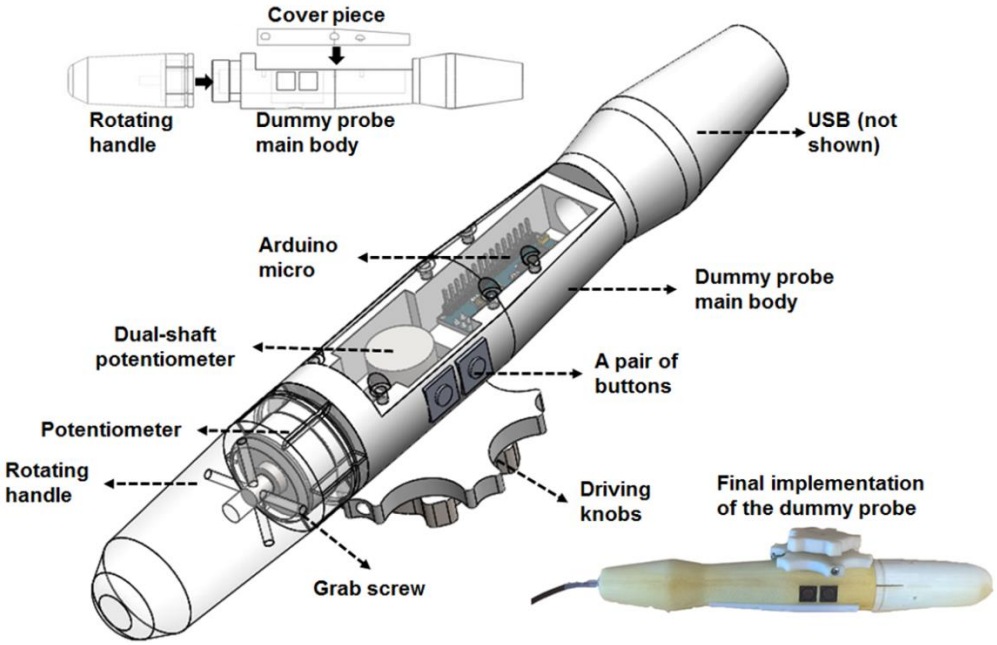


**Fig. 3.14. Design and implementation of the dummy probe control device.**

A dual-shaft driving knob pair is used for rotating the similar knobs on the original probe handle for bi-directional bending of the probe head. These knobs are mounted onto a dual-shaft potentiometer with grab screws so the input movements of the knobs can be sensed. Inside of the dummy probe, the cavity is designed for housing an Arduino Micro microcontroller (Adafruit Industries). Potentiometers and buttons are electronically connected to the microprocessor and the data inputs are transmitted to the PC via a USB cable extending out from the dummy probe.

- Control of the TOE robot using a haptic device

The last option to control the TOE robot provided in this study is to use a commercial haptic device (Phantom Omni® Haptic Device, Sensable & Geomagic). Though force sensing is not primarily required for this robotic application, the haptic device can generate constraints on the movement with its built-in force generating law. This feature

enables the haptic device's movements to be limited in certain ranges and exaggerated forces are required in order to overcome the constraints and move the robot beyond the designed working range. The haptic device used in this study has 6-DOF movement. Four axes of the joystick are mapped to the TOE robot. These are the rotation of the pointer mapped to the rotation of the probe, the left-right (X) and up-down (Y) translation of the pointer mapped to the bi-directional steering of the probe, and the forward-backward (Z) translation of the pointer mapped to the linear motion of the probe (Fig. 3.15). With the constraint function included, the pointer's X and Y axis movements are limited to designed boundaries, corresponding to the maximum movements allowed for the bi-directional steering axes of the robot. With the IEEE-1394a FireWire cable for data transmission and the OpenHaptics API (Sensable & Geomagic) for program design [189, 190], the haptic device is interfaced with the main robot control software to communicate with the robotic system.


**Fig. 3.15. Control of the TOE robot with a haptic device. (a) Phantom Omni haptic device and its axes definition. Figure adapted from [191]. (b) Photo showing the probe tip bending controlled with the haptic device.**

## 3.4 Safety Features of the TOE Robot

### 3.4.1 Overall safety control of the robot

The general safety design of the TOE robot includes several features to allow the probe to work in a safe state (Fig. 3.16). To address the concerns of manipulating the TOE probe, which could potentially result in injuries to patients as reviewed in Section 1.4, active safety sensors and passive safety feature are employed. The active safety sensors are designed to measure the neutralization of the TOE probe tip (not in any flexion

state), as translating the probe when it is in a flexion state could result in injuries to tissues. This includes two magnetic sensors monitoring the neutralization of the driving discs, which will be explained in Section 3.4.2. The passive force limiting feature includes motor current limiting for the two bending axes to guarantee that the maximum force generated due to the bending of the probe tip is less than the maximum force generated manually. Details of the experiments measuring the force and setting the current are explained in Section 3.4.3. Additionally, several safety features have been included in the software for safe operation. This includes a watchdog between the microcontrollers and the PC which continually monitors the connection by checking periodically refreshed signals and various software logics to ensure that motor actuation works in conjunction with the safety sensors. Furthermore, the stepper motors are powered in a range such that their maximum generated torque would not break the internal mechanisms of the probe. Thus the safety features of the original TOE probe [186], which have been clinically tested for many years, are still available in the robotic system. With the add-on design, The TOE operator can also manually retract the probe from the patient or unplug the probe from the robotic holder to switch back to manual control.

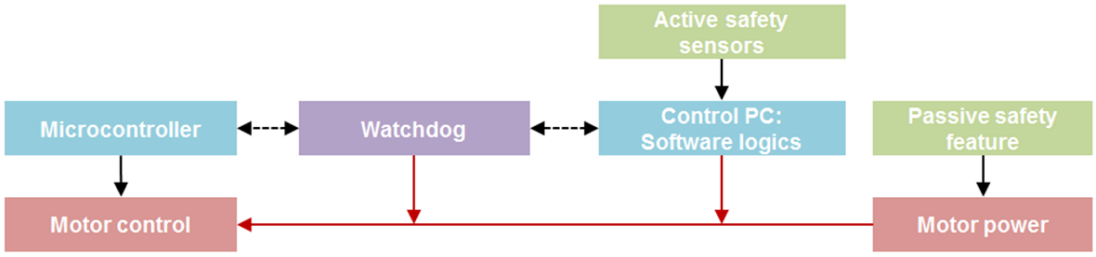


**Fig. 3.16. Overview of the safety features implemented in the motor control of the TOE robot.**

### 3.4.2 Active safety sensors

As reviewed in Section 1.4, one of the most serious potential injuries due to probe manipulation results from moving the probe when it is in a flexion state; either left-right bending or anteflex-retroflex bending. This could happen when the probe is bent in the pharynx, middle oesophagus, or stomach and gastroesophageal junction. Considerable tension is applied on the tissue if the probe is forcefully retrograded or advanced. To address this concern when a robotic TOE system is utilized, it was stated in Section 1.6 that an active safety sensor should be included into the robotic system for measuring the neutralization of the probe tip. With this neutralization sensing device, the TOE robot should only be actuated for translational movements when the probe is not in any flexion state.

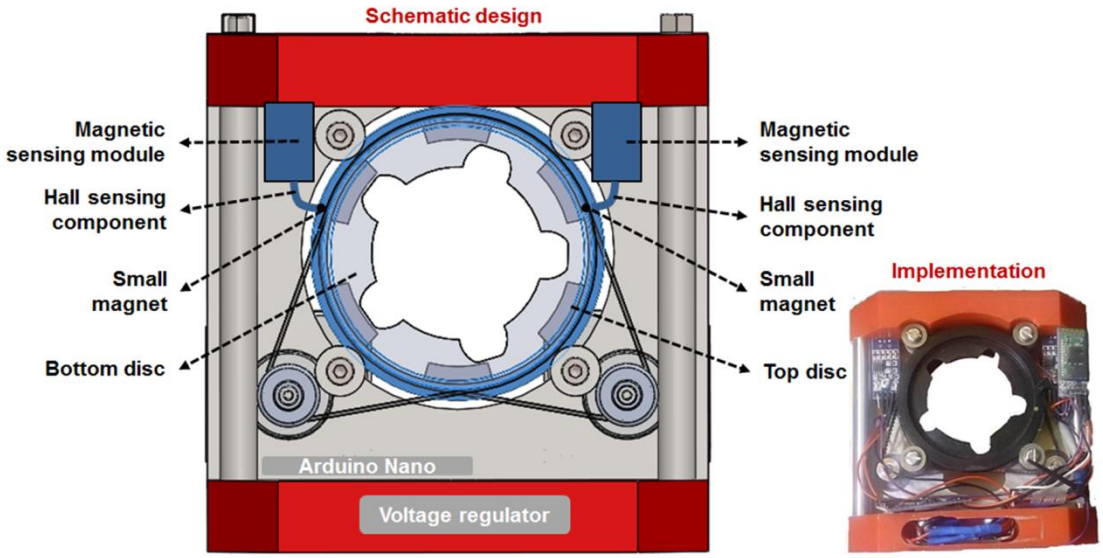


**Fig. 3.17. Schematic illustration and implementation of the design for monitoring the neutralization of the two driving discs. The electronic wiring and Bluetooth module are not shown in the schematic drawing. Details of these components are presented in the previous sections.**

In the proposed TOE robot design, the flexion of the probe tip is directly controlled by the handle control structure, which includes two mating discs driven by belt mechanisms. These two discs control the movements of the knobs on the original TOE probe, thus operating the bi-directional bending of the probe tip. With such a configuration, the neutralization of the probe tip is directly determined by whether the two driving discs are in the home or neutral position. In the current design, two small circular magnets (1mm diameter) are embedded into the two discs' flanges by machining and supergluing. These serve as two trackers to locate the initial home or neutral position of the two driving discs, so as to neutralize the tip of the TOE probe. These magnets have been tested to verify that they can provide enough magnetic field for the sensing devices to detect.

To track these two magnets, two Hall-effect magnetic sensing modules are included into the handle control structure. The sensing components (A3144EUA, Allegro MicroSystems) of the magnetic sensing module extend into the discs actuating mechanisms, facing downward to the flanges of the two discs where two magnets are embedded. The supporting circuits for the sensing components, as parts of the module, are mounted to the plastic block of the handle structure. As the discs rotate, the embedded magnets rotate as well. For the sensing devices, when the magnetic field rises above a threshold level (35-450 Gauss), an open-collector output transistor switches on. This then gives a digital output immediately (< 2us) to the Arduino Nano microcontroller, indicating that the embedded magnets are in the place where the

sensing components are mounted. The magnets are embedded in special locations on the discs so that they arrive at the sensing components only when the driving discs of the knobs are in neutral positions. For better accuracy of the triggering level, the analog output of the sensing components was used and a custom threshold could be defined to accurately control the rotational position of the discs. The whole schematic design and implementation are shown in Fig. 3.17.

With the magnetic position sensing of the discs, the outputs of the two sensors are recorded by the microcontroller almost in real time (clock speed: 16 MHz). This information is sent to the PC master software and monitored in a background thread continuously. For any command given by the master software to translate the probe, including commands from any other input devices (gamepad, dummy probe, or haptic device), this can only be sent to the microcontroller when the sensing information indicates that the discs are in neutral positions. Furthermore, the microcontroller is programmed with the logic that the motor for the translational mechanism is disabled when the discs are not in the neutral positions. Therefore, the probe can only be removed or translated to a new position when the knobs, and the probe tip, are in the neutral position.

### 3.4.3 Passive safety

The passive safety feature focuses on motor current limiting for the two bending axes to guarantee that the maximum force due to the bending of the probe tip generated robotically is less than the maximum force generated manually. As reviewed in Section 1.4, though compression due to bending of the probe tip has the potential to cause injury, only limited case reports have been found in the literature. Other research reviewed also indicates that prolonged TOE use with excessive probe bending has no clear harmful effects on the oesophagus. In addition, the bending mechanism of the original TOE probe had the force limiting factor suggested by the patent [186]. Therefore, it is believed that the force due to the tip bending is not the primary concern for the safety of TOE and a passive current limiting method for the robotic system would be adequate to address the concern.

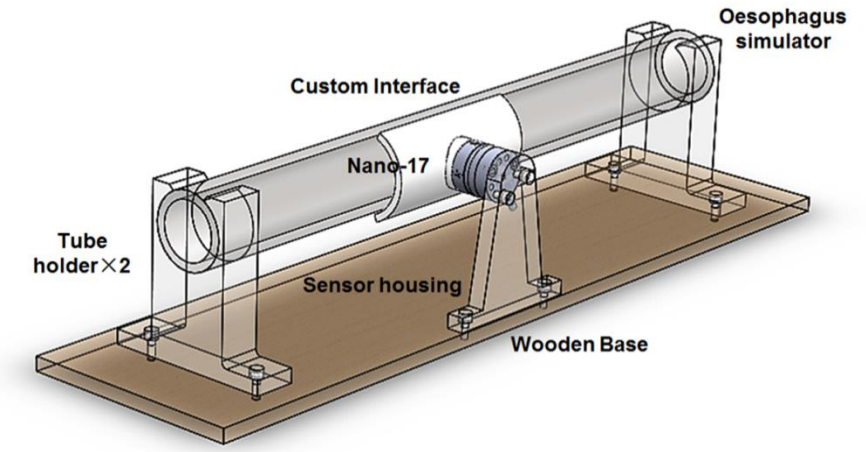


**Fig. 3.18. Schematic illustration of the experimental setup for measurement of the force due to the bending of the probe tip using an oesophagus simulator and a commercial force sensor Nano-17.**

Since the handle control structure drives the probe tip bending in two axes which cause radial contact force to the oesophagus, the robotic motor current limiting method focuses on the investigation of handle control. The handle control structure consists of two rotational wheels precisely formed to mate with and drive the two knobs on the original TOE probe handle via belt mechanisms controlled by two stepper motors. In the design of the original TOE probe, the probe tip is bent by pulling and extending control wires from a control portion coupled to the proximal end and the control portion is attached to two control knobs. Therefore, the contact force generated in the tip is related to the tension on the wires, and so to the torque applied to the control knobs. In the robotic system, the torque applied to the control knobs is determined by the driving motors. Electronically, the two stepper motors driving the knobs of the TOE handle are controlled by two stepper motor drivers (A4988, Pololu). The motor's torque would be proportional to ampere-turns (the number of turns of wire in the motor's stator multiplied by the current passing through those turns of wire). The A4988 stepper motor driver provides an active current limiting method in which each full-bridge is controlled by a fixed off-time PWM current control circuit that limits the load current to a desired value. The maximum value of current limiting is set by a trimmer potentiometer on the board and the voltage at the reference pin. This can be measured and adjusted to set the current limiting value of the two motors.

To measure the maximum force generated manually and robotically by the probe tip, a commercial 6-axis force/torque sensor (Nano-17, ATI Industrial Automation) is employed for the measurement. The Nano-17 is made from two stainless steel attachment flanges separated by a silicon sensing layer. The sensing flange of the sensor

is connected to a 3D printed Acrylonitrile butadiene styrene (ABS) plastic sphere placed against different oesophagus simulators in two different experiments (Fig. 3.18). This enables assessment of the simulated oesophagus's ability to push the plastic sphere against a known resistance. The housing flange of the sensor is connected to a 3D printed sensor holder (ABS plastic) providing a mean of securing the sensor to the supporting base. Mechanically, there is no bridge between the mounting and the tool sides as this could lead to incorrect readings of the force/torque. The oesophagus simulator is held by two 3D printed holders (ABS plastic) mounted onto a wooden supporting base.

The oesophagus simulators used in the measurements include a silicone tube (Advanced Fluid, Ltd., Essex, United Kingdom) of 5mm thickness and two custom-made polyvinyl alcohol (PVA) oesophageal phantoms (5mm and 3mm thicknesses respectively). The use of different materials and thicknesses is intended to provide more variations for the simulation of the oesophagus. The PVA oesophageal phantoms are made with PVA cryogel of 10 wt% (Fig. 3.19a). The PVA liquid was first poured into 3D printed ABS plastic moulds (Fig. 3.19b). The liquid was then allowed to rest for 12 hours for air bubbles to rise to the surface. The phantoms were cooled from room temperature to −20° over 2 hours in a standard chest freezer and were kept at -20° for a further 10 hours. The moulds were then removed and allowed to defrost at room temperature for 24 hours. The PVA phantoms were then removed from the mould and stored in water, ready for use (Fig. 3.19c).

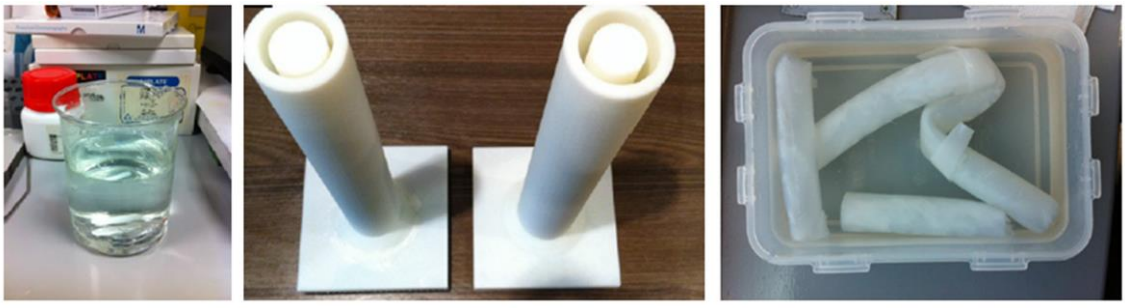


**Fig. 3.19. Custom-made oesophagus simulators using PVA. (a) Beaker with the clear PVA cryogel. (b) 3mm and 5mm wall thickness ABS plastic moulds made by 3D printing. (c) Resulting PVA oesophageal phantoms of 3mm and 5mm wall thickness stored in distilled water.**

Two positions which can generate radial contact force were evaluated by manual measurement. This includes the tip position where the ultrasound transducer is embedded and the bending segment which forms a curvature during bending (Fig. 3.20).

The initial radial force when inserting the probe and the bending force were recorded separately. The actual force during bending was then obtained by deducting the initial force from the bending force. The manual operation of the knob bending task was measured when maximum possible forces for rotating the two knobs were applied. This was performed by three different people and the average forces for the tip position and the bending segment were used as the results of the manual control. The same experiment as the manual measurement was repeated using robotic control of the TOE probe. For each of the measurements, six different current settings were adjusted in advance, covering the range from 90 mA to 560 mA, corresponding to a measured voltage ranging from 0.15V to 0.9V. It was already verified that the minimum current limiting setting required to fully rotate the TOE probe knobs using the robot is 90 mA. To achieve high step rates, the motor supply voltage (7.5V) was set higher than the rated voltage (5V). The corresponding current was required to be less than the rated current (500 mA) for continuous actuation of the motors. The current limiting setting range investigated in this study is adequate to cover the whole working range of the current setup allowed for the bending axes.

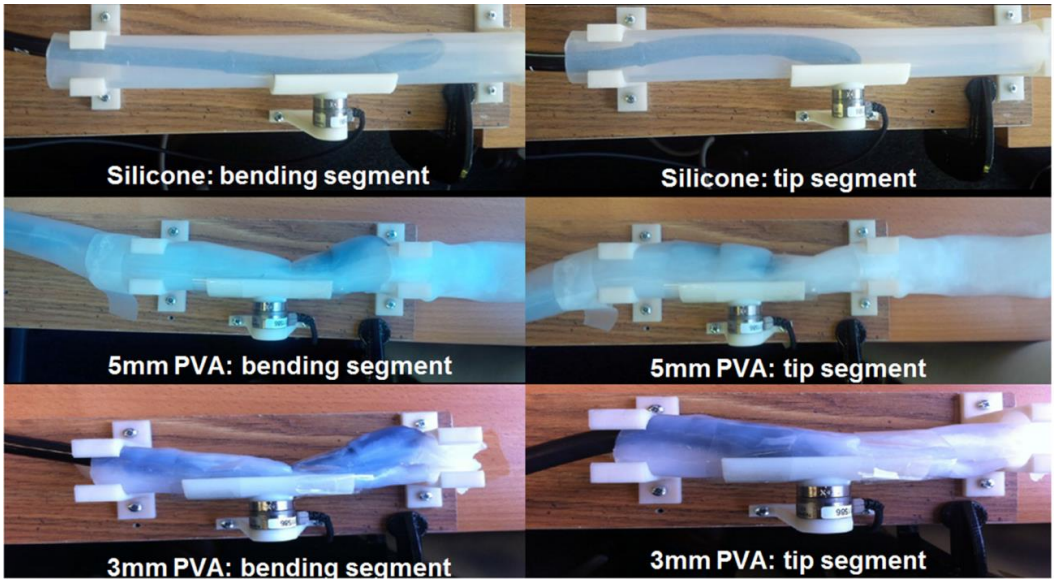


**Fig. 3.20. Force measurement experiment for two positions using different oesophagus simulators including a silicone tube, a 5mm PVA tube, and a 3mm PVA tube.**

The measurement results of three different oesophagus phantoms for both manual and robotic control are shown in Fig. 3.21. Though different oesophagus phantoms were used, all 3 oesophagus simulators (silicone, 5mm PVA and 3mm PVA) gave very similar motor current intersect values despite the spread of force data. The intersect points refer to the same radial force obtained from the robotic and manual measurement. In general, the value of the current limiting setting less than the corresponding value of

the intersect points for the robotic control yields less resulting force compared with the manual operation for all the three setups. Therefore, in the same experimental setup (same material and thickness), it is concluded that the relationship between manual and robotic control is similar. The intersect values for the two different measured points in a similar setup tends to be slightly different to each other. The smaller one with its corresponding current setting is selected as the resulting value as this guarantees that in both of the two measured points the robot generates less maximum force than the manual control. Among the three different setups, the minimum resulting current setting was selected as the final target as this guarantees that below this value in all the setups the robot generates less maximum force than the manual control. Therefore, a reasonable working region of the motor current setting is then identified within the range (90-220mA) where the maximum force generated robotically is less than that generated manually. This also indicates that the robotic system can manipulate the probe at a motor current which generates less force compared to human operation therefore reducing the force applied to the oesophagus and reducing the risk of injury.

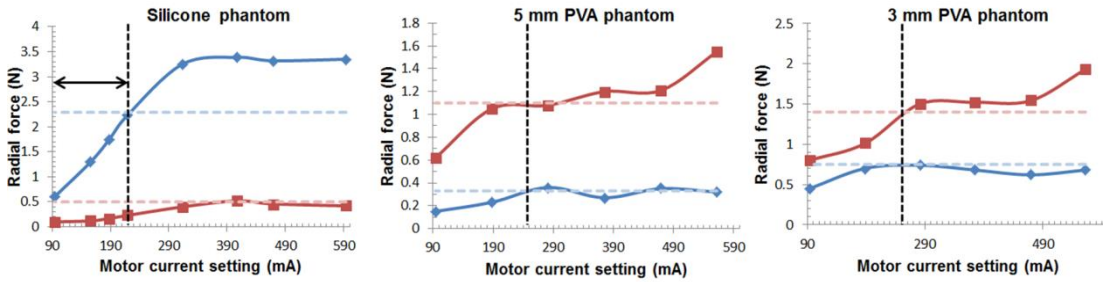


**Fig. 3.21. Force measurement results on different oesophagus simulators both manually (dotted lines) and robotically (full lines) for the bending segment (blue) and tip segment (red).**

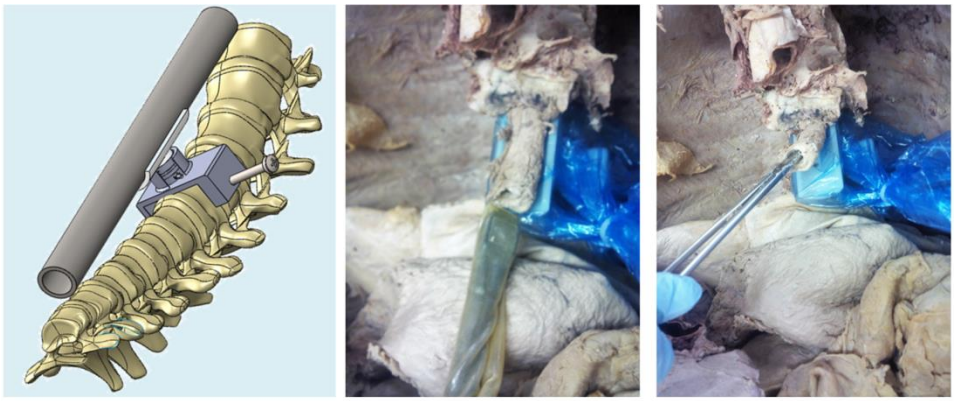


**Fig. 3.22. Cadaver force measurement experiment. (a) Schematic illustration of the G-clamp with sensor housing and oesophagus support/interface. (b) The TOE probe in a sterile cover and the sensor housing under the oesophagus (blue protection cover). (c) Surgical forceps inserted into the oesophagus showing the narrow calibre of the orifice which prevented probe insertion.**

The same force measurement experiment was also attempted in cadavers in order to obtain more realistic data. The sensing flange of the sensor was still attached with the plastic sphere as described above to make contact with the cadaveric oesophagus. In order to secure the sensor, a custom designed G-clamp was employed serving as the housing structure of the sensor. The clamp can be adjusted by a screw and attached to the cadaveric spine as shown in Fig. 3.22a. This mechanical housing has two functions: (1) secure the Nano-17 sensor; (2) protect the Nano-17 from contacting with internal body structures. In the design, there is a small gap between the Nano-17 and the housing structure to ensure the sensor is not in contact with the housing. When placed in the human cadaver, there is fluid present (usually water which is sprayed to prevent specimens drying) so a plastic wrap was placed to waterproof the sensor. The use of the cadaveric human oesophagus for the force measurement experiment proved unsuccessful due to technical difficulties with inserting the TOE probe into an inelastic oesophagus (it was unable to fit as shown in Fig. 3.22b and Fig. 3.22c). When the deceased person is embalmed for educational purposes, the chemical used (formalin) in the process fixes the tissues in the rigor state. As the oesophagus is a muscle with both circular and longitudinal fibre, loss of circulation (which occurs in death) leads to an inability of the muscle to relax. In the living oesophagus, passage of the probe is permitted due to muscle relaxation and peristaltic movements.

### 3.4.4 Risk assessment

With the general safety parameters described in the previous sections, a Risk Assessment (also known as Hazard Analysis) is presented in this section. This is one step of an overall Risk Management process, as required by ISO 14971 (Application of risk management to medical devices). Here in this thesis, a simplified Failure Modes Effects Analysis (FMEA) [192] is performed (Table 3.1). The FMEA is a bottom-up analysis, where the potential system failure is determined for each possible component failure [193]. Methods of control are devised to mitigate the hazards associated with these failures. It should be noted that the FMEA is a proactive analysis that should begin early in the design phase and evolve repeatedly as hazards are identified and methods of control are developed. To this stage, the simplified FMEA analysis performed in this thesis focuses on analysing the use of the proposed TOE robot via software from a PC under the control of a trained operator.

**Table 3.1. Simplified FMEA risk assessment of the TOE robot (MCU, Microcontroller)**

| Failure Mode | Effects on System | Potential Cause | Proposed Control |
|---|---|---|---|
| Uncontrolled stepper motor current | Excessed bending/ rotational/translational force generated | Failure of stepper motor | Use of low-power motor |
| | | Failure of motor driver | |
| | | Failure of MCU | Watchdog to stop robot operation |
| | | Failure of power system | |
| Incorrect step counting of stepper motor | Incorrect bending/ rotational/translational motion | Failure of stepper motor | Additional tip tracking methods (sensor/image-based) |
| | | Failure of motor driver | |
| | | Failure of MCU | Watchdog to stop robot operation |
| | | Failure of power system | |
| Loss of home position monitoring | Unknown neutralization state of the bending tip | Failure of Hall sensor | Additional tip tracking methods (sensor/image-based) |
| | | Failure of MCU | Watchdog to stop robot operation |
| | | Failure of power system | |
| Probe tip remains at previous position when new command is given | Incorrect bending/ rotational/translational motion | Failures of driving mechanism (pulley-belt/gear train/linear belt) | Manual override of the probe from the operator |
| | | Failure of stepper motor | |
| | | Failure of motor driver | |
| | | Failure of MCU | Watchdog to stop robot operation |
| | | Failure of power system | |
| Probe tip cannot retain its position | Cannot lock the probe | Failures of driving mechanism (pulley-belt/gear train/linear belt) | Manual override of the probe from the operator |
| | | Failure of stepper motor | |
| | | Failure of motor driver | |
| | | Failure of MCU | Watchdog to stop robot operation |
| | | Failure of power system | |
| Probe cannot be plugged in/taken out from the robot mechanism | Unable to use the robot/ release the probe | Failures of knob driving mechanism | Manual override of the probe from the operator |
| Robot does not respond/ cannot be connected | Unable to use the robot | Failure of Bluetooth/Serial communication | Manual override of the probe from the operator |
| | | Failure of MCU | |
| | | Failure of power system | |

## 3.5 Repeatability of the TOE Robot

To evaluate the basic performance of the TOE robot, a repeatability test was performed. The primary goal of this experiment was to assess the reliability of the mechanical and

electronic design of the robot system. This can be verified by investigating the repeatability of the probe tip position when the same sets of motor parameters are given. The experimental setup is shown in Fig. 3.23. The robotic TOE system was placed on a desk with the TOE probe inserted. The flexible gastroscope section of the TOE probe was constrained using a guide tube. An Optotrak system (Northern Digital Inc.) was employed to measure the position and orientation of the TOE probe tip. The Optotrak system is a non-contact motion measurement system where high accuracy (0.1 mm) is expected to measure movements up to the speed of 4600 Hz based on the manufacturing data. Independent accuracy evaluation studies for several similar optical tracking systems from literatures have indicated an accuracy ranging from 0.2 to 1.15 mm when in practical use [194, 195]. Because of the verified high accuracy performance of the system working in different environments, the optical tracking method with the selected device is believed to be an ideal choice to reliably evaluate the performance of the robot. The measurement is achieved by tracking numbers of small infrared (IRED) position markers which are attached to a subject. Three position markers are needed to determine the 3D orientation of a body. However more markers are preferred since they can be blocked by movement. The movements of the subject are usually measured by recording the 3D poses of the subject relative to a fixed coordinate system. The positions of the cameras that track the sensors are pre-calibrated. The position sensor must not be blocked at any time since it is an optical system. If markers go out of view, they will be automatically identified by the system. The three dimensional positions of markers are determined in real-time for viewing and processing. At the same time, data can be saved to file for post-analysis.

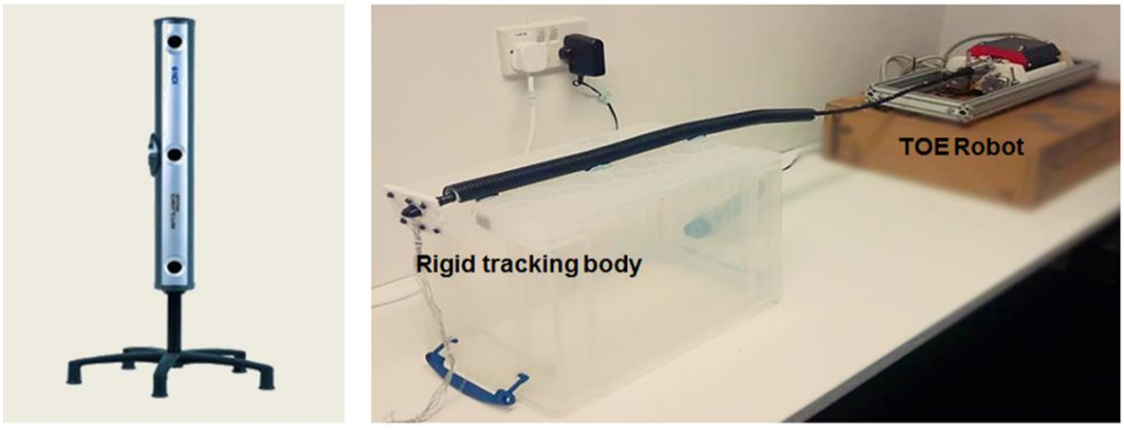


**Fig. 3.23. Repeatability experimental setup. (a) Optotrak measurement system from Northern Digital Inc. (b) Bench setup with the rigid tracking body and the TOE robot.**

In this experiment, a rigid tracking body with six IRED sensors was attached at the rigid section of the probe tip and used for validation. By investigating the transformation between the tracking and reference coordinates, the position of the probe tip was located and the repeatability was assessed. The tracking coordinates representing the rigid tracking body specify the pose of the probe tip. This is defined arbitrarily by the IRED sensors but fixed during the experiment. The amount of movement of the probe tip can be analysed by the changes of the pose of the tracking coordinates recorded relative to the reference coordinates. The reference coordinates are defined by another rigid body (not shown in Fig. 3.23) which is fixed onto the table during the whole experiment.

During the experiment, the robotic system was controlled via a computer, which steered the tip of the probe in two planes, rotated the probe about its shaft, and translated the probe along its axis. For each of the steering processes, the bending tip was curved from -40 degrees to +40 degrees with a difference of four degrees in each step. For the rotation and translation processes, the probe was rotated 0 degrees to 360 degrees with a difference of 18 degrees in each step and translated from the initial position to 50cm with steps of 2.5cm. For each of the axes, the measurement process was repeated four times (N=84) to acquire the repeatability performance of the robotic system. Each set of data (N=21) for each axis was compared with the other three sets. For the same motor inputs, the differences of the orientation and position outputs between different sets were defined as orientation and position errors. This were quantified based on decomposing each transformation matrix and extracting the position vector referring to translation along and Euler angles referring to rotations about the X-, Y- and Z-axes. Root mean squares (RMS) of the differences between the X-, Y-, and Z-axes rotation ($\theta$ and $\theta'$ for two different sets) and translation ($t$ and $t'$ for two different sets) components were calculated. The results of the repeatability experiments are summarized in Table 3.1. It shows the mean and standard deviation of the error over for each axis.

**Table 3.2. Orientation and distance errors of the manipulator system**

| Axes | Orientation error (mean±std) | Position error (mean±std) |
|---|---|---|
| Left-right steering | 0.46° ± 0.18° | 0.71mm ± 0.45mm |
| Anteflex-retroflex steering | 0.82° ± 0.51° | 1.00mm ± 0.82mm |
| Handle rotation | 1.27° ± 0.44° | 0.89mm ± 0.37mm |
| Handle translation | 0.57° ± 0.34° | 0.32mm ± 0.15mm |

## 3.6 Summary and Discussion

In this chapter, a new concept and prototype to manipulate a standard TOE probe has been presented. The primary goal is to provide the cardiologist a remote control approach for standard TOE scanning so they can work in a zero radiation environment with a comfortable posture for the duration of long cardiac procedures. The design and implementation of the proposed system has been described, which is the first TOE robotic system introduced. A complete list of the manufacturers' details of the current prototype is summarized in Table 3.3.

**Table 3.3. Manufacturers' details of the current robot prototype**

| | Components | Details | Vendors |
|---|---|---|---|
| **Handle control** | Knob driving discs | 110-tooth MXL pulley | Retailer from *BeltingOnline* (www.beltingonline.com) |
| | Timing pulleys | 10-tooth MXL T5 Pulley | Machined by Xtronics, Ltd. (Gravesend, Kent, UK) |
| | Timing belts | 112 MXL O-ring timing belt | Retailer from *AliExpress* (https://www.aliexpress.com) |
| | V-groove pulleys | V623ZZ 3 x 12 x 4mm | Retailer from *AliExpress* |
| | Supporting steel plate | Custom-made from machining | Machined by Xtronics, Ltd. |
| **Rotational** | Spur gears | 3D printing - ABS plastic (ProJet™ 3000 HD printer) | 3D Printing services, King's College London |
| | Front and back blocks | | |
| | Rotational bearing | VSB 20mm ball bearing | NationSkander California Corp. (Anaheim, US) |
| **Translational** | Linear motor seat | 3D printing - ABS plastic (ProJet™ 3000 HD printer) | 3D Printing services, King's College London |
| | Linear steel guide rails | V-Slot® Linear Rail | Provided by OpenBuilds (http://openbuildspartstore.com) Manufactured by Xtronics, Ltd. |
| **Electronics** | Microcontrollers | Arduino Nano | Adafruit Industries (New York, United State) |
| | Stepper motors | NEMA 17 - 37mm | Adafruit Industries |
| | Bluetooth module | HC-06 Bluetooth to Serial module | Retailer from *Ebay* (http://www.ebay.co.uk) |
| | Magnetic sensors | A3144EUA Hall sensor | Allegro MicroSystems (Massachusetts, US) |
| | Stepper motor drivers | A4988 micro-stepping bipolar driver | Pololu Robotics & Electronics (Pololu Corporation, Las Vegas, US) |
| | Voltage regulator | 9V-to-5V voltage regulator module | Adafruit Industries |
| **Software** | The robot software was developed using Visual Studio C# 2015 and Arduino IDE | | |

The current implementation manipulates four of the five DOFs of the manual TOE controls. A mechanism for the remaining electronic steering DOF was not included in this preliminary prototype. The described system is lightweight and has a small footprint with all the electronics and control devices built in. The handle control piece for knob control can work stand alone for individual purposes. The proposed driving mechanism can easily be adapted to work with other types of TOE probe on the market by simply changing the shape and dimension of the structure. In addition, the proposed add-on system doesn't change any internal structure of the standard TOE probe. The TOE probe can be easily removed from the robotic system, quickly switching back to manual control mode if necessary. The whole system is designed to work as an individual piece next to the surgical bed, such as standing on a trolley (Fig. 3.24). Different options to manipulate the TOE robot have also been provided, including control from software, a gamepad, a dummy probe, and a haptic device. Preliminary bench testing has been performed sufficient to verify the correct working of these control options.

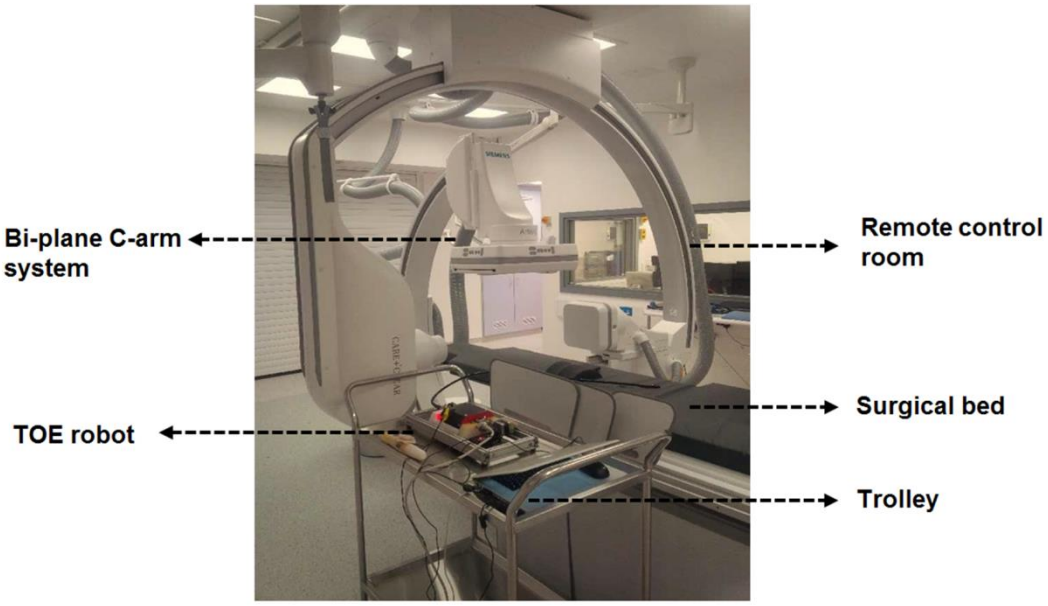


**Fig. 3.24. Possible clinical setup for the TOE robot in the surgical room with the robot sitting on a trolley. The echocardiographer to control the robot could be in the remote control room.**

For the practical clinical use of the robot, the entire clinical scenarios including equipment and room set-ups are shown in Fig. 3.25. The prior art (Fig. 3.25a) shows a typical distribution of theatre staff for cardiac surgical procedures performed using ultrasound and x-ray guidance. During the operation, an echocardiographer holds a TOE probe, which passes through into the patient's oesophagus to monitor the heart. A surgeon is located on an opposite side of the X-ray C-arm and an operating table. The

surgeon navigates devices (not shown) (e.g., catheters and guidewires) for the surgery under X-ray guidance and ultrasound guidance via a manually held TOE probe in order to perform different diagnostic or therapeutic procedures. For the use of the proposed TOE robot, an exemplary embodiment is shown in Fig. 3.25b with a remote controlled actuation of a TOE probe in accordance with the present invention. In this configuration, the TOE probe, manipulated by the proposed robot, is controlled by the echocardiographer (either a cardiologist or an anaesthetist) from a separate room (e.g. the monitoring room) with a robot workstation. The workstation is structurally configured with hardware and software to generate motor commands to the TOE robot via different user inputs as introduced in this Chapter (e.g., joystick, mouse, dummy probe, etc.). The ultrasound images shown on the ultrasound machine inside the surgical room are also fed back to the robot workstation for the echocardiographer. Additionally in a collaborative control scheme between the echocardiographer and the surgeon, appropriate user interfaces for facilitating additional control of the TOE probe from the surgeon could also be included.

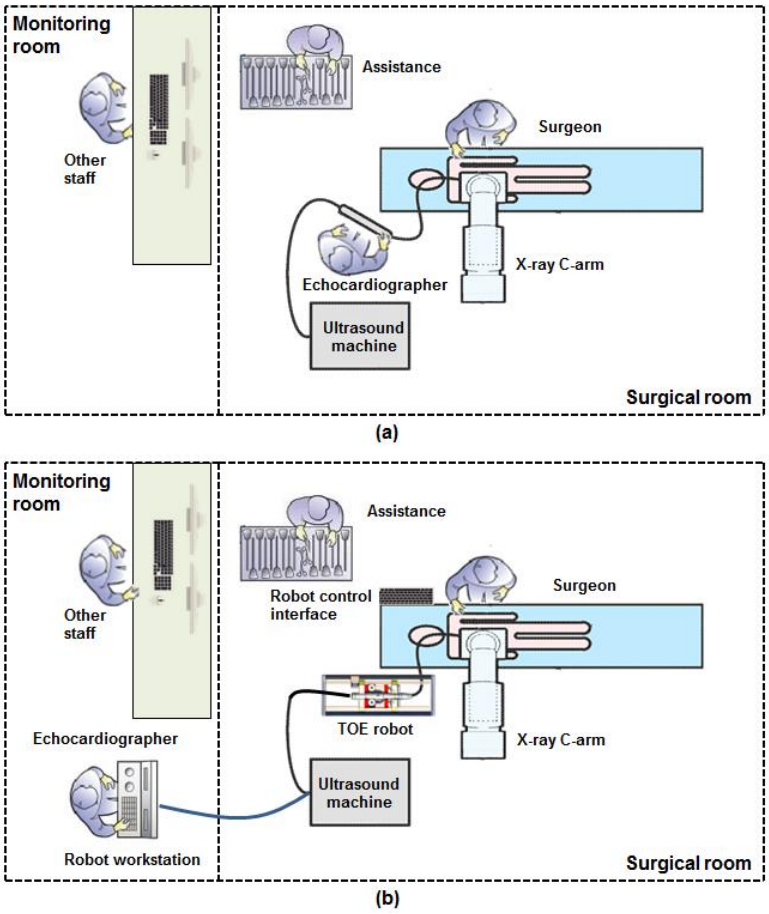


**Fig. 3.25. Entire clinical scenarios including equipment and room set-ups for (a) the current use of TOE in the surgical room and (b) the potential use of robotic TOE system in the surgical and monitoring rooms for cardiac procedures.**

In terms of patient safety using the TOE robot, several features targeted at addressing the concerns of different potential injuries when manipulating the probe, as reviewed in Section 1.4, have been proposed. This includes active position sensing for the neutralization of the probe tip, passive motor current limiting for restricting the maximum bending force, and several software safety features. To understand the reliability of the proposed system, repeatability experiments using an optical tracking method have been performed and it was determined that the repeatability error of the robotic system is less than 1mm. Comparing to the workspace of the TOE probe tip, which is a half sphere with 40mm radius, the evaluation of the entire data indicates the driving mechanism and electronics of the designed robotic system are reliable and the repeatability of the probe tip position and orientation is therefore acceptable.

From the experiments and experience using the TOE robot, several drawbacks were identified which could be improved in a future design. The comparison experiment for the bending force generated manually and robotically indicated smaller motors with less power could be used to further minimize the size of the design of the handle control structure. For a commercial implementation in the future, the flexion of the probe tip needs to be relaxed immediately if the probe needs to be removed as the flexion can potentially cause damage to the tissue, especially when the probe is inserted deeply into the stomach. As for the electronics, the whole robotic system is now powered from two different sources: the chargeable batteries and the external power supply. This is because the whole handle control structure is designed without any electronic wires coming out in order to be safe when it rotates. However, this may cause inconvenience to the operator as the batteries need to be charged over a period of use. Therefore in a future design, a more convenient powering solution for the TOE robot is needed.

It should also be noted that the current inability of the proposed TOE robot to quickly disengage the probe and revert to manual guidance would potentially be a problem for the practical use of the system. This could happen at the time when an operator wants to take over the control by using the original probe, such as when failures of the robot occur or when complications of the patient have been identified. The manual override for the original probe using the current robotic system requires the operator to open the cover piece of the handle control structure, shown in Fig. 3.9, and remove the probe from the knob driving discs. Although this is not considered as a difficult operation, a more effective manual override facility would be necessary for the future practical use of the system. This requires an eject mechanism which enables the user to relax the

flexion of the probe tip and release the probe from the mechanism by pressing a single button on the robot. The relaxing of the tip flexion can be achieved by the current knob driving mechanisms with the assistances from the magnetic home sensors introduced in this chapter. Additionally, a mechanism to disengage the probe handle could be included in the future design. This can be achieved with a 1-DOF linear push-pull mechanism to lower the two knob driving discs as a way to disengage the probe handle. The push-pull mechanism can be designed by replacing the current pin-screw structure shown in Fig. 3.4, which is to hold four pairs of small pulleys for retaining the position of the knobs driving discs, by four small linear actuators electronically connected to one motor logic drive circuit. The advantage of actuating the knobs driving discs rather than actuating the probe handle directly is because no additional disturbances would be introduced to the probe tip during the disengagement process as the probe handle is still held in place by the rotation driving blocks shown in Fig. 3.6. Furthermore, a handle could be added to the cover piece of the handle control structure, which allows easy operation to open the cover.

It will be necessary to perform studies aimed at comparing different controls in terms of usability and efficiency for the echocardiographer to use during TOE scans. This includes tests with the software control, gamepad, dummy probe, and haptic device using realistic setups with similar anatomical structures to the real TOE scan. A custom heart-oesophagus phantom has been built, which will be introduced in the subsequent chapter. However, the phantom is mainly for testing automatic TOE acquisition with a specific focus on acquiring ultrasound images. The robotic system has also been tested with cadavers as described in Section 3.4.3, and it was expected that this could provide a simulation environment for the usability study of different control options. However, the loss of circulation leads to an inability of the muscle of the oesophagus to relax for the dead bodies, which made it almost impossible to insert the probe. Alternatively, a recently released TOE simulation system [196], which provides anatomical structures of the TOE scan and simulated TOE image outputs, would be a good choice for the study, though a new TOE robot with similar mechanisms but different sizes will have to be designed in order to mate with the probe provided by the simulating system.

To summarize, this chapter describes the design, implementation, and testing of a robotic TOE system. This addresses the aim of building an add-on system for a commercial TOE probe and allowing the operator to remotely operate the device. With the developed robotic system, the following chapters will focus on its application and

try to achieve the ultimate aim of this work: the automatic acquisition. This starts with Chapter 4 describing the kinematic modelling of the robot-probe system and the design of a view-planning platform for deciding TOE views before the acquisition. The next two chapters will describe the methods using the robot with this view-planning platform to achieve the goal of automatic acquisition. All the following chapters are based on the work presented in this chapter and the robotic TOE system mentioned later in the thesis refers to the system described in this chapter.

# 4 KINEMATIC MODELLING AND VIEW-PLANNING PLATFORM

## 4.1 Introduction

This chapter describes the kinematic modelling of the TOE robotic system presented in Chapter 3 and the implementation of a view-planning platform based on the kinematics. The overall aim of this work is to provide a solution that allows the user to virtually control the TOE robot and define trans-oesophageal ultrasound views when patient heart-oesophagus models are given. This enables the user to plan TOE views for the scan in a virtual environment and obtain robotic parameters for those views.

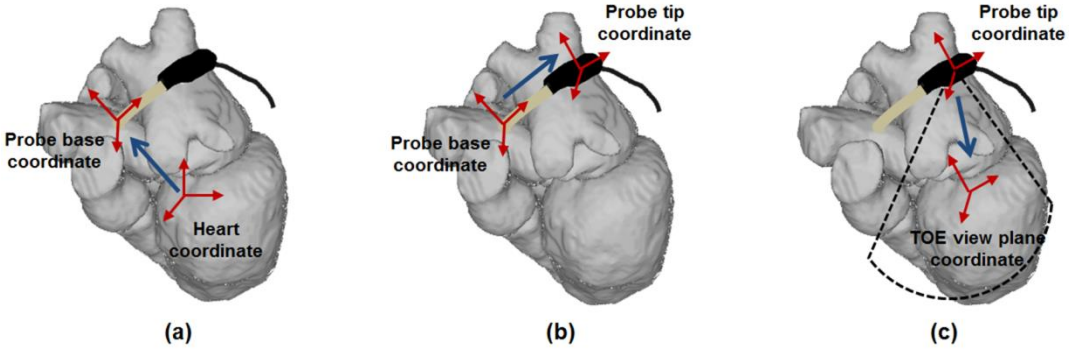


**Fig. 4.1 Schematic illustration of the forward kinematic model studied in this chapter. (a) Transformation from the probe base coordinates to the heart coordinates. (b) Transformation from the probe tip coordinates to the probe base coordinates. (c) Transformation from the TOE ultrasound view plane coordinates to the probe tip coordinates.**

The kinematic modelling describes the forward approach where a set of robotic motor parameters is given as the input and the associated TOE view is obtained as the output. This assumes the position information of the heart and oesophagus is available, which can be obtained from pre-procedure CT or MR scans. With the forward kinematics, the probe is modelled moving from the starting point of the oesophagus along the oesophagus centre line based on the robotic inputs. The complete kinematic modelling includes three steps beginning with the transformation from the probe base coordinates to the heart coordinates (Fig.4.1a), which is determined by the translational and rotational movements of the robot. The second step models the bi-directional bending of the probe tip using a constant-curvature model, giving the transformation from the probe tip coordinates to the probe base coordinates (Fig. 4.1b). The last step describes the probe tip calibration (Fig. 4.1c), defining the transformation from the TOE view plane coordinates to the probe tip coordinates. These three steps, with mathematical details, are explained in Section 4.2 individually. The experimental verification of the model and the results are presented in Section 4.3. It should be noted that the part of this work on the kinematic modelling and validation experiments has been included in the published work [184].

In the view planning platform implemented based on the forward kinematic modelling, movements of the TOE probe are modelled, including the translation, rotation, and bi-directional bending of a virtual probe head. Additionally, electronic steering of the ultrasound beam is modelled by rotating the 2D ultrasound plane. Desirable views can be found by manual interaction with the view-planning software. In the virtual setup, the five parameters are adjusted via sliders in the software, and the resulting view plane is interactively updated to show the imaged 2D slice. In this way, suitable long and short axis views of the heart are found and the corresponding robotic parameters are recorded. Therefore, the platform can be used to define a 2D ultrasound view directly or a 3D ultrasound view based on slice views. The overview of the view-planning platform and its workflow are presented in Section 4.4. It should be noted that development of the view-planning platform was based on existing software, and the kinematic modelling proposed in Section 4.2 was then added to this software for a realistic simulation of the probe's movements. At the end of this chapter in Section 4.5, summaries and discussion for the kinematic modelling and view-planning platform are presented.

For the transformation matrices notation used in this chapter and the following chapters, ${}^{A}\mathbf{T}_{\mathbf{B}}$ is defined as the $4 \times 4$ homogeneous matrix representing the transformation from the B coordinate frame to the A coordinate frame. This represents the location of the B coordinate frame with respect to the A coordinate system.

## 4.2 Forward Kinematics and Probe Calibration

### 4.2.1 Modelling of the translation and rotation

The first step of the kinematics models the translational and rotational movements of the TOE probe, which directly relate to the translational and rotational axes of the TOE robot. Based on the mechanical ratio of the mechanisms, distances and angles of the movements actuated by the robotic system are directly transferred to the distal end of the probe based on the path of movements, i.e. the oesophagus centre line. Mathematically, the translational and rotational movements can be easily modelled with standard rigid transformations using a $4 \times 4$ matrix to describe the relative positioning relationship of the probe to the heart [197]. The probe base coordinates and the heart coordinates are then defined to describe the transformation. The origin of the probe base coordinates is at the bending origin of the probe tip and the origin of the heart coordinates is located at a centre point of the heart, which is determined by the MR or CT images. The definitions of the coordinates and axes are shown in Fig 4.2a. The movements of the probe is modelled from the entrance of the oesophagus and the initial position of the probe base coordinate, i.e. the beginning point of the oesophagus, relative to the heart coordinate can be obtained from the MR or CT images. The initial orientation of the probe at the entrance of the oesophagus is assigned manually to allow the transducer of the probe to point towards the heart centre (mass centre of the segmented heart based on the vertex data) while at the same time align with the oesophagus. With the position and orientation information, the initial transformation from the probe base coordinates to the heart coordinates is determined (Fig. 4.2b), denoted as ${}^{\mathbf{heart}}\mathbf{T}_{\mathbf{oesophagus\text{-}beginning}}$. In practice, when manually inserting the TOE probe using the robot, this initial pose of the probe base relative to the heart would be different and a method to locate its initial position will be necessary. This will be discussed and addressed in the subsequent chapters under the content of probe tracking.

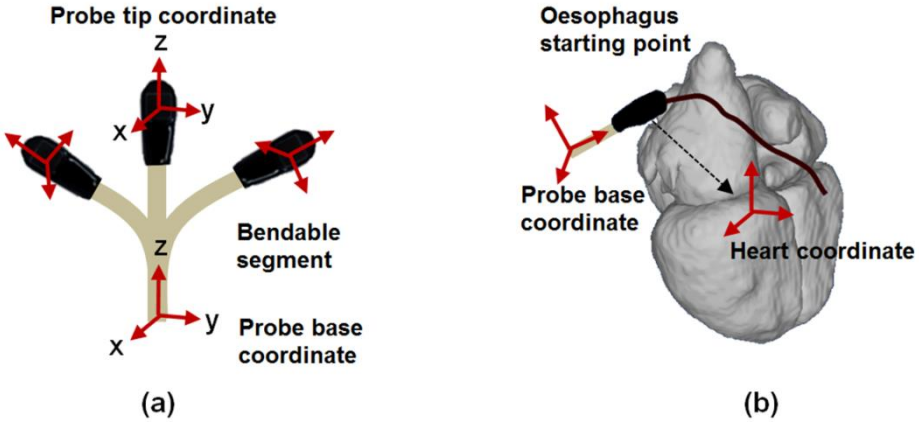


**Fig. 4.2. (a) Illustration showing the definitions of the probe base coordinates and the probe tip coordinates on the probe bending head. (b) The initial position of the probe with the probe pointing towards the heart at the entrance.**

From the initial position at the entrance of the oesophagus, the translational movement of the probe base coordinate is constrained by the path of the oesophagus. In practice, this is achieved by path interpolation based on Catmull-Rom splines [198, 199] using the 3D point set of the oesophagus centre line. For each small segment of the oesophagus, the spline interpolation method specifies four points at intervals along the oesophagus path using the point set and defines a function that allows additional points within an interval to be calculated. To calculate an additional point, two points on either side of the desired point are required as shown in Fig. 4.3. The point is specified by a value $t$ that signifies the portion of the distance between the two nearest control points. Its location $p(t)$ can be calculated using the four control points ($P_0$, $P_1$, $P_2$, and $P_3$) based on the following formula:

$$p(t) = 0.5*(2*P_1 + (-P_0 + P_2)*t + (2*P_0 - 5*P_1 + 4*P_2 - P_3)*t^2 + (-P_0 + 3*P_1 - 3*P_2 + P_3)*t^3) \quad (4.1)$$

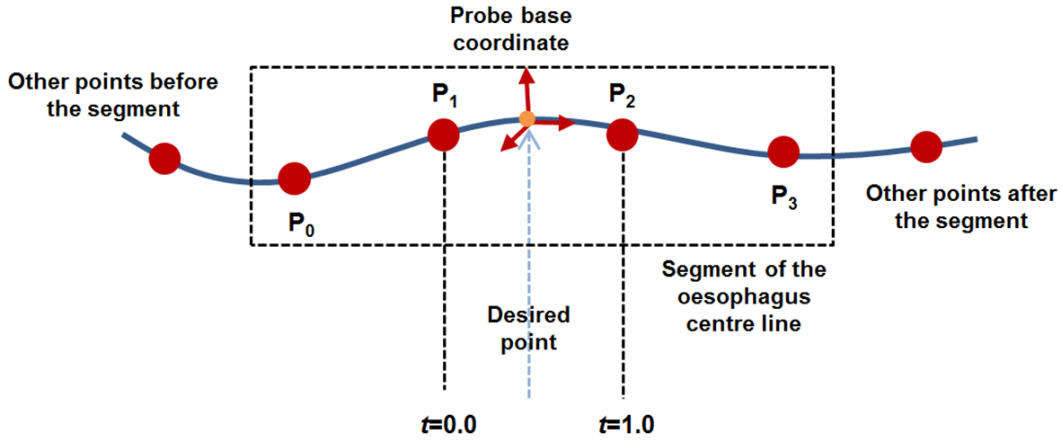


**Fig. 4.3. Illustration of the spline interpolation for calculating an additional point in between the control points obtained from the oesophagus segmentation.**

In this study, the distance between the two nearest control points is divided into 10 pieces (uniform spacing) for interpolation. From the position of the interpolated points, the translation vector is obtained for the translational movement of the probe driven by the robot along the oesophagus. The interpolated points allow the translational movement to follow the path of the oesophagus with the translation distance determining the path length along the curve. As for the rotation of the probe actuated by the rotational axis of the robot, the rotation matrix can be simply determined by the angle of the rotational mechanism. It should be noted that the rotational movement of the probe is always relative to the probe base coordinates even when the probe is bent since the actuation of the rotation is applied to the handle of the TOE probe. This is explained in Fig. 4.4. With the translation vector and rotation matrix, the transformation matrix representing the translation and rotation of the probe is obtained, denoted as ${}^{\text{oesophagus-begining}}\mathbf{T}_{\text{probe-base}}$. Therefore, the transformation from the probe base coordinates to the heart coordinates is determined.

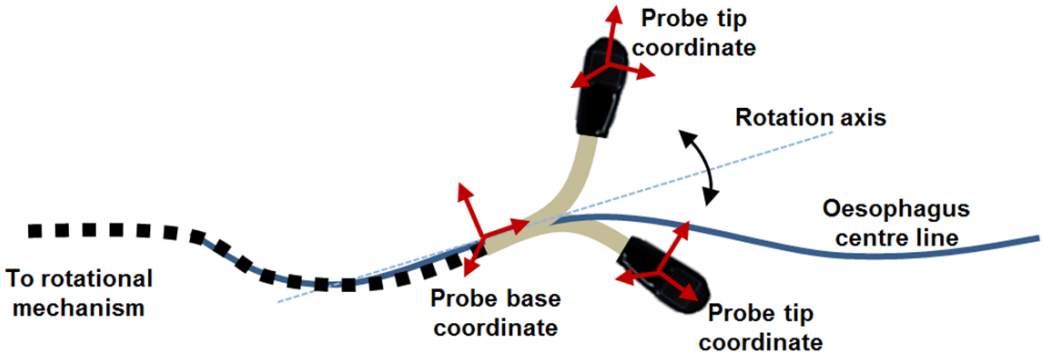


**Fig. 4.4. Illustration of TOE probe's rotational axis. The movement is relative to the probe base coordinate even if the probe is bent due to the driven mechanism being applied to the handle.**

### 4.2.2 Modelling of the bi-directional bending

Different approaches have been utilized to derive the kinematic models of bi-directional bending tips for endoscopic devices. Camarillo *et al*. used a mechanical approach to model the tendon-driven continuum manipulators and applied the method to an intra-cardiac echocardiography catheter [200]. The modified Denavit-Hartenberg approach was also employed by investigating multi-section articulation parameters of the internal structure of the endoscope [201]. As already explained in Section 2.5.3, another approach based on geometric principles, also known as the constant curvature model, was widely used in other works for modeling an add-on endoscopic robot, such as the work described for modeling an endoscope of NOTES [202] and the work for modelling an intra-cardiac echocardiography catheter [148]. The geometric approach does not

require details of the internal joint information of the endoscopic devices, but makes use of the outer measureable geometries. This makes it an ideal choice to model these commercial probes which are manipulated by add-on robots.

In this TOE probe model, a similar geometry approach is employed, i.e. the constant-curvature model, with two assumptions to describe the transformation from the probe tip coordinates to the probe base coordinates. First, it is assumed that the overall bending is independent of the order in which the individual bends in the two directions are applied. Second, plastic torsion is neglected so that the probe tip can only bend in the bending plane. The probe tip coordinate is defined with its origin located at a point on the rigid end of the probe head, which could be any point along the centre line.

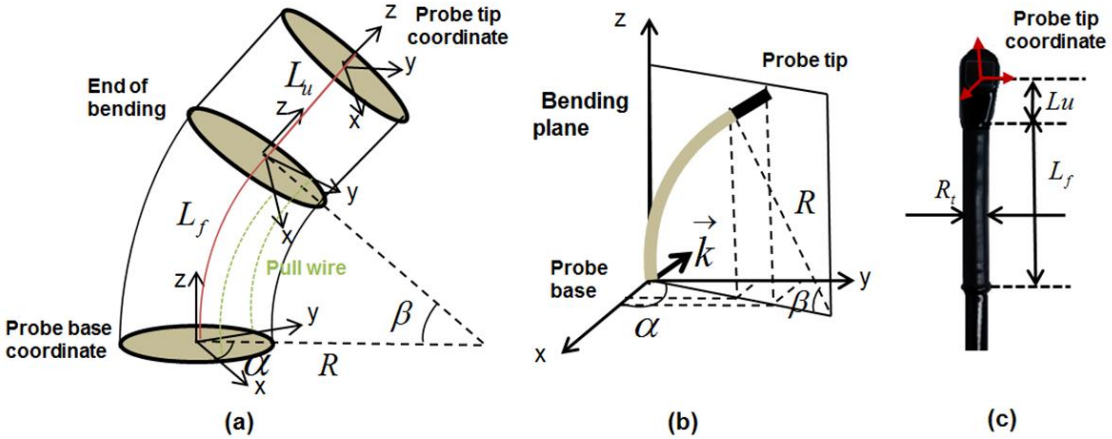


**Fig. 4.5 Geometric illustration of TOE probe tip bending. (a) The perspective view of the bending tip. (b) The projection view in the bending plane. (c) Outer geometries of the probe tip.**

The kinematic model of the tip uses the input of the TOE probe handle to calculate the orientation and position of the probe tip, where the ultrasound transducer is embedded. The calculation is relative to the probe base coordinate. The two inputs of the model are listed below:

- The rotation angle of the bending knob $\varphi_y$, which controls the bending tip pitch in the posterior-anterior plane. $\varphi_y$ is also the rotation angle of the pinion (circular gear) inside the probe;
- The rotation angle of the bending knob $\varphi_x$, which controls the bending tip yaw in the left-right plane. $\varphi_x$ is also the rotation angle of the pinion (circular gear) inside the probe;

The ratio of bending about the Y-axis to bending about the X-axis, $\alpha$, is the angle between the bending plane and the X-Z plane (Fig. 4.5(a)).

$$\alpha = \tan^{-1}(\frac{\varphi_x}{\varphi_y}) \tag{4.2}$$

Previous research has shown that a continuum robot with two bending directions follows a curve of constant radius of curvature [203] along the flexible part of the device. A rotation of angle $\varphi_x$ or $\varphi_y$ of a pulley changes the distribution of the length along the flexible part. The changes of length of the pull wires are $\delta_1$ and $\delta_2$.

$$\delta_1 = \phi_x R_p \tag{4.3}$$

$$\delta_2 = \phi_y R_p \tag{4.4}$$

where $R_p$ is the relative radius of the rack and pinion mechanism inside of the probe where the pull wires are attached [186]. The bending angle $\beta$ in the bending plane is

$$\beta = \sqrt{(\frac{\delta_1}{R_t})^2 + (\frac{\delta_2}{R_t})^2} \tag{4.5}$$

where $R_t$ is the cross-sectional radius of the TOE probe tip. The radius of curvature due to the two-direction bending is

$$R = \frac{L_f}{\beta} \tag{4.6}$$

where $L_f$ is the length of the bending section of the probe tip. The probe comprises a flexible part that follows this curvature model, with a rigid extension to the probe tip on the end. The translation from the base coordinate frame to the tip coordinate frame can be obtained from the orthogonal projection in the bending plane, as shown in Fig. 4.5(b). The translation matrix is shown below:

$$\mathbf{t}_{bend} = \begin{bmatrix} R(1-\cos\beta)\cos\alpha + L_u \sin\beta\cos\alpha \\ R(1-\cos\beta)\sin\alpha + L_u \sin\beta\sin\alpha \\ R\sin\beta + L_u\cos\beta \end{bmatrix} \tag{4.7}$$

where $L_u$ is the length of the rigid section of the probe tip. The tip orientation from the base frame to the tip frame can be calculated by Rodrigues' rotation formula [204] which transforms all three basis vectors to compute a rotation matrix from an axis-angle representation.

$$\mathbf{R} = \mathbf{I} + \sin\beta \cdot [\mathbf{k}]_\times + (1-\cos\beta)\cdot[\mathbf{k}]_\times^2 \tag{4.8}$$

The rotation axis (unit vector) **k** is orthogonal to the bending plane. In the matrix notation form of the Rodrigues' formula, $[\mathbf{k}]_x$ denotes the antisymmetric matrix with entries

$$[\mathbf{k}]_x = \begin{bmatrix} 0 & -k_z & k_y \\ k_z & 0 & -k_x \\ -k_y & k_x & 0 \end{bmatrix} \tag{4.9}$$

The rotation angle about the new axis **k** is $\beta$. Therefore, the rotation matrix $\mathbf{R}_{bend}$ is

$$\mathbf{R}_{bend} = \begin{bmatrix} k_x^2 V_\beta + C_\beta & k_x k_y V_\beta - k_z S_\beta & k_x k_z V_\beta + k_y S_\beta \\ k_x k_y V_\beta + k_z S_\beta & k_y^2 V_\beta + C_\beta & k_y k_z V_\beta - k_x S_\beta \\ k_x k_z V_\beta - k_y S_\beta & k_y k_z V_\beta + k_x S_\beta & k_z^2 V_\beta + C_\beta \end{bmatrix} \tag{4.10}$$

where $S_x$, $C_x$, and $V_x$ denote sin($x$), cos($x$), and (1-cos(x)) respectively. According to Fig. 4.5, the normal unit vector **k** to the bending plane can be expressed as (**k**=-sin α**i** + cosα**j**). The rotation matrix $\mathbf{R}_{bend}$ can therefore be written as:

$$\mathbf{R}_{bend} = \begin{bmatrix} S^2{}_\alpha + C_\beta C^2{}_\alpha & -S_\alpha C_\alpha V_\beta & C_\alpha S_\beta \\ -S_\alpha C_\alpha V_\beta & C^2{}_\alpha + C_\beta S^2{}_\alpha & S_\alpha S_\beta \\ -C_\alpha S_\beta & -S_\alpha S_\beta & C_\beta \end{bmatrix} \tag{4.11}$$

With the rotation matrix $\mathbf{R}_{bend}$ and the translation matrix $\mathbf{t}_{bend}$, a 4 by 4 transformation matrix, $\mathbf{T}_{bend}$ is then derived to bend the TOE tip with respect to the base. This gives the transformation from the probe tip coordinates to the probe base coordinates (Fig. 4.6), indicating the position and orientation of the probe tip relative to the probe base coordinates.

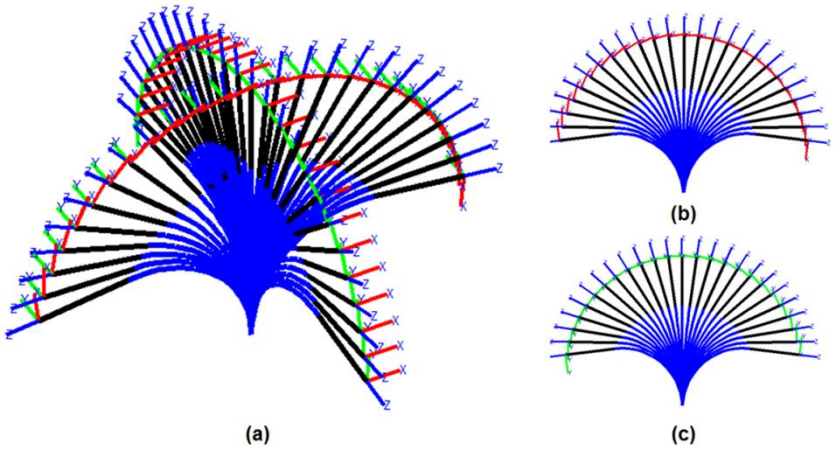


**Fig. 4.6. Simulation of the probe tip bi-directional bending in the two default planes. (a) Perspective view of the bi-directional bending in 3D space. (b) The 2D view of the X-Z bending plane. (c) The 2D view of the Y-Z bending plane.**

### 4.2.3 Probe to ultrasound image calibration

The TOE calibration procedure aims to determine the transformation from the TOE tip coordinates to the ultrasound image coordinates, i.e. the TOE view plane coordinates. Previous work has determined the transformation from the coordinates of a nano-CT image of the probe to the ultrasound image coordinates [205]. This was calculated from using a specially designed calibration phantom consisting of a water tank and two thin metal wires with nine landmark attached as described in [205]. The calibration accuracy has been studied in the same work with additional TOE volumes of the calibration phantom acquired for validation and the error was found to be 2 mm for the mean 3D Euclidean distance in the nano-CT space using the calibration result. This amount of error is considered to be acceptable and for convenience this existing calibration result is used in this thesis. The nano-CT volume (Fig. 4.7) provides a precise 3D model of the TOE probe tip, which can then be related to the model described above. The nano-CT has its own coordinate system with coordinate directions aligned to the voxels. The coordinate origin is at the centre of the voxel array of the nano-CT image, which is a point (approximately along the centre line of the probe tip) located in the rigid section of the TOE probe tip. The voxel size of the nano-CT volume is 0.2 mm in all directions.

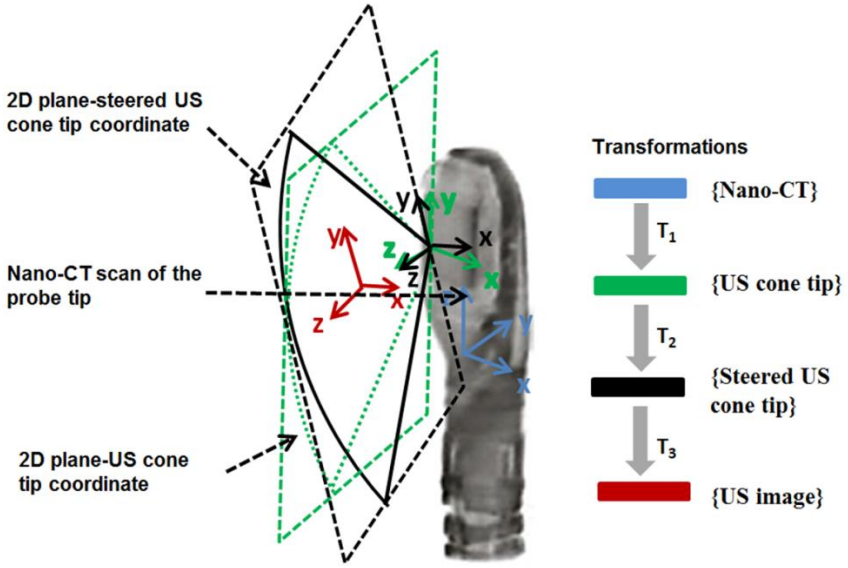


**Fig. 4.7. Illustration of the series of transformations from the nano-CT coordinates to the ultrasound image coordinates with the coordinates and image planes shown.**

The transformation from the ultrasound image coordinates to the nano-CT coordinates (Fig. 4.7) is made up of the following transformations:

- ${}^{0}\mathbf{T}_{1}$ is the transformation from the nano-CT coordinates to the ultrasound cone tip coordinates, which is already known from the previous work. Since the nano-CT

coordinate origin is in the rigid section of the TOE probe tip, this transformation remains the same for different bending inputs.

- ${}^{1}\mathbf{T}_{2}$ is a Z-axis rotation by the angle set for the electronic steering controlled by the buttons on the TOE probe handle.
- ${}^{2}\mathbf{T}_{3}$ is a translation from the cone tip coordinate origin to the ultrasound image coordinate origin. The default is to use the image centre as the image coordinate origin, with the same orientation as the steered cone-tip coordinates.

The forward kinematic model can predict any 'probe tip coordinates' located on the centre line of the probe head as described in the previous section. Therefore, it can predict the nano-CT coordinates and give the transformation from nano-CT coordinates to probe base coordinates. In summary, The overall transformation from the ultrasound image coordinates to the base coordinates is shown below:

$$^{\text{probe-base}}\mathbf{T}_{\text{us\_image}} = {}^{\text{probe-base}}\mathbf{T}_{\text{nano\_CT}}\,{}^{0}\mathbf{T}_{1}\,{}^{1}\mathbf{T}_{2}\,{}^{2}\mathbf{T}_{3} \tag{4.12}$$

## 4.3 Model Validation Experiments

### 4.3.1 Coordinate definitions

In this section, experimental methods using an Optotrak measurement system to assess the properties of the robotized TOE system and evaluate the mechanical assumptions of the forward kinematic model are presented. A quantitative analysis method based on the Optotrak measurement system to assess the targeted accuracy of the forward kinematic model and the error propagation effect in the ultrasound image space is also proposed. Considering the formation of the forward kinematic model, the bending transformation is the segment that is most likely to cause error due to the mechanical assumptions and the inaccuracy of the constant curvature model itself. In comparison, the rotation and translation of the handle are well modelled by simple rotation and translation transformations, and can be treated as accurate segments of the model. Therefore, the experiments are focused on validating the bending transformation. As already introduced in Chapter 3, the Optotrak measurement system used in the following experiments tracks the pose of an object by reporting transformations of the tracking coordinate system relative to a fixed reference coordinate. The tracking coordinate representing the rigid tracking body specifies the pose of the probe tip. Similar to the

experiment presented in Chapter 3, the tracking body is defined with six IRED sensors and the reference coordinate is defined by a rigid body fixed to the table. These are indicated in the figure of the experimental setup shown in the following Section 4.3.2. In this section, several coordinate systems used in the quantitative analysis are defined. The definitions of these coordinates with explanations are as follows (the first three of them are shown in Fig. 4.8):

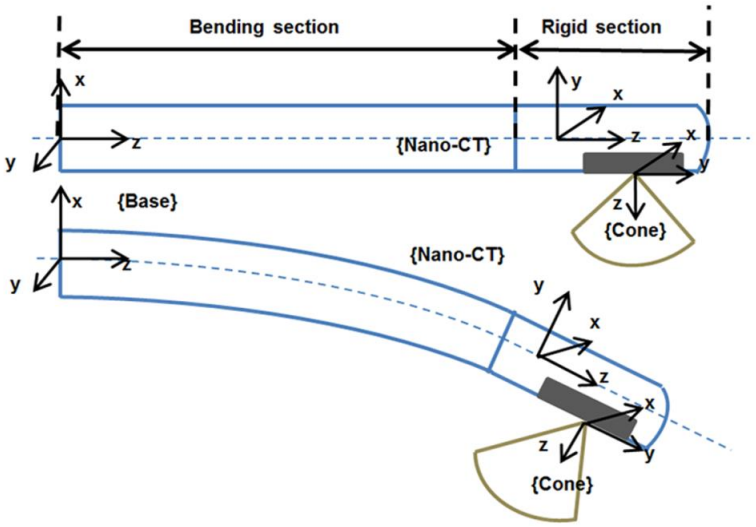


**Fig. 4.8. Coordinate definitions of the TOE probe tip: the bending section and the rigid section.**

**{Base}**: the origin is at the bending origin of the probe tip. The base coordinate is fixed, which provides a world coordinate for the analysis.

**{Nano-CT}**: the origin is at the centre of the voxel array of the nano-CT image, which is a point (approximately along the centre line of the probe tip) located in the rigid section.

**{Cone}**: the origin is at the ultrasound cone tip. For simplicity, the electronic steering of the ultrasound beam is zero in this experiment.

**{Optotrak}:** the reference coordinates of the Optotrak system. The definition is arbitrary but fixed during the experiment.

**{Plate}:** the tracking coordinate of the Optotrak, fixed to the rigid part of the probe. The axes definition is arbitrary, but the origin is at the mass centre of the tracking body.

### 4.3.2 Experimental methods

- Validation of the plastic torsion and joint coupling assumptions

In the forward kinematic model, it is assumed that the effect of plastic torsion is negligible and that the TOE tip can only bend in the bending planes. This experiment

aimed to assess the effect of plastic torsion in the TOE bending process to evaluate the assumption of the forward kinematic model. The same experimental data from the experiment described in Section 3.5 was used and the off-plane distance quantified. This includes 84 points for each of the axes. In the Optotrak coordinate system, the bending plane was defined from the measured data by utilizing vectors in the plane. Here, the vectors between the first, central, and last measured points were used. For each of the measured points, the distance from the point to the defined bending plane was calculated. The forward kinematic model also assumes that the order of knob actuation does not affect the final TOE tip position. To validate this assumption, a further experiment using the Optotrak system was performed. During the experiment, the first knob remained constant while the second knob was actuated by the TOE robot, and then the first knob was incremented while the second knob remained constant throughout the workspace. Each set of corresponding points (with the same motor inputs but different order for knob actuation) was then compared.

- Targeted accuracy of the forward kinematic model

For each of the bending inputs, the forward kinematic model gives the transformation from **{Nano-CT}** to **{Base},** which is denoted as ${}^{\mathbf{Base}}\mathbf{T}_{\mathbf{Nano\text{-}CT}}$. This transformation matrix can then be decomposed to give the transformation parameters: $\theta_x$, $\theta_y$, $\theta_z$, $t_x$, $t_y$, $t_z$. $\theta_x$, $\theta_y$, $\theta_z$ are the Cardan angles referring to rotations about the X-, Y- and Z-axes, respectively. $t_x$, $t_y$, $t_z$ are the translation distances in the X-, Y- and Z-axes.

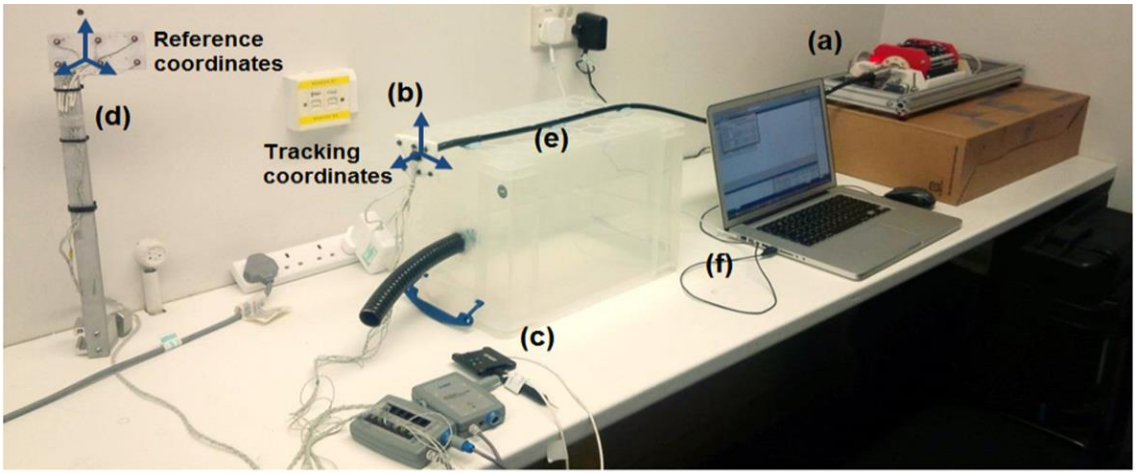


**Fig. 4.9. Experimental setup for the targeted accuracy measurement of the forward kinematic model. (a) TOE robotic system, (b) the rigid section of the TOE probe tip with the rigid tracking body attached, (c) the Optotrak pointer, (d) the rigid reference body, (e) the TOE probe flexible shaft, which was constrained onto a stand, (f) the control laptop of the robot.**

For the same bending inputs, the experiment aimed to find the transformation from **{Nano-CT}** to **{Base}** from the real Optotrak measurement result, which is denoted as ${}^{\mathbf{Base}}\mathbf{T}_{\mathbf{Nano\text{-}CT}}\mathbf{(measured)}$. Fig. 4.9 shows the experimental setup and the following steps describe the processing method.

- Transformation from **{Nano-CT}** to **{Plate}**: the position of four corresponding points (e.g. four corners of the transducer face) in both **{Plate}** and **{Nano-CT}** were acquired respectively. An Optotrak pointer was pivot calibrated, and was then utilized to pick up the four corners of the TOE transducer face, defining four points in **{Plate}**. The positions of these points in **{Nano-CT}** were acquired using the Nano-CT volume image. The transformation ${}^{\mathbf{Plate}}\mathbf{T}_{\mathbf{Nano\text{-}CT}}$ was then derived using least-squares estimation. The rigid tracking body (the plate) was tightly attached onto the rigid section of the probe tip, so this transformation remains fixed.

- Transformation from **{Optotrak}** to **{Base}**: this transformation remains the same for different bending inputs as both coordinates are fixed. The neutral position (when the probe tip is straight) was used to estimate ${}^{\mathbf{Base}}\mathbf{T}_{\mathbf{Optotrak}}$:

$$ {}^{\mathbf{Base}}\mathbf{T}_{\mathbf{Optotrak}} = {}^{\mathbf{Base}}\mathbf{T}_{\mathbf{Nano\text{-}CT}}\mathbf{(neutral)}\,{}^{\mathbf{Nano\text{-}CT}}\mathbf{T}_{\mathbf{Plate}}\,{}^{\mathbf{Plate}}\mathbf{T}_{\mathbf{Optotrak}}\mathbf{(neutral)} \quad (4.13) $$

The ${}^{\mathbf{Base}}\mathbf{T}_{\mathbf{Nano\text{-}CT}}\mathbf{(neutral)}$ transformation can be obtained from the forward kinematic model, since the constant curvature model is accurate in the neutral position when no bending occurs. ${}^{\mathbf{Nano\text{-}CT}}\mathbf{T}_{\mathbf{Plate}}$ was obtained in the first step. ${}^{\mathbf{Plate}}\mathbf{T}_{\mathbf{Optotrak}}\mathbf{(neutral)}$ can be obtained from the Optotrak measurement when placing the probe tip in its neutral position.

- Transformation from **{Nano-CT}** to **{Base}** from the measurement data: for each of the bending inputs, the Optotrak reports the transformation from the tracking coordinates (**{Plate}** coordinates) to the reference coordinates (**{Optotrak}** coordinates), which is ${}^{\mathbf{Optotrak}}\mathbf{T}_{\mathbf{Plate}}$. The transformation ${}^{\mathbf{Base}}\mathbf{T}_{\mathbf{Nano\text{-}CT}}\mathbf{(measured)}$ can be then calculated:

$$ {}^{\mathbf{Base}}\mathbf{T}_{\mathbf{Nano\text{-}CT}}\mathbf{(measured)} = {}^{\mathbf{Base}}\mathbf{T}_{\mathbf{Optotrak}}\,{}^{\mathbf{Optotrak}}\mathbf{T}_{\mathbf{Plate}}\,{}^{\mathbf{Plate}}\mathbf{T}_{\mathbf{Nano\text{-}CT}} \quad (4.14) $$

Therefore, the resulting matrix can then be decomposed to give the transformation parameters: $\theta_x'$, $\theta_y'$, $\theta_z'$, $t_x'$, $t_y'$, $t_z'$ with the same method as described previously. Eventually, the probe tip was driven bi-directionally by the PC. For each of the knobs, the stepper motor was driven from -2000 steps to +2000 steps with a 200 step division,

which covered most of the working space of the bending. For each position, the targeted accuracy of the forward kinematic model can be quantified by comparing the ${}^{\mathbf{Base}}\mathbf{T}_{\mathbf{Nano\text{-}CT}}\mathbf{(measured)}$ and ${}^{\mathbf{Base}}\mathbf{T}_{\mathbf{Nano\text{-}CT}}$. The distance error and the orientation error are defined respectively as follows:

$$\text{dis\_error}=\sqrt{(t_x'-t_x)^2+(t_y'-t_y)^2+(t_z'-t_z)^2} \tag{4.15}$$

$$\text{orien\_error}=\sqrt{(\theta_x'-\theta_x)^2+(\theta_y'-\theta_y)^2+(\theta_z'-\theta_z)^2} \tag{4.16}$$

- Ultrasound image error propagation

The TOE image error caused by the inaccuracy of the forward kinematic model will be propagated with regard to the distance from the transducer. The inaccurate prediction of the orientation and position of the TOE tip can potentially create a considerable error in the ultrasound image, especially for a target object at the far side of the ultrasound cone. In this section, a quantitative method to evaluate the error propagation due to the inaccuracy of the forward kinematic model is described.

In the previous section, the transformation from the **{Nano-CT}** to **{Base}** was described, for the theoretical model and the measurement respectively. For simplicity, the **{cone}** coordinate system was utilized as the ultrasound image coordinates in the experiment. The overall transformation from the ultrasound image coordinates to the base coordinates is

$${}^{\mathbf{Base}}\mathbf{T}_{\mathbf{US\text{-}image}}={}^{\mathbf{Base}}\mathbf{T}_{\mathbf{Nano\text{-}CT}}\,{}^{\mathbf{Nano\text{-}CT}}\mathbf{T}_{\mathbf{US\text{-}image}} \tag{4.17}$$

$${}^{\mathbf{Base}}\mathbf{T}_{\mathbf{US\text{-}image}}\mathbf{(measured)}={}^{\mathbf{Base}}\mathbf{T}_{\mathbf{Nano\text{-}CT}}\mathbf{(measured)}\,{}^{\mathbf{Nano\text{-}CT}}\mathbf{T}_{\mathbf{US\text{-}image}} \tag{4.18}$$

Points in the ultrasound image were then defined by assuming an image size (90 deg * 90 deg cone, 15 cm depth). The ultrasound cone tip was assumed to be the image coordinate centre. Ten image planes were selected within the TOE field of view (FOV) which were parallel to the transducer of the TOE probe (Fig. 4.10). The interval between two planes was 15mm. Landmarks were defined on the four corners of the image planes. The point locations relative to the cone tip are denoted as P_cone. For each set of motor settings, the following transformation was applied:

$${}^{\mathbf{Base}}\mathbf{P\_cone}={}^{\mathbf{Base}}\mathbf{T}_{\mathbf{US\text{-}image}}\,{}^{\mathbf{US\text{-}image}}\mathbf{P\_cone} \tag{4.19}$$

This calculates the positions of the landmarks relative to the base coordinate system using the forward kinematic model. The same idea of transformation was applied to calculate the landmark positions relative to the base coordinate system using the Optotrak measured data:

$$^{Base}\mathbf{P\_cone(measured)} = {}^{Base}\mathbf{T}_{US\text{-}image}\mathbf{(measured)}\,{}^{US\text{-}image}\mathbf{P\_cone} \tag{4.20}$$

The potential TOE image error at different depths was then assessed by calculating the mean position errors of the landmarks.

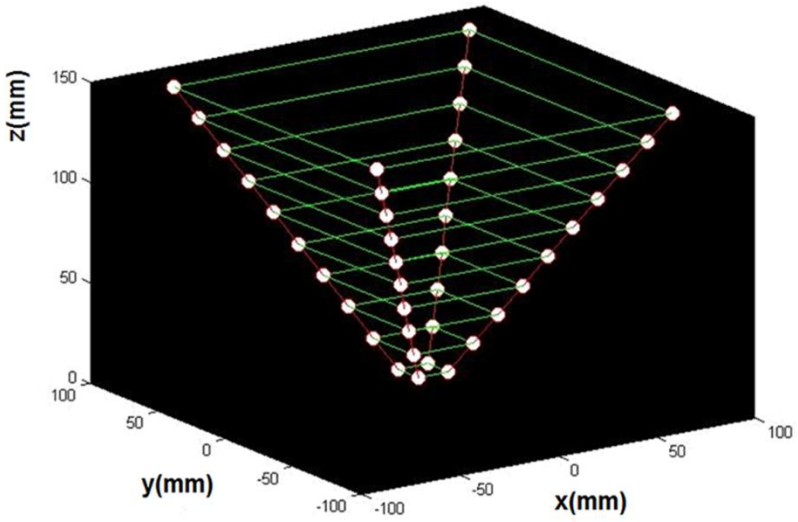


**Fig. 4.10. The FOV of the 3D TOE is a pyramid shaped structure which can be defined from any TOE volume. Ten planes were selected within the TOE FOV which were parallel to the transducer of the TOE probe. Landmarks were defined on the four corners of the image planes.**

### 4.3.3 Experimental results

- Validation of the plastic torsion and joint coupling assumptions

For the validation of the plastic torsion, the results show that for each bending axis, the mean off-plane distances are 0.14mm for the left-right bending axis and 0.21mm for the anteflex-retroflex bending axis. The maximum off-plane distances are 0.57mm for the left-right bending axis and 0.27mm for the anteflex-retroflex bending axis respectively. A histogram including both axes of the off-plane distance is shown in Fig. 4.11. According to the experimental method for joint coupling validation, each set of corresponding points was compared and it was determined that the maximum distance between two corresponding points was within 1 mm.

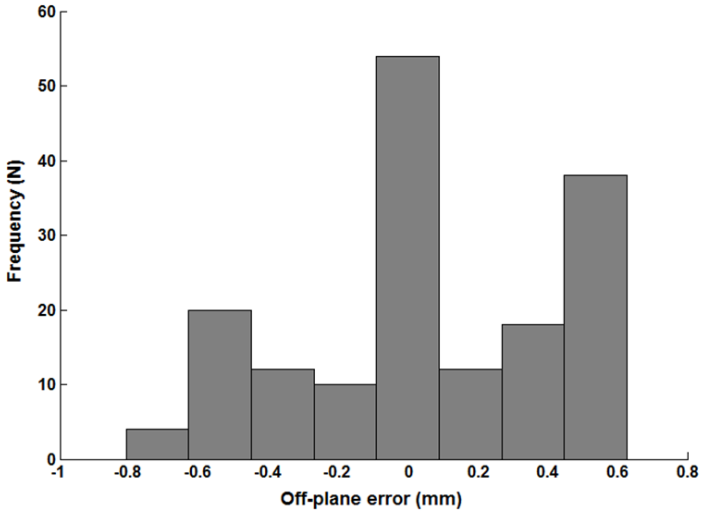


**Fig. 4.11. Histogram of the off-plane error for both the left-right and anteflex-retroflex axes.**

- Targeted accuracy of the forward kinematic model

For each of the measurements, the motor parameters were input into the forward kinematic model. The predicted nano-CT coordinates (origin position and orientation), i.e. ${}^{\mathbf{Base}}\mathbf{T}_{\mathbf{Nano\text{-}CT}}$, as described previously, were calculated. The measured data were processed by applying the method described in the previous section to calculate ${}^{\mathbf{Base}}\mathbf{T}_{\mathbf{Nano\text{-}CT}}\mathbf{(measured).}$ Fig. 4.12 shows the comparison of the measured positions of the nano-CT coordinate origin in base coordinates and the positions in the same coordinate system predicted using the forward kinematic model. The point-to-point errors were quantitatively assessed for position and orientation using the method described previously. The mean and standard deviation of the error over all the points are summarized in Table 4.1.

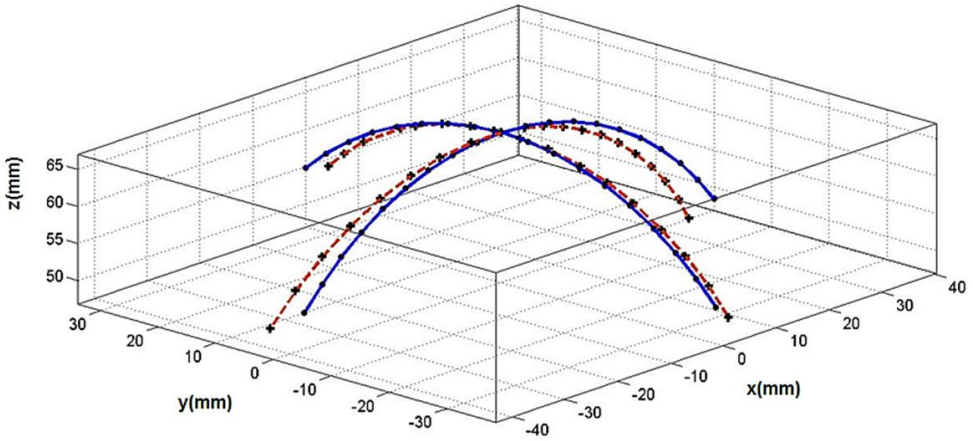


**Fig. 4.12. Comparison of the measured positions (red dotted line) from the Optotrak system and the predicted positions from the forward kinematic model (blue solid line). The data in the x-z plane is the anteflex-retroflex bending axis and the data in the y-z plane is the left-right bending axis.**

**Table 4.1. Orientation and position error of the model for the bi-directional bending**

| Axes | Orientation error (mean±std) | Position error (mean±std) |
|---|---|---|
| Left-right steering | $2.80° \pm 1.15°$ | $2.02mm \pm 1.30mm$ |
| Anteflex-retroflex steering | $4.30° \pm 2.12°$ | $3.17mm \pm 1.27mm$ |

- Ultrasound image error propagation

For each measurement, the positions of the landmarks defined in the pyramid FOV relative to the base coordinate were calculated using the method described in the previous section. This was compared with the predicted position of the landmarks based on the forward kinematic model. The mean distance errors were calculated for different ultrasound penetration depths. Fig. 4.13a and Fig. 4.13b show the mean distance error of the landmarks for different penetration depths and different bending angles of the knobs. The result shows the error is increased from 1.2 millimetres (minimum) to 19 millimetres (maximum) with increasing penetration depth.

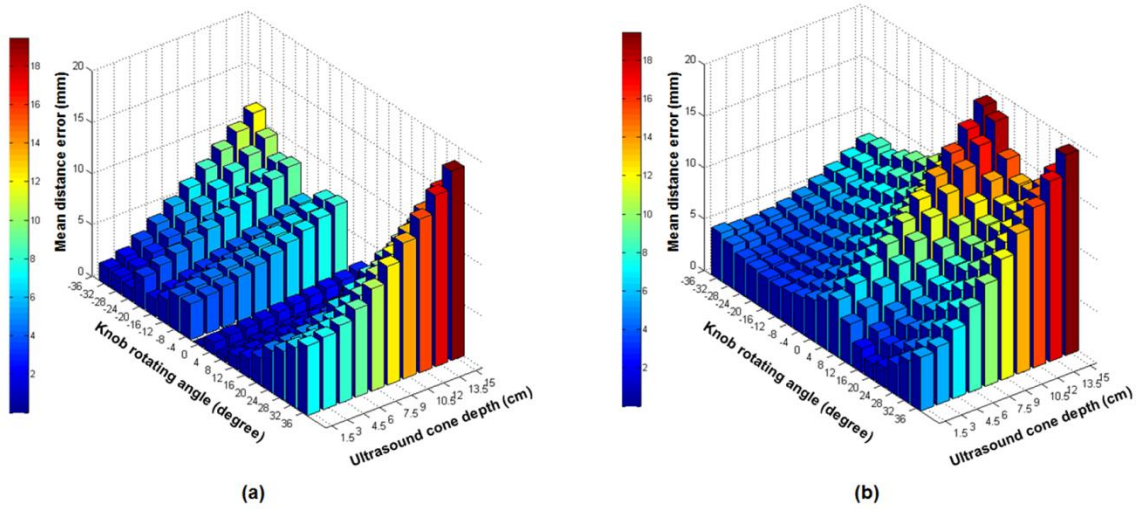


**Fig. 4.13. Mean distance error of the defined landmarks in the ultrasound image for different ultrasound penetration depth resulting from the differences of the predicted TOE probe positions and the measured TOE probe positions. (a) Errors of the anteflex-retroflex steering axis and (b) the left-right steering axis.**

## 4.4 View-planning Platform

As introduced in Chapter 1, the basis of the view-planning platform is an unpublished existing software platform developed for model visualization and user interaction with the probe's movements. Based on the existing software, the verified kinematic model described in the previous sections, along with a number of assisting functions, have been built into this existing software. This forms the final view-planning platform used with the developed TOE robot. This section aims to introduce the implementation and functionality of the view-planning platform and give examples of using this platform to define TOE views.

### 4.4.1 Segmentation of pre-scanned images

Heart-oesophagus models obtained from pre-scanned 3D images are required for the user to define TOE views based on the probe positions in the view-planning platform. The images used in this study are from pre-procedure MR scans. Segmentation of the heart and oesophagus from these images is a basic task to obtain the heart-oesophagus model for TOE view planning. In addition, it also provides the relative positioning information of the heart and oesophagus. This information is essential for the kinematics to work in patients as the model requires the oesophagus centre line's location relative to the heart as explained in Section 4.2. In this study, a fully automatic whole heart segmentation method [206], based on shape-constrained deformable models [207], is employed to process the MR image volumes in order to obtain cardiac chambers and great vessels. The method includes a 3D generalized Hough transformation to automatically localize the heart position if it is unknown prior to the processing, an image calibration method to compensate for intensity variations in the MR images, and a multi-stage adaptation scheme to extract cardiac anatomies.

The anatomy of the automatically segmented heart extracted from the MR image volume includes the four-chambers, the trunks of the aorta, the myocardium, the pulmonary artery and the pulmonary veins (Fig. 4.14). Example uses of the existing method on the MR data of two patients are shown in Fig. 4.15. The segmentation results are furthermore used for the view definition described in the following sections. This segmentation method has considered to be reliable from previous user experiences and for convenience the existing implementation of the method is used in this thesis. The oesophagus centre line is manually segmented from the same MR image. This could be done using a number of software packages: in this study the segmentation features of

the Rview software were used, in which landmarks are selected with the aid of the cursor along the course of the oesophagus in the MR image. Tracking the course along the centre of the oesophagus is easy to perform in practice. A minimum knowledge and understanding to identify the oesophagus in the mediastinum is adequate to perform the task. Besides, the task does not demand a great deal of time to carry out.

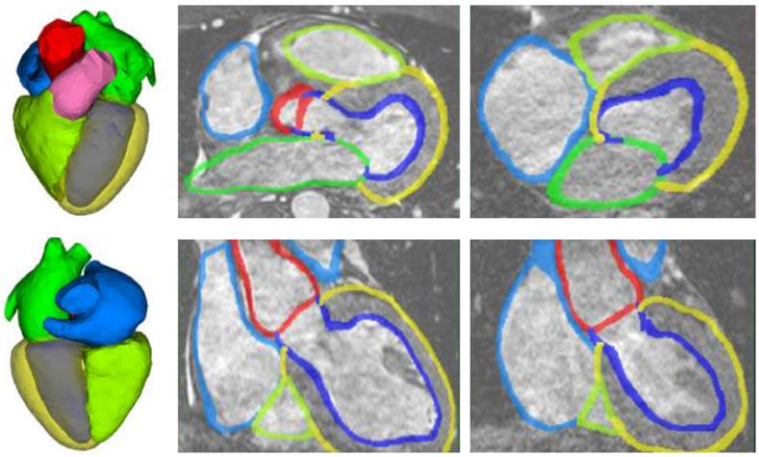

**Fig. 4.14. Two different views of the heart model using the standard 3D heart MRI after applying the shape constraint deformable automatic segmentation algorithms. Figure adapted from [206].**

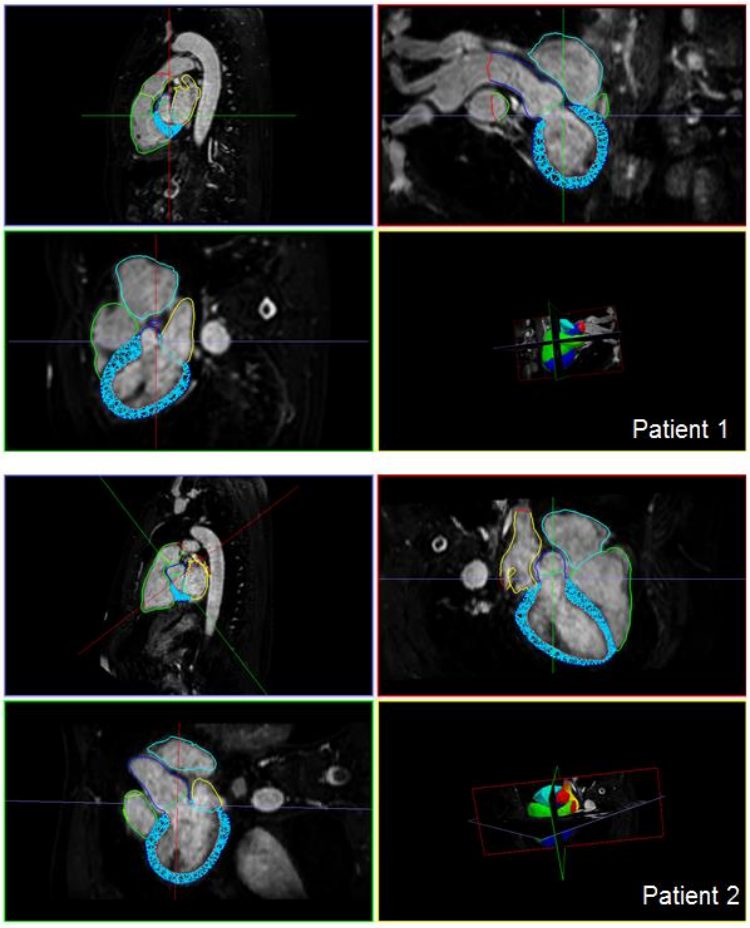


**Fig. 4.15. Example uses of the existing method on the MR data of two patients with the successful segmentation results shown. These results are furtherly used for the view definition of TOE.**

### 4.4.2 Model visualization in the Unity platform

The automatically segmented heart and the manually segmented oesophagus (in VTK format) are loaded and visualised using Unity (Unity Technologies) [208]. Unity is primarily known as a 3D game engine for the development of video games, simulation platform, etc. It integrates a custom rendering engine with the NVIDIA PhysX physics engine and Mono, the open source implementation of Microsoft's .NET libraries. With its capability in building 3D simulations, the software was selected for the development of the view-planning platform. Generally for the design using Unity, objects are loaded and viewed with its camera system to specify the view point. Each of the objects can be assigned with multiple scripts, physics, and rendering properties. Script edited using the Mono API can give objects interactive behaviors, create user interfaces, or simply manage information [209].

In the view-planning platform, custom scripts were created to load the mesh data of the segmented heart model and the line data of the segmented oesophagus model. These were assigned to two Unity objects and rendered to be viewed by the user from the front end of the software along with a virtual TOE probe head (Fig. 4.16a). In addition, methods to generate 2D clip planes for slicing the segmented heart model were developed to view the internal structures of the heart when the pose of a plane is given (Fig. 4.16b). This was further developed with the kinematic model and with user interactions to determine the pose of the plane, as explained in the next subsection. Supporting scripts were produced to control the view interactions such as rotation, translation, and magnification of the view by the user via mouse controls.

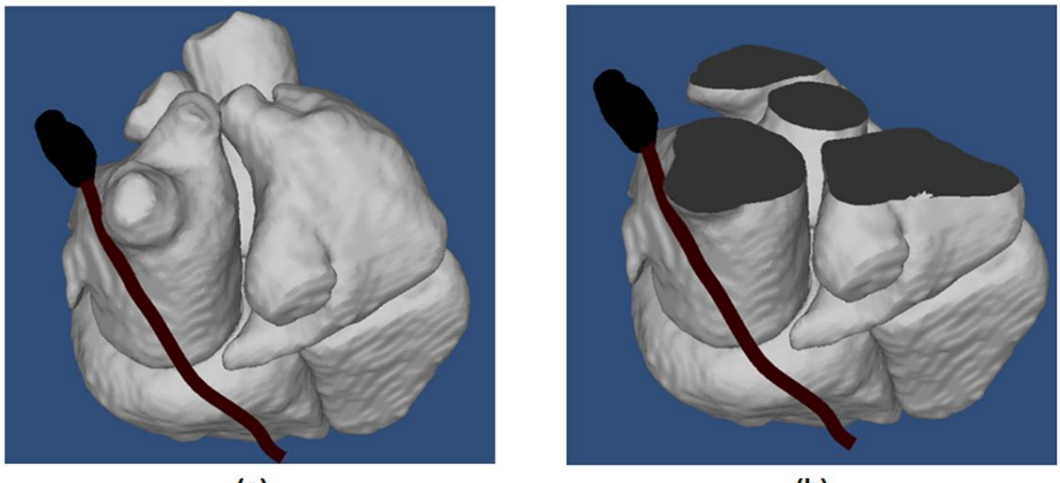

(a) (b)

**Fig. 4.16. Visualization of components in the view-planning platform using Unity: (a) heart surface, oesophagus centre line, and virtual TOE probe head; (b) 2D clip plane for the slice view.**

### 4.4.3 User interaction and implementation of kinematics

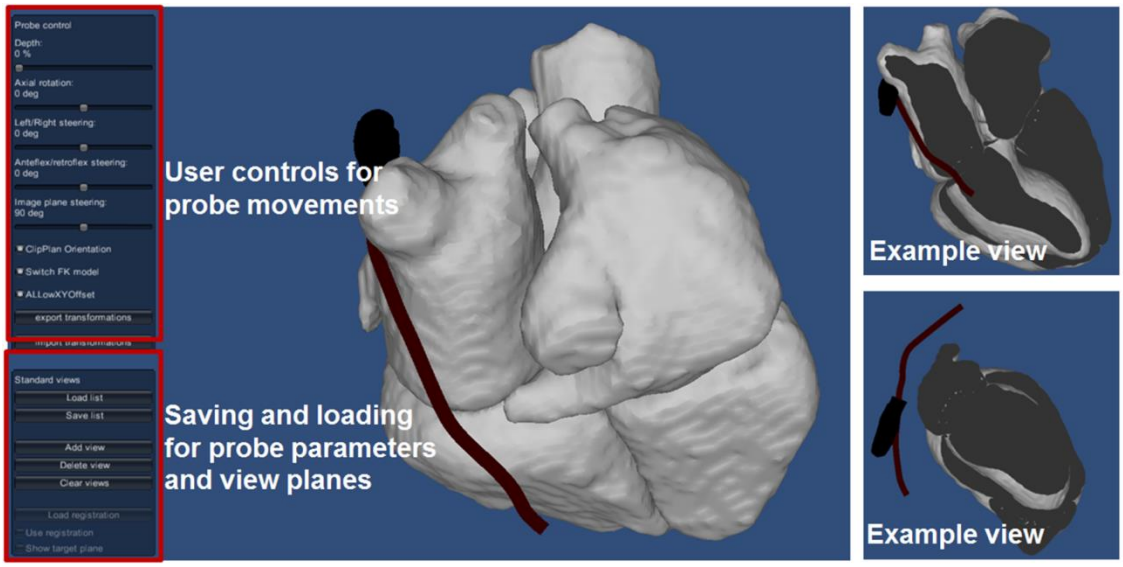


**Fig. 4.17. User interaction with the view-planning platform for controlling the probe's movements.**

The user interaction of the view-planning platform mainly includes the movement control of the probe head according to the probe manipulating parameters based on the kinematic model described in Section 4.2. This is achieved by using the GUI API in Unity and relating the user inputs to the pose of the virtual TOE probe head and the 2D clip plane using the custom scripts. In the implementation, five sliders are designed to adjust the five probe parameters: translation, rotation, bi-directional bending, and electronic steering controlled by the user from the front end. The resulting probe pose is interactively updated based on the forward kinematics calculated in the back-end scripts. In addition, the implementation of the forward kinematics also enables the calculation of the pose of the 2D view TOE planes. The pose of the view plane is then related to the pose of the clip plane and therefore updates the slice view when giving a new set of probe manipulation parameters. As explained previously, both poses are relative to the heart coordinates, which are the MR coordinates used in this study. In the view-planning platform, the MR coordinate system is set to align with the default Unity coordinate system when loading the heart model. Fig. 4.17 shows the user controls of the kinematics and several different probe poses with different 2D clip planes serving as virtual TOE image outputs. Additionally, geometry constrains of the oesophagus are applied to limit the probe's movement ranges. The platform also incorporates the function to save and load the probe manipulation parameters as well as the defined views represented by the pose of the clip planes, which is also shown in Fig. 4.17.

### 4.4.4 Intended use of the view-planning platform

Using the view-planning platform, 2D or 3D TOE standard views can be defined and the associated probe robotic manipulation parameters can be obtained. This is achieved by checking the output clip planes from manual interaction with the view-planning software. With visual inspection, a 2D TOE view can be directly defined and a 3D TOE view can be specified based on central slice views. Alternatively, several protocols have specified the probe locations which can also be used as references [36, 43, 46]. In addition, an online website (Department of Anaesthesia at the Toronto General Hospital) designed for facilitating learning of TOE provides details on brief descriptions of each 2D view including bullet point listings of the features and structures expected from each view [210, 211]. The website also states detailed information to obtain each standard view. This information can also be used as a guide to set up the standard 2D TOE views. The current platform works for the 13 oesophageal views described in the protocols. The remaining 7 gastric views are left to be implemented due to the unavailability of the patient data for the stomach. As an example, a standard patient MR image acquired with a Philips Achieva 1.5T scanner was set as a reference heart-oesophagus model and tested with the view-planning platform to define 2D TOE standard views based on the method described in the previous three subsections. Examples of 2D standard TOE views are shown in Fig. 4.18.

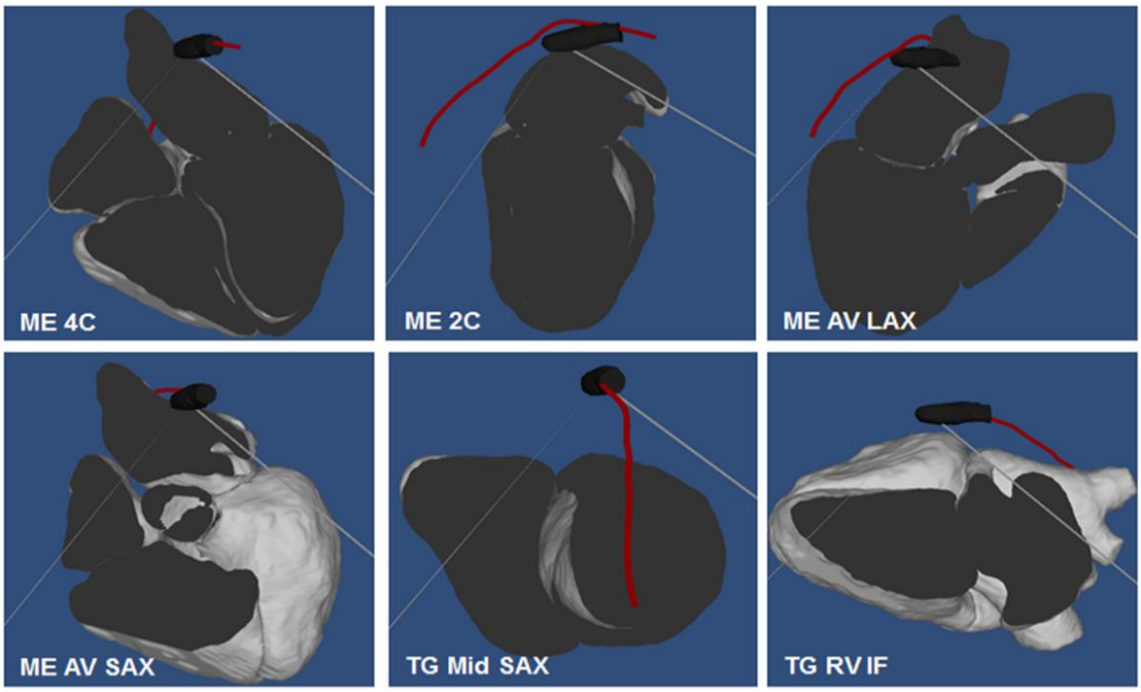


**Fig. 4.18. Examples of standard 2D TOE views (ME 4C, ME 2C, ME AV LAX, ME AV SAX, TG Mid SAX, and TG RV IF) for a patient defined in the view-planning platform. Geometry constrains of the oesophagus are applied to limit the probe's movement ranges.**

## 4.5 Summary and Discussion

In this chapter, a kinematic model of the probe-robotic system has been described in Section 4.2, including an interpolation method for translating the probe along the oesophagus centre line, a standard rigid transformation for rotation of the probe, and a geometry-based model to represent the bi-directional bending of the probe tip in Section 4.2. The model describes the mathematical relationship between the robotic motor parameters and the final pose of the probe tip relative to the heart when the heart and oesophagus's positions are known. Furthermore, the calibration of the probe tip provides the relationship between the 2D TOE view plane and the probe tip, which enables the kinematic model to be extended into the ultrasound image coordinates. The practical behaviour of the TOE probe was then examined in Section 4.3 to assess the kinematic modelling. Since the bi-directional bending is the only segment of the model which does not rely on standard rigid transformation, the modelling of the bending behaviour was the main evaluation target of the experiments. This included assessment of the model's assumption, the targeted accuracy of the probe positioning, and the error propagation in the ultrasound FOV resulting from inaccurate predictions.

The results of the experiments show that the forward kinematic model provides a good representation of the workspace of the TOE robotic system. The predicted trajectory from the forward kinematic model can accurately predict the TOE probe tip bending movement. The errors are mainly accounted for by the initial approximations of the forward kinematic model, i.e. there are non-uniformities along the TOE probe bending tip section. Additionally, the origin of the nano-CT coordinate system defined in the experiment is not exactly along the centre line of the probe tip. The approximation used here also contributes to the errors. As for the point-to-point error contributing to the inaccurate prediction of the targeted position, this is mainly accounted for by a hysteresis effect, due to the backlash in the TOE system. It was also noticed that the TOE probe has an inherent dead zone when the bending knobs cross the zero point, due to the lack of tension in the pull wires. For the experiment where the TOE tip was bent in the default two directions (left–right and anteflex–retroflex steering), the dead zone ranged over roughly ± 10° in which rotating the bending knobs resulted in no output. The systematic influences of the backlash effects and the dead zone still remain unknown without more detailed experimental analyses. The current analytical results as shown in Fig. 4.13 have not indicated observable systematic patterns of the errors. According to the existing literature for other similar types of probe, a compensation

model incorporating both effects is potentially achievable. With such an improved model, it is expected that point-to-point errors would have less variation.

Clinically, the required accuracy of manipulation of the TOE probe tip is not clearly stated in the literature, as ultrasound scanning is a feature-based feedback approach controlled by the clinician. At the beginning of this thesis in Chapter 1, an accuracy requirement of 1 cm was set as the target based on the magnitude of the heart motion and deformation. The study of the potential errors in the ultrasound cone space indicates that for 2D modes, some of the standard slice views of TOE, where the probe tip is positioned far from the heart, are likely to be missed due to errors from inaccurate manipulation. However, most structures of clinical interest during cardiac procedures, including major valves and the septum, are in the near field of ultrasound (5–6cm), where the potential error of the model is < 1 cm. Therefore, this error is considered acceptable according to the goal set in Chapter 1. The influence of the error is much less for 3D modes, where most of the investigated structures would still remain in the field of view and be displayed on the screen.

The evaluation method for the kinematic model verification has a further limitation, as the control of the probe is not performed in the real oesophagus. Although the oesophagus can be approximated to a tube-shape cavity, the performance of the TOE probe inside the oesophagus could be different due to the mechanical constraints and the curved structure from the oral cavity to the oesophagus. Despite this, the kinematic model has a significant value as it can be used to pre-plan the robotic motion for a TOE scan sequence. Based on the successful validation, the kinematic model has been built into an existing view-planning platform developed using the Unity engine to allow users to define TOE views and obtain the robotic parameters for driving the probe to these views, as described in Section 4.4. The platform requires a segmented heart-oesophagus model to be prepared as the input. The methods of automatic segmentation of the heart and manual tracing of the oesophagus have been explained. With a heart-oesophagus model imported into the platform, the software models the movement of a virtual probe head based on the proposed kinematics and interacts with the user's inputs. This allows the user to virtually drive the probe along the oesophagus and view the 2D slices of the heart. Therefore, based on the structures observed and the purpose of the procedure, the operator can obtain the robotic parameters for driving the probe to these views assuming the probe starts from the beginning of the oesophagus.

This has been tested with a reference heart-oesophagus model obtained clinically to define 2D TOE views and record robotic parameters. As for 3D TOE views, the view-planning platform can also be used for planning based on the slice views. To make the view-planning platform useful clinically, an automatic adaption method for patient-specific data which can automatically calculate standard 2D TOE views for new patient data based on a reference heart is necessary. This allows the user to quickly prepare the plan for a patient if only standard views are required. This problem will be addressed in the automatic TOE acquisition described in the next chapter. In addition, several other functions of the view-planning platform related to the automatic acquisition will be described in the following chapters.

# 5 ROBOTIC TOE AUTOMATIC ACQUISITION WORKFLOW

## 5.1 Introduction

In Chapter 3, the development of a remote controlled TOE robotic system was presented. This enables the operator to perform TOE scans in a non-radiation environment with a comfortable posture for operation. However, remote controlled ultrasound systems are not adequate to solve the problem of general usability of TOE as they still require a manual control approach which is tedious, time consuming, and most of all totally operator-dependent. These problems with manual control and training experience have been discussed in Section 1.5. Therefore intelligence towards automatic or semi-automatic TOE acquisition has to be built into the developed robotic system in order to achieve a breakthrough in the utilization of TOE with robots.

In Chapter 4, a view-planning platform was presented with robotic kinematics to enable users to define standard 2D or 3D TOE views. This was intended to provide a pre-planning system to decide the robotic movements during an automatic scan. This chapter further describes an automatic acquisition workflow (Fig. 5.1) using the developed TOE robot based on an auto-patient adaption method for pre-planning and an ultrasound-to-MR registration method for locating the probe position. With a pre-scanned 3D model of a patient imported to the view-planning platform, the auto-patient adaption method rapidly calculates the standard views for the patient based on views defined in a reference heart model. The pre-planned movements are performed by the

TOE robot during the scan and feedback adjustments are made based on the ultrasound-to-MR registration method.

The auto-patient adaption method explained in Section 5.2 is intended to allow users to rapidly define TOE views for a new patient when standard views for a reference heart model have already been defined before the procedure. The auto-adaption method originally described in [212] is a joint effort by the author and other colleagues as described in Chapter 1. Since this is an essential step in the automatic acquisition workflow and relates to the rest of the work, details of the method and its evaluation are presented in this chapter. As only one heart-oesophagus phantom was available for the robotic-based experiment described in this chapter, the auto-adaption experiments were performed separately using different heart models from real clinical scans.

The ultrasound-to-MR registration method described in Section 5.3 works as a tracking approach for locating the probe's pose, thus providing feedback adjustments during the real TOE scan. In Section 5.4 a design of a heart-oesophagus phantom is proposed and custom views are defined based on this phantom. This was used as the experimental platform for testing the whole automatic acquisition workflow. The experiments, post-processing, and analysis of the results are presented in Section 5.5. In Section 5.6, a summary and discussion of the whole workflow are given. It should be noted that the work on the automatic acquisition workflow and the experimental validation have been included in the published paper [212].

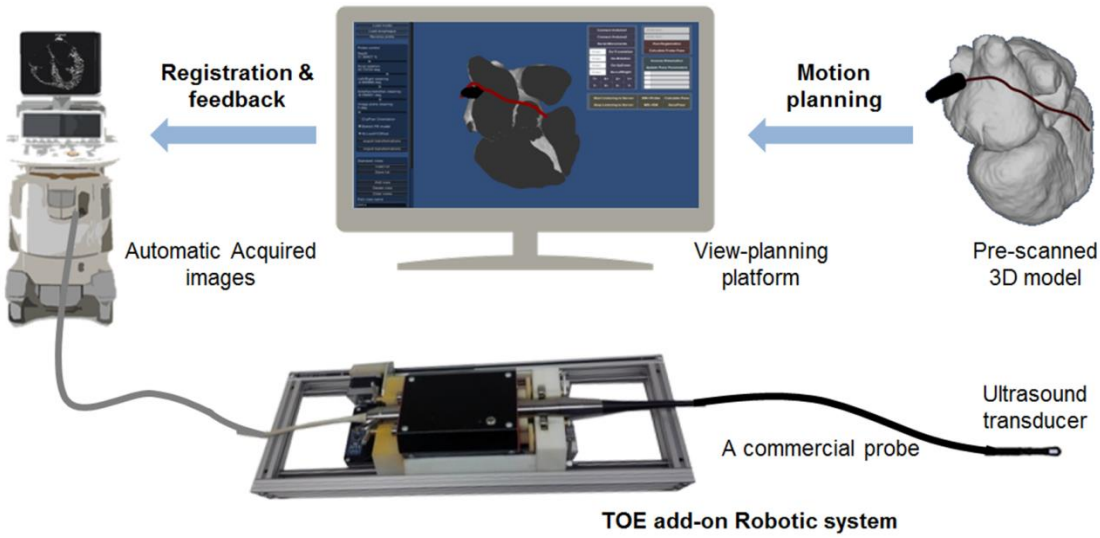


**Fig. 5.1. Overview of the automatic acquisition workflow based on the TOE robot for remote operation, view-planning platform for motion planning, and the ultrasound-to-MR registration method for tracking.**

## 5.2 Auto-adaption to Patient-specific Data

### 5.2.1 Overview of the method

The developed workflow (Fig. 5.2) aims to calculate new patient-specific probe robotic parameters for standard views before the TOE scanning procedure. Once a set of standard views of TOE are defined in the reference heart-oesophagus model, the platform allows users to import any patient-specific data comprising a new heart model and oesophagus centre line. These are obtained using the same automatic segmentation and manual tracing methods used for the reference heart explained in Section 4.4. The method automatically calculates the specific probe robotic parameters for this patient based on the following steps in order to obtain the standard views defined in the reference model.

1. One time system setup: in the reference heart and oesophagus model, standard TOE views are defined by adjusting probe position using the view definition function based on the probe kinematics. This has been already introduced in Section 4.4.4 as the basic function of the view-planning platform. The reference heart model in this study is from a clinical scan of a patient heart.

2. Patient-specific heart models: a new patient-specific heart model is derived from a 3D MR image. Cardiac chambers and great vessels are automatically segmented and the oesophagus centre line is manually located as introduced in Section 4.4.1 and 4.4.2.

3. Adapting reference views to new data: the reference heart and associated standard views are registered to the new patient-specific heart model, using affine registration of the segmented surfaces. As a result, a new set of standard view planes for this patient is obtained. This is achieved by the iterative closest point (ICP) registration method which will be explained in Section 5.2.2.

4. Patient-specific probe positions: optimum probe locations to obtain each view in the patient-specific heart are calculated using an optimization method applied to the new oesophagus. This optimization method employs a gradient descent search algorithm based on the probe kinematics and tries to locate the probe position along the oesophagus to generate the new set of standard view planes for the patient. This will be explained in Section 5.2.3.

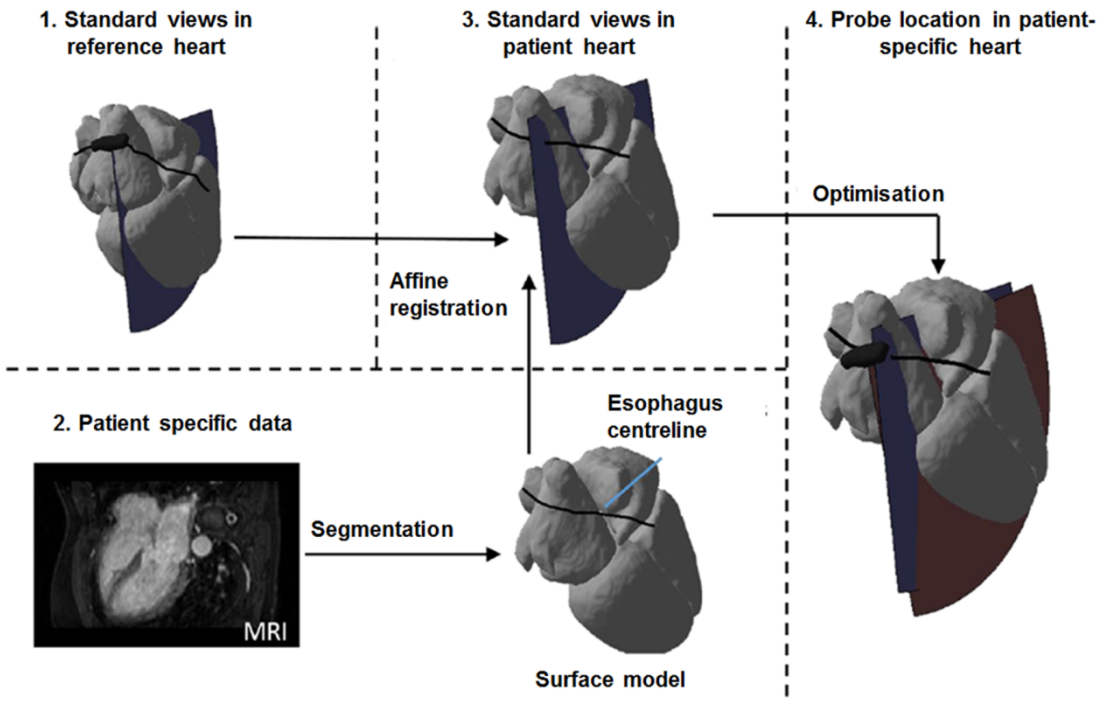


**Fig. 5.2. Overview of the workflow to automatically calculate the probe location in patient-specific data that gives a view as close as possible to the standard view defined in the reference heart model.**

### 5.2.2 Registration of new patient heart models

The adaption to the patient-specific heart uses iterative closest point (ICP) registration [213, 214] to determine an affine warping of the reference 3D heart model (along with the predefined views) to the new patient heart data ICP is used because of the simplicity and relatively quick performance of the method. The affine transformation allows more flexibility than a rigid registration while ensuring that the pre-defined view planes remain as planes after the transformation. In this process, the point sets defining the segmented surfaces of the new patient model are set as the target and kept fixed. The point sets of the reference heart model are transformed to best match the target. The algorithm iteratively revises the transformation (combination of translation, rotation, scaling and shearing) needed to minimize the distance from the source to the reference point cloud. For increased robustness, the heart model is divided up into separate chambers and vessels as provided by the automatic segmentation, and points in a particular section of the reference model are matched only to points in the corresponding section of the new patient model. Essentially, the algorithm steps are briefly summarized as follows:

1. For each point in the source point cloud, find the closest point in the corresponding subsection (chamber or vessel) of the reference point cloud.

2. Estimate the combination of rotation, translation, scaling and shearing using a mean squared error cost function that will best align each source point to its match found in the previous step.

3. Transform the source points using the obtained transformation, re-associate the points and iterate.

By employing this method, a set of new standard views for the patient-specific data after registration is obtained based on the transformation obtained from the registration result of the two heart models and (Fig. 5.3) the original standard views defined in the reference heart model. However, the probe locations defined in the reference heart model cannot be directly transformed to the new patient data, as the transformed probe is possibly not located on the new patient's oesophagus centre line because of the variation of the oesophagus's location relative to the heart. Therefore, for each of the patient-specific standard views, the corresponding probe robotic parameters that provide this view, within the constraints of allowed probe motions along the oesophagus centre line, must be found with a separate method to obtain the best pose of the probe and the electronic steering angle.

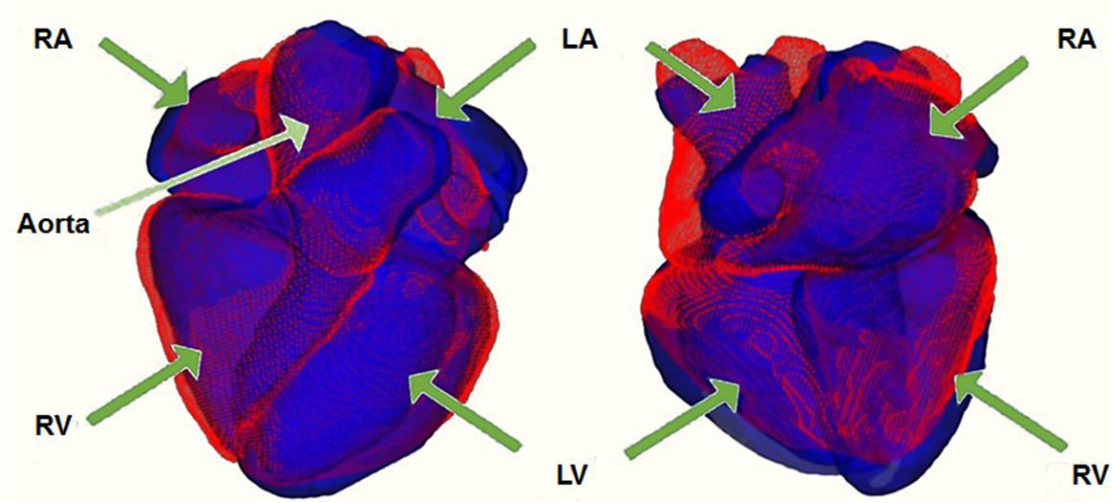


**Fig. 5.3. Visualization of the reference heart model (red) registered with the experimental patient-specific heart models (blue): heart model one (left) and heart model two (right).**

### 5.2.3 Optimization of probe robotic parameters

The optimization strategy defines a single objective function in order to optimize the robotic probe parameters $\mathbf{p} = (x, \theta, \alpha, \beta, \varphi)$, where x is the translation parameter, θ is the axial rotation parameter, α, β are the bi-directional bending parameters, and φ is the angle of the electronic steering. The forward kinematic model introduced in Chapter 4, denoted as F, gives the transformation from the ultrasound image coordinates (TOE

view plane) to the heart coordinates (MR coordinates in practice) based on the information of the oesophagus path for the patient-specific data:

$$^{MR}\mathbf{T}_{US\_Image} = F(\mathbf{p}) = F(x, \theta, \alpha, \beta, \varphi) \quad (5.1)$$

The objective function uses nine reference points defined on the TOE view plane, denoted as $\mathbf{R_i}$. These nine points are defined based on the projection point of the heart centre on the TOE view plane (Fig. 5.4a). The pose of the ultrasound TOE view plane after affine registration is denoted as $^{MR}\mathbf{T}_{US\_Image}\mathbf{*}$, and the objective function f(**p**) used for optimization is based on the in-plane lateral and out-of-plane distance components between corresponding points within the heart on the current and required planes (Fig. 5.4b). The depth component of the distance between corresponding points is not included in the objective function as the same view at a different depth in the image should be acceptable. This avoids the optimization moving the probe into a large angle which is not achievable in practice.

During the search and step approach, the parameter $p_i$ in the parameter space **p** which gives the maximum partial derivative is selected as the step parameter to be updated. The best step direction $d_i = -\nabla f(p_i) / \|\nabla f(p_i)\|$ in the step direction space **d** is the forward direction of the selected parameter. The step size, **σ**, is initially defined based on the dimension scale of each parameter and then reduced after each convergence when $\nabla f(p_i) = 0$. A new parameter set $\mathbf{p}_+$ is of the form: $\mathbf{p}_+ = \mathbf{p} + \boldsymbol{\sigma} \cdot \mathbf{d}$. The search strategy starts from $\mathbf{p} = \mathbf{0}$ and ends when the step size **σ** reaches its minimum pre-set value. The final parameter set **p***, representing the current pose of the probe, is the best probe location which generates a similar TOE view plane as the registered views for the patient-specific data.

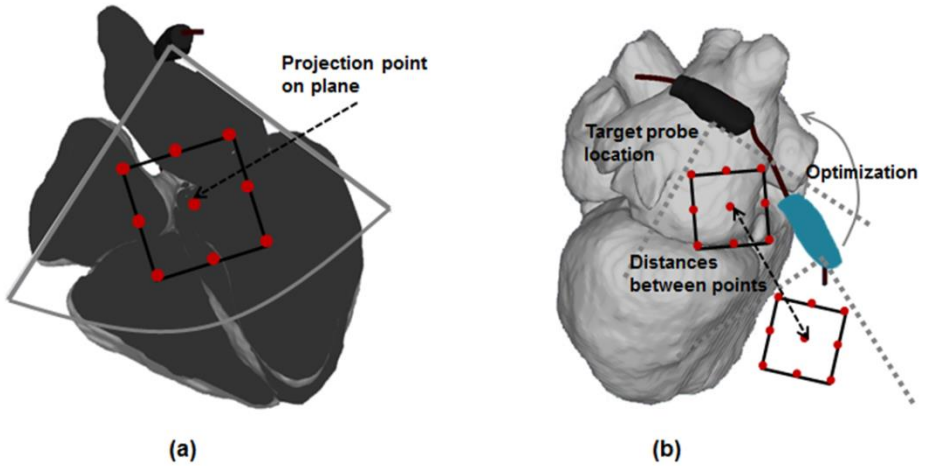


**Fig. 5.4. Optimization of probe robotic parameters for the registered view planes. (a) Definition of the reference points defined on the sliced view plane. (b) Illustration of the optimization method.**

### 5.2.4 Validation experiments and results

To study the performance of the ICP registration and the optimization of probe robotic parameters, 26 standard views were defined in the reference heart model. The reference heart model was registered to two real clinical MR data and the standard views for the two patients were obtained using the registration results. The probe position optimization method was then applied to the registered heart model for the new views. The final locations of the probe, as the output of the optimization method, were obtained for the patient-specific oesophagus locations. The results of the sliced views during the workflow are shown in Fig. 5.5.

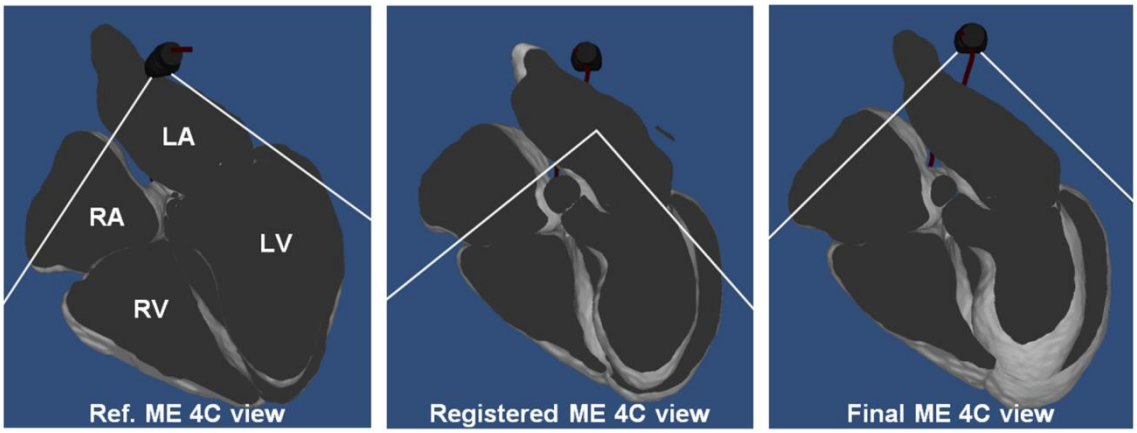


**Fig. 5.5. An example of a standard view slice (mid-oesophagus four chamber view), at different stages of the workflow (view in the reference heart, view after affine registration, and view after probe position optimization), shown with the heart surface mesh cropped at the view plane.**

Correctness of the obtained views was measured as the RMS distance error between surface points on the obtained view plane and a manually-located gold-standard view plane. The gold-standard view plane was achieved by manually adjusting the probe position according to the standard approach to obtain the view (as given in Virtual Transoesophageal Echocardiography, Toronto General Hospital Department of Anesthesia and Pain Management). This educational tool provides details on brief descriptions of each view including the features and structures expected from each view. The website also states detailed information to obtain each standard views. This information was used as a guide to set up the manually-located gold-standard views.

For the affine registration, the target views after adapting the reference model were evaluated to assess the affine registration step alone. The median (IQR) error of affine registration was 11.1 (7.4–15.8) mm. The time required for the registration is within a few seconds, although this is not critical for pre-procedure planning. The final views output from the system, including the effect of the optimization method, probe

kinematics and oesophagus position, were also evaluated. This was found to be 11.5 (8.9–15.1) mm.

To qualitatively analyze the performances of the method, a classification criteria based on the degree of match to the standard view requirements are defined. These guidelines, as listed below, are used when visually observing and categorising each view plane:

A: All required features are present in the image;

B: Close but can be easily corrected by adjusting probe parameters;

C: Same as Category B, but cannot be easily corrected by adjusting the probe positions;

D: View is completely wrong.

The qualitative assessment examined whether the obtained view plane contained all the required anatomical features of the standard TOE view listed in the protocol, and found that 21 of the 26 views needed small adjustments (category B) while the remaining 5 needed no adjustment (category A). No view has been found that cannot be easily adjusted to get all the features (category C) or is completely wrong (category D).

## 5.3 Image-based Probe Position Tracking

### 5.3.1 Overview of the registration method

Once standard views for the patient-specific data are created, corresponding probe robotic parameters can be imported into the robot control system, driving the probe to perform an automatic acquisition sequence. However, considering the practical scan, manual insertion of the probe into the patient is still required for the robotic TOE approach. Therefore, knowing the initial pose of the probe head after manual insertion is essential in order to start the automatic sequence. Additionally, knowing the pose of the probe head is also important for providing feedback adjustments to improve the accuracy of the positioning. In this study, due to the verified performance of the method and the availability of the code, an existing method [93] of model-based registration of pre-procedure volumetric images with TOE images was adapted to work with the view planning platform (Fig. 5.6). This allows estimation of the current probe robotic parameters from the acquired 3D ultrasound image. The images were acquired in the

scanner's full-volume mode, which produces a large pyramidal 3D image by stitching sub-volumes acquired over a few consecutive heartbeats.

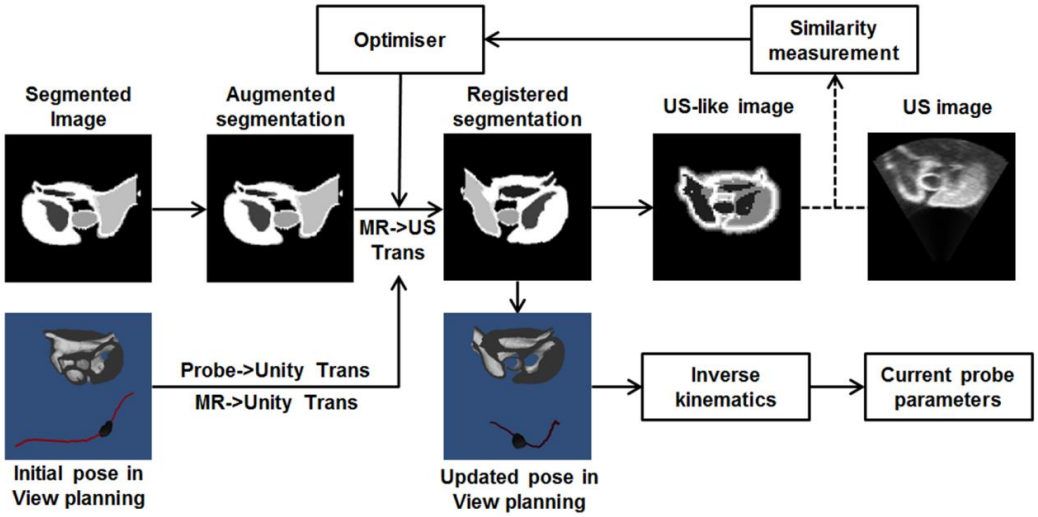


**Fig. 5.6. Overview of the workflow to register the MR image to the TOE image. This forms a probe position tracking method which is used to calculate the probe pose relative to the MR coordinates.**

The pre-procedure MR image is segmented using an automatic method and augmented with prior knowledge of the acoustic properties of the segmented regions' tissue types. The initial estimate of the probe pose is obtained from the view-planning platform, and defines a relative transformation from MR segmentation coordinates to ultrasound image coordinates ${}^{US}\mathbf{T}_{MR\_estimate}$. An ultrasound-like image is generated from the MR using the acoustic property information and an ultrasound imaging model [215]. This is then registered to the real US image using a monogenic phase similarity measure [216]. The optimization method attempts to maximize this similarity measure to find the true pose of the TOE probe relative to the heart segmentation ${}^{MR}\mathbf{T}_{Probe}$. The tracked probe information is used for feedback adjustment which will be introduced in the following subsection 5.3.3.

The registration method has previously been shown in phantom experiment to have a capture range of 9 mm and a median error of 2.9 mm in the registration accuracy [93]. For the phantom setup used in this study, a separate study of the capture range and accuracy was performed, which will be introduced in the following subsections. For the initial estimate ${}^{US}\mathbf{T}_{MR\_estimate}$ obtained from the view-planning platform required for the registration, two different cases exist during an automatic TOE scan sequence:

1. Initialization: this happens at the time when the probe is manually inserted into the oesophagus at a random starting pose with the probe pointing towards the heart. By visually looking at the first output ultrasound image, a similar view can be manually

selected from the view-planning platform, giving an estimate of the current probe pose in the MR coordinates ${}^{US}\mathbf{T}_{MR\_estimate}$. The ultrasound image is then registered to the MR image starting from this estimation, giving an accurate probe pose in the MR coordinates ${}^{MR}\mathbf{T}_{Probe}$. This is a once-only manual operation for each scan of a patient. Clinically, this could be achieved relatively easily by an experienced TOE operator by requiring that they position the probe to one of the standard views when it is first inserted into the oesophagus.

2. Scan: this happens when the probe is driven by the robot to a target location pre-planned from the view-planning platform during the normal scan sequence. In this situation, the initial estimate of the probe's pose relative to the MR coordinates ${}^{US}\mathbf{T}_{MR\_estimate}$ has been already decided during the procedure of pre-planning using the developed platform.

### 5.3.2 Optimization-based inverse kinematics

The registration result of the updated probe pose is then input to an inverse kinematic model to find the corresponding probe robotic parameters using the same optimization method to that introduced in Section 5.2.3 but with only four parameters $\mathbf{p} = (x, \theta, \alpha, \beta)$ representing the probe pose to optimize. A different objective function $f(\mathbf{p})$ is used to best align the positions of the four corners of the transducer face, defined as $\mathbf{R_i}$. The illustration of the optimization is shown in Fig. 5.7. Compared with the method in Section 5.2.3, the use of a different objective function is because the probe pose itself, rather than an image plane, is set as the target for the optimization.

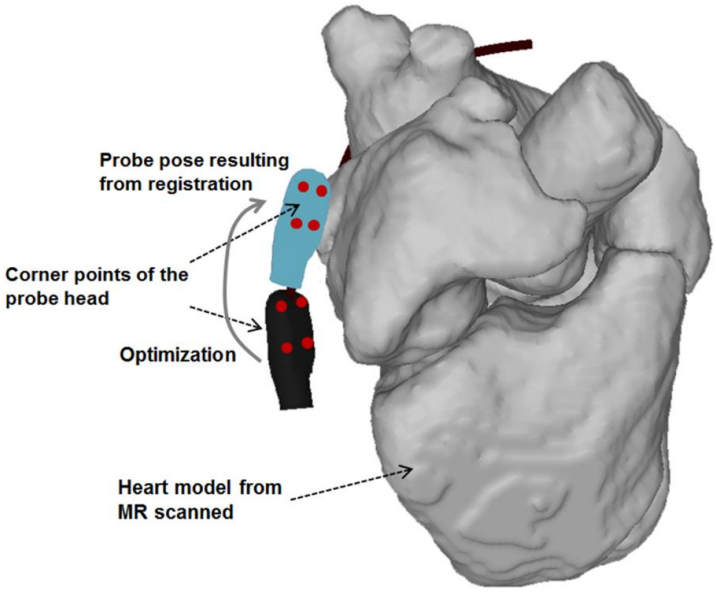


**Fig. 5.7. Optimization of the robotic parameters based on the four corner points of the probe head.**

Different to the description in Section 5.2.3 which estimates the TOE image plane's pose, the forward kinematics F used in this optimization only estimates the probe pose ${}^{\mathbf{MR}}\mathbf{T}_{\mathbf{probe}} = F(\mathbf{p}) = F(x, \theta, \alpha, \beta)$. The current probe pose relative to the MR coordinates resulting from the registration is denoted as ${}^{\mathbf{MR}}\mathbf{T}_{\mathbf{Probe}}{}^{*}$ and the objective function is defined as:

$$f(\mathbf{p}) = \frac{1}{4}\sum_{i=1}^{4} || {}^{\mathbf{MR}}\mathbf{T}_{\mathbf{probe}} * \mathbf{R}_i - F(\mathbf{p})\mathbf{R}_i || \tag{5.2}$$

Similar to the method introduced in Section 5.2.3, the search strategy for the probe robotic parameters in a defined range uses the gradient-descent iteration method and results in the best-fit probe robotic parameters **p*** to represent the probe pose ${}^{\mathbf{MR}}\mathbf{T}_{\mathbf{Probe}}{}^{*}$.

With the tracking information and the inverse kinematics, a simple feedback position controller is designed as shown in Fig. 5.8. Based on the method of position pre-planning using the forward kinematics of the probe described in Chapter 4, the target position of the probe is set for a required view. The corresponding robotic movements obtained from the view-planning platform are executed by the robot based on parameters for each joint (axis), driving the original probe mechanisms to change the location of the ultrasound transducer. After the robot finishes its movements, a full-volume 3D ultrasound is acquired and the MR-to-US registration described in Section 5.3.1 is performed to provide position feedback and check the difference between the current probe pose and the target. This information is further interpreted by the optimization-based inverse kinematics described in Section 5.3.2 to calculate the current parameter for each joint (axis) and find the difference to the target in robotic parameters. This correction is then executed by the robot in an attempt to move the probe closer to the target. The appropriate number of iterations of this loop will be decided from the experimental performance.

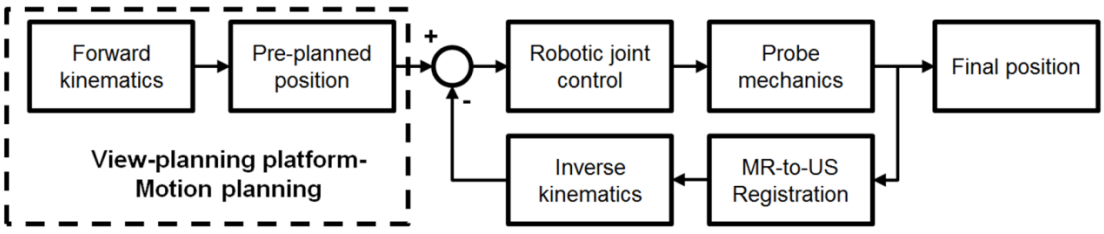


**Fig. 5.8. Diagram of the feedback position controller based on the MR-to-US registration and inverse kinematic model. The segmentation from the pre-scanned MR image is registered to the acquired 3D TOE image based on to provide the current probe pose and the inverse kinematics computes the best-fit robotic parameters to represent the obtained probe pose.**

## 5.4 Heart-oesophagus Phantom and Pre-defined Views

### 5.4.1 Design of the phantom and preparation

A custom made heart-oesophagus phantom (shown in Fig. 5.9) was built in order to provide a simulation environment for the TOE approach in terms of the movements of the probe and the image quality. With a large plastic box, a hole was made into one side to insert a silicone tube. This tube, representing the pathway of the oesophagus, was fixed to plastic tubing to ensure a waterproof seal. The box is filled with water to ensure transmission of ultrasound (holes are also made in the silicone tube to allow it to fill with water). The angle of travel for the probe to enter the tube serves to ensure no water leaks from the box whilst the probe is fully submerged. The heart phantom used is an ultrasound/MRI heart phantom (#CIRS 067, Computerized Imaging Reference Systems, Incorporated (CIRS), USA.), which is designed for viewing the heart from the anterior view. The phantom is made of echogenic material and is embedded in a clear anechoic medium protected by a layer of clear Polyvinyl chloride then mounted on a base. Imaging from below when the phantom is placed upside-down on the box, the views of the heart are in a different anatomical orientation to those obtained in a real TOE scan. However, the proposed phantom meets most of the requirements for testing the view planning and automatic acquisition method for robotic TOE.

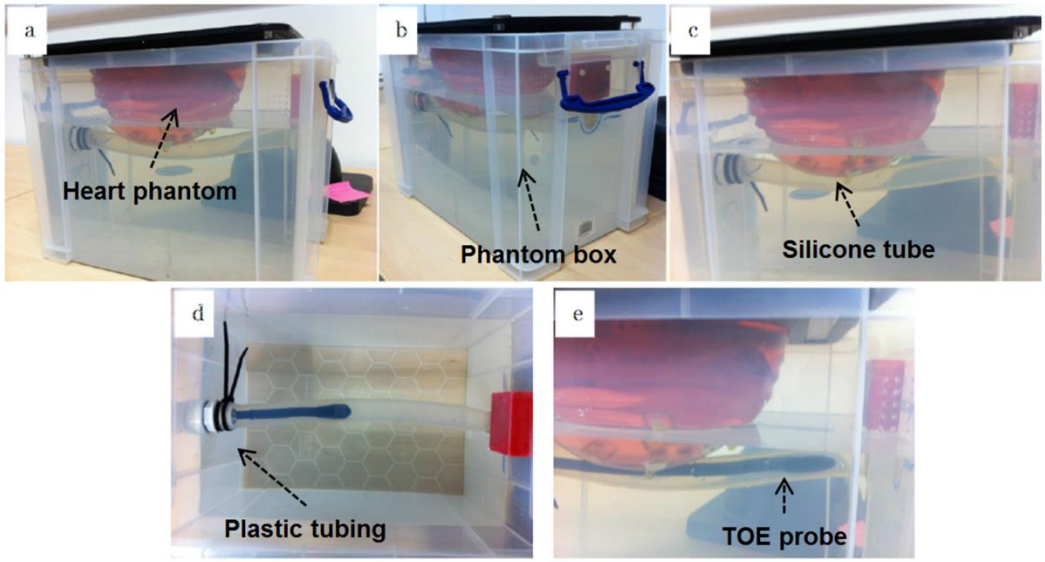


**Fig. 5.9. (a)-(c) show the ultrasound heart phantom mounted on the box containing the silicone tube. This is then filled with water to ensure the TOE probe has no air interface during scanning. The TOE probe fits into the submerged silicone tube as shown in (d) and (e).**

### 5.4.2 Definition of the pre-planned views

Using the custom heart-oesophagus phantom, non-standard heart views were defined (Fig. 5.10). A 3D automatically segmented model of the heart was created based on an existing MR scan of the heart phantom using the method introduced in Section 4.4.1. The centre line of the tube was manually segmented from a CT scan of the phantom box with the commercial heart phantom mounted. The CT image was then manually registered to the MR image of the heart phantom to align the position of the tube and the heart in the same coordinates (the MR coordinates). Both the segmented heart model and the tube's centre line were loaded into the view-planning platform. Based on feature structures (chambers, valves, vessels) shown in either long-axis view or short-axis view, five views (for either 2D or 3D), at different depths and scanning orientation, were defined as follows:

• View 1: right and left atria, pulmonary valve and aortic arch.

• View 2: pulmonary artery, left atrium, left ventricle and pulmonary valve.

• View 3: right atrium, right ventricle, and tricuspid valve.

• View 4: left atrium, left ventricle, mitral valve, aortic arch, and aortic valve.

• View 5: right and left ventricles at mid chamber.

There are a few differences in the phantom compared to real TOE views in addition to the scanning direction, such as the penetration depth of the ultrasound wave emitted from the transducer to the heart structures is longer than in real TOE scans. However, it is difficult to improve on these drawbacks as there are no commercially available TOE cardiac phantoms appropriate for these experiments.

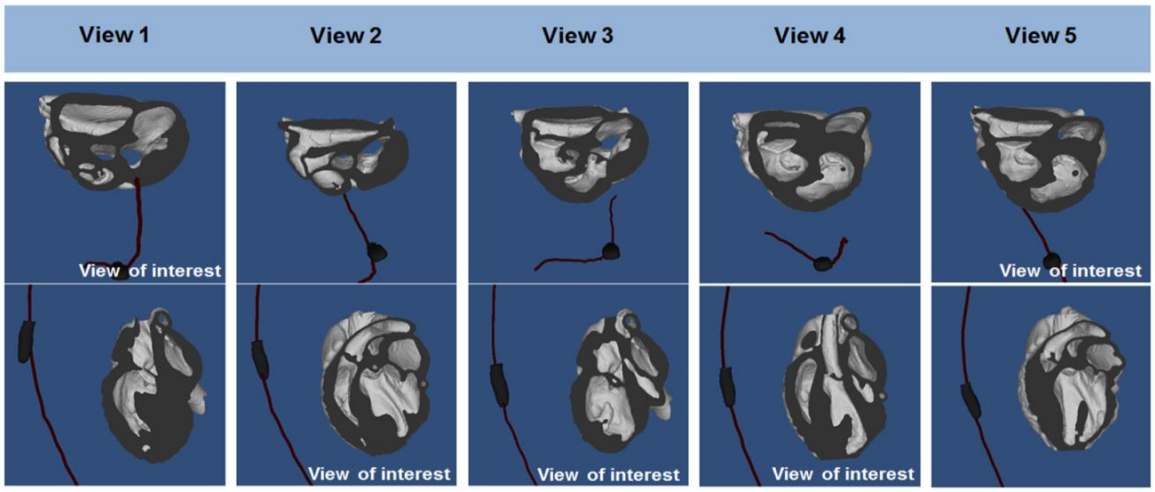


**Fig. 5.10. Definition of the custom standard views using the heart-oesophagus phantom: (top row) long-axis 2D slices of the defined views and (bottom) corresponding short-axis 2D slices.**

## 5.5 Validation Experiments and Results

### 5.5.1 Experimental methods

For the validation experiment to evaluate the automatic TOE acquisition workflow, the TOE ultrasound probe was inserted into the robotic system with an ultrasound machine (iE33, Philips Healthcare, The Netherlands) connected. The guiding mechanism for the translation of the probe uses articulating arms and a few guiding connectors (Fig. 5.11) as introduced in Section 3.2.4. In these experiments, the mechanism was set with the most distal part at 10 cm from the entrance of the phantom (or oral cavity). This distance was found to be short enough preventing the probe from buckling for this phantom experimental setup. Depending on the future practical use of the system in the human body, the distance could be adjusted to different values. From there to the tip of the probe, the endoscopic portion was constrained by the silicone tube. The acquired 3D image data was streamed out to a PC in real time via TCP/IP using an existing software. Simulated human ECG signals were generated for the static phantom in order to obtain the 3D full-volume TOE images. Two experiments using this setup were designed in order to test the automatic acquisition of TOE.

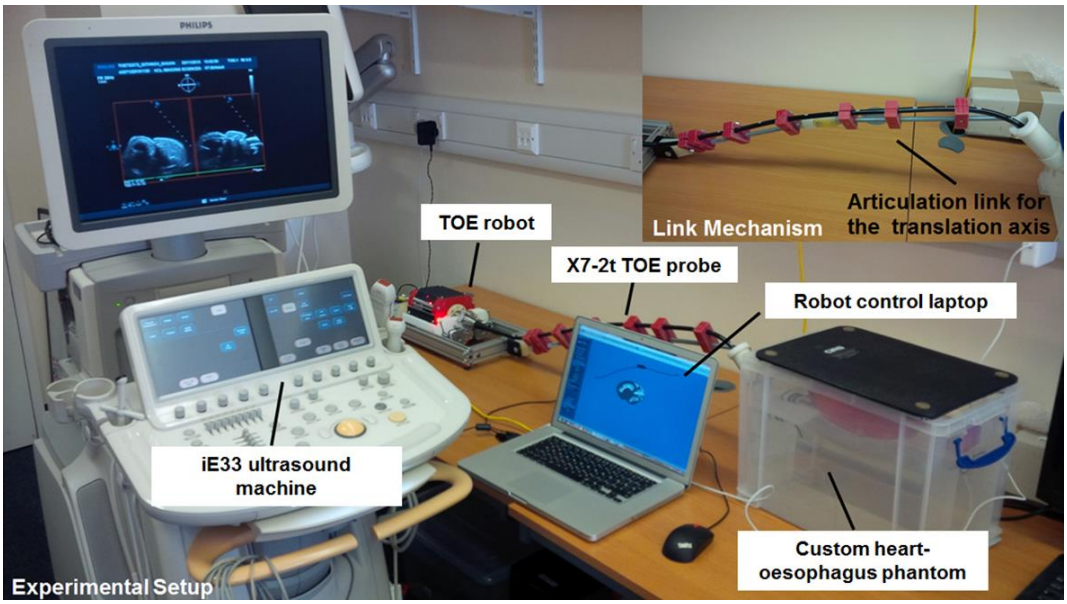


**Fig. 5.11. Experimental setup for the phantom experiment with the TOE robot, ultrasound machine and heart-oesophagus phantom. An enlarged photo of the link mechanism is shown in the top right.**

The first experiment aimed to test the feasibility and accuracy of automatic acquisition using open-loop control. During the experiment, the probe head was manually inserted into the heart-oesophagus phantom with a random starting position. A full-volume acquisition was performed and the acquired 3D ultrasound image was registered to the

MR segmentation to define the initial position. As described in the previous section, this involved using the image-based probe tracking method to obtain the current probe pose. From this starting position, the robotic movement needed to obtain each target view was calculated. This step is defined as the initialization. The robot was then actuated to obtain each view relative to the known initial pose based on position information defined in the view-planning platform. 3D full-volume images were acquired at each view position. This was repeated five times with different initial positions. For each of these initial positions, each view was acquired two times with the probe moving through the sequence from View 1 to View 5, then from View 5 to View 1.

The second experiment aimed to test the improvement in the accuracy of the automatic acquisition using the image-based probe tracking method to provide feedback adjustments. At each iteration of adjustment, the actual position was determined by the image-based tracking and a new movement was calculated to obtain the required view. If the registration failed during the image-based tracking method, feedback adjustments were not performed and the current view was skipped. In this study, the experiments were run and the accuracy improvement quantified over three iterations of feedback adjustments. This experiment used four different initial poses and five views for each.

### 5.5.2 Post-processing and evaluation methods

For analysis of the performances of the automatic acquisition, accurate measures of the probe positions at each view were obtained using the automatic registration method described previously followed by manual corrections as needed. Errors in the probe positioning and image space were calculated by comparing the resulted real positions to the initially planned positions. For the probe pose error, transformations from probe coordinates to the MR coordinates for planned and acquired views were calculated and decomposed to give the transformation parameters: the Cardan angles referring to rotations about the X-, Y- and Z-axes ($\theta_x'$, $\theta_y'$, $\theta_z'$, $\theta_x$, $\theta_y$, $\theta_z$) and the translation distances in the X-, Y- and Z-axes ($t_x'$, $t_y'$, $t_z'$, $t_x$, $t_y$, $t_z$). The distance and the orientation error were defined separately as the root sum square (RSS) of the differences between the X-, Y-, and Z-axis components.

$$\text{dis\_error}=\sqrt{(t_x'-t_x)^2+(t_y'-t_y)^2+(t_z'-t_z)^2} \tag{5.3}$$

$$\text{orien\_error}=\sqrt{(\theta_x'-\theta_x)^2+(\theta_y'-\theta_y)^2+(\theta_z'-\theta_z)^2} \tag{5.4}$$

For the open-loop experiment, the distance and the orientation errors of each view were calculated. For the closed-loop experiment, the distance and the orientation errors after each feedback adjustment were calculated to quantify the improvement in probe positioning accuracy after different numbers of feedback adjustments. Statistical tests were performed to evaluate the reduction in error after feedback by testing differences between means of the error using a t-test.

To quantify the error in the image space, a number of marker points in the ultrasound image coordinates (90 deg * 90 deg cone, 10 cm depth) were then defined. Ten image planes were selected within the TOE field of view, each parallel to the transducer of the TOE probe. The interval between two planes was 10 mm. The marker points were defined on the four corners of the image plane (Fig. 5.12a). From the initial pre-planned views in the view-planning platform and the acquired ultrasound views, the locations of corresponding marker points were obtained and compared in MR coordinates. As shown in Fig. 5.1b, this is done by transforming the marker point locations from the ultrasound image coordinates to the MR coordinates based on the probe positions defined by the view-planning platform for planned views and by the registration result for real acquired views. Mean position errors between corresponding marker points were then calculated for both open- and closed-loop at different depths. Using marker points to quantify the error in the imaging space, rather than directly comparing features obtained from images, is mainly because the penetration depth of the ultrasound beam in the custom heart-oesophagus phantom (> 10 cm) is deeper than the normal scanning depth of the real TOE (5–6 cm). With the pseudo marker points defined covering the entire depth for the normal TOE scan, it is expected that this error quantification will be more reliable to judge the performance of the workflow. Similar statistical tests were performed to evaluate the reduction in error after feedback by testing differences between means of the error using a t-test. Since most structures of clinical interest during cardiac procedures are in the near field of ultrasound (5-6 cm), the statistical test was performed based on the data within this penetration depth. To analyze the influence of the initial position of the manually-inserted probe on the performance of the automatic acquisition, the mean probe pose errors of each whole sequence of five views (five sets for open-loop, four for closed-loop) were calculated. The standard deviation of these mean errors, which resulted from different initial positions of the probe, was calculated to evaluate the impact of the initial probe positioning.

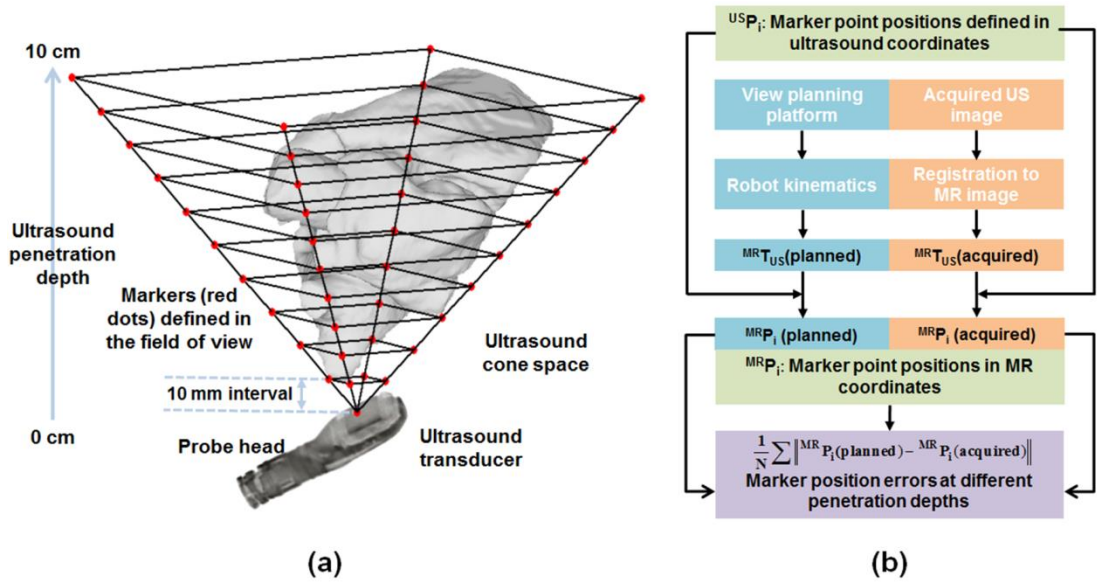


**Fig. 5.12. (a) Marker points (red dots) defined in the ultrasound image field of view (pyramid shaped, 90 deg * 90 deg cone, 10 cm depth). Ten image planes (10 mm interval) were selected within the TOE field of view, each parallel to the transducer of the TOE probe. (b) Overview of the method using marker points defined in ultrasound coordinates to quantify the error.**

To evaluate the performance of the registration-based tracking method, the correct registration was defined by manual initialisation followed by automatic registration of the ultrasound image to the pre-scanned MR image. Final registrations from three people performing independent manual initialisations were averaged. The capture range was tested by running the registration using different initial estimated positions of the probe generated at a range of offsets from the correct position of the probe (100 for each view). These 100 initial positions were split evenly between 10 groups with each of them representing a range of possible error offsets which were applied to the initial position. The registration accuracy could be tested by comparing output from each automatic registration with the correct registration based on the distances between equivalent points on the surfaces of the cardiac chambers of each ultrasound image. A distance of 5 mm, which is smaller than most anatomical features, was used as the maximum mean surface error for a successful registration.

### 5.5.3 Performance of the automatic acquisition

- Probe head positioning errors

For the open-loop method, over all the sample views, the mean position error of the probe head was 8.1 ± 2.7 mm and the mean orientation error was 11.8 ± 4.1 deg. For each of the views, the error distributions of the probe head position and orientation are

summarized in Fig. 5.13. In the closed-loop experiment, with three iterations of the feedback adjustment, the overall mean position error of all sample views reduced from 8.5 ± 3.6 mm to 6.4 ± 2.8 mm and the overall mean orientation error reduced from 10.6 ± 4.7 deg to 8.4 ± 3.6 deg (Fig. 5.14).

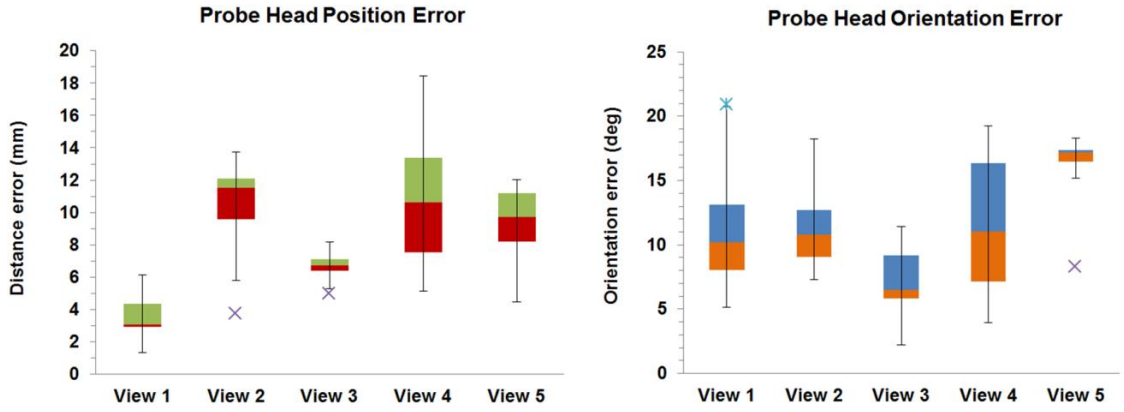


**Fig. 5.13. Distributions of position and orientation errors (box-whisker chart) of the probe head positioning for the open-loop acquisition experiment.**

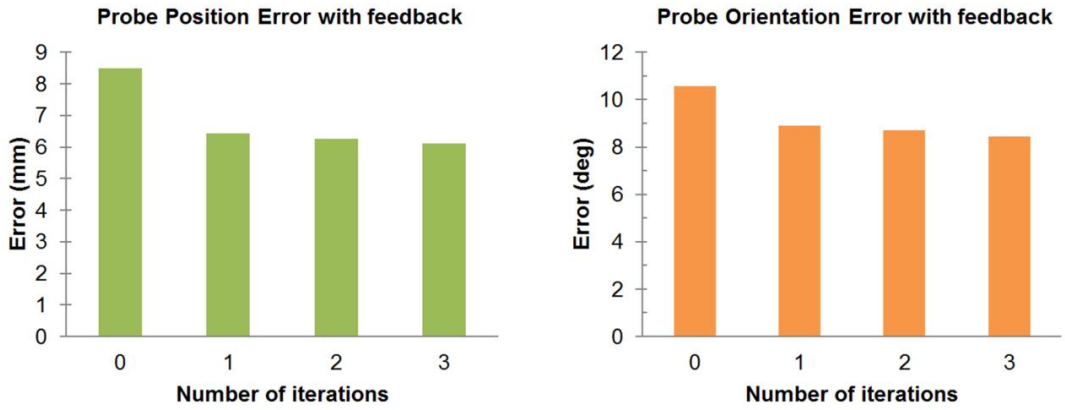


**Fig. 5.14. Changes of the mean position and orientation errors of the probe head with different numbers of feedback adjustments employed.**

Since it has been observed that only the first closed-loop has an important contribution to the error reduction, the statistical test of the difference between means was performed using the open-loop values and the first closed-loop values first with the null hypothesis $H_0$ stating that there is no difference between the means of the two sets. The P-value was found to be 0.018 (< 0.05) for the positioning error comparison and 0.191 (> 0.05) for the orientational error comparison.

- Error in the ultrasound image space

One example sequence of acquired ultrasound views using the closed-loop method is shown in Fig. 5.15. The ultrasound is overlaid on the MR segmentation data with long axis and short axis views shown in order to intuitively compare with the views originally defined in the view planning software. The resulting 2D images of the long and short axis indicate a good alignment with the planned views in the view-planning platform. However, some small structures are noticed to be missing due to the inaccurate probe location. As for the quantitative error in the ultrasound image space for open-loop and closed-loop methods, the error propagation with depth is summarized in Fig. 5.16, with mean errors and standard deviations for different depths. For the statistic test, the P-value for the difference comparison of the mean errors between the open-loop and the closed-loop data within the depths of 5-6 cm was found to be 5.4×10-5 (< 0.05).

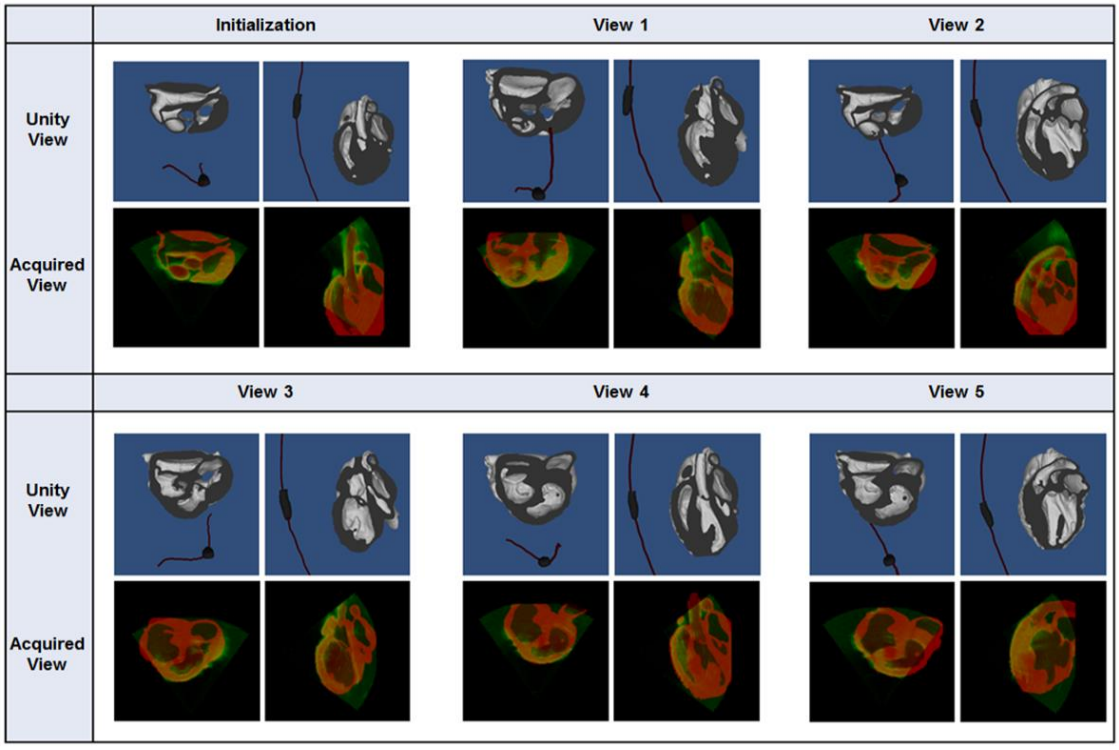


**Fig. 5.15. Pre-planned views (long and short axis) in Unity (apart from initialization) and an example of the acquired ultrasound views (green) from the closed-loop experiment overlaid on the MR segmentation (red). For initialization, the Unity view was obtained from the acquired initial ultrasound view afterwards based on the registration and inverse kinematics.**

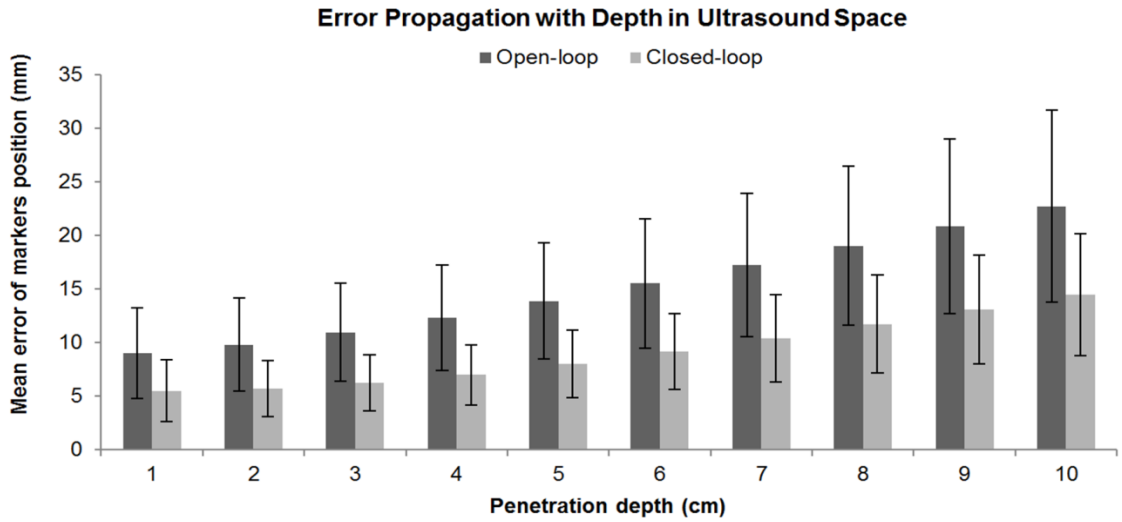


**Fig. 5.16. Error propagation of the marker points' positions with depths in the ultrasound space for the open-loop and closed-loop method from 0 to 10 cm.**

- Reliability and repeatability of the method

Considering the reliability using the registration-based tracking method as feedback, of all the 20 sample views acquired in the closed-loop experiment, 3 initial registrations failed and caused failures of the feedback adjustments. Over different initial probe positions, the standard deviation in the open-loop experiment was 1.3 mm and 2.5 deg while in the closed-loop experiment it was 0.9 mm and 2.5 deg.

- Performance of the registration-based tracking method

The success rate of the registration with different initial positions was analysed (Fig. 5.17). The registration always succeeds when the initial position is close to the correct initial position. When the offset for the initial position is below 10 mm there is a 100% success rate in the registration. However at offsets greater than 10mm the success of the registration quickly drops reaching complete failure of registration at offsets above 30mm. Therefore, the capture range was determined to be offsets less than 10 mm. As for the accuracy of the registration, the mean error for successful registrations was 1.4503mm in a total of 366 successful registrations. This error was found to be smaller than that described in the earlier work [93] which had a similar experiment but different phantom setup and a different definition of the correct reference alignment.

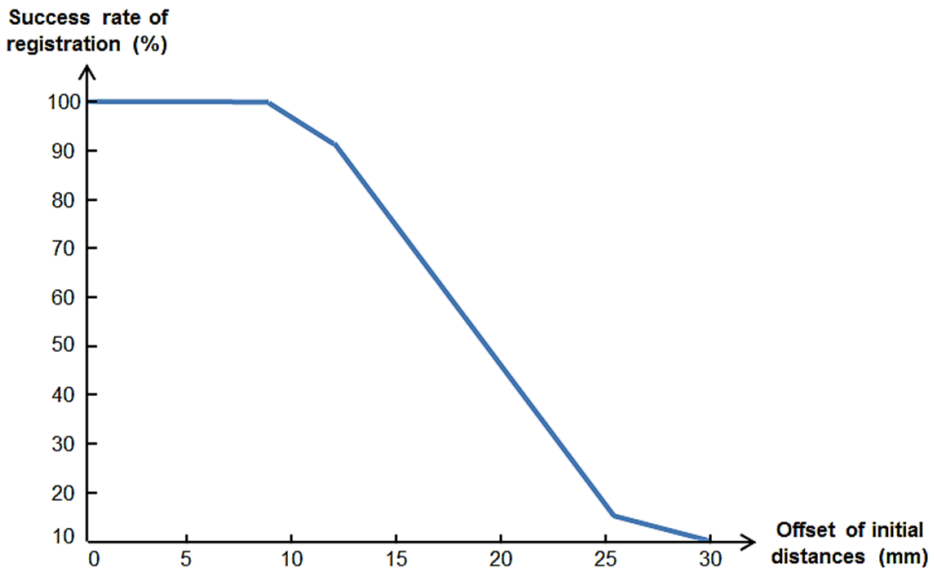


**Fig. 5.17. Success rate of the registration using initial positions with increasing offset. A 100% success rate in the registration is found when the offset for the initial position is below 10 mm.**

## 5.6 Summary and Discussion

In this chapter, the aim was to provide a TOE automatic acquisition solution for any patient-specific data during cardiac procedures based on a pre-procedure MR scan. The method of auto-adaption to patient data has been tested with real clinical data and an average error less than 1 cm was found. With small manual adjustments, the overall approach is sufficiently accurate to position the view plane close to the desired view in all cases. The source of this error is mainly the ICP registration method, in which the affine registration is not able to represent all variations in heart anatomy. Other non-rigid registration methods, such as proposed in the study [217, 218], may give a better alignment of the heart but the corresponding methods of identifying the standard planes and probe poses would need to be changed. As for the image-based probe tracking method, the experimental result indicates a high accuracy of the registration which is sufficient for locating the probe pose in this application. The capture range of the registration indicates a close estimation of the probe pose obtained from robotic kinematics is required in order to guarantee the success of the registration.

For the open-loop acquisition method, quantitative analysis of the error propagation in 3D ultrasound space indicates that the error is less than 23 mm within the imaging depth of 10 cm. In a real TOE acquisition, most structures of clinical interest during cardiac procedures, including major valves and the septum, are in the near field of ultrasound

(5-6 cm) where the error of the open-loop method is in the range 13.8 to 15.5 mm. With this order of magnitude of the error, it is expected that the majority of planned structures will be in the field of view and appear on the screen in 3D mode. Therefore the open-loop method is suitable for view planning in the 3D mode. There are a number of error sources in the method itself contributing to the overall error, including the error from initial registration, inverse kinematics, and forward modelling of the probe bending. The different errors for each view evident in Fig. 5.13 are mainly due to the difference between the view-planning software and the experimental setup. The probe is constrained to move along the oesophagus centre line in the view-planning software, which in reality might be different in the silicone tube. Additionally, large bi-directional bending in the silicone tube is not possible due to the rigidity of the tube. Different views defined in this study are in different portions of the silicone tube and required different ranges of bending, both of which contribute to variations of the errors. These errors will also occur in the real human body and are difficult to quantify and eliminate. Therefore, the best way to improve the accuracy is to perform acquisitions with closed-loop feedback adjustment. Considering the effect of different initial positions on the overall performance, the standard deviation results indicate that the initial position causes only small variations in the accuracy of the final probe locations. Provided the initial registration is successful, this initial position has little impact on the robustness of the solution.

Results from the second experiment using feedback adjustments indicate an obvious improvement in the accuracy of the probe positioning. Both the position and the orientation error have been reduced. From the results over multiple iterations, it is seen that the errors are mainly reduced in the first registration and feedback adjustment. The statistical test indicates there is a significant difference between the positional errors of the open-loop and the closed-loop methods but no significant difference between the orientational errors. However, this cannot fully represent the improvement of the feedback as the probe pose error has complicated effects on the errors in the ultrasound image depending on the different combinations of position and orientation errors. The statistical test for the error reduction in the ultrasound image space at the depth of 5-6 cm clearly indicates an improvement with the feedback in terms of the accuracy of obtaining the target. The error of points in 3D ultrasound space at the depth of 5-6 cm ranges from 8.0 to 9.2 mm, which is less or similar to the amount of movement and deformation of the beating heart. With the increase in accuracy, the centre slices of the

obtained ultrasound image align better with the original slice view planned in Unity (shown in Fig. 5.15). Therefore the method with one or more feedback adjustments has great potential in providing accurate automatic acquisition not only for 3D mode but also for 2D mode. However, such a deviation might still cause significant challenges for the 2D mode if a small structure is required in the view plane. In that case, a precision of a few millimetres might need to be achieved, which is still challenging using the current method. The feedback method using registration has the advantage of not requiring any other sensor or equipment. However, the registration method, serving as a means of tracking, currently has limitations of computational time and reliability. The current registration method takes 10-15 seconds and has a chance of failure due to a limited capture range of 10 mm as indicated from the capture range study. Therefore, either improvement in the registration method or a failure remedy method is necessary to provide a more reliable feedback method. In order to provide a faster and more reliable tracking method for feedback adjustments, electromagnetic tracking, which doesn't rely on image quality, would be an ideal choice working with the current image-based probe position tracking method. Motivated by this idea, the use of electromagnetic tracking on its own and combined use with the image registration to work with the current automatic acquisition workflow will be investigated and presented in the next chapter.

# 6 IMPROVED TRACKING AND VARIATIONS OF THE WORKFLOW

## 6.1 Introduction

In Chapter 5, an intelligent TOE robotic solution was presented which enables automatic acquisition of ultrasound images. This was addressed using a view-planning platform in which the robot is controlled according to a pre-planned path during the acquisition. The problem with patient variations was solved with an auto-patient adaption method described in the previous chapter. Considering the real mechanical movement, feedback of the probe position is essential in ensuring the success of the automatic acquisition. As described in the previous chapter, an ultrasound-to-MR registration method was employed for locating the probe pose when applying feedback.

However, in the workflow described in Chapter 5, the probe tracking method based on registering 3D ultrasound images to pre-scanned MR models requires a close initial estimate of the probe pose. This was estimated based on the robotic kinematics, which could result in failures because the mechanical performance of the probe driven by the robot mechanism within the real oesophagus could be different to the kinematics in the simulation environment. The experimental results from the previous chapter indicated a 10 mm capture range of the registration method which the initial estimation should meet. Therefore, a method of more reliable tracking of the probe's pose is a key component for automatic TOE acquisition to be reliable. Motivated by this requirement,

this chapter further investigates possible tracking methods of the probe and explores the applications of the new tracking method.

As an alternative to the image-based tracking, EM tracking systems are widely used for medical device tracking and have been reported for tracking the TOE probe [219]. However, registering the EM tracking coordinates to the patient coordinates is required which is difficult to achieve using the EM tracking system on its own and the accuracy of EM tracking could also be influenced by the electromagnetic environment. To solve the problem of reliable tracking, a method is introduced to combine the EM tracking system with image-based registration for probe tracking and integrate this method into the workflow as shown in Fig. 6.1. This tracking method is tested with a phantom experiment in which the tracking information provides feedback for the robot. The performances of the combined tracking method and the automatic acquisition are analysed and discussed. In this chapter, details of the new probe tracking method and the utilization of this new tracking method are presented in Section 6.2. Based on these methods, experiments and results for using this new tracking method in the application of automatic TOE acquisitions are presented in Section 6.3. It should be noted that this work on the improved tracking methods and its use in the automatic acquisition workflow has been included in the published work [220].

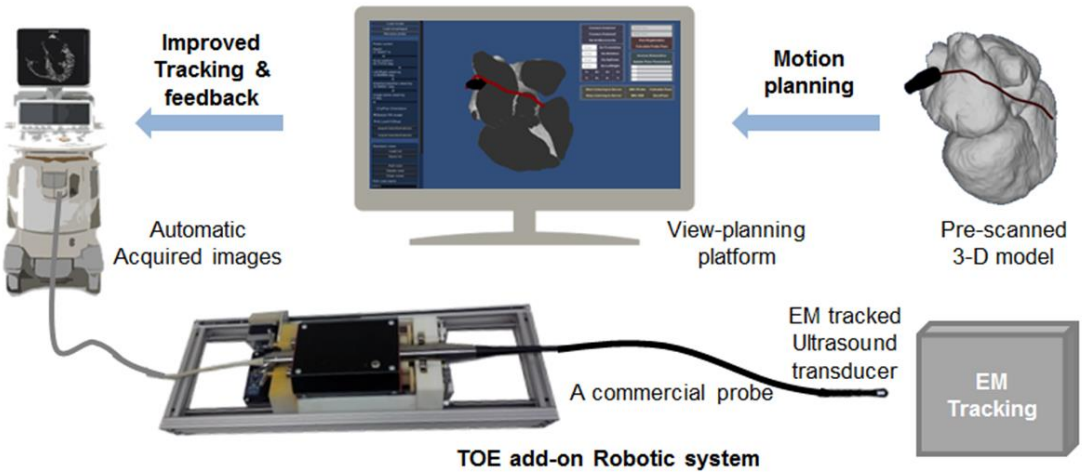


**Fig. 6.1. Overview of the TOE automatic acquisition workflow with the improved tracking method.**

The reliable tracking of the TOE probe improves the performance of the automatic TOE acquisition described in both Chapter 5 and Chapter 6. Up to Section 6.3, the whole workflow of the robot-based automatic TOE acquisition has been completed including the robotic TOE system described in Chapter 3, the kinematic modelling and view-planning platform described in Chapter 4, the auto-patient adaption method and registration-based feedback method described in Chapter 5, and the improved combined

tracking described in this chapter. The proposed workflow, though originally designed for automatic acquisitions of standard 2D or 3D TOE views, has variations that can also be used in several different applications. This includes pre-planning strategy for monitoring cardiac surgical devices as a variation of monitoring standard views. This also includes robot-assisted semi-automatic acquisitions and robot-based manual acquisitions as variations of the original automatic workflow. The second part of this chapter aims to present and discuss these variations of the proposed robot-based automatic acquisition workflow and demonstrate the potential uses of its components in different applications.

## 6.2 Improved Tracking with Electromagnetic Sensing

### 6.2.1 Spatial calibration

In the workflow, EM tracking is done using the Aurora Electromagnetic Measurement System (Northern Digital Inc., Waterloo, Canada). An EM sensor has been tightly mounted onto the tip of the probe using low friction taping and the extension wire of the EM sensor has been embedded into a tough protection sheath. Spatial calibration of the ultrasound image to the EM tracker was by a simple registration-based method using a phantom comprising several crossed wires [221]. This was to find the transformation which aligns the EM sensor's coordinates and the ultrasound image coordinates produced from the TOE probe. The phantom comprises two elastic bands stretched across a small open topped box with each elastic band hooked around tabs on opposite sides of the box (Fig. 6.2a). One of the elastic bands is stretched across with both sides parallel to each other. The other elastic band is stretched across to the first elastic band and has each side of the elastic band overlap to form a crossing in the middle of the box. The overlap is placed so that it is nearer to one of the sides of the parallel elastic band than the other. A piece of foam is placed at the bottom of the box to prevent rebounding of the ultrasound wave and the circular box is then placed into a box which is filled with water.

During the spatial calibration experiment, the EM tracker system was connected to a computer, which was used to store the location of the EM tracker in the EM space. The ultrasound machine was also connected to a computer, which stored the 3D image acquired by the probe via TCP/IP. For each image that was acquired in the experiment a

corresponding EM tracked location was measured. The probe was manually held in a certain position whilst readings from the EM tracker and the ultrasound probe were recorded. The probe poses at different positions and orientations were chosen in a way that the image encompassed the overlap of the elastic bands and all the lines formed from the elastic bands. Once the probe was in place the EM tracker position and the image from the ultrasound probe were recorded at the same time. This process was repeated 15 times at different positions to give 15 ultrasound images and their corresponding EM tracker location.

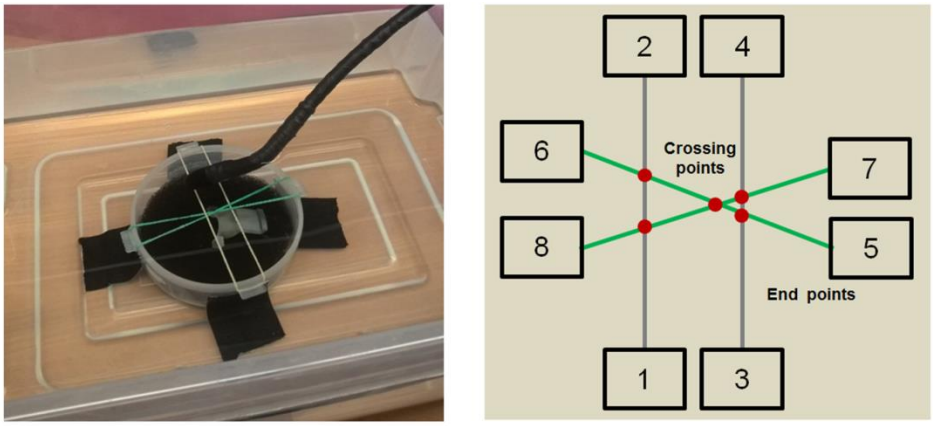


**Fig. 6.2. Illustration of the spatial calibration experiment. (a) Cross-line phantom and experimental setup for the calibration. (b) The ordering of the points extracted from the acquired 3D ultrasound images.**

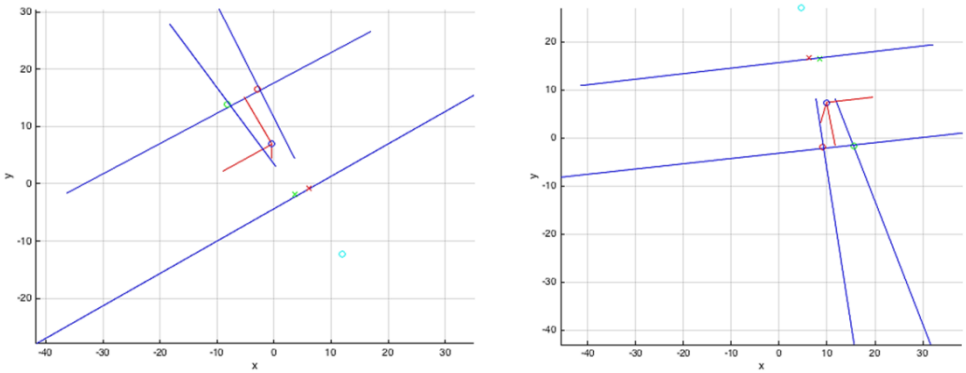

**Fig. 6.3. Examples of the coordinate system's definition with the extracted and calculated points.**

For post-processing, the straight lines and crossing points of the wires were extracted manually and logged in the order given in Fig. 6.2b. With the end points extracted and the crossing points calculated, a coordinate system with its origin and orientation for the phantom in each image is defined (Fig. 6.3), denoted as ${}^{\mathbf{US}}\mathbf{T}_{\mathbf{Phantom}}$. The calibration transformation is that which satisfies the fixed transformation:

$$ {}^{EM}T_{Phantom} = {}^{EM}T_{Tracker}\ {}^{Tracker}T_{US}\ {}^{US}T_{Phantom} \quad (6.1) $$

where ${}^{\text{Tracker}}\mathbf{T}_{\text{US}}$ is the unknown calibration and ${}^{\text{EM}}\mathbf{T}_{\text{Tracker}}$ is the measured position of the EM tracking device. The calibration was solved for iteratively to minimise the alignment error between a grid of reference points centred on phantom coordinates in each image. From this the targeted transformation ${}^{\text{tracker}}\mathbf{T}_{\text{probe}}$ was obtained using a prior known transformation from the probe coordinates to the ultrasound image coordinates. Using this spatial calibration, a measured pose of the EM tracker in the EM coordinate system can be converted to the pose of the probe in the EM coordinates ${}^{\text{EM}}\mathbf{T}_{\text{probe}}$ (Fig. 6.4) for locating the probe coordinates.

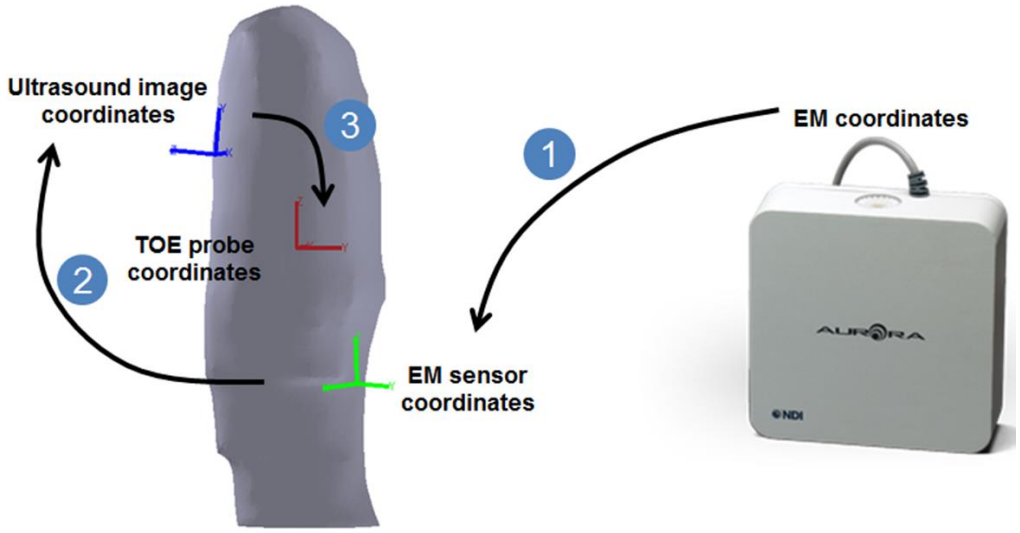


**Fig. 6.4. Illustration of the probe tracking with EM sensing using the spatial calibration result. Step 1 describes the position recording of the EM sensor in the EM coordinates. Step 2 is the calibration between the EM sensor coordinates and the TOE probe coordinates described in the spatial calibration. Step 3 uses a pre-known relationship between the ultrasound image coordinates and the TOE probe coordinates.**

### 6.2.2 Initialization and patient calibration

In order to provide the probe pose in the MR coordinates, another calibration between the EM coordinates and the MR coordinates must be obtained. This can be done at the time when the probe is manually inserted into the esophagus at a random starting pose with the probe pointing towards the heart. By visually looking at the first output ultrasound image, an estimated similar view can be manually selected from the view-planning platform, giving an estimate of the current probe pose in the MR coordinates ${}^{\text{MR}}\mathbf{T}_{\text{probe}}\mathbf{(initial)}$. The ultrasound image is then registered to the MR image starting from this estimation, giving an accurate probe pose in the MR coordinates ${}^{\text{MR}}\mathbf{T}_{\text{probe}}\mathbf{(reg)}$. The current probe pose ${}^{\text{EM}}\mathbf{T}_{\text{probe}}$ is also measured from the EM system. Therefore, an estimate of the transformation from the EM coordinates to the MR coordinates ${}^{\text{MR}}\mathbf{T}_{\text{EM}}$

can be obtained. The workflow of the patient calibration is shown in Fig. 6.5. It is important to understand that this is a once-only manual operation for each TOE scan of a patient. Clinically, this could be achieved relatively easily by an experienced TOE operator by requiring that they position the probe to one of the standard views when it is first inserted into the oesophagus. This is similar to the initialization procedure introduced in Chapter 5.

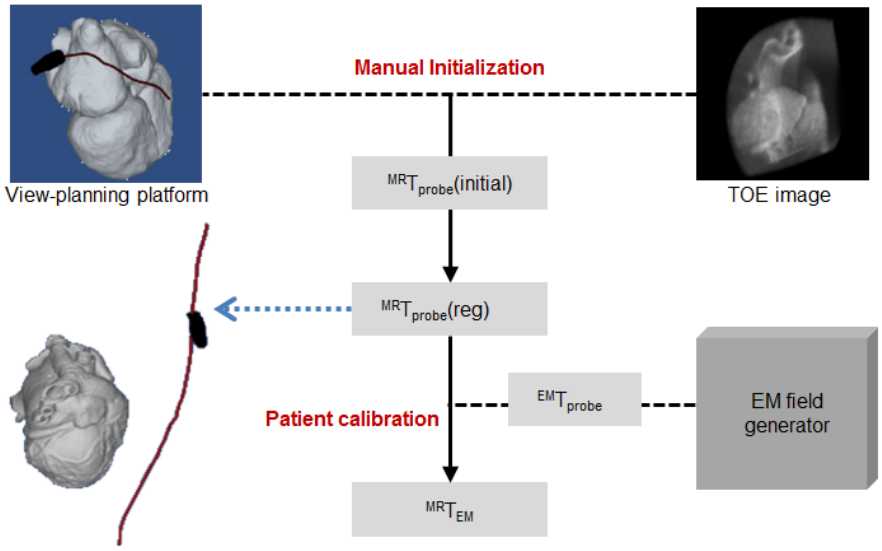


**Fig. 6.5. Diagram of the initialization and patient calibration based on image registration.**

### 6.2.3 Improved combined tracking

After initialization, the probe pose $^{MR}\mathbf{T}_{probe}\mathbf{(EM)}$ can be tracked automatically in any position inside of the oesophagus by the EM tracking system using $^{MR}\mathbf{T}_{EM}$ and $^{EM}\mathbf{T}_{probe}$. To further eliminate the influence of the environment on EM tracking and the inaccuracy of the initial calibration $^{MR}\mathbf{T}_{EM}$, registration of the current ultrasound image to the MR image is performed from the current $^{MR}\mathbf{T}_{probe}\mathbf{(EM)}$. The output from the registration is expected to give a more accurate pose of the probe in the MR coordinates $^{MR}\mathbf{T}_{probe}\mathbf{(EM\text{-}reg)}$ as shown in Fig. 6.6, which is used to provide feedback for the robot.

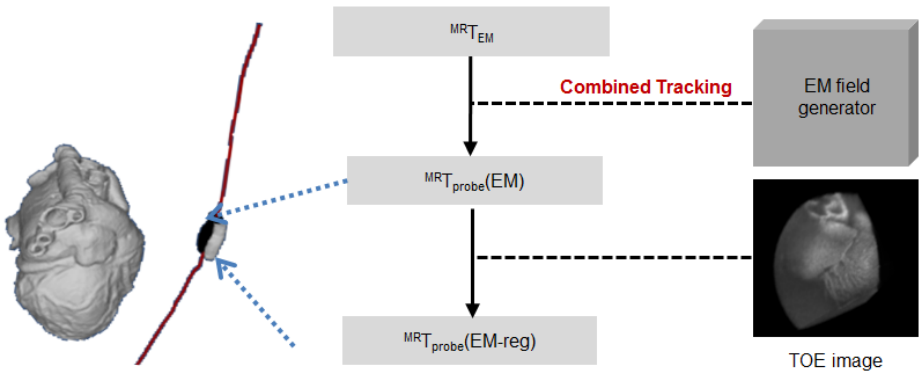


**Fig. 6.6. Diagram of the combined tracking method after initialization and patient calibration.**

## 6.3 Automatic Acquisitions for Standard Views

### 6.3.1 Overview

In this section, the aim is to evaluate the performances of the combined tracking method in the application of automatic TOE acquisitions for standard views presented in Chapter 5. The original workflow described includes the pre-planning procedure, auto-patient adaption, registration-based probe tracking and feedback. As a replacement of the original tracking method which is not reliable due to the limited capture range of registration, the improved tracking method described in this chapter is utilized and incorporated into the workflow for the application. Therefore, though the new experiment uses the same experimental setup and has the same targeting task, the aim of the experiment is mainly to test the performance of the new tracking method and compare the improved tracking method with the previous tracking approach. More specifically, this is to evaluate the following assumptions:

1. The proposed combined tracking method using EM sensing as the estimate of the registration has an improvement in reliability compared with the previous tracking method using kinematics as the estimate of the registration. This is important to understand the necessity of incorporating an additional positioning sensor in the robotic system and the automatic acquisition workflow.

2. The proposed combined tracking method using EM sensing as the estimate of the registration has an improvement in accuracy compared with using EM tracking on its own. This is important to understand the necessity of using ultrasound-to-MR registration as an additional step to achieve high accuracy for the tracking as this requires extra time for the tracking.

In addition to the analysis of the combined tracking, the performance of the automatic acquisition using the new tracking method in terms of the error in the ultrasound space is also studied in this experiment similarly to the experiment described in Chapter 5. Since the combined tracking method also uses the ultrasound-to-MR registration as the final step to provide feedback for probe positioning, similar experimental results and error magnitudes as presented in Chapter 5 are expected. Consequently, more detailed analysis as already performed in Chapter 5 will not be repeated in this section.

### 6.3.2 Experimental methods

A similar phantom experiment (Fig. 6.7) as described in Section 5.5 was performed to test the proposed tracking method and its performance in automatic TOE acquisition. During the experiment, the initial calibration between the EM coordinates and the MR coordinates was performed at the very beginning using the method described in Section 6.2.2. After initialization, the probe was tracked by the proposed tracking method described in Section 6.2.3. Based on the 5 pre-planned poses of the probe introduced in Chapter 5, the robotic system was actuated, driving the probe towards the targeted poses. When the probe arrived, the tracked probe pose was used as feedback information with the inverse kinematics method described in Section 5.3.2. The adjustments of the probe parameters were calculated and performed, and the ultrasound image was streamed to PC using TCP/IP. The experiment was repeated three times with different random initial poses of the probe.

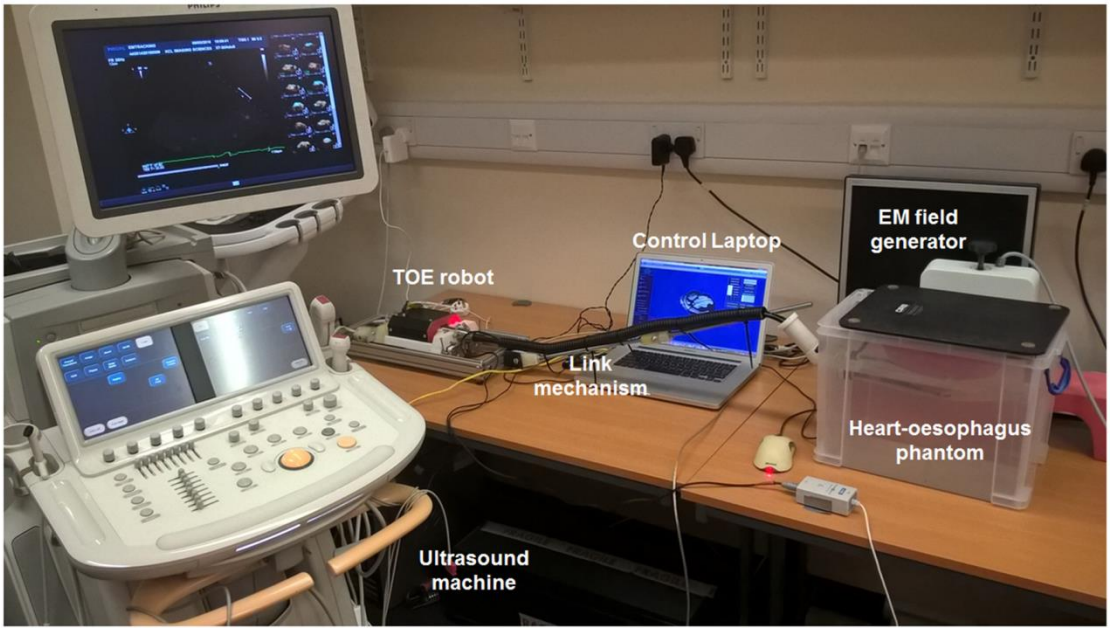


**Fig. 6.7. Experimental setup for the automatic acquisition using the TOE robot, custom heart-oesophagus phantom, and the EM tracking system.**

For post-processing, to understand the improvement in accuracy using the combined tracking method over the EM tracking method, the tracked probe poses reported by the EM tracking system $^{MR}\mathbf{T}_{probe}\mathbf{(EM)}$ and the combined tracking method $^{MR}\mathbf{T}_{probe}\mathbf{(EM\text{-}reg)}$ were compared. Root sum square (RSS) of the differences between the X-, Y-, and Z-axes rotation and translation components were calculated after decomposing each matrix. This is the same as the analysis method described in Section 5.5.2 to compare two poses. To understand the need for using the EM tracking system to provide the

initial estimate of registration for tracking, robot kinematics were used as an alternative initialization for the registrations similar to the tracking method described in Chapter 5 and the success rate was compared with the proposed combined tracking method.

The accuracy of automatic acquisition was quantified by comparing the final probe pose determined by registration $^{MR}\mathbf{T}_{probe}\mathbf{(EM\text{-}reg)}$ with the planned probe pose $^{MR}\mathbf{T}_{probe}\mathbf{(planned)}$. 60 marker points were defined in the ultrasound image field of view (90 deg * 90 deg cone) at a depth of 5-6 cm where most structures of clinical interest during cardiac procedures are located, including major valves and the septum. The locations of corresponding marker points in the MR coordinates were obtained and compared. The analysis is similar to the method described in Section 5.5.2 but focuses on the depth of 5 -6 cm with more marker points defined in this distance range to provide a more accurate evaluation of the error in the ultrasound space at the depth of clinical interest in TOE. Additionally, the acquired real ultrasound images were compared with the planned views in the view planning platform visually.

### 6.3.3 Results and comparisons

Results from the experiments indicate that the proposed tracking method is suitable for the robotic-based automatic TOE acquisition. Fig. 6.8a shows one of the tracking examples where the EM tracking provided a close estimation and the image-based registration calculated an accurate probe pose. Visual examination of the registration results found that the combined registration result could not be improved by manual adjustments, whereas the EM-only registration had some clear misalignment. Quantitatively, the proposed combined tracking method has a relatively high tracking accuracy with a median registration error of 1.45 mm. This has been shown previously from the investigation of the registration method itself in Section 5.5.3. Therefore, the combined tracking result is used as the reference to compare with the EM tracking result. The analysis indicates a difference of 7.96 mm and 3.42 deg between EM tracking and the combined methods for reporting probe poses during the experiment. The success rate is 11 out of 15 (73%) using the kinematics to provide the initial estimate of registration while all registrations succeed (100%) using the EM tracking result as the initial estimate of registration.

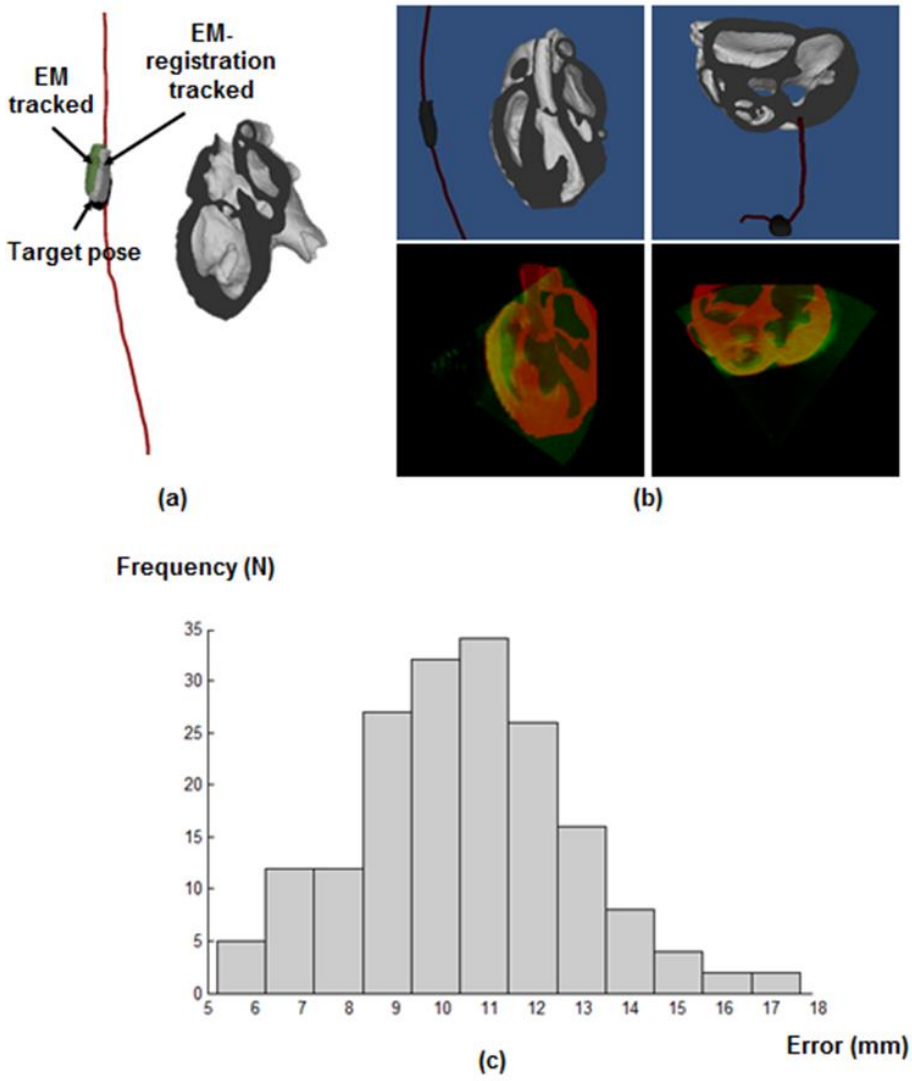


**Fig. 6.8. (a) Example of tracking with target probe pose (black), EM tracked pose (green), and EM-registration tracked pose (white) shown. (b) Examples of automatic acquisition results with planned view (top row) and acquired TOE images (bottom row). (c) Histogram of the error at 5-6 cm depth.**

For the performance of the automatic acquisition, the ultrasound images were overlaid on the MR segmentation data in order to intuitively compare the acquired ultrasound views with the views originally defined in the view planning software (example views are shown in Fig. 6.8b). The results show that all planned structures were in the 3D field of view and most of the centre slices of the obtained ultrasound images aligned with the original slice planned in the view-planning platform. Quantitatively, the overall error of marker points defined in the ultrasound field of view at the depth of interest over all three experiments is 10.44 ± 2.30 mm (mean ± standard deviation). A histogram of this error is shown in Fig. 6.8c.

## 6.4 Variations of the Robotic TOE Acquisition Workflow

### 6.4.1 Pre-planning strategy for device monitoring

- Overview of the application

In the previous sections described in this chapter, a combined tracking method using the EM tracking system with the ultrasound-to-MR registration was presented and its feasibility for incorporation into the automatic acquisition workflow initially described in Chapter 5 in order to obtain TOE standard views was shown. Based on the work of automatic standard view acquisitions, another use of the workflow with a separate probe positioning strategy is to plan and automatically position the probe to monitor devices for cardiac surgeries, such as catheters. This is to drive the robotic TOE system and automatically adjust the probe pose in order to accurately monitor and image the intra-operative devices in 3D modes (live 3D or 3D full-volume) during cardiac procedures. The motivation for this application is similar to the motivation of automatic view acquisitions where experience of the operator and continuous adjustments of the probe are required when TOE is used, especially in live 3D mode where the FOV is usually narrow.

In this section, a variation of the workflow is proposed to automatically monitor a device and place the device in an ideal location within the ultrasound FOV. The automatic positioning of the TOE probe is achieved using the proposed possible tracking methods and the robot kinematics with an automatic probe positioning strategy. The kinematic modelling described in Section 4.2 requires working in the patient coordinates with the information of oesophagus path provided by the pre-scanned MR image. Therefore, an initialization method based on the ultrasound-to-MR image registration is also required in the workflow in order to calibrate the EM tracking coordinates and the patient coordinates, similar to the method described in Section 6.2.2. The combined tracking method described in Section 6.2.3 can be used for tracking of the TOE probe as a way of providing feedback to accurately position the probe to image the defined target.

Additionally for this application, the accurate position of the target device must be known in the patient coordinates (the MR coordinates in practice). As a general approach, the device's location can be pre-planned in the MR coordinates. Alternatively, efficient tracking methods of the device based on image analysis or an

additional physical sensor can be used if real-time adjustments are required. However, considering the effect of cardiac motion and the reasonable adjustment rate of the TOE probe, the middle of the complete movement range of the device could be defined as the target to be imaged in the centre of the TOE FOV instead of the real-time device location. In practice, required target positions can be defined by the surgeon before the procedure using the view-planning platform based on the potential movement range of the device during the procedure.

- Probe positioning strategy based on device's location

In the application of automatic device monitoring, the tracking and feedback strategy of the probe is the same as used for automatic standard view acquisitions described in Section 6.2. However, the pre-planning strategy is different to the definition of standard views as this application takes the device location into consideration. The desired robotic parameters for the TOE system in order to image the device continuously are decided by the middle of the complete movement range of the device. This is defined as the target and its position in the ultrasound image coordinates is used for pre-planning. Ideally, as a way of optimizing the target position in the FOV, the defined target should be positioned at the centre of the TOE FOV. However, the Z-distance between the probe's transducer face and the target, measured along the Z-axis of the ultrasound image coordinates, is constrained by the heart-to-oesophagus distance and therefore the Z-distance optimization is limited. Moreover, most of the structures of clinical interest, where devices are likely to be placed, are already at good positions in the ultrasound image space (near field). Therefore, the focus of this work is on optimizing the X-axis distance and Y-axis distance measured along the X- and Y axes of the ultrasound image coordinates, in which case the two distances are zero if the target is placed at the centre of the X-Y plane (Fig. 6.9).

An objective function based on the X- and Y-axial distances from the origin of the ultrasound image coordinates to the target is defined for the inverse kinematics to optimize the robotic parameters using the gradient-descent search strategy described in Section 5.2.3. As described previously, the forward kinematic model F(**p**), where **p** is the robotic parameter set, gives the transformation from the patient coordinates to a predicted probe pose in the patient coordinates if the probe's initial pose is known. With

the combined tracking information for the current probe pose ${}^{Patient}\mathbf{T}_{Probe}$ serving as the initial pose, a predicted probe pose in the patient coordinates is:

$$ {}^{Patient}\mathbf{T}_{Probe}(\mathbf{p}) = {}^{Patient}\mathbf{T}_{Probe}\mathrm{F}(\mathbf{p}) \quad (6.2). $$

The position vector of the device defined in the patient coordinates is known as ${}^{Patient}\mathbf{T}_{target}$. Therefore, the position of the device in the ultrasound image coordinates based on the predicted probe pose is calculated using the known calibration between the probe and ultrasound image:

$$ {}^{US}\mathbf{T}_{Target}(\mathbf{p}) = {}^{US}\mathbf{T}_{Probe}\,{}^{Probe}\mathbf{T}_{Patient}(\mathbf{p})\,{}^{Patient}\mathbf{T}_{Target} \quad (6.3) $$

The objective function is then defined based on the target position in the ultrasound image coordinates. Since both X- and Y- components of this position vector are expected to be zero to locate the target at the centre, the objective function is defined as the root sum square of the X and Y components extracted from ${}^{US}\mathbf{T}_{Target}(\mathbf{p})$. Similarly to the method introduced in Section 5.2.3, the search strategy for the probe robotic parameters in a defined range uses the gradient-descent iteration and results in the best-fit probe robotic parameters **p*** to represent the desired probe pose ${}^{Patient}\mathbf{T}_{Probe}{}^{*}$. Based on the calculated desired probe robotic parameters, the TOE robot drives the probe and re-positions the probe's location with tracking and feedback in order to image the device accurately, similar to the automatic acquisition workflow for standard views described in Section 6.2.

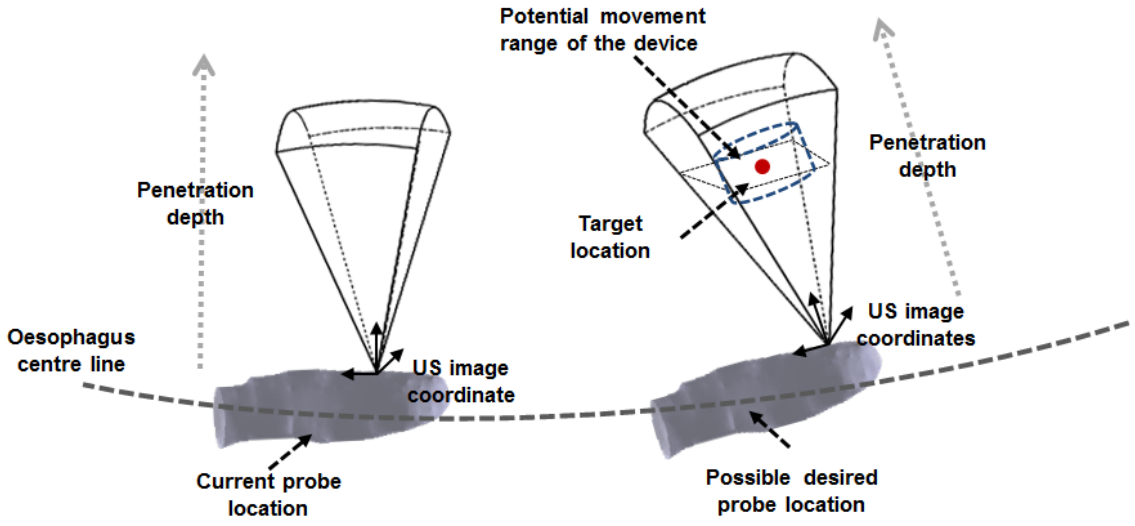


**Fig. 6.9. Illustration of the strategy for probe optimization in order to image the device accurately. The target location (red point) is defined as the centre point of the potential movement range of the device (dotted blue line). This can be selected by the user during the pre-planning process.**

- Verification of the pre-planning strategy

To verify the correct working of the pre-planning strategy in the view-planning platform, 100 random points are defined within the heart segments to simulate the planned targets defined by the user. The automatic probe positioning method is applied to calculate the desired probe pose to image the defined point at the centre of the ultrasound FOV. Based on the resulting calculated probe pose ${}^{US}\mathbf{T}_{\mathbf{Target}}$, the error function is defined as the root sum square of the X and Y components extracted from the matrix. This quantifies the offset error from the centre of the ultrasound FOV. This evaluation indicates a mean error less than 0.5 mm for the pre-planning of the 100 target points.

### 6.4.2 Robot-assisted semi-automatic TOE and robot-based manual TOE

From the view of automation level, robot-assisted semi-automatic TOE and robot-based manual TOE are variations of the proposed automatic TOE acquisition workflow described in Chapter 5 and earlier in this chapter. The robot-assisted semi-automatic TOE acquisition aims to solve a potential problem with the translational axis which requires a guiding mechanism for the endoscopic portion of the probe to be led into the patient's oral cavity. This requires the guiding mechanism to be extended and placed relatively close to the patient. Therefore, it may introduce more safety concerns in the robotic system as well as a space concern. As a variation, the semi-automatic TOE acquisition could use the translational axis of the robot as a passive axis without the guiding mechanism and require the operator to manually set the depths of the TOE probe according to the probe parameters obtained from the pre-planning process. This could be achieved since distance markers exist on the endoscope which itself can guide the operator without any additional requirement of expertise. After setting the depth of the probe manually, the other three axes of the robot will be controlled robotically using the automatic-acquisition workflow presented in Chapter 5 and Chapter 6. Additional changes to the original workflow may be required to limit translational movements of the probe during automatic feedback adjustments and rely on the other three axes to obtain the target view.

The robot-based manual TOE approach intends to give the operator more priority when controlling the robot for TOE acquisitions, as a variation of the proposed automatic acquisition workflow. In this situation, the pre-planning process based on the view-planning platform is still required to give an unexperienced TOE operator clear

indications of where to place the probe. The robotic-probe parameters for each view, together with the predicted output ultrasound images generated from the view-planning platform, will be written into a guiding protocol for using the robot to set up required views. Based on the pre-planning platform and the generated protocol, the operator is required to control the robot by themselves to set up a view and let the robot continuously hold the probe and monitor the procedure. It is expected that the robot-based manual TOE might be less accurate at acquiring the pre-planned probe pose and view compared with the automatic or semi-automatic TOE acquisition. However, it does not require any additional tracking and feedback methods but relies on the user's visual feedback. This makes it more easy to incorporate into the clinical workflow and there is less chance of mistakes compared with probe control methods using higher automation strategies.

As variations of the proposed automatic-acquisition workflow, robot-assisted semi-automatic TOE and robot-based manual TOE use existing methods described in the workflow but with minor adjustments. Independent experiments to evaluate these two variations are not included into this thesis but are left as future works for testing the most feasible robotic acquisition workflow clinically and in cadaver experiments.

## 6.5 Summary and Discussion

Derived from the problem with tracking reliability identified in Chapter 5, this chapter further investigated the tracking strategies and proposed a new combined tracking method described in Section 6.2. The proposed combined tracking method uses the combination of the EM tracking system and the image-based registration method. This aims to provide a reliable and accurate tracking solution for the TOE probe in order to guide the robot for automatic standard view acquisition, as initially described in Chapter 5. Therefore, the automatic view acquisition experiment was re-performed but the analysis of the results was more focused on validating the new proposed tracking solution. These experiments were described in Section 6.3. From the results, it was identified that using the image-based registration and an EM tracking system together enables a more accurate tracking performance than using the EM sensor alone. This is because the EM sensor could be influenced by the environment and an inaccurate calibration. As one of the most well-known problems with the EM tracking, distortions induced by ferromagnetic materials and electronic circuits from the clinical environment

may have an impact on the accuracy of tracking. In the use of the TOE robot, this might include influences from several sources, e.g. the general clinical set-up, the imaging devices in the surgical room, and the electronic and mechanical components of the TOE robot itself, such as the stepper motor and drive circuits. From existing literature such as reviewed in [222], it is apparent that generalizing results obtained in one environment to others is not straightforward. As a result, the current accuracy evaluation study should be re-performed in the exact clinical environment to re-evaluate its feasibility. For the current experiment, compared with using kinematics as the initial estimate of registration described in Chapter 5, the EM tracking system provides a more reliable estimate and ensures the success rate of the tracking. Therefore the proposed combined tracking method is believed to be suitable for automatic TOE acquisition in terms of both accuracy and reliability.

It should be noted that the gold standard for the error measurement of the tracking method was to run the registration from a good initial alignment, and then to manually correct any visible alignment errors, although in the experiment there was almost no visible misalignment after this registration. Therefore, while the gold standard is not truly independent, it is thought to be accurate, and certainly shows that registration is better than using EM tracking alone. As for the accuracy of probe positioning for automatic acquisition, the error in the ultrasound space at the depth of clinical interest due to the probe positioning error is similar to the amount of movement and deformation of the beating heart (1 cm). This is similar to the results found in Chapter 5. The result is reasonable as both experiments utilized the same pre-planning method, experimental setup, and kinematic-based feedback. Importantly, though the new tracking method was employed, the tracking accuracy is still decided by the image-based registration method. Therefore, using the new tracking approach for the automatic standard view acquisition was mainly to improve the reliability and not the probe positioning accuracy. In that case, a number of error sources contributing to the overall error discussed in Section 5.6 also account for the re-performed experiment. As a summary, with the new combined tracking method incorporated into the automatic standard view acquisition, the complete workflow has great potential to be used clinically in terms of both accuracy and reliability. This work is the last main aim of the thesis as planned initially and the whole solution is now ready to be tested using suitable cadaver facilities to validate the concept in real human bodies.

In the final part of this chapter in Section 6.4, several variations of the complete workflow have been proposed and described. From the view of the object to be imaged, a different pre-planning method was proposed for monitoring devices during cardiac procedures using 3D TOE with the robot, as described in Section 6.4.1. The simulation result indicates the planning method can accurately find desired probe poses to image the targets at the centre of the ultrasound FOV. The target is set at the middle of the complete movement range of the device. For probe automatic positioning with the robot, similar performance and the magnitude of error as presented in Section 6.3 are expected. This is because the probe tracking and feedback methods are the same as automatic probe positioning for standard view acquisitions. To further evaluate the performance on acceptance of automatic device monitoring, experiments using anatomically-correct phantoms or cadavers with cardiac surgical devices incorporated should be performed in the future. In Section 6.4.2, variations of the workflow from the view of automation level were presented to indicate potential use of the robot with the current designed techniques. This section briefly described the concept of using the current workflow with minor changes to do robot-assisted semi-automatic TOE acquisitions and robot-based manual TOE acquisitions. These variations should be tested and compared in the future using cadavers to evaluate their feasibilities and performances. The ultimate goal is to find the best clinically acceptable option of the workflow for using the robot to assist TOE acquisitions.

# 7 CONCLUSION AND FUTURE WORK

## 7.1 Summary and Discussion

### 7.1.1 Design and implementation of the TOE robot

The work presented in this thesis aims to develop a robotic TOE system that can be used during cardiac procedures as a remote operated device and can be automatically controlled to perform ultrasound acquisitions. This is motivated by several challenges for the echocardiographer with manual operation of the traditional TOE probe discussed in Chapter 1, such as long-term radiation exposure, potential orthopaedic injuries, and advanced training requirements. Though numerous works have been presented for the concepts of robotic ultrasound and robotic endoscopic systems, including different designs and various automatic control approaches as reviewed in Chapter 2, no previous work in the literature has demonstrated the motorization of a TOE probe and the utilization of a robotic TOE system as an automatic device to perform cardiac ultrasound scanning.

Based on a commercial TOE probe, the design and implementation of a robotic TOE system was first proposed. The add-on device holds the probe handle and manipulates four degrees of freedom (DOFs) that are available in manual handling of the probe, including the rotation about and translation along the length of the TOE probe and additional manipulators with 2-DOFs to bend the probe head. This was achieved by several unique mechanisms described in Chapter 3. These mechanisms are primarily

designed for the X7-2t TOE probe used in this study but can be easily adapted to meet the particular dimensions and shapes of other available TOE probes. The described system is lightweight and has a small footprint with all the electronics and control devices built in. The basis of remote control for the current robot was achieved using Bluetooth communication working with the integrated microcontrollers. However, other remote communication methods such as wireless communication could also be easily implemented. To verify the correct working of the mechanisms and electronics, a repeatability experiment was performed using an optical tracking system to investigate the positioning of the probe tip. The experimental results indicated that the repeatability error of the robotic system is less than 1mm. Therefore, the mechanical design and the basic electronic controls of the robot are reliable.

### 7.1.2 Safety issues and intuitive control of the robot

The safety of a medical robotic system has always been an important concern. This is particularly decided by the safety status and requirement of the original device, which is the TOE probe in this study. The safety and complications of TOE have been reviewed in Chapter 1 and it was identified that TOE has been well proved clinically over many years since it was introduced with a low rate of complications. It is a highly safe procedure when performed by a trained clinician. However, actuating the probe when the tip is in flexion states is the most dangerous operation and needs to be avoided. Therefore a design was proposed using magnetic sensors as the safety sensor to detect the neutralization of the probe knob driving discs, to monitor the bending state of the tip. In addition, a current limiting strategy was employed as a passive safety feature to limit the bending forces generated by the probe tip based on comparative force measurement experiments using manual and robotic control. Though other safety features may need to be incorporated into the robot in order to meet the regulation of medical devices for a commercial product, the current safety feature of bending monitoring and limiting meets the safety objective set in Chapter 1 for this research prototype. Additionally, a watchdog system was designed to monitor the availability of the microcontrollers. These safety features were presented and studied in Chapter 3. In the same chapter, several different control choices for the TOE robot were explored including using custom software, a gamepad, a specially designed dummy probe, or a haptic device. Preliminary bench experiments were performed to verify the correct operations of these remote control devices.

### 7.1.3 View-planning platform and kinematic modelling

With the proposed robotic TOE system, intelligence towards automatic or semi-automatic TOE acquisition is expected beyond the function of manual remote control, in order to improve the utilization of TOE and deskill the operation for acquiring standard views. This started with the development of a view-planning platform which enables the user to virtually drive the TOE probe and define required ultrasound views when an MR or CT scan is performed before the cardiac surgeries. In Chapter 4, a kinematic modelling method for the TOE probe, given the information of the oesophagus and heart, was presented to provide the relationship between motor parameters, poses of the probe tip, and output ultrasound images. This modelling method was tested in terms of the targeted accuracy using the optical tracking method. The results indicate the feasibility of employing this model to represent the movements of the tip, though point-to-point errors of the order of millimetres were identified, as was discussed in more detail in Chapter 4. Based on the kinematics, a view-planning platform built in Unity was presented. The platform loads the segmented heart and oesophagus model for visualization and takes the motor parameters as user inputs. A virtual TOE probe head is driven along the oesophagus based on the kinematics, and the corresponding virtual 2D slice view is generated as the output to indicate the structures imaged when the TOE probe is placed at that location. The whole platform is designed to define either 2D or 3D TOE views before a cardiac surgery, and the feasibility of the software has been tested by setting up the 2D TOE standard views described in the standard protocol. As a pre-planning process operated by the professional surgeon or echocardiographer, the whole view-planning platform allows for defining TOE standard views and obtaining robotic parameters. The design of the platform meets the objective defined in Chapter 1 for having a method to plan TOE views for a TOE acquisition before the robot-assisted procedure.

### 7.1.4 Automatic TOE acquisition workflow

The workflow of the automatic TOE acquisition using the view-planning platform and the robot was presented in Chapter 5. This includes the ingredient of the auto-patient adaption method for patient specific data. This is intended to allow the user to quickly decide the standard views for new patient data taking the variations of the heart and oesophagus between patients into consideration once standard views for a reference heart-oesophagus model are defined. For the auto-adaption, ICP registration was

utilized with a probe parameter optimization method to determine the best parameters for the new patient. The method was tested using two patient data sets and the results from the quantitative and qualitative analysis indicate that the error has a magnitude of 1 cm and small manual adjustments are required to correct the error induced from the affine registration and probe parameter optimization. However, the adjustments are easy to perform for an echocardiographer and could be done rapidly before the cardiac surgeries in the pre-planning step. Moreover, this error in the pre-planning step for the view might not influence the correct acquisition if 3D mode for a volume is used. Another ingredient for the automatic TOE acquisition aims to provide position tracking information of the probe tip for feedback control, in order to reduce the probe positioning error during the acquisition. This was achieved by adapting previous work of registering the TOE images to pre-scanned MR images. Details of the method have been explained and a separate experiment was performed to verify the accuracy and capture range of this image-based tracking method. With these ingredients, automatic acquisition experiments using a custom heart-oesophagus phantom were performed to verify the feasibility of the whole workflow. Different analyses were performed to evaluate the positioning accuracy of the TOE probe and the error's effect on the ultrasound image, as discussed in Chapter 5. With feedback adjustments, the error of points in 3D ultrasound space at the depth of 5-6 cm ranges from 8.0 to 9.2 mm, which is less or similar to the amount of movement and deformation of the beating heart. This meets the goal for the accuracy of automatic acquisition set in Chapter 1. However, it is noted that such a deviation can still cause significant challenges for the 2D mode if a small structure is required in the view plane. As a conclusion, the performance of the automatic TOE acquisition workflow using the robotic TOE system in the phantom is encouraging for the eventual clinical application. Using the proposed method, TOE standard views can be acquired automatically or semi-automatically with minor manual assistance.

The current experiments for the automatic acquisition workflow described in Chapter 5 and Chapter 6 of this thesis relied on pre-surgical MR scans. However, the workflow could also handle CT images as the input to the planning and acquisition workflow with minor adjustments. In the pre-planning process, alternative existing automatic, semi-automatic, or manual segmentation methods for cardiac CT images should be adapted as the replacement of the current segmentation method for MR images described in Chapter 4. The image-based tracking method used in the workflow, though referring to

MR to ultrasound registration for simplicity in the thesis, was initially proposed for registering preprocedure volumetric images to the 3D TOE images based on using simulated ultrasound images generated from the segmentation and therefore is also able to handle the CT segmentation once it has been prepared. In addition, the rest of the components in the workflow also remain the same if CT images are used. The use of MR or CT as the pre-planned images for the robotic TOE has no preference and should be based on the specific availability, which is decided by the original clinical decision on the pre-scanning modality for diagnosis and surgical planning. For more realistic oesophageal position modelling during the robotic TOE, dummy probes might be used with either MR or CT pre-scans to simulate the influence of the TOE probe on the oesophagus position relative to the heart.

### 7.1.5 Improved tracking and catheter monitoring

The most important problem identified in the automatic TOE acquisition experiments is several failures of the image-based tracking as discussed in Chapter 5. These failure cases were due to the inaccurate estimation of the probe pose provided by the kinematics and used for the registration. This is the result of differences between the mechanical performance of the probe driven by the robot within the real esophagus and the simulated movements in the view-planning environment. This problem with tracking was further investigated and addressed using a combined tracking method incorporating EM sensing, as presented in Chapter 6. For this improved tracking method, an EM tracking system was used to provide the initial estimation of the probe pose after a sensor has been attached to the tip of the probe. Calibration methods between the tracker coordinates and the probe coordinates, as well as between the EM coordinates and the MR coordinates, were developed. The whole combined tracking method was included into the automatic TOE acquisition workflow, and experiments similar to those in Chapter 5 were re-performed, but focusing on the validation and comparison of the combined tracking method. As summarized in Chapter 6, the combined tracking method has 100% success rate, indicating an improvement over the tracking method that uses kinematics as the estimate of the registration. The improvement in accuracy of the combined tracking over the tracking method using EM sensing alone indicates the necessity of keeping registration in the workflow for tracking of the TOE probe. The whole workflow of reliable automatic TOE acquisition was completed with the combined tracking method described in the first half of Chapter

6 and other ingredients described in Chapter 3, Chapter 4 and Chapter 5. To summarise, the combined tracking can provide both reliability and accuracy for locating the probe during the automatic TOE acquisition. This meets the objective set in Chapter 1 for having an accurate tracking method which is sufficient enough to control the TOE robot for its application in automatic acquisitions.

### 7.1.6 Variations of the automatic acquisition workflow

In the second half of Chapter 6, in Section 6.4, some variations of the proposed automatic acquisition workflow were presented. These include a different pre-planning strategy focusing on monitoring devices rather than standard views. This aims to keep the device at the centre of the ultrasound FOV and use the automatic acquisition workflow to drive the probe to the planned position. The strategy was verified in the view-planning platform with highly accurate probe positioning, giving an error less than 0.5 mm. Further experiments with real surgical devices and anatomically correct phantoms or cadavers are required to test the whole method. The second variation described is for the level of automation. The concept of robot-assisted semi-automatic acquisitions and robot-based manual acquisitions were proposed. Though further experiments need to be performed to understand the best option of the workflow for the clinical environment, these variations mainly use the existing methods already presented in Chapter 5 and Chapter 6 with minor adjustments to a few steps.

## 7.2 Limitations and Future Work

### 7.2.1 Design and implementation of the TOE robot

The proposed TOE robotic system was primarily designed to work as an add-on device for TOE acquisition. The current design does not include the actuation DOF for the electronic steering of ultrasound controlled by two small buttons on the handle of the TOE probe. For the second clinical prototype, this could be addressed by adding additional mechanisms to push the buttons from the inside of the handle control structure if mechanical actuation is selected as the approach to control the electronic steering. Alternatively, a better solution would be to directly access the electronic signal which is used to control the electronic steering internally from the probe and the

ultrasound machine. This would require modification of the original ultrasound and probe system working with the probe manufacturer.

In addition to adding another DOF to control the electronic steering buttons, several improvements could be incorporated into the future design of the robot, based on the findings of the current version:

- The size of the robot can be reduced by using smaller motors which will still generate enough torque for turning the knobs on the probe for the handle control structure.
- To better integrate the system into the clinical environment, the future design could have accessories including a mechanical mounting solution for the robot to work in the catheter lab.
- The current guiding mechanism for the translational axis described in Chapter 3 is designed for the phantom and cadaver experiments and includes metal links and joints. For a second clinical prototype, improved safety features should be one of the future development tasks.

### 7.2.2 Safety issues and intuitive control of the robot

In terms of the safety of the current TOE robot, additional torque sensors actively monitoring the rotation of the knobs could be useful for tracking the force at the tip of the probe if a second clinical prototype is built. The most important safety sensor for the current design is the neutralization monitoring device for the knobs, which is to ensure the probe tip is not in its flexion states while actuated. However, the current sensor has the limitation of only sensing when the knobs are in their neutral positions and not indicating their distances away from the neutral positions. In the future design, angle sensing devices will be incorporated to address this limitation. If a second clinical prototype is built, an auto-eject mechanism could be designed which enables the user to release the probe from the mechanism immediately by pressing a single button on the robot. This will actuate another motor or a magnetic clutch ejecting the probe from the robotic manipulator. The design is to allow a quick switch from robotic to manual control if this is required by the echocardiographer. The mechanism requires an ejection of the handle control part of the TOE probe while at the same time keeping the endoscopic part of the probe as steady as possible to ensure minimum movement of the probe inside of the patient.

Several control modalities have been investigated in this study as the master device for the echocardiographer to operate, and the correct operation of each method has been verified. However, the current study has the limitation that these devices have not been studied and compared with each other by cardiologists. This is mainly due to unavailability of a realistic TOE simulation environment, as the current heart-oesophagus phantom is mainly designed for imaging but not the simulation of the oral cavity. In the future, cadaver experiments or a more realistic TOE phantom including the body structures will be useful for the comparative study of different control modalities of the robot.

### 7.2.3 Kinematic modelling and view-planning platform

The current view-planning platform models the movements of the TOE probe along the centre line of the oesophagus, and the kinematic model was built in free space to predict the pose of the probe tip relative to the heart. However, the actual performance of the head of the probe in the real oesophagus can be different as the bending of the tip will have interactions with the oesophagus wall. This is the main limitation of the view-planning platform and the future work for this topic will focus on an interactive kinematic model of the TOE probe inside of the oesophagus taking the effects of the wall into consideration.

The current view-planning platform built by the Unity engine requires automatic segmentation and manual segmentation performed in advance using separate software. For an improved platform to be used clinically and which incorporates all required steps of view planning, the segmentation functions should be included into the main view-planning software as well. The current view-planning platform defines TOE views using the clip planes generated from the pose of the probe tip. This is ideal for defining 2D TOE views as it clearly shows potential structures to be imaged with the current parameters. However, defining 3D TOE views using the clip planes might not be intuitive enough and improved methods for visualization are required.

### 7.2.4 Automatic TOE acquisition workflow

The current experiment using the heart-oesophagus phantom has the limitation that the custom views are not natural to the real TOE views. The most important next step would be to test the whole view planning and the automatic acquisition method in cadavers with real TOE views to further evaluate the whole workflow in the real human

body. This would require specially preserved cadavers using the Thiel embalming method to allow life-like TOE acquisitions. These experiments would provide a more realistic environment in which the required level of accuracy for 3D and 2D imaging could be verified. In the current work, the accuracy requirements for the error in the ultrasound space were decided by the level of the heart deformation movement as a reference. However, it was noted that this level of accuracy might not be adequate if small structures are required to be viewed in 2D mode. Therefore, an important future task should be to re-evaluate the accuracy requirements for the automatic TOE acquisition workflow in this less rigid environment based on a qualitative study judging whether the planned structures are successfully obtained in a real human body.

The problem of reliable tracking of the TOE probe in the automatic acquisition workflow has been addressed using the improved combined tracking method with EM sensing incorporated. Though the method has a high success rate, it still requires time for registration to obtain high accuracy. In the future, using the EM tracking method on its own could be investigated in order to improve the real-time performance of the tracking. The error of the EM tracking should be broken down and analysed. This will indicate the error contribution from the calibration and the environmental influences. The variations of the automatic acquisition workflow presented in the second half of Chapter 6 require further clinical experiments to understand their feasibilities in real TOE scans. These works should be done using cadavers to be able to have a realistic anatomically-correct setup. These proposed variations of the workflow also require surgeons and echocardiographers to operate the robot and evaluate the performance. These tests should be included in future clinical evaluations of the TOE robot.

Additionally, physiological movements, such as respiratory and cardiac motions, are not specifically studied and addressed in the current automatic acquisition workflow. For the pre-planning step using the pre-scanned images, deformation and motion artefacts caused by the beating heart and vascular pulsation might require extensive correction to the automatic segmentation results for either modalities. For the auto-positioning step using the robotic TOE system, the influence of the organ motion would be less when it is used for acquiring standard views as these views usually have an adequate FOV to tolerate the motions of organs and many of these views are inherently designed to investigate the movements of the heart. However, when the automatic acquisition is used for monitoring devices as one of the variations discussed in Chapter 7, additional methods for motion compensation might be necessary to keep the device in the centre of

the FOV, especially when live 3-D mode with a relative narrow FOV is used. Potentially, methods of image servoing with robotic differential kinematics, which relate the movements of the structures in image space to the changes of the joint space parameters, could be a method to reject the physiological movements, similar to the work described in [179], although additional image-based tracking methods for the device are required. Furthermore, it is known that the physiological movements might also result in translational movement of the probe coming out from the oral cavity by a few centimetres. Without an appropriate way to maintain the probe and compensate the movement, this could cause risks to the patient, such as complications related to the oesophagus injuries listed in Chapter 1. For future work, a comprehensive study of the TOE operator's role in controlling the probe to deal with the physiological movements should be performed. The results from the study can be used to guide a new design of the probe translational mechanism for maintaining the probe's position near the oral cavity.

### 7.2.5 Cadaver experiment

The initial trial of cadaver experiments in this work was to use the normal cadaveric human oesophagus from dissected bodies (for educational purposes) preserved in formalin for the force measurement experiment. This proved unsuccessful due to technical difficulties with inserting the TOE probe into an inelastic oesophagus. As described in Chapter 3, when the deceased person is embalmed, the chemical in the process fixes the tissues in the rigor state. The loss of circulation leads to an inability of the oesophagus muscle to relax, whereas in a living person the passage of the probe is permitted due to muscle relaxation and peristaltic movements. For these reasons, the planned cadaver experiments, such as for testing the automatic acquisition, were not performed due to lack of facilities in the limited time period of this work. In the future, an alternative way to conduct cadaver experiments is to use the advanced Thiel cadaver technique as mentioned in previous sections. The Thiel embalming soft-fix method would allow preservation of the oesophagus in its life-like flexible state and quality, as well as allow ultrasound imaging of the heart from the oesophagus. This would be ideal for testing the proposed TOE robotic system and as discussed previously to revalidate the system design and the acquisition workflow.

## 7.3 Conclusion

The research work presented in this thesis was motivated by the difficulties of the current use of trans-oesophageal echocardiography for diagnosis and cardiac procedure monitoring, including the radiation exposure to the user, the orthopaedic injury concern, and the requirements of training and experience. The first main contribution of this work was developing an add-on robotic system to be able to remotely control a commercial TOE probe. As presented in Chapter 3, the developed robotic system has a small footprint and its reliable performance with 1 mm magnitude repeatability error has been verified in support of the hypothesis. For safety, several features to avoid TOE complications have been built into the system. These functionalities have been tested in phantom for validation. To incorporate intelligence into this robotic system, a view-planning platform based on a kinematic modelling of the robot was successfully developed as the second main contribution of this work presented in Chapter 4. This provides the user with a way to plan and define robotic TOE procedures based on pre-scanned MR images. The accuracy of the kinematic modelling with a mean predication error less than 5 mm in free space has been verified in support of the hypothesis.

Based on the robotic system and the view-planning platform, the third main contribution of this work was building a whole automatic acquisition workflow and designing individual components required for this workflow presented in Chapter 5 and Chapter 6. This includes an auto-patient adaption method for finding standard views for a new patient, different probe tracking methods to locate the probe, and optimisation-based inverse kinematic modelling for applying feedback control of the robot. Phantom experiments were designed to verify the whole workflow and an error of 1 cm magnitude in the ultrasound image space was identified as an overall effect of the error in each component. This supports the hypothesis and is concluded to be adequate for 3D TOE but still challenging for 2D TOE if small structures in a particular plane need to be monitored. Particularly for the tracking method in the workflow, several different options were investigated based on robotic kinematics, ultrasound to MR registration, and electromagnetic sensing. It is concluded that the combined tracking using EM sensing first for the estimation and ultrasound to MR registration as the improvement provides both accuracy with an error magnitude less than 2 mm and reliability with 100% success rate in support of the hypothesis. The whole design of the automatic TOE acquisition workflow using the robot has been verified and proved to be achievable.

The study presented in this thesis is encouraging for eventual clinical experiments using the TOE robot in cadaver facilities and *in vivo*. The proposed future development of this system requires building a second clinical prototype and performing cadaver experiments to verify the automatic acquisition workflow and its possible variations. This second clinical prototype will require more professional safety features and a clinically acceptable mounting option for the robot in the surgical room. The cadaver experiment will re-perform the experiment introduced in this work but with the correct anatomical relationship and constraints. Different variations of the workflow such as semi-automatic acquisition or manual robotic acquisition will be evaluated and the best clinically acceptable option of the workflow will be decided. A commercial TOE robotic system and a robot-assisted workflow will be the focus in order to bring the robot into an eventual first in man study.

# 8 REFERENCES


1. Hunt, F.V., *Electroacoustics: the analysis of transduction, and its historical background*. 1954: Harvard University Press.

2. Woo, J. *A short history of the development of ultrasound in obstetrics and gynecology*. [cited 2016; Available from: http://www.ob-ultrasound.net/.

3. Gohe, H. and T. Wedekind, *Der Ultraschall in der Medizin.* Klinische Wochenschrift, 1940. **19**(2): p. 25-29.

4. Ludwig, G.D. and F.W. Struthers, *Considerations underlying the use of ultrasound to detect gallstones and foreign bodies in tissue*. 1949, DTIC Document.

5. Dussik, K.T., *Über die Möglichkeit, hochfrequente mechanische Schwingungen als diagnostisches Hilfsmittel zu verwerten.* Zeitschrift für die gesamte Neurologie und Psychiatrie, 1942. **174**(1): p. 153-168.

6. Goldberg, B.B., *Medical diagnostic ultrasound: a retrospective on its 40th anniversary*. 1988: Kodak Health Sciences.

7. Hueter, T.F. and R.H. Bolt, *Sonics: Techniques for the use of Sound and Ultrasound in Engineering and Science*. 1955: Wiley New York.

8. Duck, F.A., A.C. Baker, and H.C. Starritt, *Ultrasound in medicine*. 1998: CRC Press.

9. Rovner, A. *Physics of ultrasound as it relates to echocardiography*. The principle of ultrasound [cited 2016; Available from: http://www.echopedia.org/.

10. Gray, A.T., *Atlas of Ultrasound-Guided Regional Anesthesia: Expert Consult-Online and Print*. 2012: Elsevier Health Sciences.

11. Sprawls, P., *Physical principles of medical imaging*. 1987: Aspen Publishers.

12. Herring, W., *Learning radiology: Recognizing the basics*. 2015: Elsevier Health Sciences.

13. Shung, K.K., *Diagnostic ultrasound: Past, present, and future.* J. Med. Biol. Eng. **31**(6): p. 371-374.

14. Byrne, S.F., *A-scan axial eye length measurements: a handbook for IOL calculations*. 1995: Grove Park Publishers.

15. Lang, R., et al., *ASE's Comprehensive Echocardiography*. 2015: Elsevier Health Sciences.

16. Jensen, J.A., *Medical ultrasound imaging.* Progress in Biophysics and Molecular Biology, 2007. **93**(1–3): p. 153-165.

17. Kollár, A. *The clinical importance of diagnostic modalities: Ultrasound Imaging*. [cited 2016; Available from: http://oftankonyv.reak.bme.hu/.

18. Kremkau, F.W. and F. Forsberg, *Sonography principles and instruments*. 2015: Elsevier Health Sciences.

19. Whittingham, T., *Medical diagnostic applications and sources.* Progress in biophysics and molecular biology, 2007. **93**(1): p. 84-110.

20. Powers, J. and F. Kremkau, *Medical ultrasound systems.* Interface focus, 2011. **1**(4): p. 477-489.

21. Bjåstad, T.G., *High frame rate ultrasound imaging using parallel beamforming*. 2009, Norwegian University of Science and Technology.

22. Barthez, P.Y., R. Leveille, and P.V. Scrivani, *Side lobes and grating lobes artifacts in ultrasound imaging.* Vet Radiol Ultrasound, 1997. **38**(5): p. 387-93.

23. Tchacarski, V., et al., *Atlas of diagnostic Ultrasound: Ultrasonography*. 2015: Valery Tchacarski.

24. Matsumoto, M., et al., *Three-dimensional echocardiography for spatial visualization and volume calculation of cardiac structures.* Journal of Clinical Ultrasound, 1981. **9**(4): p. 157-165.

25. Badano, L.P., R.M. Lang, and J.L. Zamorano, *Textbook of real-time three dimensional echocardiography*. 2011: Springer.

26. Fenster, A., D.B. Downey, and H.N. Cardinal, *Three-dimensional ultrasound imaging.* Physics in medicine and biology, 2001. **46**(5): p. R67.

27. Buck, T. and E.K. Thiele, *Basic principles and practical application,* in *Three-dimensional Echocardiography*. 2015, Springer. p. 21-57.

28. Savord, B. and R. Solomon. *Fully sampled matrix transducer for real time 3D ultrasonic imaging*. in *Ultrasonics, 2003 IEEE Symposium on*. 2003. IEEE.

29. Vegas, A. and M. Meineri, *Three-dimensional transesophageal echocardiography is a major advance for intraoperative clinical management of patients undergoing cardiac surgery: a core review.* Anesthesia & Analgesia, 2010. **110**(6): p. 1548-1573.

30. Gibbs, V., D. Cole, and A. Sassano, *Ultrasound physics and technology: how, why and when*. 2011: Elsevier Health Sciences.

31. Cheitlin, M.D., et al., *ACC/AHA guidelines for the clinical application of echocardiography. A report of the American College of Cardiology/American Heart Association Task Force on Practice Guidelines (Committee on Clinical Application of Echocardiography).* Circulation, 1997. **95**(6): p. 1686-1744.

32. Stec, S., et al., *First experience with microprobe transoesophageal echocardiography in non-sedated adults undergoing atrial fibrillation ablation: feasibility study and comparison with intracardiac echocardiography.* Europace, 2011. **13**(1): p. 51-56.

33. Szili-Torok, T. and J.G. Bosch, *Transnasal transoesophageal ultrasound: the end of the intracardiac echocardiography age?* Europace, 2011. **13**(1): p. 7-8.

34. Jongbloed, M., et al., *Clinical applications of intracardiac echocardiography in interventional procedures.* Heart, 2005. **91**(7): p. 981-990.

35. Hijazi, Z.M., K. Shivkumar, and D.J. Sahn, *Intracardiac echocardiography during interventional and electrophysiological cardiac catheterization.* Circulation, 2009. **119**(4): p. 587-596.

36. Hahn, R.T., et al., *Guidelines for performing a comprehensive transesophageal echocardiographic examination: recommendations from the American Society of Echocardiography and the Society of Cardiovascular Anesthesiologists.* Journal of the American Society of Echocardiography, 2013. **26**(9): p. 921-964.

37. *What To Expect During Transesophageal Echocardiography*. Explore Transesophageal Echocardiography 2012 [cited 2016; Available from: https://www.nhlbi.nih.gov/health/health-topics/topics/tee/during.

38. Side, C.D. and R.G. Gosling, *Non-surgical assessment of cardiac function.* Nature, 1971. **232**(5309): p. 335-6.

39. Frazin, L., et al., *Esophageal echocardiography.* Circulation, 1976. **54**(1): p. 102-8.

40. Hisanaga, K., et al., *A new transesophageal real-time two-dimensional echocardiographic system using a flexible tube and its clinical application.* Proc Jpn Soc Ultrason Med, 1977. **32**: p. 43-44.

41. Hisanaga, K., A. Hisanaga, and Y. Ichie, *A new transesophageal real-time linear scanner and initial clinical results.* Reflections, 1978. **4**: p. 203-206.

42. Seward, J.B., et al. *Multiplane transesophageal echocardiography: image orientation, examination technique, anatomic correlations, and clinical applications*. in *Mayo Clinic Proceedings*. 1993. Elsevier.

43. Shanewise, J.S., et al., *ASE/SCA guidelines for performing a comprehensive intraoperative multiplane transesophageal echocardiography examination: recommendations of the American Society of Echocardiography Council for Intraoperative Echocardiography and the Society of Cardiovascular Anesthesiologists Task Force for Certification in Perioperative Transesophageal Echocardiography.* Anesthesia & Analgesia, 1999. **89**(4): p. 870.

44. Lang, R.M., et al., *EAE/ASE Recommendations for Image Acquisition and Display Using Three-Dimensional Echocardiography*. European Heart Journal – Cardiovascular Imaging, 2012. **13**(1): p. 1-46.

45. Douglas, P.S., et al., *Appropriate Use Criteria for Echocardiography. A Report of the American College of Cardiology Foundation Appropriate Use Criteria Task Force, American Society of Echocardiography, American Heart Association, American Society of Nuclear Cardiology, Heart Failure Society of America, Heart Rhythm Society, Society for Cardiovascular Angiography and Interventions, Society of Critical Care Medicine, Society of Cardiovascular Computed Tomography, and Society for Cardiovascular Magnetic Resonance Endorsed by the American College of Chest Physicians.* J Am Coll Cardiol, 2011. **57**(9): p. 1126-66.

46. Cheitlin, M.D., et al., *ACC/AHA/ASE 2003 guideline update for the clinical application of echocardiography: summary article: a report of the American College of Cardiology/American Heart Association Task Force on Practice Guidelines (ACC/AHA/ASE Committee to Update the 1997 Guidelines for the Clinical Application of Echocardiography).* Circulation, 2003. **108**(9): p. 1146-62.

47. Perrino, A.C. and S.T. Reeves, *Prosthetic Valves*, in *A practical approach to transesophageal echocardiography*. 2008, Lippincott Williams & Wilkins.

48. Perrino, A.C. and S.T. Reeves, *Transesophageal Echocardiography in the Intensive Care Unit*, in *A practical approach to transesophageal echocardiography*. 2008, Lippincott Williams & Wilkins.

49. Pearson, A.C., R. Castello, and A.J. Labovitz, *Safety and utility of transesophageal echocardiography in the critically ill patient.* American heart journal, 1990. **119**(5): p. 1083-1089.

50. Huttemann, E., *Transoesophageal echocardiography in critical care.* Minerva Anestesiol, 2006. **72**(11): p. 891-913.

51. Oh, J.K., J.B. Seward, and A.J. Tajik, *The echo manual*. 2006: Lippincott Williams & Wilkins.

52. Khandheria, B.K., J.B. Seward, and A.J. Tajik, *Transesophageal echocardiography.* Mayo Clin Proc, 1994. **69**(9): p. 856-63.

53. Lambert, A.-S., et al., *Improved evaluation of the location and mechanism of mitral valve regurgitation with a systematic transesophageal echocardiography examination.* Anesthesia & Analgesia, 1999. **88**(6): p. 1205-1212.

54. Couture, P., et al., *Impact of routine use of intraoperative transesophageal echocardiography during cardiac surgery.* Canadian Journal of Anesthesia, 2000. **47**(1): p. 20-26.

55. Peterson, G.E., M.E. Brickner, and S.C. Reimold, *Transesophageal echocardiography clinical indications and applications.* Circulation, 2003. **107**(19): p. 2398-2402.

56. Perk, G., et al., *Use of real time three-dimensional transesophageal echocardiography in intracardiac catheter based interventions.* Journal of the American Society of Echocardiography, 2009. **22**(8): p. 865-882.

57. Silvestry, F.E., et al., *Echocardiographic guidance and assessment of percutaneous repair for mitral regurgitation with the Evalve MitraClip: lessons learned from EVEREST I.* Journal of the American Society of Echocardiography, 2007. **20**(10): p. 1131-1140.

58. Faletra, F.F., S.Y. Ho, and A. Auricchio, *Anatomy of right atrial structures by real-time 3D transesophageal echocardiography.* JACC: Cardiovascular Imaging, 2010. **3**(9): p. 966-975.

59. Faletra, F.F., G. Nucifora, and S.Y. Ho, *Imaging the atrial septum using real-time three-dimensional transesophageal echocardiography: technical tips, normal anatomy, and its role in transseptal puncture.* Journal of the American Society of Echocardiography, 2011. **24**(6): p. 593-599.

60. Altiok, E., et al., *Real-time 3D TEE allows optimized guidance of percutaneous edge-to-edge repair of the mitral valve.* JACC: Cardiovascular Imaging, 2010. **3**(11): p. 1196-1198.

61. Faletra, F.F., et al., *Role of real-time three dimensional transoesophageal echocardiography as guidance imaging modality during catheter based edge-to-edge mitral valve repair.* Heart, 2013. **7**(3): p. 292-308.

62. Faletra, F.F., et al., *3D TEE during catheter-based interventions.* JACC: Cardiovascular Imaging, 2014. **7**(3): p. 292-308.

63. Daniel, W.G., et al., *Safety of transesophageal echocardiography. A multicenter survey of 10,419 examinations.* Circulation, 1991. **83**(3): p. 817-821.

64. Min, J.K., et al., *Clinical features of complications from transesophageal echocardiography: a single-center case series of 10,000 consecutive examinations.* Journal of the American Society of Echocardiography, 2005. **18**(9): p. 925-929.

65. Kallmeyer, I.J., et al., *The safety of intraoperative transesophageal echocardiography: a case series of 7200 cardiac surgical patients.* Anesthesia & Analgesia, 2001. **92**(5): p. 1126-1130.

66. Hilberath, J.N., et al., *Safety of transesophageal echocardiography.* Journal of the American Society of Echocardiography, 2010. **23**(11): p. 1115-1127.

67. *American Society of Anesthesiologists and Society of Cardiovascular Anesthesiologists Task Force on Transesophageal Echocardiography, Practice guidelines for perioperative transesophageal echocardiography. An updated report by the American Society of Anesthesiologists and the Society of Cardiovascular Anesthesiologists Task Force on Transesophageal Echocardiography.* Anesthesiology, 2010. **112**(5): p. 1084-96.

68. Seward, J.B., et al., *Critical appraisal of transesophageal echocardiography: limitations, pitfalls, and complications.* Journal of the American Society of Echocardiography, 1992. **5**(3): p. 288-305.

69. Chan, K.-L., et al., *Complications of transesophageal echocardiography in ambulatory adult patients: analysis of 1500 consecutive examinations.* Journal of the American Society of Echocardiography, 1991. **4**(6): p. 577-582.

70. Lennon, M.J., et al., *Transesophageal echocardiography-related gastrointestinal complications in cardiac surgical patients.* Journal of cardiothoracic and vascular anesthesia, 2005. **19**(2): p. 141-145.

71. O'Shea, J.P., et al., *Effects of prolonged transesophageal echocardiographic imaging and probe manipulation on the esophagus—an echocardiographic-pathologic study.* Journal of the American College of Cardiology, 1991. **17**(6): p. 1426-1429.

72. McIlwain, E.F., et al., *Radiation Safety for the Cardiac Sonographer: Recommendations of the Radiation Safety Writing Group for the Council on Cardiovascular Sonography of the American Society of Echocardiography.* Journal of the American Society of Echocardiography, 2014. **27**(8): p. 811-816.

73. Brenner, D.J., et al., *Cancer risks attributable to low doses of ionizing radiation: assessing what we really know.* Proceedings of the National Academy of Sciences, 2003. **100**(24): p. 13761-13766.

74. Valentin, J., *The 2007 recommendations of the international commission on radiological protection*. 2007: Elsevier Oxford, UK.

75. Stewart, F., et al., *ICRP publication 118: ICRP statement on tissue reactions and early and late effects of radiation in normal tissues and organs–threshold doses for tissue reactions in a radiation protection context.* Annals of the ICRP, 2012. **41**(1): p. 1-322.

76. Barr, J.M.B. and A.D. Schiska, *Radiologic safety: historical perspectives and contemporary recommendations.* Journal of Radiology Nursing, 2005. **24**(1): p. 6-10.

77. *National Research Council, Health risks from exposure to low levels of ionizing radiation: BEIR VII phase 2*. 1900: National Academies Press.

78. Einstein, A.J., *Effects of radiation exposure from cardiac imaging: how good are the data?* Journal of the American College of Cardiology, 2012. **59**(6): p. 553-565.

79. Bushberg, J.T. and J.M. Boone, *The essential physics of medical imaging*. 2011: Lippincott Williams & Wilkins.

80. *Minimize Your Exposure*. 2014 [cited 2016; Available from: http://www.nrc.gov/about-nrc/radiation/protects-you/protection-principles.html#tds.

81. Hart, D. and B.F. Wall, *UK population dose from medical X-ray examinations.* Eur J Radiol, 2004. **50**(3): p. 285-91.

82. Hart, D. and P.C. Shrimpton, *Fourth review of the UK national patient dose database.* The British Journal of Radiology, 2012. **85**(1018): p. e957-e958.

83. *1990 Recommendations of the International Commission on Radiological Protection.* Ann ICRP, 1991. **21**(1-3): p. 1-201.

84. Vano, E., et al., *Lens injuries induced by occupational exposure in non-optimized interventional radiology laboratories.* Br J Radiol, 1998. **71**(847): p. 728-33.

85. *Interview: Interventionalists in surgical rooms with radiation risks* 2016 [cited 2017; Available from: http://www.xinhuanet.com/photo/zhuanti/bt/btgs17/index.htm.

86. Ross, A.M., et al., *Prevalence of spinal disc disease among interventional cardiologists.* Am J Cardiol, 1997. **79**(1): p. 68-70.

87. Goldstein, J.A., et al., *Occupational hazards of interventional cardiologists: prevalence of orthopedic health problems in contemporary practice.* Catheter Cardiovasc Interv, 2004. **63**(4): p. 407-11.

88. Magnavita, N., et al., *Work-related musculoskeletal complaints in sonologists.* Journal of Occupational and Environmental Medicine, 1999. **41**(11): p. 981-988.

89. Mercer, R.B., et al., *Occupational health hazards to the ultrasonographer and their possible prevention.* J Am Soc Echocardiogr, 1997. **10**(4): p. 363-6.

90. Shah, S., et al., *Perceived barriers in the use of ultrasound in developing countries.* Critical ultrasound journal, 2015. **7**(1): p. 1-5.

91. LaGrone, L.N., et al., *A review of training opportunities for ultrasonography in low and middle income countries.* Tropical Medicine & International Health, 2012. **17**(7): p. 808-819.

92. Housden, R.J., et al. *Automated view planning of robotic trans-esophageal ultrasound imaging for interventional guidance*. in *MEIbioeng15*. 2015. Leeds.

93. Housden, R.J., et al. *Three-modality registration for guidance of minimally invasive cardiac interventions*. in *International Conference on Functional Imaging and Modeling of the Heart*. 2013. Springer.

94. *Webpage on da Vinci clinical evidence*. 2016 [cited 2016; Available from: http://www.intuitivesurgical.com/company/clinical-evidence/.

95. Lavery, H., D. Samadi, and A. Levinson, *Not a zero-sum game: the adoption of robotics has increased overall prostatectomy utilization in the united states*. The Journal of Urology, 2011. **185**(4): p. e33.

96. Moustris, G., et al., *Evolution of autonomous and semi-autonomous robotic surgical systems: a review of the literature*. The International Journal of Medical Robotics and Computer Assisted Surgery, 2011. **7**(4): p. 375-392.

97. Singh, I., *Robotics in urological surgery: review of current status and maneuverability, and comparison of robot-assisted and traditional laparoscopy*. Computer Aided Surgery, 2011. **16**(1): p. 38-45.

98. Stüer, C., et al., *Robotic technology in spine surgery: current applications and future developments*. 2011: Springer.

99. Najarian, S., M. Fallahnezhad, and E. Afshari, *Advances in medical robotic systems with specific applications in surgery—a review*. Journal of medical engineering & technology, 2011. **35**(1): p. 19-33.

100. Beasley, R.A., *Medical robots: current systems and research directions*. Journal of Robotics, 2012. **2012**.

101. Gomes, P., *Surgical robotics: Reviewing the past, analysing the present, imagining the future*. Robotics and Computer-Integrated Manufacturing, 2011. **27**(2): p. 261-266.

102. Okamura, A.M., M.J. Mataric, and H.I. Christensen, *Medical and health-care robotics*. Robotics and Automation Magazine, 2010. **17**(3): p. 26-27.

103. Priester, A.M., S. Natarajan, and M.O. Culjat, *Robotic ultrasound systems in medicine*. Ultrasonics, Ferroelectrics, and Frequency Control, IEEE Transactions on, 2013. **60**(3): p. 507-523.

104. Salcudean, S., et al. *Robot-assisted diagnostic ultrasound–design and feasibility experiments*. in *Medical Image Computing and Computer-Assisted Intervention–MICCAI'99*. 1999. Springer.

105. Salcudean, S.E., et al., *Robotically assisted medical ultrasound*. 2002, Google Patents.

106. Abolmaesumi, P., et al., *Image-guided control of a robot for medical ultrasound*. Robotics and Automation, IEEE Transactions on, 2002. **18**(1): p. 11-23.

107. Abolmaesumi, P., et al. *A user interface for robot-assisted diagnostic ultrasound*. in *Robotics and Automation, 2001. Proceedings 2001 ICRA. IEEE International Conference on*. 2001. IEEE.

108. Zhu, W.-H., et al. *Motion/force/image control of a diagnostic ultrasound robot*. in *Robotics and Automation, 2000. Proceedings. ICRA'00. IEEE International Conference on*. 2000. IEEE.

109. Abolmaesumi, P., S. Salcudean, and W. Zhu. *Visual servoing for robot-assisted diagnostic ultrasound*. in *Engineering in Medicine and Biology Society, 2000. Proceedings of the 22nd Annual International Conference of the IEEE*. 2000. IEEE.

110. Abolmaesumi, P., M.R. Sirouspour, and S. Salcudean. *Real-time extraction of carotid artery contours from ultrasound images*. in *Computer-Based Medical Systems, 2000. CBMS 2000. Proceedings. 13th IEEE Symposium on*. 2000. IEEE.

111. Nakadate, R., et al. *Development of a robotic carotid blood measurement wta-1rii: mechanical improvement of gravity compensation mechanism and optimal link position*

*of the parallel manipulator based on ga*. in *Advanced Intelligent Mechatronics, 2009. AIM 2009. IEEE/ASME International Conference on*. 2009. IEEE.

112. Nakadate, R., et al., *Development of the Ultrasound Probe Holding Robot WTA-1RII and an Automated Scanning Algorithm based on Ultrasound Image Feedback*. 2010: Springer.

113. Nakadate, R., et al. *Implementation of an automatic scanning and detection algorithm for the carotid artery by an assisted-robotic measurement system*. in *Intelligent Robots and Systems (IROS), 2010 IEEE/RSJ International Conference on*. 2010. IEEE.

114. Nakadate, R., et al. *Out-of-plane visual servoing method for tracking the carotid artery with a robot-assisted ultrasound diagnostic system*. in *Robotics and Automation (ICRA), 2011 IEEE International Conference on*. 2011. IEEE.

115. Seabra, J., J.S. Suri, and J.M. Sanches, *Three-Dimensional Ultrasound Plaque Characterization*, in *Ultrasound Imaging*. 2012, Springer. p. 203-221.

116. Seabra, J.C., et al., *A 3-D ultrasound-based framework to characterize the echo morphology of carotid plaques.* Biomedical Engineering, IEEE Transactions on, 2009. **56**(5): p. 1442-1453.

117. Gourdon, A., et al. *A new robotic mechanism for medical application*. in *Advanced Intelligent Mechatronics, 1999. Proceedings. 1999 IEEE/ASME International Conference on*. 1999. IEEE.

118. Arbeille, P., et al., *Echographic examination in isolated sites controlled from an expert center using a 2-D echograph guided by a teleoperated robotic arm.* Ultrasound in medicine & biology, 2003. **29**(7): p. 993-1000.

119. Arbeille, P., et al., *Fetal tele-echography using a robotic arm and a satellite link.* Ultrasound in obstetrics & gynecology, 2005. **26**(3): p. 221-226.

120. Arbeille, P., et al., *Use of a robotic arm to perform remote abdominal telesonography.* American journal of Roentgenology, 2007. **188**(4): p. W317-W322.

121. Vieyres, P., et al., *A tele-operated robotic system for mobile tele-echography: The OTELO project*, in *M-Health*. 2006, Springer. p. 461-473.

122. Delgorge, C., et al., *A tele-operated mobile ultrasound scanner using a light-weight robot.* Information Technology in Biomedicine, IEEE Transactions on, 2005. **9**(1): p. 50-58.

123. Courreges, F., P. Vieyres, and R. Istepanian. *Advances in robotic tele-echography services-the OTELO system*. in *Engineering in Medicine and Biology Society, 2004. IEMBS'04. 26th Annual International Conference of the IEEE*. 2004. IEEE.

124. Courreges, F., et al., *Clinical trials and evaluation of a mobile, robotic tele-ultrasound system.* Journal of telemedicine and telecare, 2005. **11**(suppl 1): p. 46-49.

125. Courrèges, F., et al. *Ergonomic mouse based interface for 3D orientation control of a tele-sonography robot*. in *Intelligent Robots and Systems, 2009. IROS 2009. IEEE/RSJ International Conference on*. 2009. IEEE.

126. Masuda, K., et al. *Three dimensional motion mechanism of ultrasound probe and its application for tele-echography system*. in *Intelligent Robots and Systems, 2001. Proceedings. 2001 IEEE/RSJ International Conference on*. 2001. IEEE.

127. Masuda, K., et al. *Development and experience of tele-echography systems with and without robotics*. in *Proc. of the 3rd Biomedical Engineering International Conference, Kyoto*. 2010.

128. Masuda, K. and H. Kato, *Development of a twist pantograph mechanism for robotic tele-echography.* Proc. of 3rd European Medical & Biological Engineering Conference (EMBEC'05), 2005: p. 1661-1664.

129. Vilchis, A., et al., *A new robot architecture for tele-echography.* Robotics and Automation, IEEE Transactions on, 2003. **19**(5): p. 922-926.

130. Vilchis Gonzales, A., et al. *TER: a system for robotic tele-echography*. in *Medical Image Computing and Computer-Assisted Intervention–MICCAI 2001*. 2001. Springer.

131. Vilchis, A., et al. *Robotic tele-ultrasound system (TER): slave robot control*. in *1st IFAC Conference on Telematics Application in Automation and Robotics*. 2001.

132. Vilchis, A., et al., *Experiments with the TER tele-echography robot*, in *Medical Image Computing and Computer-Assisted Intervention—MICCAI 2002*. 2002, Springer. p. 138-146.

133. Koizumi, N., et al., *Construction methodology for a remote ultrasound diagnostic system.* Robotics, IEEE Transactions on, 2009. **25**(3): p. 522-538.

134. T-MedRobotics. *Tele-Echography Scientific Recognition*. 2014 [cited 2016; Available from: http://www.t-medrobotics.com/scientific-recognition.html.

135. *Long-distance ultrasound exams controlled by joystick*. 2010 [cited 2016; Available from: http://phys.org/news/2010-12-long-distance-ultrasound-exams-joystick.html.

136. AdEchoTech. *Telemedecine : MELODY, a remote, robotic ultrasound solution*. 2013 [cited 2016; Available from: http://www.adechotech.com/products/.

137. Janvier, M.-A., et al., *Validation of 3D reconstructions of a mimicked femoral artery with an ultrasound imaging robotic system.* Medical physics, 2010. **37**(7): p. 3868-3879.

138. Vilchis-Gonzalez, A., J. Avila-Vilchis, and A. Garcia-Torres. *TERMI robot*. in *null*. 2007. IEEE.

139. Ma, Y., et al., *Hybrid echo and x-ray image guidance for cardiac catheterization procedures by using a robotic arm: a feasibility study.* Physics in medicine and biology, 2010. **55**(13): p. N371.

140. Ma, Y., et al. *Using a Robotic Arm for Echocardiography to X-ray Image Registration during Cardiac Catheterization Procedures*. in *CI2BM09-MICCAI Workshop on Cardiovascular Interventional Imaging and Biophysical Modelling*. 2009.

141. Han, M., et al., *Tandem-robot assisted laparoscopic radical prostatectomy to improve the neurovascular bundle visualization: a feasibility study.* Urology, 2011. **77**(2): p. 502-506.

142. Kim, C., et al. *Robot for ultrasound-guided prostate imaging and intervention*. in *Intelligent Robots and Systems (IROS), 2011 IEEE/RSJ International Conference on*. 2011. IEEE.

143. Han, M., et al., *Geometric evaluation of systematic transrectal ultrasound guided prostate biopsy.* The Journal of urology, 2012. **188**(6): p. 2404-2409.

144. Adebar, T., et al., *A robotic system for intra-operative trans-rectal ultrasound and ultrasound elastography in radical prostatectomy*, in *Information Processing in Computer-Assisted Interventions*. 2011, Springer. p. 79-89.

145. Adebar, T.K., O. Mohareri, and S.E. Salcudean. *Instrument-based calibration and remote control of intraoperative ultrasound for robot-assisted surgery*. in *Biomedical Robotics and Biomechatronics (BioRob), 2012 4th IEEE RAS & EMBS International Conference on*. 2012. IEEE.

146. Yu, Y., et al., *Robotic system for prostate brachytherapy*. Computer Aided Surgery, 2007. **12**(6): p. 366-370.

147. Schneider, C.M., A.M. Okamura, and G. Fichtinger. *A robotic system for transrectal needle insertion into the prostate with integrated ultrasound*. in *Robotics and Automation, 2004. Proceedings. ICRA'04. 2004 IEEE International Conference on*. 2004. IEEE.

148. Loschak, P.M., L.J. Brattain, and R.D. Howe. *Automated pointing of cardiac imaging catheters*. in *Robotics and Automation (ICRA), 2013 IEEE International Conference on*. 2013. IEEE.

149. Brattain, L.J., et al., *Instrument tracking and visualization for ultrasound catheter guided procedures*, in *Augmented Environments for Computer-Assisted Interventions*. 2014, Springer. p. 41-50.

150. Loschak, P.M., L.J. Brattain, and R.D. Howe, *Algorithms for automated pointing of cardiac imaging catheters*, in *Computer-Assisted and Robotic Endoscopy*. 2014, Springer. p. 99-109.

151. Loschak, P.M., et al., *A 4-DOF Robot for Positioning Ultrasound Imaging Catheters.* Proc ASME Des Eng Tech Conf, 2015.

152. De Cunha, D., et al. *The MIDSTEP system for ultrasound guided remote telesurgery*. in *Engineering in Medicine and Biology Society, 1998. Proceedings of the 20th Annual International Conference of the IEEE*. 1998. IEEE.

153. Stolka, P.J., et al. *First 3D ultrasound scanning, planning, and execution of CT-free milling interventions with a surgical robot*. in *Engineering in Medicine and Biology Society, 2008. EMBS 2008. 30th Annual International Conference of the IEEE*. 2008. IEEE.

154. Budde, R.P., et al., *Endoscopic localization and assessment of coronary arteries by 13 MHz epicardial ultrasound.* The Annals of thoracic surgery, 2004. **77**(5): p. 1586-1592.

155. Leven, J., et al., *DaVinci canvas: a telerobotic surgical system with integrated, robot-assisted, laparoscopic ultrasound capability*, in *Medical Image Computing and Computer-Assisted Intervention–MICCAI 2005*. 2005, Springer. p. 811-818.

156. Schneider, C., et al., *Intra-operative "Pick-Up" ultrasound for robot assisted surgery with vessel extraction and registration: a feasibility study*, in *Information Processing in Computer-Assisted Interventions*. 2011, Springer. p. 122-132.

157. Schneider, C.M., et al., *Robot-assisted laparoscopic ultrasound*, in *Information Processing in Computer-Assisted Interventions*. 2010, Springer. p. 67-80.

158. Billings, S., et al. *System for robot-assisted real-time laparoscopic ultrasound elastography*. in *SPIE Medical Imaging*. 2012. International Society for Optics and Photonics.

159. Davies, B., et al. *Neurobot: A special-purpose robot for neurosurgery*. in *Robotics and Automation, 2000. Proceedings. ICRA'00. IEEE International Conference on*. 2000. IEEE.

160. Ahmadi, S.-A., et al. *Advanced planning and intra-operative validation for robot-assisted keyhole neurosurgery In ROBOCAST*. in *Advanced Robotics, 2009. ICAR 2009. International Conference on*. 2009. IEEE.

161. Novotny, P.M., et al. *Real-time visual servoing of a robot using three-dimensional ultrasound*. in *Robotics and Automation, 2007 IEEE International Conference on*. 2007. IEEE.

162. Vitrani, M.-A., et al. *Robust Ultrasound-Based Visual Servoing for Beating Heart Intracardiac Surgery*. in *ICRA*. 2007. Citeseer.

163. Ortmaier, T., G. Morel, and M.-A. Vitrani, *Real-time instrument tracking in ultrasound images for visual servoing*, in *Bildverarbeitung für die Medizin 2005*. 2005, Springer. p. 232-236.

164. Stoll, J., et al. *Real-time 3D ultrasound-based servoing of a surgical instrument*. in *Robotics and Automation, 2006. ICRA 2006. Proceedings 2006 IEEE International Conference on*. 2006. IEEE.

165. Yuen, S.G., et al., *Robotic motion compensation for beating heart intracardiac surgery.* The International journal of robotics research, 2009. **28**(10): p. 1355-1372.

166. Thienphrapa, P., et al., *Tracking and characterization of fragments in a beating heart using 3D ultrasound for interventional guidance*, in *Medical Image Computing and Computer-Assisted Intervention–MICCAI 2011*. 2011, Springer. p. 211-218.

167. Megali, G., et al. *A computer-assisted robotic ultrasound-guided biopsy system for video-assisted surgery*. in *Medical Image Computing and Computer-assisted Intervention–MICCAI 2001*. 2001. Springer.

168. Kettenbach, J., et al., *Robot-assisted biopsy using ultrasound guidance: initial results from in vitro tests.* European radiology, 2005. **15**(4): p. 765-771.

169. Mallapragada, V.G., N. Sarkar, and T.K. Podder, *Robot-assisted real-time tumor manipulation for breast biopsy.* Robotics, IEEE Transactions on, 2009. **25**(2): p. 316-324.

170. Fichtinger, G., et al., *Robotic assistance for ultrasound-guided prostate brachytherapy.* Medical image analysis, 2008. **12**(5): p. 535-545.

171. Kheng, N.C., et al. *A HIFU robot for transperineal treatment of prostate cancer*. in *Control, Automation, Robotics and Vision, 2002. ICARCV 2002. 7th International Conference on*. 2002. IEEE.

172. Chauhan, S., *Image guided robotic systems for focal ultrasound based surgical applications*. 2008: INTECH Open Access Publisher.

173. Koizumi, N., et al. *Integration of diagnostics and therapy by ultrasound and robot technology*. in *Micro-NanoMechatronics and Human Science (MHS), 2010 International Symposium on*. 2010. IEEE.

174. Xiao, X., et al. *Focused ultrasound ablation using real time ultrasound image guidance*. in *Biomedical Engineering and Informatics (BMEI), 2011 4th International Conference on*. 2011. IEEE.

175. Fang, C., et al. *First clinical application of a robotics-based hand-held manipulator to steer a flexible endoscope in rhinoscopy*. in *IEEE-ICBBE 2012, The 6th International Conference on Bioinformatics and Biomedical Engineering*. 2012.

176. Fang, C., et al. *A motorized hand-held flexible rhino endoscope in ENT diagnoses and its clinical experiences*. in *Biomedical Robotics and Biomechatronics (BioRob), 2012 4th IEEE RAS & EMBS International Conference on*. 2012. IEEE.

177. Olds, K., et al., *A robotic assistant for trans-oral surgery: the robotic endo-laryngeal flexible (Robo-ELF) scope*. Journal of Robotic Surgery, 2012. **6**(1): p. 13-18.

178. Olds, K., et al., *Robotic endolaryngeal flexible (Robo-ELF) scope: A preclinical feasibility study*. The Laryngoscope, 2011. **121**(11): p. 2371-2374.

179. Ott, L., et al., *Robotic assistance to flexible endoscopy by physiological-motion tracking.* Robotics, IEEE Transactions on, 2011. **27**(2): p. 346-359.

180. Reilink, R., S. Stramigioli, and S. Misra. *Image-based flexible endoscope steering*. in *Intelligent Robots and Systems (IROS), 2010 IEEE/RSJ International Conference on*. 2010. IEEE.

181. Reilink, R., et al., *Evaluation of flexible endoscope steering using haptic guidance*. The International Journal of Medical Robotics and Computer Assisted Surgery, 2011. **7**(2): p. 178-186.

182. Ruiter, J., et al. *Design and evaluation of robotic steering of a flexible endoscope*. in *Biomedical Robotics and Biomechatronics (BioRob), 2012 4th IEEE RAS & EMBS International Conference on*. 2012. IEEE.

183. Peszynski, M., *Ultrasound imaging system with remote control and metod of operation thereof*. 2009, Google Patents.

184. Wang, S., et al., *Design, testing and modelling of a novel robotic system for trans-oesophageal ultrasound.* Int J Med Robot, 2016. **12**(3): p. 342-54.

185. Wang, S., et al. *Development of a robotic trans-esophageal ultrasound probe manipulator*. in *Design of medical device conference-Europe*. 2014. Delft, the Netherland.

186. Peszynski, M., *Control mechanism for an endoscope*. 2009, Google Patents.

187. Badamasi, Y.A. *The working principle of an Arduino*. in *Electronics, Computer and Computation (ICECCO), 2014 11th International Conference on*. 2014. IEEE.

188. Harrison, L.T., *Introduction to 3D game engine design using DirectX 9 and C#.* Computing Reviews, 2004. **45**(5): p. 277.

189. Geomagic. *OpenHaptics Toolkit*. [cited 2016; Available from: http://www.geomagic.com/en/products/open-haptics/overview/.

190. Itkowitz, B., J. Handley, and W. Zhu. *The openhaptics™ toolkit: a library for adding 3d touch™ navigation and haptics to graphics applications*. in *First Joint Eurohaptics Conference and Symposium on Haptic Interfaces for Virtual Environment and Teleoperator Systems. World Haptics Conference*. 2005. IEEE.

191. Brouwer, I. *Haptic Interfaces*. 2012 [cited 2016; Available from: http://www.bracina.com/haptichardware.html.

192. Kazanzides, P., *Safety design for medical robots.* Conf Proc IEEE Eng Med Biol Soc, 2009. **2009**: p. 7208-11.

193. Mikulak, R.J., R. McDermott, and M. Beauregard, *The basics of FMEA*. 2008: CRC Press.

194. Rudolph, T., L. Ebert, and J. Kowal, *Comparison of three optical tracking systems in a complex navigation scenario.* Comput Aided Surg, 2010. **15**(4-6): p. 104-9.

195. Koivukangas, T., J.P.A. Katisko, and J.P. Koivukangas, *Technical accuracy of optical and the electromagnetic tracking systems.* SpringerPlus, 2013. **2**: p. 90.

196. Inventive-Medical. *TEE Simulator-Product Overview*. 2016 [cited 2016; Available from: http://www.inventivemedical.com/tee-simulator/.

197. Corke, P., *Robotics, vision and control: fundamental algorithms in MATLAB*. Vol. 73. 2011: Springer.

198. Twigg, C., *Catmull-rom splines.* Computer, 2003. **41**(6): p. 4-6.

199. Catmull, E. and R. Rom, *A class of local interpolating splines.* Computer aided geometric design, 1974. **74**: p. 317-326.

200. Camarillo, D.B., et al., *Mechanics modeling of tendon-driven continuum manipulators.* IEEE Transactions on Robotics, 2008. **24**(6): p. 1262-1273.

201. Jones, B.A. and I.D. Walker, *Kinematics for multisection continuum robots.* IEEE Transactions on Robotics, 2006. **22**(1): p. 43-55.

202. Ott, L., et al., *Robotic assistance to flexible endoscopy by physiological-motion tracking.* IEEE Transactions on Robotics, 2011. **27**(2): p. 346-359.

203. Lipkin, H., et al. *Endoscope Kinematics*. in *12th IFToMM World Congress, Besanon*. 2007.

204. Murray, R.M., et al., *A mathematical introduction to robotic manipulation*. 1994: CRC press.

205. Gao, G., et al., *Registration of 3D trans-esophageal echocardiography to X-ray fluoroscopy using image-based probe tracking.* Medical image analysis, 2012. **16**(1): p. 38-49.

206. Peters, J., et al. *Automatic whole heart segmentation in static magnetic resonance image volumes*. in *International Conference on Medical Image Computing and Computer-Assisted Intervention*. 2007. Springer.

207. Weese, J., et al. *Shape constrained deformable models for 3D medical image segmentation*. in *Biennial International Conference on Information Processing in Medical Imaging*. 2001. Springer.

208. *Unity Game Engine-Official Site*. 2016 [cited 2016; Available from: http://unity3d.com.

209. Goldstone, W., *Unity game development essentials*. 2009: Packt Publishing Ltd.

210. Jerath, A., et al., *An interactive online 3D model of the heart assists in learning standard transesophageal echocardiography views.* Canadian Journal of Anesthesia/Journal canadien d'anesthésie, 2011. **58**(1): p. 14-21.

211. Hospital, D.o.A.a.t.T.G. *Virtual Transesophageal Echocardiography*. 2013 [cited 2016; Available from: https://pie.med.utoronto.ca/TEE/index.htm.

212. Wang, S., et al., *Robotic Ultrasound: View Planning, Tracking, and Automatic Acquisition of Transesophageal Echocardiography.* IEEE Robotics & Automation Magazine, 2016. **23**(4): p. 118-127.

213. Besl, P.J. and N.D. McKay. *Method for registration of 3-D shapes*. in *Robotics-DL tentative*. 1992. International Society for Optics and Photonics.

214. Zhang, Z., *Iterative point matching for registration of free-form curves and surfaces.* International journal of computer vision, 1994. **13**(2): p. 119-152.

215. King, A.P., et al., *Registering preprocedure volumetric images with intraprocedure 3-D ultrasound using an ultrasound imaging model.* IEEE Transactions on Medical Imaging, 2010. **29**(3): p. 924-937.

216. Grau, V., H. Becher, and J.A. Noble, *Registration of multiview real-time 3-D echocardiographic sequences.* IEEE transactions on medical imaging, 2007. **26**(9): p. 1154-1165.

217. Myronenko, A. and X. Song, *Point set registration: Coherent point drift.* IEEE transactions on pattern analysis and machine intelligence, 2010. **32**(12): p. 2262-2275.

218. Fuerst, B., et al., *Automatic ultrasound–MRI registration for neurosurgery using the 2D and 3D LC 2 Metric.* Medical image analysis, 2014. **18**(8): p. 1312-1319.

219. Lang, A., A. Jain, and V. Parthasarathy, *Calibration of EM sensors for spatial tracking of 3D ultrasound probes*. 2012: INTECH Open Access Publisher.

220. Wang, S., et al. *Probe Tracking and its Application in Automatic Acquisition Using a Trans-esophageal Ultrasound Robot*. in *3rd International Workshop on Computer-Assisted Robotic Endoscopy, MICCAI 2016*. 2016. Athens, Greece: Springer.

221. Bergmeir, C., et al., *Comparing calibration approaches for 3D ultrasound probes.* International journal of computer assisted radiology and surgery, 2009. **4**(2): p. 203-213.

222. Yaniv, Z., et al., *Electromagnetic tracking in the clinical environment.* Medical Physics, 2009. **36**(3): p. 876-892.

# 9 APPENDIX

## LIST OF PUBLICATIONS DURING PHD STUDY

*Journal papers:*

- Design, testing and modelling of a novel robotic system for trans-oesophageal ultrasound. Wang, S., Housden, J., Singh, D., Althoefer, K. & Rhode, K. International Journal of Medical Robotics and Computer-assisted Surgery. 2016. 12(3): p. 342-54.
- Robotic ultrasound: view planning, tracking, and automatic acquisition of trans-esophageal echocardiography. Wang, S., J., Singh, D., Althoefer, K. Rhode, K. & J., Housden. IEEE Robotics and Automation Magazine. 2016. 23(4): p. 18-127.

*Conference proceedings:*

- Development of a robotic trans-esophageal ultrasound probe manipulator. Wang, S., Housden, R. J., Singh, D., Althoefer, K. A. & Rhode, K. Design of Medical Device Conference - Europe. 2014. Delft, the Netherland.
- Probe tracking and its application in automatic acquisition using a trans-esophageal ultrasound robot. Wang, S., J., Singh, D., Althoefer, K. Rhode, K. & J., Housden. The 3rd International Workshop on Computer-assisted Robotic Endoscopy - MICCAI. 2016. Athens, Greece. 2017. Springer.

*Conference abstracts:*

- Development of a Robotic Trans-esophageal Ultrasound Probe Manipulator. Wang, S., Housden, R. J., Singh, D., Althoefer, K. A. & Rhode, K. MEC Annual Meeting and Bioengineering 2014. London, UK.
- Robotic Trans-oesophageal ultrasound system: control, force limiting, and modelling Wang, S., Housden, R. J., Singh, D., Althoefer, K. A. & Rhode, K. MEIbioeng 2015. Leeds, UK.
- Development of a Robotic Trans-esophageal Ultrasound Probe Manipulator. Wang, S., Housden, R. J., Singh, D., Althoefer, K. A. & Rhode, K. MEIbioeng 2016. Oxford, UK.